A Multidisciplinary Investigation on the Influence of Archean Seawater Composition and UV radiation levels on the Survival and Evolution of Early Microorganisms

by

Aleksandra Magdalena Mloszewski

A thesis submitted in partial fulfillment of the requirements of the degree of

Doctor of Philosophy

Department of Earth and Atmospheric Sciences

University of Alberta

Abstract

Life evolved in the oceans nearly four billion years ago, but the environmental conditions surrounding its evolution remains poorly understood. While Archean seawater (2.5 to 3.8 Ga) provided ancient microorganisms with the bioactive trace metals needed to sustain their metabolic requirements, it also presented high levels of UV radiation and toxic iron levels that made early marine environments inhospitable to life. Nevertheless, the existence of Archean-aged fossil evidence suggests that early microorganisms overcame these challenges and thrived in ancient shallow marine communities. The answer to how they achieved this lies in the composition of Archean seawater. Using the composition of banded iron formations (BIF) from the recently discovered ≥3.75 Ga Nuvvuagittuq Supracrustal Belt and the ≥ 3.77 Ga Nulliak Supracrustal Association as proxies for Eoarchean seawater composition, we show that the early oceans were rich in Ni and Zn. In methanogens (methane-producing bacteria), Ni is a key metal co-factor in the enzymes responsible for methane production. High Ni abundances in Eoarchean seawater facilitated the proliferation of large communtities of methanogens, which were responsible for much of the methane production in the early atmosphere. In terms of Zn, the relatively late appearance of Zn enzymes in eukaryotes has been previously linked to biolimiting marine Zn abundances in the Archean oceans. Instead, this study shows that Zn only varied within an order of magnitude of modern levels. These new observations decouple the relatively late appearance of eukaryotes from the

geochemical evolution of Zn in ancient seawater. Much as the rise of oxygen was important to the proliferation of eukaryotes, this study also demonstrates that high concentrations of iron and silica may have been instrumental to the initial survival of the most ancient planktonic bacteria, as well as to the early colonization of littoral marine environments. High UV radiation levels are detrimental to living organisms by causing lesions on DNA molecules, producing critical errors during the transcription of genetic material. Furthermore, the high iron concentrations present in Archean seawater were toxic to cells, through the production of reactive oxygen species (ROS). The intracellular accumulation of ROS has significant metabolic consequences, such as damage to genetic material (DNA and RNA), as well as protein deterioration and lipid peroxidation, any of which can lead to cell death. Silica played an important protective role for ancient planktonic bacteria by complexing with the iron in Archean seawater. The effects of this reaction were twofold: it lowered the level of soluble, bioavailable iron to more biologically manageable levels, enabling the survival and evolution of early bacteria under high iron conditions. Soluble iron is known for its efficiency at absorbing UV radiation. Aqueous silica delays the precipitation of ferric oxyhydroxide minerals through the formation of nanometer-sized iron-silica colloids. By keeping iron suspended in the water column in this way, silica maintained the role of iron as an effective UV shield. Thus protected from conditions that would otherwise be detrimental to life, early microorganisms were able to thrive in Archean marine habitats. By applying information from the Archean rock record to geochemical and biological models, this

multidisciplinary approach has allowed the elucidation of a number of important interactions between the hydro-, litho- and atmosphere and early life.

Preface

The research conducted for this thesis forms part of a research program led by Dr. Kurt Konhauser at the University of Alberta.

Chapter 2 of this thesis has been published as: Mloszewska, A.M., Pecoits, E., Cates, N.L., Mojzsis, S.J., O'Neil, J., Robbins, L.J., Konhauser, K.O., 2012. The composition of Earth's oldest iron formations: The Nuvvuagittuq Supracrustal Belt (Québec, Canada). Earth and Planetary Science Letters, 317:331-352. E. Pecoits and I were responsible for sample collection. L.J Robbins assisted with geochemical modeling. I was responsible for manuscript composition. Drs. S.J Mojzsis, J. O'Neil and K.O Konhauser contributed to manuscript edits.

Chapter 3 of this thesis has been submitted to The Canadian Journal of Earth Sciences as: Mloszewska, A.M., Haugaard, R., Lalonde, S.V., Ryan, B., Konhauser, K.O., Petrography and composition of chemical sedimentary rocks from the ≥3.77 Ga Nulliak Supracrustal Association (Labrador, Canada). Bruce Ryan of the Newfoundland and Labrador Geological Survey provided samples. R. Haugaard and Dr. S.V Lalonde provided assistance with petrological analyses and geochemical modeling, respectively. I was responsible for manuscript composition. Dr. K.O Konhauser contributed to manuscript edits.

Chapter 4 of this thesis has been submitted to Nature Geoscience as: Mloszewska, A.M., Owttrim, G.W., Whitford, D.S., Lalonde, S.V., Kappler, A. and Konhauser, K.O. Sunscreen-like properties of Archean seawater facilitated the initial colonization

of early shallow-marine environments. I conducted data collection and analysis, and was responsible for manuscript composition. G.W Owttrim and D.S Whitford contributed to experimental design and set up. Dr. S.V Lalonde assisted with geochemical modeling. Drs. S.V Lalonde, G.W Owttrim, A. Kappler, K.O Konhauser contributed to manuscript edits.

Chapter 5 of this thesis has been prepared for publicartion as: Mloszewska, A.M., Owttrim, G.W., Whitford, D.S., Kappler, A. and Konhauser, K.O. The success of Archean marine cyanobacteria depended on Si-rich seawater. I conducted data collection and analysis, and was responsible for manuscript composition. G.W Owttrim and D.S Whitford contributed to experimental design and set up. Dr. S.V Lalonde assisted with geochemical modeling. Drs. S.V Lalonde, G.W Owttrim, A. Kappler and K.O Konhauser contributed to manuscript edits.

Acknowledgements

First and foremost, I would like to thank Dr. Kurt Konhauser for all his advice, guidance and support over the past five years. His steadfast patience and encouragement were essential parts of the successful completion of this thesis. I would also like to thank Dr. George Owttrim for all his guidance and support in teaching me how to think like a microbiologist, and for welcoming me as an adoptive member of his research group.

Dr. Don Francis of McGill University and the Pituvik Landholding Corporation are thanked for facilitating fieldwork in Inukjuak, northern Quebec.

A special thank you to Bruce Ryan of the Newfoundland and Labrador Geological Survey for providing the samples from the Nulliak Supracrustal Association (northern Labrador).

Sergei Matveev and Guangcheng Chen are thanked for their assistance on the electron microprobe and quadrupole mass spectrometer (Department Earth and Atmospheric Sciences, University of Alberta). Thanks also to Arlene Oatway and Troy Locke for their support in the Advanced Microscopy Facility and in the Microbiology Service Unit (Biological Sciences Department, University of Alberta). Thanks also to the Goss and Barreda labs (Biological Sciences, University of Alberta) for the use of their UV spectrophotometer and fluorescence plate reader.

Thank you to the National Science and Engineering Research Council of Canada for their financial support in the form of a PGS-D award from 2010 to 2013.

Many thanks to Denise Whitford and Alex Dececchi for listening and advising as I hashed out various ideas with them.

Thanks especially to Rasmus Haugaard and Michelle Speta, for their constant friendship, emotional support and for never letting me take myself too seriously. Last but certainly not least, a very big thank to my parents and to my godmother. Without their love, support and constant faith in my abilities, none of this would have been possible.

CONTENTS

LIST OF TABLES

LIST OF FIGURES

Chapter 1. Introduction

Life evolved in the oceans at least 3.8 billion years ago (Ga) (Rosing, 1999) and its subsequent development was greatly influenced by changing seawater composition (Saito et al., 2003; Dupont et al., 2006, 2010). Archean (3.8 to 2.5 Ga) seawater environments deviated significantly from our own (Holland, 2006). They were largely anoxic, with increased UV radiation levels penetrating the first few meters of the water column, and contained greater quantities of dissolved iron, silica, and trace metals that were related to enhanced hydrothermal fluid fluxes at that time (Kasting and Catling, 2003). Vestiges of these ancient environmental pressures still exist in the genetic makeup of extant organisms. For example, the high iron and cobalt requirements of many modern bacteria are thought to be a conserved trait from their initial evolution when these metals occurred in significantly higher concentrations in their living environments (Dupont et al., 2010). While Archean seawater may have been high in bioactive trace metals beneficial to microbial growth (Frausto da Silva and Williams, 2001), other factors such as high UV fluxes may have deterred their proliferation (Knoll, 1979). Thus, the way these abiotic factors influenced the evolution and proliferation of early life remains poorly understood.

1.1 The oxygenation state of the Archean atmosphere

1.1.1 A reducing Archean environment

Our understanding of the state of the ocean-atmosphere system on early Earth is largely derived from the composition of Archean-aged meta-sedimentary rocks (Holland, 2006). The oxygenation state of the atmosphere influences important biogeochemical cycles (Fe, S, N, C) and causes the enrichment or depletion of various bioactive trace metals and nutrients. One of the most compelling pieces of evidence for a reducing Archean atmosphere is the large degree of mass-independent suphur isotope fractionation (S-MIF) in sulphide and sulphate minerals from pre-2.5 Ga meta-sedimentary rocks ($\delta^{34}S$ = -1.29‰ to +2.04‰) (Farquhar et al., 2000). While mass-dependant sulphur isotope signatures are characteristic of post-2.5 Ga rocks, the mass-independent fractionations observed in older rocks were likely produced by photochemical reactions between atmospheric sulphur particles and a high UV flux penetrating the Earth's ozoneless atmosphere (Farquhar and Wing, 2003). Atmospheric models estimate that levels of free oxygen were no higher than ~10^{-5} PAL (present atmospheric levels) during much of the Archean (Kasting et al., 2001; Pavlov and Kasting, 2002). Consequently, the deep oceans at this time were almost certainly anoxic, with the possibility that surface waters were partially oxygenated in so-called "oxygen oases" (Kasting, 1993). This is evidenced by the widespread occurrence of oxide-facies banded iron formations (BIF: Fe- and Si-rich chemical sedimentary rocks) and large-scale marine manganese deposits. These

mineral deposits require reducing conditions under circum-neutral pH for the transport of both Fe^{2+} and Mn^{2+} in seawater, and oxidizing conditions for mineral precipitation (Roy, 1997; Klein, 2005).

1.1.2 High fluxes of surface UV radiation

The absence of an ozone layer was another major consequence of an atmosphere devoid of detectable free oxygen (Kasting, 1987). Indeed, the Earth's ozone layer is formed photochemically from O_2 gas in the atmosphere. A radiative-photochemical modeling study by Segura et al., (2003) estimates that, at oxygen levels of 10^{-5} PAL, Archean UV-B fluxes may have been up to 11 times higher than they are today. While virtually all UV-C radiation today is attenuated by the ozone layer, this shortwave radiation is estimated to have been 4 times higher at the Archean Earth's surface (Segura et al., 2003). Importantly, UV-C is the most harmful form of ultraviolet radiation to life, causing mutagenic lesions on DNA molecules, which often produce deleterious effects (Sinha and Hader, 2002). Of the three types of UV radiation, UV-C can also penetrate the farthest in the water column, presenting a danger to microorganisms living in the top few meters of the ocean (Cockell, 2000). Indeed, early mat-forming communities of microorganisms were largely protected from incident UV radiation by virtue of their aggregate lifestyle as evidenced by ca. 3.5 Ga stromatolite fossils (Hoffman et al., 1999). While it has been suggested that planktonic (free-floating) microorganisms in the ancient water column would have been unable to withstand such high UV fluxes (Knoll, 1979), there is geological

evidence for a thriving planktonic community perhaps as early as 3.8 Ga (Rosing, 1999). Consequently, how did these organisms survive the high incident UV fluxes during the Archean?

1.1.3 A prolonged transition period leading up to the Great Oxidation Event

In the past decade, several geochemical studies have been suggestive of oxidative continental weathering occurring at ca. 2.4-2.3 Ga, prior to the Great Oxidation Event (GOE). For example, increases in molybdenum (Mo), rhenium (Re) and osmium (Os) concentrations, fractionation of Mo isotopes (yielding light $\delta^{98/95}$Mo values), and Platinum Group Element (PGE) abundance patterns (giving the typical "U-shaped" pattern of Phanerozoic shale) in black shale units of the 2.7 Ga old Manjeri Formation in Zimbabwe suggest that oxidising conditions already existed at that time. Through oxidative weathering, these metals were solubilised from their sulphide host minerals into their soluble oxyanion forms (e.g., MoO_4^{2-}). They were then transported to the oceans where they could be fractionated and scavenged into shales (Siebert et al., 2005). Similar patterns of these metals have been reported in the 2.64-2.50 Ga Ghaap Group in South Africa (Wille et al., 2007). Stueken et al., (2012) suggested that an increase in the total S and Mo supply to marginal marine sediments at 2.8 Ga is best explained by the biological oxidation of crustal sulphide minerals. Most recently, it was reported that the 2.95 Ga shallow-water Sinqeni iron formation (Pongola Supergroup, South Africa) contains molybdenum isotope signatures consistent with the sorption of Mo onto Mn oxide minerals (Planavsky et al., 2014).

The oxidation of Mn(II) to form these minerals requires the presence of free oxygen. The distribution of chromium isotopes in the ~3.0 Ga Nsuze paleosol, also part of the Pongola Supergroup, further suggests mobilization of redox-sensitive metals through oxidative weathering (Crowe et al., 2013). Collectively these results imply that detectable levels of free oxygen existed in the atmosphere and/or shallow water column at that time.

By ~2.3 Ga, the rock record suggests an irreversible appearance of free oxygen, the GOE. Briefly, this includes the disappearance of detrital pyrite, uranitite and siderite from fluvial and deltaic deposits (e.g., Rasmussen and Buick, 1999), an increase in the retention of iron in paleosols (e.g., Rye and Holland, 1998), an enrichment of Cr and U in iron formations (Konhauser et al., 2011; Partin et al., 2013), and the disappearance of S-MIF anomalies indicative of atmospheric SO_2 processing in the absence of appreciable ozone (e.g., Farquhar et al., 2000). In the case of the latter, meta-sedimentary pyrite devoid of a MIF sulphur isotope signal and oxidized ironstones in the ~2.32 Ga Rooihoogte and Timeball Hill iron formations (South Africa) might be the best indicators that atmospheric oxygen values had increased above levels of 10^{-5} PAL (Bekker et al., 2004).

One interesting aspect pertaining to the GOE that has received little attention is the role of increasing oxygenation of the surface environment on the existing biosphere. In particular, it is well known that oxygen is toxic to cells when it reacts with elements such as iron, nitrogen and copper to produce oxidative stress agents (Malick, 2004; Latifi et al., 2009; Rastogi et al., 2010). Its appearance in significant

amounts would certainly have changed the abundance of bioactive trace metals such as iron and other nutrients such as phosphate (Planavsky et al., 2010). Therefore, the episodic transition period leading up to the GOE may have presented significant challenges to the survival of early microorganisms.

1.2 The composition of Archean seawater

The Archean mantle was thought to have been hotter than at later times in Earth's history, due to higher rates of radioactive elemental decay, the exothermic crystallization of Earth's core, and residual heat from planetary accretion (Nisbet, 1993). The most direct evidence for a hotter Archean mantle is the occurrences of komatiites, ultramafic rocks unique to the Archean eon. These rocks have eruption temperatures several hundred degrees higher than that of modern basalts (Arndt et al., 1998). Consequently, positive europium anomalies characteristic of pre-2.5 Ga BIF suggest an increase in high-temperature (>350°C) hydrothermal fluxes during the Archean (Bolhar et al., 2004). This europium was sourced from the high temperature alteration of oceanic crust where Eu^{3+} is reduced to the more soluble Eu^{2+}, which fractionates preferentially into the hydrothermal fluid (Michard, 1986). These higher hydrothermal fluid fluxes stripped ions more readily from rocks deep within the Earth during their ascent to the surface, before ejecting them into overlying seawater.

1.2.1 Iron

In modern seawater, iron occurs in trace amounts (<2nM; Bruland and Lohan, 2004), and it is the second most important nutrient apart from phosphorus (Da Silva and Williams, 2001). In contrast, iron in Archean seawater was several orders of magnitude higher (Czaja et al., 2012). In terms of provenance, the mantle-like ε_{Nd} values of pre-2.5 Ga BIF suggest that this iron was primarily hydrothermally derived (Jacobsen and Pimentel-Klose, 1988). This is in contrast with the largely negative ε_{Nd} values of younger, Phanerozoic seawater (542 Ma to the modern), which suggest a dominantly continental iron source. Conventional ε_{Nd} notation is defined as the departure of $^{143}Nd/^{142}Nd$ from the chondrite uniform reservoir (CHUR) evolution line. Dissolved (ferrous) iron levels in Archean seawater are thought to have occurred at background concentrations of 30 μM in areas isolated from iron-rich upwelling currents (Holland, 1984). They may have reached levels as high as 1000 μM and perhaps even 1800 μM in parts of the ocean exposed to iron-upwelling currents (Morris and Horowitz, 1983; Edmond et al., 1986). The widespread occurrence of Archean-aged BIF is evidence that dissolved iron occurred at considerable concentrations (Klein, 2005). Toward the end of the Archean eon, iron deposition rates are estimated to have topped 4.53×10^{12} mol/year, during the deposition of the hundreds-of-meters thick Hamersley BIF, ca. 2.5 Ga (Konhauser et al., 2002).

Although iron is depleted in the modern ocean and acts as a micronutrient to many organisms, it can also be toxic to them in the quantities present in Archean

seawater. By reacting with hydrogen peroxide, it produces reactive oxygen species ($^1O_2$; O_2^-; H_2O_2; $OH\cdot$), which damages genetic material, deteriorates proteins and causes lipid peroxidation. (Touati et al., 2000). How then did microbes living in the Archean ocean survive the effects of iron toxicity?

1.2.2 Silica

The abundance of voluminous, pre-2.5 Ga chert deposits is a characteristic feature of Archean greenstone belts (Condie, 1981). Modern seawater has very low Si concentrations (<180 μM, Bruland and Lohan, 2004). This is due to organisms, such as diatoms and radiolarians, removing virtually all dissolved silica in seawater to precipitate their tests (Siever, 1992). In contrast, aqueous Si concentrations in Archean seawater, prior to the evolution of these Si-secreting organisms, occurred at concentrations between 0.67 mM and 2.2 mM, which designate the saturation with respect to the minerals cristobalite and amorphous silica, respectively (Maliva et al., 1989). Both of these minerals are thought to have been the precursor minerals of Archean chert deposits.

The source of Si to the modern oceans can either be from hydrothermal fluids derived from the alteration of basaltic oceanic crust at mid-ocean ridges, or from continental runoff via rivers and groundwater (Froelich et al., 1992; Mortlock et al., 1993). In early Archean seawater, aqueous Si was largely hydrothermally sourced from hot, highly alkaline SiO_2-enriched fluids emanating from hydrothermal vents (Shibuya et al., 2010). Because modern hydrothermal plumes extend horizontally for

thousands of kilometers, it is thought that Archean hydrothermal fluids could have led to the extensive silicification observed in the Archean geological terranes (Lupton, 1995; Shibuya et al., 2010). The large variation in the ^{30}Si isotopic composition of 3.0 to 3.5 Ga cherts from the Pilbara Craton (Western Australia) suggest mixing of seawater-derived Si and freshly sourced hydrothermal Si (van den Boorne et al., 2007). These two sources can be distinguished isotopically. The heavy ^{30}Si isotopic composition of Archean seawater is caused by an isotopic enrichment due to SiO_2 precipitation. In contrast, the zero to slight negative ^{30}Si isotopic compositions of hydrothermal fluids resemble the basaltic oceanic crust from which it was derived (van den Boorne et al., 2007). Sources of Si to the oceans shifted toward the end of the Archean with an identifiable contribution by continentally derived sources as evidenced by an inverse proportionality between the concentrations of hydrothermally-derived Ge, and continentally-derived Si in chert layers in the ca. 2.5 Ga Dales Gorge BIF (Hamade et al., 2003).

1.2.3 Trace elements

The composition of bioactive trace metals (e.g., Mo, Co, Cu, Zn, Ni) in ancient seawater played a significant role in influencing the evolution of early microbial metabolisms (Zerkle et al., 2005). Studies comparing the trace metal requirements and sensitivities of extant Archaea and Bacteria, with modeled abundances of trace metals in seawater through time, suggest preferences consistent with an evolution in anoxic seawater environments (Saito et al., 2003; Dupont et al., 2006, 2010). A

greater abundance of ultramafic rocks in the Archean, in combination with higher hydrothermal fluid fluxes, implies a higher concentration of metals associated with these rocks in ancient seawater (e.g., Ni, Co, Cr; Arndt, 1991). For instance, a recent study of Ni in BIF through time ties a sudden decrease in seawater Ni concentrations prior to the GOE (ca. 2.7 Ga) to a decrease in biogenic methane production, facilitating the accumulation of atmospheric free oxygen (Konhauser et al., 2009). Ni is a key co-factor in the metallo-enzyme required for biogenic methane production (Jaun and Thauer, 2007; Konhauser et al., 2009). Contrary to previous findings, a recent study on Zn in BIF and other iron rich sediments suggested that during conditions of BIF deposition (i.e., high Fe^{2+}concentrations, anoxic conditions, circum-neutral pH), the marine Zn reservoir would have remained unchanged throughout geologic time (Robbins et al., 2013). This is in contrast with previous studies suggesting that low Archean marine Zn concentrations due to sulphide complexation caused evolutionary pressure for the delay in the rise of eukaryotes (Dupont et al., 2010).

Phosphorus in hydrothermal sedimentary rocks and BIF through time also suggests noticeably higher P levels in Archean seawater compared with younger, Phanerozoic (542 Ma to recent) seawater (Planavsky et al., 2010). These recent findings are important, as it was previously believed that P limitation existed in the Archean. The cause of this P depletion was thought to have been the high affinity of P for the ferric oxyhydroxide particles that formed BIF. As a critical nutrient, this would have had deleterious effects on the marine plankton, resulting in low O_2

production by cyanobacteria (Bjerrum and Canfield, 2002). However, subsequent studies have since shown that P was likely never a limiting nutrient given that, in a silica-rich Archean ocean, Si preferentially binds to ferric oxyhydroxides instead of P (Konhauser et al., 2007).

1.2.4 Salinity, temperature and pH of the Archean ocean

Fluid inclusions containing trapped hydrothermal fluids from well-preserved ca. 3.2 Ga ironstones from the Barberton Greenstone Belt (South Africa) suggest seawater salinity was within an order of magnitude of modern seawater values (Cl, Br, SO_4, I, Na, NH_4, K, Mg, Ca, and Sr; de Ronde et al., 1997). In terms of pH, mass balance calculations and geochemical modelling based on the Archean carbonate-evaporite rock record seems to suggest high bicarbonate to calcium ratios, which may have counteracted a high CO_2 atmosphere. This implies that seawater pH may not have differed from the 8.1 pH of modern seawater (Grotzinger and Kasting, 1993).

Much debate still exists regarding Archean seawater temperature. The isotopic compositions of ^{30}Si and ^{18}O in well-preserved Archean-aged cherts and carbonate rocks can change as a result of temperature, and are often used to derive ancient seawater temperatures. A number of studies have suggested drastically higher Archean surface ocean temperatures compared to modern conditions. Early diagenetic cherts of the ca. 3.5 Ga Barberton Greenstone Belt preserve low $\delta^{18}O$ values (averaging ~1.22‰) which correspond to ocean surface temperatures of 55 to

80°C, 40°C warmer than modern ocean water (Knauth and Lowe, 2003). A correlation between ^{30}Si and ^{18}O isotopes in cherts, ranging in age from 3.5 to 0.8 Ga, support these results, suggesting temperatures of up to 70°C at 3.5 Ga, decreasing to below 20°C by 0.8 Ga (Robert and Chaussidon, 2006). However, it has also been argued that Archean seawater may have naturally had isotopically light ^{18}O values by up to 10‰ (Kasting and Howard, 2006). Instead of being due to higher sea surface temperatures, this modeling study by Kasting and Howard (2006) hypothesizes that thicker oceanic crust due to hotter mantle temperatures and more intense hydrothermal circulation would have shifted the ^{18}O of hydrothermal fluid flux emissions toward lighter values. Furthermore, a number of studies show that paleo-weathering indices of 3.5 to1.0 Ga Precambrian rocks were significantly lower than would have been expected at high temperatures in a CO_2-rich Archean atmosphere (Condie, 2001; Sleep and Hessler, 2006). This evidence implies that Archean seawater temperatures may have not different significantly from the modern.

1.2.5 The use of banded iron formation as palaeo-seawater proxies

BIF are iron rich (20-40 wt. %) and siliceous (40-60 wt. % SiO_2) sedimentary deposits that precipitated throughout much of the Archean (2.5-3.8 Ga) and Paleoproterozoic (2.5-1.8 Ga). The "Superior" type BIF, including those in the Hamersley Group, Western Australia and the Transvaal Supergroup, South Africa, are hundreds of meters thick, over 10^5 km^2 in areal extent, and contain $>10^{13}$ tons of

iron (Trendall, 2002; Klein, 2005). These chemical sedimentary rocks are typically laminated, with banding observed on a wide range of scales, from coarse macrobands (meters in thickness) to mesobands (centimeter-thick units) to millimeter and submillimeter layers (Trendall and Blockley, 1970). Among the latter is the wide variety of varve-like repetitive laminae, known as microbands.

BIF are among the best lithologies to use as proxies for ancient seawater composition because having precipitated directly from seawater, they retain some of its compositional signature in the process. Studies using chemical sedimentary rocks as proxies for changes in seawater composition through time are fairly recent. To derive the abundance of metals in early seawater, laboratory-derived partitioning coefficients between trace metals and ferric oxyhydroxide are applied to the trace metal composition in BIF. Much of the focus of recent research in this field has been directed at the composition of redox-sensitive metals during the transition period preceding or just after the GOE (Bjerrum and Canfield, 2002; Saito et al. 2003; Konhauser et al., 2009). However, there has been little focus on the composition of Eoarchean seawater. Indeed, the paucity of pre-3.6 Ga year old BIF puts a constraint on establishing the composition of early seawater, and emphasizes the importance of exploiting any known occurrence.

Some of the trace metals abundant in Eoarchean seawater served as important nutrients for early microorganisms, for example, Ni^{2+}. The presence of Ni-containing metallo-enzymes commonly found in most living species on Earth is a testament to the importance of this metal in early seawater (urease, dehydrogenase, and some

superoxide dismutases; da Silva and Williams, 2001). Therefore, expanding our knowledge of the composition of Eoarchean seawater would also establish some of the biological constraints the nutritional demands for producing important microbial metallo-enzymes.

1.3 Evidence for the antiquity of life

1.3.1 Isotopes

Geological evidence for the existence of life by as early as ~3.8 Ga occur as isotopically light carbon globules in meta-sedimentary rocks from the Eoarchean-aged Isua Supracrustal Belt (southern West Greenland) (Rosing, 1999). These globules contain a ^{13}C isotopic value of -19‰ and are thought to have had a biogenic origin, possibly being derived from the remains of planktonic organisms raining down onto the sea floor (Rosing, 1999). Similarly, isotopically light ^{13}C signatures are found in carbonaceous inclusions within apatite grains in BIF from the ca. 3.85 Ga year old Akilia association, South Greenland (Mojzsis et al., 1996). However, the origins of these rocks have been questioned, where Fedo and Whitehouse (2002) have alternately proposed that these Akilia rocks are in fact metasomatically altered mafic rocks, not meta-sediments precipitated from ancient seawater. Debate regarding the origins of these rocks is ongoing (Manning et al., 2006). Most Eoarchean terranes have been heavily deformed and highly metamorphosed, sometimes up to granulite facies (>700°C, >2 kbar) as in the case of the Akilia rocks (Klein, 2005). With ca 3.8 Ga rocks, it is especially important to combine field observations with petrographic

and geochemical data in order to confirm their origins as well as determine the effects of high-grade metamorphism of the primary composition.

1.3.2 Stromatolites

The earliest microbial mats date back to the Mesoarchean, with the stromatolites of the ca. 3.45 Ga Strelly Pool Chert (Pilbara Craton, Western Australia; Allwood et al., 2006), and the microbially induced sedimentary structures (MISS) of the ca. 3.48 Ga Dresser Formation also in the Pilbara (Heubeck, 2009). These fossilized organo-sedimentary structures were emplaced in shallow coastal environments such as lagoons and estuaries, and imply a thriving benthic microbial community by ca. 3.5 Ga. Indeed, they were likely produced by anoxygenic photosynthesizing bacteria (Byerly et al., 1986; Hoffman et al., 1999). Anoxygenic photosynthesis uses reductants such as H_2S, Fe^{2+}, H_2, SO_3^{2-}, S^0 or S_2O_3 as electron donors instead of H_2O, and is commonly thought to predate oxygenic photosynthesis (Nisbet et al., 1995). However, there is geological evidence for the early evolution of oxygenic photosynthesis (and by association, cyanobacteria) by as early as ca. 2.7 Ga. Stromatolites from the 2.72 Ga year old Tumbiana Formation (Pilbara Craton, Western Australia) that formed in saline Archean lakes are thought to have been constructed by cyanobacteria. This is evidenced by a deficit in reduced compounds such as ferrous iron and sulphate, implying oxygenic photosynthesis as the main mechanism for microbial growth (Buick, 1992). Similarly, sulphur and iron depleted kerogenous shales of the 3.2 Ga Gorge Creek Group (northwestern Australia) are

consistent with an oxygenic photosynthetic source for the kerogen (Buick, 2008). Recent isotopic studies of redox-sensitive Cr isotopes (Ijzermyn iron formation and Nsuze paleosol) and Mo isotopes (2.95 Ga year old Sinqeni Formation) in the Pongola Supergroup (South Africa) also suggest that the first cyanobacteria may have evolved by as early as ca. 3.0 Ga (Crowe et al., 2013; Planavsky et al., 2014).

1.3.3 Microfossils

Microfossil-like structures have been described in over 14 Archean-aged geological units (Schopf et al., 2010). The earliest of these occurrences was also considered the oldest reported evidence of life on Earth, which occurs in the ca. 3.5 Ga year old Apex Chert of the Warrawoona Group, Western Australia (Schopf, 1993). Filamentous structures in the Apex Chert range in width from less than a micron to several microns in size, and superficially resemble extant filamentous bacteria and cyanobacteria in both size and shape (Schopf, 1993, 2000). However, the age and origin of these structures is still a controversial matter. Indeed, it has been argued that one of the two fossil localities is not even a metasediment, but instead is a hydrothermal vein. Correspondingly, the structures described as microfossils are thought to be secondary artifacts formed by amorphous graphite (Brasier et al., 2002). The origins of the fossil-like structures at the second Apex Chert locality have also been questioned, as they show similarities to scoriaceous volcanic ash grains inside a tuffaceous host rock (Buick, 2008). The robustness of this microfossil evidence is

therefore questioned, forcing us to search for additional forms of evidence supporting the existence of a thriving Archean microbial community.

1.3.4 Biomarkers

Some of the molecular skeletons may remain as residues in a sedimentary rock, when microbial lipid and pigment biomolecules degrade. If they are unique enough in composition, they may be used as environmental and even taxonomical indicators (Buick, 2008). Hopanes and steranes are the most common biomarkers used, as they are robust under diagenetic conditions (Brocks and Pearson, 2005). Hopanes are used by bacteria to stabilize the cellular membrane (Ourisson et al., 1987), while steranes are eukaryotic in origin and are used by such organisms to modify the cell membrane for processes such as phagocytosis (Summons et al., 2006). Despite most Archean-aged rocks having succumbed to metamorphic temperatures greater than 350°C, biomarkers have been reported in rocks as old as 2.7 Ga. Traces of 2α-methylhopanes were found in Neoarchean shale units of the Pilbara Craton, Western Australia (Brocks et al., 1999). Given that these lipids rarely occur outside of cyanobacteria (Summons et al., 1999), this discovery was thought to be indicative of early oxygenic photosynthesis. The possibility of contamination cannot be excluded however, due to the permeability of the host rock and the low abundances in which the biomarkers were found (Brocks, 2001).

Other biomarker evidence comes from oil-bearing fluid inclusions in sandstone and conglomerate units from the 2.45 Ga Matinenda Formation (Huronian Supergroup, Canada). Their antiquity is emphasized by the geological context of the fluid inclusions, which are found in intra-granular fractures within quartz and potassium feldspar grains in the sedimentary rocks. This suggests that the oil was entrapped during compactional diagenesis, prior to peak metamorphism ca. 2.2 Ga (Dutkiewicz et al., 2003). A relative abundance of 2α-methylhopanes, as well as some steranes were recovered from these inclusions, suggesting at the ancient existence not only of cyanobacteria, but also of early Eukaryotes, by ca. 2.45 Ga (Dutkiewicz et al., 2006).

1.3.5 Proteomics

Over the last decade, the combined efforts of the fields of proteomics and geochemistry have led to the realization that early seawater composition and the metabolic trace metal demands of early microorganisms were probably linked. A geochemical modeling study taking into consideration the trace metal sensitivities of extant cyanobacteria put forth that modern cyanobacteria show trace metal preferences (Fe>Mn,Ni,Co>>Cd,Zn,Cu) consistent with their initial evolution in a ferro-sulfidic marine environment (Saito et al., 2003). In support of this idea, a phylogenetic study looking at the evolutionary timing of several important prokaryotic metallo-enzymes suggests that the redox state of Earth's atmosphere and

oceans has largely controlled the biological use of bioactive trace metals throughout geologic time (Zerkle et al., 2005). In fact, the relative abundance of Fe, Mn, Zn and Co binding structures in the proteomes of Prokarya and Eukarya appear to correspond with the theoretical changes in the abundances of these metals after the oxygenation of deep ocean waters (Dupont et al., 2006). While most prokaryotic proteomes appear to reflect evolution under anoxic conditions, most eukaryotic proteomes reflect an evolution under oxygenic conditions (Dupont et al., 2006). An evolutionary timeline based on the protein structures and genomic characteristics in prokaryotes and eukaryotes suggest that the development of proteins controlling metal homeostasis coincided with theoretical abundances of metals in the Archean ocean (Dupont et al. 2010). Based on the later appearance of Cu and Zn binding proteins compared with Fe, Ni and Mo binding protein structures, it has been suggested that the bioavailability of Zn was particularly low in the Archean, which could have been a limiting factor in the late appearance of eukaryotes (Dupont et al., 2010). By using Archean BIF as an archive of ancient seawater composition, we will be able to put these biological observations directly into the physical context of pre-2.5 Ga seawater.

1.4 Objectives

Much of our understanding about ancient seawater, the state of the atmosphere and the evolution of the biosphere comes from analyses of the Archean rock record. The paleo-environmental model that can be obtained from these rocks, when combined

with experimentally derived microbiological data, forms the basis for the theoretical predictions of the relationship between early life and its environment. The aim of this thesis is to elucidate some of the complex interactions between the hydrosphere, lithosphere and atmosphere on early life. Specifically, I focus on abiotic factors that would influence the proliferation of early microorganisms such as Fe, Si, trace metals, high UV radiation, and changing oxygen levels. I accomplish this by combining geochemical data derived from the rock record with experimental data to form the basis of a geochemical and microbiological model designed to mimic Archean seawater conditions. This multidisciplinary approach allows me to construct a more dynamic picture of the interplay between the survival and thus, evolution of ancient life and seawater composition.

In the first half of this thesis, I use Eoarchean-aged BIF (ca. 3.8 Ga) as proxies for ancient seawater composition in order to infer a more global picture of the bioactive trace element composition of Eoarchean-aged seawater. I focus on establishing a detailed geochemical-petrographic framework of BIF from the recently discovered ≥3.75 Ga Nuvvuagittuq Supracrustal Belt (Quebec, Canada) and the lesser-known ≥3.77 Ga Nulliak Supracrustal Association (Labrador, Canada). I then incorporate this new data with existing data on the extensively researched Eoarchean BIF occurrences of South and West Greenland (3.7-3.8 Ga Isua Supracrustal Belt; Akilia Island; Appel, 1980; Dymek and Klein, 1988; Dauphas et al., 2004, 2007; Mojzsis et al., 1996; Fedo and Whitehouse, 2002).

How life survived to evolve in these harsh Archean marine environments is the focus of the second half of my thesis. Geochemical analyses of the Archean rock record indicate that the water column was anoxic, containing high levels of aqueous Si and a profusion of trace metals from the weathering and dissolution of an abundance of ultramafic rocks (Barley et al., 1998). Significantly, Archean seawater also contained high concentrations of soluble, hydrothermally sourced iron, which was toxic to early life. Furthermore, the upper water column, where photosynthetic organisms resided, was bathed in high intensity UV radiation due to the absence of an atmospheric ozone layer. Overall, these conditions would have been inhospitable to life as we know it on Earth today, leading to the question of how early life survived and evolved in these extreme conditions. In this regard, I examine how life may have overcome these challenges by mimicking Archean seawater conditions predicted by the rock record, using living bacterial systems as proxies. By growing the marine planktonic cyanobacterium *Synechococcus* sp. PCC 7002 in high iron- and/or silica supplemented growth media under a range of Eh conditions (from microaerophilic to fully oxic) and high UV radiation levels, I experimentally model the conditions predicted to be present in the Archean oceans. Using a combination of microbiological and molecular techniques as well as geochemical modeling, I infer some important implications for biodiversity in the oceans in the few hundred million years leading up to the GOE, and during the transition period directly preceding that event.

These two main areas of investigation for this thesis are subdivided into 4 distinct chapters that are composed of work that is either published or in review:

Chapter 2. A detailed geochemical and petrographic study of banded iron formations from the ≥3.75 Ga Nuvvuagittuq Supracrustal Belt (northern Québec) and their use as a proxy for Eoarchean seawater composition.

The recent discovery of Eoarchean BIF units in the ≥3.75 Ga year old Nuvvuagittuq Supracrustal Belt (Inukjuak, Québec) has opened up exceptional opportunities to investigate the composition of early seawater. Based on fieldwork in the Nuvvuagittuq belt, I conducted detailed sampling of the chemical sedimentary lithologies with the guidance of outcrop-scale mapping in order to better direct sample collection. Here I link the Nuvvuagittuq BIF composition to the seawater chemistry in the Nuvvuagittuq depositional basin at the time of BIF precipitation more than ~3.8 Ga years ago. This is accomplished through multiple sorption experiments between ferric oxyhydroxide minerals and important bioactive trace metals (Ni and Zn), which allows me to calculate the paleo-environmental trace metal concentrations. By combining these results with those from previous work on the ca. 3.7-3.8 Ga year old Isua Supracrustal Belt (southern West Greenand; Konhauser et al., 2009), I determined how global oceanic processes in the Eoarchean, and trace metals in seawater could have influenced the evolution of early life.

A modified version of this chapter has already been published:

Mloszewska, A.M., Pecoits, E., Cates, N.L., Mojzsis, S.J., O'Neil, J., Robbins, L.J., Konhauser, K.O., 2012. The composition of Earth's oldest iron formations: The Nuvvuagittuq Supracrustal Belt (Québec, Canada). Earth and Planetary Science Letters, 317:331-352.

Chapter 3. A detailed geochemical and petrographic study of chemical sedimentary rocks from the ≥3.77 Ga Nulliak Supracrustal Association (Labrador, Canada).

Pre-3.6 Ga year old BIF have generally suffered complex metamorphic and deformation histories as compared with their younger counterparts. In order to use Eoarchean-aged BIF as seawater proxies, it is especially important to ascertain how these post-depositional events changed the primary composition, on both a whole rock and a mineral scale. The difficulty in preserving primary lithological signatures has been effectively demonstrated by the debate on the ca. 3.85 Ga year old banded quartz-pyroxene rocks from Akilia Island in southern Greenland (Manning et al., 2006). In the pyroxene bands, the light $\delta^{13}C$ signatures in the carbonaceous inclusions within the apatite have been interpreted to be indicative of the remains of early microorganisms (Mojzsis et al., 1996; Manning et al., 2006). However, Fedo and Whitehouse (2002) challenge this interpretation. The paucity of pre-3.6 Ga year old BIF occurrences emphasizes the importance of exploring any such occurrence. The

extensive cost of doing fieldwork in remote areas of northern Labrador (Canada) has likely deterred detailed sampling of the chemical sedimentary rocks of the ≥3.77 Ga Nulliak Supracrustal Association. With some rare samples provided by the Newfoundland and Labrador Geological Survey, I integrated petrographic and geochemical data (major and trace elements, as well as Fe isotopes) for the Nulliak rocks on both a whole-rock and mineral scale. I thereby create a framework for better understanding the bulk and microscale variations in these samples. This work provides insights into how post-depositional processes affect the primary geochemical composition of Eoarchean-aged BIF.

A modified version of this chapter is now in review:

Mloszewska, A.M., Haugaard, R., Lalonde, S.V., Ryan, B., Konhauser, K.O., Petrography and composition of chemical sedimentary rocks from the ≥3.77 Ga Nulliak Supracrustal Association (Labrador, Canada). Canadian Journal of Earth Sciences.

Chapter 4. A geochemical and microbiological study assessing the UV attenuating effects of Fe and Si on the survival of early plantkonic cyanobacteria in Archean seawater.

Fossil evidence suggests the presence of thriving photosynthetic communities living in shallow coastal and lagoonal settings by as early as 3.5 Ga (Hoffman et al., 1999; Allwood et al., 2006; Heubeck, 2009), and perhaps even by ca. 3.8 Ga (Rosing,

1999). However, planktonic organisms are especially susceptible to UV damage, and all mat-forming organisms have a motile, free-living stage in their life cycle with which they propagate to new environments (Stoodley et al., 2002). Furthermore, a radiative transfer model of the Neoarchean water column suggests that only at a depth of 30 m would the DNA damage rate to organisms have reached levels at the modern ocean's surface (Cockell, 2000). Therefore, how did early photosynthetic microorganisms survive and evolve under these conditions? Previous work suggests that biomineralized Fe(III)-Si crusts effectively protect microbial mats against UV radiation while transmitting photosynthetically active radiation (Pierson et al., 1993; Phoenix et al., 2001). It is known that iron has a high affinity for silica and likely complexed in the Archean water column as evidenced by the abundance of iron-silicate minerals in Archean-aged BIF. In this chapter I addressed whether iron-silica complexes, which likely formed in the Archean water column, could have effectively protected early photosynthetic microorganisms from the high levels of incident UV radiation penetrating the ozone-less Archean atmosphere.

A modified version of this chapter is now in review:

Mloszewska, A.M., Owttrim, G.W., Whitford, D.S., Lalonde, S.V., Kappler, A. and Konhauser, K.O. Sunscreen-like properties of Archean seawater facilitated the initial colonization of early shallow-marine environments. Nature Geoscience.

Chapter 5. A geochemical and microbiological study assessing the effects of aqueous Si on Fe toxicity in Archean marine cyanobacteria.

Despite being one of the most limiting nutrients in modern marine environments, disolved Fe can be extremely toxic to cells (Winterbourn, 1995). By reacting with hydrogen peroxide, harmful reactive oxygen species (ROS) are produced, causing significant intracellular damage with fatal consequences when present in quantities that overwhelm the cell (Touati et al., 2000). However, iron concentrations in Archean seawater were up to 3 orders of magnitude higher than in the modern ocean (Morris and Horrowitz, 1983; Czaja et al., 2012). Apart from protecting microorganisms from UV radiation, I investigate whether iron-silica complexes forming in Archean seawater could have also reduced the amount of soluble, bioavailabile iron, thereby reducing its toxicity.

A modified version of this chapter has been prepared for publication:

Mloszewska, A.M., Owttrim, G.W., Whitford, D.S., Kappler, A. and Konhauser, K.O. The success of Archean marine cyanobacteria depended on Si-rich seawater.

Chapter 6. Conclusions

Studying the evolution of the earliest forms of life and the extrinsic factors influencing its subsequent evolution must necessarily be multifaceted. This is best done with a thorough knowledge not only of the rock and fossil records, but also of bacterial systems and their chemical signatures. Thus, throughout this thesis, I have strived to take into account the finer points of the abiotic-biotic feedback system that may be lost by focusing on either of these two fields independently.

What my research has shown is that the Archean oceans were rich in multiple bioactive trace metals (Ni and Zn), used in primitive metallo-enzymes. I further demonstrate that elevated iron and silica concentrations in ancient seawater played key roles in the survival of early photosynthetic microorganisms. Silica played a dual role by lowering toxic iron levels to more manageable concentrations. Through the formation of iron-silica complexes, silica also kept iron in suspension in the water column, enabling its role as an effective UV shield. By using multidisciplinary methodologies, I build a dynamic picture of the interplay between the evolution of ancient life and Archean seawater composition.

References

Allwood, A.C., Walter, M.R., Kamber, B.S., Marshall, C.P., Burch, I.W., 2006. Stromatolite reef from the early Archean era of Australia. Nature 44:714-718.

Appel, P.W.U., 1980. On the early Archean Isua iron-formation, West Greenland. Precambrian Research 11:73-87.

Arndt, A., Ginibre, C., Chauvel, C., Albareded, F., Cheadle, M., Herzberg, C., Jenner, G., Lahaye, Y., 1998. Were komatiites wet? Geology 26:739-742.

Barley, M.E., Krapez, B., Groves, D.I., Kerrich, R., 1998. The Late Archean bonanza: metallogenic and environmental consequences of the interaction between mantle plumes, lithospheric tectonics and global cyclicity. Precambrian Research 91:65-90.

Bekker, A., Holland, H.D., Wang, P-L., Rumble III, D., Stein, H.J., Hannah, J.L., Coetzee, L.L., Beukes, N.J., 2004. Dating the rise of atmospheric oxygen. Nature 427:117-120.

Bekker, A., Holland, H.D., Wang, P-L., Rumble III, D., Stein, H.J., Hannah, J.L., Coetzee, L.L., Beukes, N.J., 2004. Dating the rise of atmospheric oxygen. Nature 427: 117-120.

Bjerrum, C.J., Canfield, D.E., Ocean productivity before about 1.9 Gyr ago limited by phosphorus adsorption onto iron oxides. Nature 417:159-162.

Bolhar, R., Kamber, B.S., Moorbath, S., Fedo, C.M., Whitehouse, M.J., Characterization of early Archean chemical sediments by trace element signatures. Earth and Planetary Science Letters 222:43-60.

Brasier, M.D., Green, O.R., Jephcoat, A.P., Kleppe, A.K., Van Kranendonk, M., Lindsay, J.F., Steele, A., Grassineau N., 2002. Questioning the evidence for Earth's oldest fossils. Nature 416:76-81.

Brocks, J.J., Logan, G.A., Buick, R., Summons, R.E.,1999. Archean molecular fossils and the early rise of eukaryotes. Science 285:1033-1036.

Brocks, J.J., 2001. Molecular fossils in Archean rocks. PhD thesis. University of Sidney.

Brocks, J.J., Pearson A., 2005. Building the biomarker tree of life. Reviews in Mineral Geochemistry 59:233-258.

Bruland, K.W., Lohan, M.C., 2004. The Control of trace metals in seawater. In: Elderfield, H., Ed. The Oceans and Marine Geochemistry. The Treatise of Geochemistry p. 33 to 47.

Buick, R., 1992. The antiquity of oxygenic photosynthesis: evidence from stromatolites in sulphate-deficient Archean lakes. Science 255:74-77.

Buick, R., 2008. When did oxygenic photosynthesis evolve? Philosophical Transactions of the Royal Society B. 363:2731-2743.

Byerly, G.R., Lower, D.R., Walsh, M.W., 1986. Stromatolites from the 3,300-3,500-Myr Swaziland Supergroup, Barberton Mountain Land, South Africa. Nature 319:489-491.

Condie, K.C., 1981. Archean Greenstone Belts. Elsevier Amsterdam, 434 p.

Condie, K.C., 2001. Mantle plumes and their record in Earth history. Cambridge University Press. 305 p.

Czaja, A.D., Johnson C.M., Roden, E.E., Beard, B.L., Voegelin A.R., Nagler, T.F., Beukes, N.J., Wille M., 2012. Evidence for free oxygen in the Neoarchean ocean based on coupled iron-molybdenum isotope fractionation. Geochimica et Cosmochimica Acta 86:118-137.

Cockell, C.S., 2000. Ultraviolet radiation and the photobiology of Earth's early oceans. Origin of Life and Evolution of the Biosphere 30:467-499.

Crowe, S.A., Dossing, L.N, Beukes, N.J., Bau, M., Kruger, S.J., Frei, R., Canfield, D.E., 2013. Atmospheric oxygenation three billion years ago. Nature 501:535-538.

Da Silva, J.J.R.F, Williams, R.J.P., 2001. The biological chemistry of the elements. New York, Oxford University Press, 575 p.

Dauphas, N., Van Zuilen, M., Wadhwa, M., Davis, A.M., Marty, B., Janney, P.E., 2004. Clues from Fe isotope variations on the origin of Early Archean BIFs from Greenland. Science 306:2077-2080.

Dauphas, N., Van Zuilen, M., Busigny, V., Lepland, A., Wadhwa, M., Janney, P.E., 2007. Iron isotope, major and trace element characterization of Early Archean

supracrustal rocks from SW Greenland: protolith identification and metamorphic overprint. Geochimica et Cosmochimica Acta 71:4745-4770.

De Ronde, C.E.J., Channer, D.M.D., Faure K., Bray, C.J., Spooner, E.T.C., 1997. Fluid chemistry of Archean seafloor hydrothermal vents: implications for the composition of circa. 3.2 Ga seawater. Geochimica et Cosmochimica Acta 61:4025-4042.

Dupont, C.l., Yang, S., Bourne, P.E., 2006. Proteomes contain putative imprints of ancient shifts in trace metal geochemistry. PNAS 103:17822-17827.

Dupont, C.L., Butcher, A., Valas, R.E., Bourne, P.E., Caetano-Anolles, G., 2010. History of biological metal utilization inferred through proteomic analysis of protein stuctures. PNAS 107:10567-10572.

Dutkiewicz, A., Ridley, J., Buick, R., 2003. Oil-bearing CO2-CH4-H2O fluid inclusions: oil survival since the Palaeoproterozoic after high temperature entrapment. Chemical Geology 194:51-79.

Dutkiewicz, A., Volk, H., George, S.C., Ridley, J., Buick, R., 2006. Biomarkers from Huronian oil-bearing fluid inclusions: an uncontaminated record of life before the Great Oxidation Event .Geology 34:437-440.

Dymek, R.F., Klein, C., 1988. Chemistry, petrology and origin of banded iron-formation lithologies from the 3800 Ma Isua Supracrustal Belt, West Greenland. Precambrian Research 39:247-302.

Edmond, J.M., Von Damm, K.L., McDuff, R.E., Measures, C.I., 1982. Chemistry of hot springs on the East Pacific Rise and their effluent dispersal. Nature 297:187-191.

Falkowski, P.G., 1997. Evolution of the nitrogen cycle and its influence on the biological sequestration of CO_2 in the ocean. Nature 387:272-275.

Farquhar, J., Bao, H., Thiemens, M., 2000. Atmospheric influence of Earth's earliest sulfur cycle. Science 289:756-758.

Farquhar, J., Wing, B.A., 2003. Multiple sulfur isotopes and the evolution of the atmosphere. Earth and Planetary Science Letters 213:1-13.

Fedo, C.M., Whitehouse, M.J., 2002. Metasomatic origin of quarz-pyroxene rock, Akilia, Greenland, and implications for Earth's earliest life. Science 296:1448-1452.

Froelich, P.N., Blanc, V., Mortlock, R.A., Chillrud, S.N., Dunstan, W., Udomkit, A., Peng, T-H., 1992. River fluxes of dissolved silica to the ocean were higher during glacials: Ge/Si in diatoms, rivers and oceans. Paleoceanography 7:739-767.

Grotzinger, J.P., Kasting, J.F., 1993. New constraints on Precambrian ocean composition. Geology 101:235-243.

Hamade, T., Konhauser, K.O., Raiswell, R., Goldsmight, S., Morris, R.C., 2003. Using Ge/Si ratios to decouple iron and silica fluxes in Precambrian banded iron formations. Geology 31:35-38.

Heubeck, C., 2009. An early ecosystem of Archean tidal microbial mats (Moodies Group, South Africa, ca. 3.2 Ga). Geology 37:931-934.

Hoffman, H.J., Grey, K., Hickmann, A.H., Thorpe, R.I., 1999. Origin of 3.45 Ga coniform stromatolites in Warrawoona Group, Western Australia. GSA Bulletin 111:1256-1262.

Holland, H.D., 1984. The chemical evolution of the atmosphere and oceans. Princeton NJ: Princeton Univesity Press. 582 p.

Holland, H.D., 2006. The oxygenation of the atmosphere and oceans. Transactions of the Royal Society B 361:903-915.

Jacobsen, S.B., Pimentel-Klose, M.R., 1988. A Nd isotopic study of the Hamersley and Michipictoten banded iron formations: the souce of REE and Fe in Archean oceans. Earth and Planetary Science Letters 87:29-44.

Jaun, B., Thauer, R.K., 2007. Methyl-coenzyme M reductase and its nickel corphin coenzyme F430 in methanogenic archaea. Metal Ions in Life Sciences 2:323-356.

Kasting, J.F., 1987. Theoretical constraints on oxygen and carbon dioxide concentrations in the Precambrian atmosphere. Precambrian Research 34:205-229.

Kasting, J.F., 1993. Earth's early atmosphere. Science 259:920-926.

Kasting, J.F., Pavlov, A.A., Sieffert, J.L., 2001. A coupled ecosystem-climate model for predicting the methane concentration in the Archean atmosphere. Origins of Life and Evolution of the Biosphere 31:271-285.

Kasting, J.F., Catling, D., 2003. Evolution of a habitable planet. Annual Review of Astronomy and Astrophysics 41:429-463.

Kasting, J.F., Howard, M.T., 2006. Atmospheric composition and climate on early Earth. Philosophical Transactions of the Royal Society B 361:1733-1742.

Klein, C., 2005. Some Precambrian banded iron formations (BIFs) from around the world: their age, geological setting, mineralogy, metamorphism, geochemistry, and origin. American Mineralogist 90:1473-1499.

Knauth, L.P., Lowe, D.R., 2003. High Archean climatic temperature inferred from oxygen isotope geochemistry of cherts in 3.5 Ga Swaziland Supergroup, South Africa. GSA Bulletin 115:566-580.

Knoll, A.H., 1979. Archean photoautotrophy: some alternatives and limits. Origins of Life 9:313-327.

Konhauser, K.O., Hamade, T., Raiswell, R., Morris, R.C., Ferris, F.G., Southam, G., Canfield, D.E., 2002. Could bacteria have formed the Precambrian banded iron formations? Geology 30:1079-1082.

Konhauser, K.O., Lalonde, S.V., Arnskold, L., Holland, H.D., 2007. Was there really an Archean Phosphate crisis? Science 315:1234.

Konhauser, K.O., Pecoits, E., Lalonde, S.V., Papineau, D., Nisbet, E.G., Barley, M.E., Arndt, N.T., Zahnle, K., Kamber, B.S., 2009. Nickel depletion and a methanogen famine before the Great Oxidation Event. Nature 458:750-753.

Konhauser, K.O., Lalonde, S.V., Planavsky, N.J., Pecoits, E., Lyons, T.W., Mojzsis, S.J., Rouxel, O.J., Barley, M.E., Rosière, C., Fralick, P.W., Kump, L.R., Bekker, A., 2011. Aerobic bacterial pyrite oxidation and acid rock drainage during the Great Oxidation Event. Nature 478:369-373.

Latifi, A., Ruiz, M., Zhang, C-C., 2009. Oxidative stress in cyanobacteria. FEMS Microbiology Reviews 33:258-278.

Lupton, J.E., 1995. Hydrothermal plumes: near and far field. *In*: Humphris, S.E., Zierenberg, R.A., Mullineau, L.S., Thomson, R.E Eds. Seafloor hydrothermal systems: Physical, chemical, biological, and geological interactions. Geophysical Monograph: 91. Washington, DC. American Geophysical Union, 317-346p.

Manning, C.E., Mojzsis, S.J., Harrison, T.M., 2006. Geology, age and origin of supracrustal rocks at Akilia,West Greenland. American Journal of Science 306:303-366.

Maliva, R.G., Knoll, A.H., Simmonson, B.M., 2005. Secular change in the Precambrian silica cycle: insights from chert petrology. GSA Bulletin 117:835-845.

Mallick, N. Cu-induced Oxidative stress in chlorophycean microalga Chlorella vulgaris. Journal of Plant Physiology 161:591-597.

Michard, A., 1986. The REE content of some hydrothermal fluids. Chemical Geology 55:51-60.

Mojzsis, S.J., Arrhenius, G., McKeegan, K.D., Harrison, T.M., Nutman, A.P., Friend, C.R.L., 1996. Evidence for life on Earth before 3,800 million years ago. Nature 387:55-59.

Morris, R.C., Horowitz, R.C., 1983. The origin of the iron-formation-rich Hamersley Group of Western Australia – deposition on a platform. Precambrian Research 21:273-297.

Mortlock, R.A., Froelich, P.N., Feely, R.A., Massoth ,G.J., Butterfield, D.A., Lutpon, J.E., 1993. Silica and germanium in Pacific Ocean hydrothermal vents and plumes. Earth and Planetary Science Letters 119:365-378.

Nisbet, E.G., Cheadle, M.J., Arndt, N.T., Bickle, M.J., 1993. Constraining the potential temperature of the Archean mantle: a review of the evidence from komatiites. Lithos 30:291-307.

Nisbet, E.G., Cann, J.R., Van Dover, L., 1995. Origin of Photosynthesis. Nature 373:479.

Ourisson, G., Rohmer, M., Porella, K., 1987. Prokaryotic hopanoids and other ploy terpenoid stero surrogates. Annual Reviews in Microbiology 41:301-333.

Partin, C.A., Bekker, A., Planavsky, N.J., Scott, C.T., Gill, B.C., Li, C., Podkoryrov, V., Maslov, A., Konhauser, K.O., Lalonde, S.V., Love, G.D., Poulton, S.W., Lyons, L.W., 2013. Large-scale fluctuations in Precambrian atmospheric and oceanic oxygen levels from the record of U in shales. Earth and Planetary Science Letters, 369-370:284-293.

Pavlov, A.A., Kasting, J.F., 2002. Mass-independent fractionation of sulfur isotopes in Archean sediments: strong evidence for an anoxic Archean atmosphere. Astrobiology 2: 27-41.

Pierson, B.K., Mitchell, H.K., Ruff-Roberts, A.L., 1993. Chloroflexus aurantiacus and ultraviolet radiation: implications for Archean shallow-water stromatolites. Origins of Life and Evolution of the Biosphere 23:243-260.

Phoenix, V.R., Konhauser, K.O., Adams, D.G., Bottrell S.H., 2001. Role of biominiralization as an ultraviolet shield: implications for Archean life. Geology 29:823-826.

Planavsky, N.J., Rouxel, O.J., Bekker, A., Lalonde, S.V., Konhauser, K.O., Reinhard, C.T., Lyons, T.W., 2010. The evolution of the marine phosphate reservoir. Nature 467:1088-1090.

Planavsky, N.J., Asael, D., Hofmann, A., Reinhard, C.T., Lalonde, S.V., Knudsen, A., Wang, X., Ossa Ossa, F., Pecoits, E., Smith, A.J.B., Beaukes, N.J., Bekker, A., Johnson, T.M, Konhauser, K.O., Lyons, T.W. & Rouxel, O.J. Evidence for oxygenic photosynthesis half a billion years before the great oxidation event. Nature Geoscience 7:283-286.

Rasmussen, B., Buick, R., 1999. Redox state of the Archean atmosphere: evidence from detrital heavy minerals in ca. 3250-2750 Ma sandstones from the Pilbara Craton, Australia. Geology 27:115-118.

Rastogi, R.P., Singh, S.P., Häder, D-P., Sinha, R.P., 2010. Detection of reactive oxygen species (ROS) by the oxidant-sensing probe 2', 7'-dichlorodihydrofluorecein diacetate in the cyanobacterium Anabaena variabilis PCC 7937. Biochemical and Biophysical Research Communications 397:603-607.

Robbins, L.J., Lalonde, S.V., Saito, M.A., Planavsky, N.J., Mloszewska, A.M., Pecoits, E., Scott, C., Dupont, C.L., Kappler, A., Konhauser, K.O., 2013. Authigenic iron oxide proxies for marine zinc over geological time and implications for eukaryotic metallome evolution. Geobiology 11:295-306.

Robert, F., Chaussidon, M., 2006. A paleotemperature curve for the Precambrian oceans based on silicon isotopes in cherts. Nature 443:969-972.

Rosing, M.T., 1999. 13C-depleted carbon microparticles in >3700 Ma sea floor sedimentary rocks from West Greenland. Science 283:674-676.

Roy, S., 1997. Genetic diversity of manganese deposition in the terrestrial geological record. Geological Society of London Special Publications 119:5-27.

Rye, R., Holland, H.D., 1998. Paleosols and the evolution of atmospheric oxygen: a critical review. American Journal of Science 298:621-672.

Saito, M.A., Sigman, D.M., Morel, F.M.M., 2003. The bioinorganic chemistry of the ancient ocean: the co-evolution of cyanobacterial metal requirements and biogeochemical cycles at the Archean-Proterozoic boundary? Inorganica Chimica Acta 356:308-318.

Segura, A., Krelove, K., Kasting, J.F., Sommerlatt, D., Meadows, V., Crisp, D., Cohen, M., Mlawer, E., 2003. Ozone concentrations and ultraviolet fluxes on Earth-like planets around other stars. Astrobiology 3:689-708.

Schopf, J.W., 1993. Microfossils of the early Archean Apex chert: new evidence of the antiquity of life. Science 26:640-646.

Schopf, J.W., 2000. The fossil record: tracing the roots of the cyanobacterial lineage. In: Whitton, B.A., Potts, M., Eds. The ecology of cyanobacteria: their diversity in time and space. Kluwer Academic, p.13 to 35.

Schopf, J.W., Kudryavtsev, A.B., Sugitani, K., Water, M.R., 2010. Precambrian microbe-like pseudofossils: a promising solution to the problem. Precambrian Research 179:191-205.

Siebert, C., Kramers, J.D., Meisel, T., Morel, P., Nägler, T.F., 2005. PGE, Re-Os, and Mo isotope systematics in Archean and early Proterozoic sedimentary systems as proxies for redox conditions of the early Earth. Geochimica et Cosmochimica Acta 69:1787-1801.

Siever, R., 1992. The silica cycle in the Precambrian. Geochimica et Cosmochimica Acta. 56:3265-3272.

Sinha, R.P., Häder, D-P., 2002. UV- induced DNA damage and repair: a review. Photochemical and Photobiological Science 1:225-236.

Shibuya, T., Komiya, T., Nakamura, K., Takai, K., Maruyama, S., 2010. Highly alkaline, high-temperature hydrothermal fluids in the early Archean ocean. Precambrian Research 182:230-238.

Sleep, N.H., Hessler, A.M., 2006. Weathering of quartz as an Archean climatic indicator. Earth and Planetary Science Letters 241:594-602.

Stoodley, P., Sauer, K., Davies, D.G., Costerton, J.W., 2002. Biofilms as complex differentiated communities. Annual Reviews in Microbiology 56:187-209.

Stueken, E.E., Catling, D.C., Buick, R., 2012. Contributions to late Archean sulphur cycling by life on land. Nature Geoscience. 5:722-725.

Summons, R.E., Jahnke, L.L., Hope, J.M.M., Logan, G.A., 2-Methylhopanoids as biomarkers for cyanobacterail oxygenic photosynthesis. Nature 400:554-557.

Summons, R.E., Bradley, A.S., Jahnke, L.L., Waldbauer, J.R., 2006. Steroids, triterpenoids and molecular oxygen. Philosophical Transactions of the Royal Society B 361:951-968.

Trendall, A.F., Blockley, J.G., 1970. The iron formations of the Hamersley Group, Western Australia with special references to the associated crocodilite. Western Australia Geological Survey Bulletin 119:353p.

Trandall, A.F., 2002. The significance of iron-formation in the Precambrian stratigraphic record. In: Altermann, W., Corcorane, P.L. Eds. Precambrian sedimentary environments: a modern approach to depositional systems. Internationa Association of Sedimentologists Special Publication 44:22-66.

Touati, D., 2000. Iron and oxidative stress in bacteria. Archives of biochemistry and biophysics 373:1-6.

Van den Boorne, S.H.J.M., Van Bergen, M.J., Nijman, W., Vroon, P.Z., 2007. Dual role of seawater and hydrothermal fluids in Early Archean chert formation: evidence from silicon isotopes. Geology 35:939-942.

Viollier E., Inglett, P.W., Roychoudhury, N., Van Cappellan, P., The ferrozine method revisited: Fe(II)/Fe(III) determination in natural waters. Applied Geochemistry 15:785-790.

Winterbourne, C.C., 1995. Toxicity of iron and hydrogen peroxide: the Fenton reaction. Toxicology letters. 82/83: 969-974.

Wille, M., Kramers, J.D., Nägler, T.F., Beukes, N.J., Shröder, S., Meisel, T., Lacassie, J.P., Voegelin, A.R., 2007. Evidence for a gradual rise of oxygen between 2.6 and 2.5 Ga from Mo isotopes and Re-PGE signatures in shales. Geochimica et Cosmochimica Acta. 71:2417-2435.

Zerkle, A.L., House, C.H., Brantley, S.L., 2005. Biogeochemical signatures through time as inferred from whole microbial genomes. Americal Journal of Science 306:467-502.

Chapter 2. A detailed geochemical and petrographic study of banded iron formations from the ≥3.75 Ga Nuvvuagittuq Supracrustal Belt (northern Québec) and their use as a proxy for Eoarchean seawater composition.

2.1 Introduction

Banded iron formations (BIF) are iron- and silica-rich marine, chemical sedimentary precipitates that were deposited with some hiatuses throughout the Archean and much of the Proterozoic. Because the precursor minerals of these rocks precipitated directly out of seawater, the primary ferric-oxyhydroxide minerals that comprised the initial sediments retained chemical signatures of the seawater. In this regard, BIF compositions have long been used as proxies for the compositional evolution of seawater over time (e.g., Bau and Dulski, 1996; Bolhar et al., 2004; Jacobsen and Pimentel-Klose, 1988), and ultimately for the types of nutrients that were available to ancient planktonic life (e.g., Bjerrum and Canfield, 2002; Konhauser et al., 2009). For instance, based on documented P:Fe ratios in 3.2 to 1.9 Ga BIF, Bjerrum and Canfield (2002) proposed that the Archean-Paleoproterozoic oceans may have been phosphate limited. This condition could have hindered initial cyanobacterial phytoplanktonic growth, and consequently delayed the rise of oxygen until the demise of Fe(II)-rich marine waters that accompanied the decline of BIF deposition

in the Paleoproterozoic. Konhauser et al., (2009) used Ni/Fe ratios to infer a trace metal crisis starting at around 2.7 Ga for methanogenic bacteria, and proposed that the subsequent decline of methanogens aided in the rise of atmospheric oxygen. It is noteworthy that the metabolic trace metal requirements of ancient microbes could have been established by their bioavailability in the ancient oceans, and that a record of this is preserved in the genomes of their modern descendants (Da Silva and Williams, 1991; Saito et al., 2003).

Although banded iron formations formed throughout much of the Precambrian, the paucity of pre-3.6 Ga supracrustal rocks severely hampers the use of BIF for discerning compositional changes in Earth's earliest oceans and hence of the nature of habitats for putative early life forms. By far the most intensely studied Eoarchean BIF are from the Isua Supracrustal Belt, as well as various BIF enclaves (termed the Akilia association) scattered throughout the ca. 3000 km^2 Itsaq Gneiss Complex in West Greenland (Nutman et al., 1996). Much of the published work from these complex BIF has focused on describing (and debating) their origins (e.g., Cates and Mojzsis, 2006; Dauphas et al., 2004; Dauphas et al., 2007b; Dymek and Klein, 1988; Frei and Polat, 2007; Manning et al., 2006; Polat and Frei, 2005; Whitehouse and Fedo, 2007). The recent discovery of well-preserved, banded quartz-magnetite units of BIF protolith, and another composed of banded quartz and Fe-silicate minerals (hereafter termed BSF), in the Nuvvuagittuq Supracrustal Belt in Northern Québec provides an excellent opportunity to study the early oceans especially in the context of global environmental conditions which led to BIF

sedimentation. The belt is at least 3.75 Ga in age, and perhaps as old as 4.28 Ga (cf. Cates and Mojzsis, 2007, 2009; O'Neil et al., 2008, 2011 - see section 2.2).

While research on the Nuvvuagittuq rocks is still in its infancy, preliminary chemical and isotopic work has conclusively shown that the BIF, and a representative portion of the BSF, possess many distinguishing characteristics of rocks of chemical sedimentary protolith (Cates and Mojzsis, 2007; Dauphas et al., 2007a,b; O'Neil et al., 2007). Bulk chemical analyses further indicate that these rocks retain seawater-like rare earth element and yttrium (REE+Y) signatures such as concave-upward profiles, positive La and Eu anomalies and superchondritic Y/Ho ratios (Bolhar et al.. 2004; Cates and Mojzsis, 2007; Dauphas et al., 2007a; O'Neil et al., 2007).

A currently acknowledged possibility for the origins of the Fe-oxide layers in BIF is that they were a by-product of microbial metabolism (Konhauser et al., 2002). Dauphas et al., (2007a) pointed out that the relatively heavy Fe-isotope compositions of Nuvvuagittuq ferruginous quartz -amphibole rocks of chemical sedimentary protolith can be most simply explained by a microbial oxygenic or anoxygenic photosynthetic origin. If correct, this underscores the notion that microbial life was already established at the beginning of the sedimentary rock record. Hence, any reliable means to estimate concentrations of solutes in pre-3.6 Ga seawater would reveal new insights into the nutrient status of the oceans from which key microbial metallo-enzymes first evolved. BIF compositions also potentially provide a measure of the balance that both mantle and surface processes had on seawater composition

through time (e.g., Isley, 1995), and it is well established that seawater composition as reflected in BIF is influenced by both hydrothermal, and in many cases, terrestrial inputs (Bau, 1993; Bolhar et al., 2004).

In this study, we performed detailed geochemical mapping of candidate Nuvvuagittuq chemical sediments (BIF, BSF) that integrated the petrologic and geochemical relationships between mineral phases in thin section and whole-rock chemistry to provide a framework for interpreting their bulk and microscale variations. These data were used to construct a model of seawater compositions in the Nuvvuagittuq basin as a first-order constraint on the geochemical evolution of seawater on the post-bombardment Earth.

2.2 Geological Setting

The geology of the Nuvvuagittuq belt and surrounding gneisses has been reviewed elsewhere (Boily et al., 2009; Cates and Mojzsis, 2007, 2009; David et al., 2009; O'Neil et al., 2007; Stevenson et al., 2006), and hence, only a brief synopsis is provided here. Tonalite gneisses immediately surrounding the belt are dated at ca. 3.66 Ga (David et al., 2009). Zircons recovered from trondhjemitic gneisses within the mostly mafic Nuvvuagittuq succession provide $^{207}Pb/^{206}Pb$ ages of 3751± 10 Ma (Cates and Mojzsis, 2007), and a similar age of 3817±16 Ma was obtained from zircons from the same unit (David et al., 2009), which establishes that the belt is at least Eoarchean in age. Also, intruding gabbros give a ^{147}Sm-^{143}Nd isochron age of

4023± 110 Ma, while cummingtonite-rich amphibolites provide ^{146}Sm-^{142}Nd vs. ^{147}Sm-^{143}Nd isochron age of 4280±$^{53}_{81}$ Ma (O'Neil et al., 2008).

Subsequent to re-working in the Eo- and Mesoarchean, the terrane was intruded by Neoarchean, εNd depleted TTG (tonalite-trondhjemit-granodiorite) and GGM (granite-granodiorite-monazite) suites (where the εNd notation defines the departure of ^{143}Nd/^{144}Nd from the Chondrite Uniform Reservoir evolution line), as well as by mafic to felsic volcanic suites with enriched εNd signatures thought to have been derived from the recycling of Mesoarchean crust (Boily et al., 2009). The Nuvvuagittuq belt is an isoclinal, north-plunging synform that has been refolded into a more open, south-plunging antiform (Figure 2.1; David et al., 2009; O'Neil et al., 2007, 2011). It has undergone extensive retrograde metamorphism from (upper-amphibolite/lower granulite to greenschist facies) and thermobarometry experiments by Cates and Mojzsis (2009) suggest that metamorphic temperatures were as high as ~640°C. At least three major metamorphic events are recorded through U-Pb zircon dating methods at ca. 3.6 Ga, 3.3 Ga and 2.7 Ga; the latest event is thought to be related to the juxtaposition of the Hudson Bay and Arnaud River terranes (Cates and Mojzsis, 2009; David et al., 2009).

In the broadest of terms, the Nuvvuagittuq belt can be divided up into three main units: (1) a CaO-poor (cummingtonite-rich) amphibolite previously referred to as the "faux-amphibolite" (O'Neil et al., 2007, 2008) because of its lack of

hornblende as in more common amphibolitized basalts, and now referred to as the Ujaraaluk unit by O'Neil et al., (2011); (2) gabbroic and ultramafic conformable bodies interpreted by O'Neil et al., (2007, 2008, 2011) as sills (cf. Cates and Mojzsis, 2007); and (3) rocks of likely chemical sedimentary protolith, including banded iron formation (Figure 2.1). The amphibolite unit is the most voluminous of the three main rock types. It has a generally basaltic to andesitic composition and locally preserves millimetre- to meter-scale compositional layering, and has been interpreted to be an altered mafic volcanic pyroclastic deposit (O'Neil et al., 2011). The progression from chlorite-epidote-bearing rocks and garnet-free cummingtonite amphibolites in the western portion of the belt, to garnet-bearing cummingtonite amphibolites in the east suggests a map-scale metamorphic gradient from upper-greenschist-facies in the west to upper-amphibolite facies in the east (O'Neil et al., 2007).

The amphibolite unit can be divided into three stratigraphically superimposed, geochemically distinct groups (O'Neil et al., 2011) with the iron formation units positioned between two of these groups. The group stratigraphically below these units has high Ti content, low Al/Ti ratios and relatively flat REE profiles, whereas the two groups above are characterized by low Ti contents and higher Al/Ti ratios. The group directly above has the highest Al/Ti ratios and displays distinct U-shape REE profiles with low Ta and Nb. The group at top of the sequence also has large negative Ta and Nb anomalies, but is characterized by enriched LREE profiles. The transition

between low Al/high Ti amphibolites to the high Al/low Ti amphibolites is interpreted by O'Neil et al., (2011) to represent a transition from rocks resembling those of oceanic tholeiites to rocks sharing chemical features typically observed in a volcanic island arc setting. Regardless of tectonic setting, the iron formation units occur stratigraphically at the transition between the geochemically distinct amphibolites.

The 5-30 meter wide BIF is composed of alternating bands of magnetite and grunerite with variable amounts of, locally, finely layered quartz (0.1-0.3cm), which outcrops continuously along the western limb of the synform and discontinuously along the eastern limb (Figure 2.1). Positioned ~50 m up section from this unit is a fine- to coarsely-banded unit (0.1-1 cm) of alternating Fe-Ca-Mg silicate (grunerite, actinolite and pyroxene) and quartz bands (Figure 2.1). It can be traced continuously down the western limb of the fold and discontinuously around to the southern tip of the belt. This unit grades into a 100 m-wide cherty unit composed of recrystallized quartz with minor amounts of disseminated pyrite, on the western limb of the fold (O'Neil et al., 2007). The repetitive sequence of these units on either limb of the fold suggests that some of the original volcano-sedimentary succession of the belt has been preserved despite numerous post-depositional disturbances.

2.3 Methods

Polished thin sections of samples were prepared and used for reflected and transmitted light microscopy in order to establish the mineralogy and petrology. Nine representative samples of the BIF and BSF were selected for bulk trace element analysis; rocks were broken and sub-sampled to avoid secondary veining and strongly recrystallized areas. Samples were crushed in a tungsten-carbide mill and the rock powder submitted for bulk XRF and ICP-MS analysis on a PerkinElmer Elan6000 quadrupole inductively coupled plasma mass spectrometer (Quad-ICP-MS) at the University of Alberta (Edmonton, Canada). Mineral-phase chemistry of major (K, Na, Si, Fe, P, Mg, Al, Mn) and trace elements was determined and backscattered-electron images as well as elemental maps produced on the University of Alberta's JEOL 900 electron microprobe. Analytical conditions used on the electron microprobe were: beam diameter (3 μm); voltage (20 kV); current (20 nA); and concentrations were calculated using ZAF matrix correction. Mineral-phase trace element chemistry was analyzed using a Quad-ICP-MS coupled to a laser ablation system with the following analytical conditions: PR power (1200 W); peak hopping acquisition (50 ms dwell time); spot diameter (between 60 μm and 100 μm depending on grain size); repetition rate (5 Hz); and energy density (~13 J/cm^2). The international glass standard NIST SRM 610 was used to calibrate the instrument and Fe concentrations from the electron microprobe was used as an internal standard for each analysis. GLITTER© (XP version, New Wave Research) software were used for data reduction. Bulk XRF analyses were carried out at Activation Laboratories Ltd. (Ancaster, Ontario).

2.4 Results

2.4.1 Petrography and mineral chemistry

Rocks of chemical sedimentary protolith in the Nuvvuagittuq belt preserve an upper amphibolite (locally to lower granulite facies) metamorphic assemblages, are coarsely crystalline and are well-banded where silica mobility did not result in complete recrystallization. The BSF consists of fine to coarse (>0.1 mm-wide) bands of quartz which alternate with bands consisting of grunerite [$(Fe,Mg)_7(Si,Al)_8O_{22}$], augite [$Ca(Fe,Mg)(Si,Al)_2O_6$], and actinolite[$(Ca,Na,Mn)_2(Fe,Mg)_5(Si,Al)_8O_{22}$] (Figure 2.2A). Actinolite, which was only observed in the BSF, typically occurs as lamellae within a grunerite host. Magnetite (Fe_3O_4) is scattered throughout these Fe-bearing silicate layers, while calcite, pyrite and anorthite (in one sample only, 090709-3) occur as accessory phases (together making up <2 modal % of the rock). The BIF ranges from fine (<300 μm to 0.3 cm-thick) alternating bands of quartz, magnetite and grunerite (<70 μm-wide), to the more common assemblage of fine, alternating bands of grunerite and magnetite with quartz and augite scattered throughout (Figure 2.2B,C). The occurrence of pyroxene in these samples corroborates with observations in previously published work on the Nuvvuagittuq chemical sediments (Cates and Mojzsis, 2007; Dauphas et al., 2007a; David et al., 2009). A summary of mineral grain geochemical analyses are presented in Table 2.1, and full analyses are available in Appendix A.

Magnetite

Magnetite is the only Fe-oxide mineral component of the Nuvvuagittuq chemical sediments, occurring as a dominant constituent of the BIF (<40 modal %) and as a minor constituent of the BSF (<10 modal %). In both units, magnetite occurs as anhedral to subhedral grains typically between 50 and 200 μm in size. Magnetite in the BSF occurs as individual grains typically associated with the grunerite, and are found both in grain-boundary contact with and as inclusions in grains of grunerite, quartz and augite (Figure 2.2A,D). In contrast, magnetite in the BIF comprises defined Fe-oxide bands that range in size from 250 μm to 0.3 cm thick, occurring both as individual grains and as large aggregates. Smaller individual magnetite grains are typically found as inclusions within grains of grunerite, quartz and clinopyroxene (Figure 2.2E).

Chemical analyses of magnetite in both BIF and BSF show that they are overwhelmingly iron-rich (FeO_{total} 93-94 wt%) with BIF magnetite slightly more Al and Si-rich (Al_2O_3 0.5 wt% and SiO_2 0.2 wt.% vs. <0.1 wt.%). In BSF magnetite, Cr, Ni and V occur in the highest concentrations of all the trace elements while in BIF magnetite Ni and Zn occur in the highest concentrations, and average concentrations of all other trace elements are below 35 ppm. For most trace metals BIF magnetite is also enriched compared to BSF magnetite (Table 2.1, Figures 2.3A,B).

Quartz

Quartz makes up to 60 modal% of the BSF and 20-60 modal% of the BIF (Figure 2.2A-C). Quartz in the BSF occurs as bands and as individual grains within grunerite bands, and is often found as inclusions within grains of grunerite and clinopyroxene. Much of the quartz has a granoblastic-texture, suggestive of static recrystallization. In some BSF samples the quartz is large and has an anhedral habit, extending to over 0.5 cm in size. This larger quartz component shows signs of deformation such as the presence of subgrains, undulose extinction and sutured grain margins. In most of the BIF samples, quartz occurs as individual, 50 to 300 μm-large anhedral to euhedral grains as well as granoblastic-textured aggregates within the grunerite and magnetite bands; aggregates commonly grade into individual grains along a particular band, and some aggregates cross-cut the banding. In one BIF sample (090709-5), quartz makes up regular, 0.5 mm to 2 mm wide, granoblastic-textured bands alternating with the magnetite bands.

Major element composition for quartz is ~100 wt% SiO_2. The average trace element composition of BSF quartz is below 35 ppm. In BIF quartz, only Zn occurs at concentrations >36 ppm. Similar to the magnetite, BIF quartz is higher in most trace elements than the BSF quartz (Table 2.1; Figure 2.3C,D).

Grunerite

Grunerite in the BSF is composed of <0.3cm-wide bands that alternate with quartz bands, and occurs as anhedral to subhedral grains. Grunerite grains are hosts to

lamellae of actinolite, a feature not observed in the BIF (Figure 2.2F). In the BIF, grunerite tends to be noticeably larger in size, varying from 50μm to at least 2 cm in length, often making up the whole grunerite band along the length of the thin section. Magnetite, quartz and augite grains can be found as inclusions within the grunerite (Figure 2.2C, E). In BIF sample 090709-5, bands of magnetite and quartz alternate with thin (<70μm-wide) bands of grunerite, however the inconsistent distribution of these bands between the magnetite and quartz banding might suggest that this is a primary texture (Figure 2.2B).

Major element analyses for grunerite show SiO_2 of 50-52 wt%. BIF grunerite has higher average FeO_{total} than BSF grunerite (47 wt% compared to 30 wt%), while average MgO is lower in the BIF grunerite (5 wt% compared to 13 wt%). Of all the trace elements, grunerite has the highest Zn and Ni concentrations while all other trace elements have concentrations below 35 ppm. In contrast to magnetite and quartz, BSF grunerite has higher average trace element concentrations than BIF grunerite (Table 2.1; Figures 2.3E,F).

Augite

Augite in the BSF is associated with the grunerite bands, while in the BIF, it is associated with both grunerite and magnetite bands. In both units, it occurs as individual, 20 to 150 μm large, anhedral to subhedral grains, commonly with

inclusions of quartz and magnetite, and can also be found as an inclusion in grunerite (Figure 2.2C). Within a single crystal, bands of different interference colors under polarized light points to compositional zoning; exsolved lamellae of orthopyroxene are reportedly common in calcic clinopyroxenes (Deer et al., 1992).

Major element analyses for augite show SiO_2 around 51 wt% and CaO between 21 and 23 wt%. FeO_{total} for BIF augite if higher than for BSF augite (21 wt% compared to 12 wt%), while MgO is slightly lower in the BIF augite (7 wt% compared to 11 wt%). Trace element analyses show that BSF augite is significantly more enriched in Sc, V, Ni, Co and Zn than in the BIF augite where Sr and Y occur in higher concentrations (Table 2.1; Figures 2.3G,H**)**. The augite in sample 090709-3 is especially high in Cr compared to augite in the other BSF samples (500 ppm compared to below detection limit).

Actinolite

Actinolite was only observed in the BSF, but is also mentioned in previous publications on the Nuvvuagittuq chemical sediments as a minor component of the BIF unit (e.g., O'Neil et al., 2007). Actinolite is associated with the grunerite bands of the BSF, and occurs most commonly as lamellae within a grunerite host. They can also be found as anhedral to subhedral, >50μm-large grains (Figure 2.2F).

Major element analyses of actinolite show average compositions of SiO_2 at ~ 53 wt%; FeO_{total} at ~ 20 wt%; CaO at ~13 wt%, and MgO at 12 wt%. In terms of the trace elements, actinolite contains high Zn (198 ppm), Ni (66 ppm) and Cr (47 ppm,)

while the average composition of most other trace elements is below 37 ppm (Figure 2.3I).

2.4.2 BSF whole rock geochemistry

The BSF is characterized by high, but variable, concentrations of SiO_2 (28-90 wt%), $Fe_2O_{3\ total}$ (2-55 wt%), MgO (2-12 wt.%) and CaO (3-16 wt.%) while all other oxides occur in concentrations below 2 wt% (Figure 2.4A, Appendix B). The concentrations tend to vary from sample to sample depending on the relative percentage of each mineral phase; sample 090709-3 has the highest Si, Al, and Ti concentrations and the lowest Fe concentrations. Ni, Cu and Zn vary greatly from sample to sample, sometimes by up to three orders of magnitude (Figure 5A). All the BSF samples are highest in Ni and Zn compared to the other trace elements. Sample 090710-13 is significantly higher in Cu and S compared to the other samples suggesting the presence of sulphide grains, and has the highest concentrations of incompatible elements. The other samples have concentrations of Hf and Th <0.5 ppm, Zr <3 ppm, and Y <5 ppm. The remainder of the trace elements generally have concentrations <35 ppm. Bulk Post Archean Average Shale composite (PAAS - Taylor and McLennan, 1985) normalized REE+Y profiles for the BSF show; (i) positive La/La* anomalies (2.31±1) (Figure 2.7A); (ii) strong positive Eu/Eu* anomalies (1.84±0.16) (Figure 7B); (iii) superchondritic Y/Ho ratios (37.40±6.83); (iv) depleted LREE relative to HREE (Pr/Yb_{sn}: 0.30±0.19), and (v) MREE relative to HREE (La_{sn}/Yb_{sn}: 0.70±0.23). With the exception to Eu and Ce anomalies, the overall REE+Y profile is

similar to that of modern-day seawater (Figure 2.6A; e.g., Bolhar et al., 2004). Sample 090710-13 has the highest REE+Y concentrations of all the samples and the flattest overall profile.

2.4.3 BIF whole rock geochemistry

The BIF is characterized by high, variable concentrations of SiO_2 (33-63 wt%) and Fe_2O_{3total} (32-66 wt%), while the other major element oxides occur in concentrations <3 wt% (Figure 2.4B, Supplementary Data). Only P is slightly higher in the BIF (0.01-0.09 wt%) when compared to the BSF. Sample 090710-12 has the highest SiO_2 and lowest Fe_2O_3 concentrations of all the BSF samples; the simultaneously high Cu and S concentrations suggest a contribution by sulphide minerals to the composition of this sample (Appendix B). Similar to the BSF, Ni and Zn have the highest concentrations for transition metals in the BIF, while all others are <15 ppm (Figure 2.5B). In terms of incompatible elements, Hf and Th have average concentrations of 0.3 ppm; Zr has slightly higher average concentrations of 2 ppm, while Y is even higher at 9 ppm. The shale-normalized REE+Y profile is characterized by; (i) positive La/La* anomalies (1.73±0.34) (Figure 2.7A); (ii) strong positive Eu/Eu* anomalies (2.21±0.44) (Figure 2.7B); (iii) superchondritic Y/Ho ratios (33.82±2) (Figure 2.7C); and (iv)depleted LREE relative to HREE (Pr/Yb_{sn}: 0.16±0.17) and MREE relative to HREE (La_{sn}/Yb_{sn}: 0.47±0.27). The overall REE+Y profiles, which resemble ones from BIF analysed by O'Neil et al., (2007), are similar to that of modern-day seawater (Figure 2.6B), with the exception of Eu and Ce anomalies (e.g.

Bolhar et al., 2004). Sample 090710-12 has the highest REE+Y abundances of all the samples, and the flattest overall profile.

2.5 Discussion

2.5.1 Paragenesis

In order to infer the initial mineralogy of the Nuvvuagittuq BSF and BIF units, it is necessary to assess the metamorphic modifications that took place and establish the different stages of mineral genesis. The mineral assemblages in both units (i.e. magnetite, grunerite, actinolite, augite and quartz) are typical of an upper amphibolite/lower granulite facies assemblage for banded iron formation (e.g., Klein, 2005); these minerals are similarly well-represented in the quartz-magnetite BIF of the Isua Supracrustal Belt (Dymek and Klein, 1988). Despite the multiphase metamorphic history of the Nuvvuagittuq belt (Cates and Mojzsis, 2009), petrographic evidence leads us to infer that the precursors of the BSF and BIF units consisted of ferric oxyhydroxides, amorphous carbonate and silicate phases rich in Ca-Mg-Fe and amorphous silica. There was an insignificant clastic component.

Magnetite in BIF is generally thought to be a secondary product of diagenetic/metamorphic alteration of certain pre-existing Fe-rich mineral phases (Ayres, 1972). In the Nuvvuagittuq BSF and BIF, magnetite is the only Fe-oxide mineral present in either unit. It can commonly be found as inclusions within all the other mineral phase types suggesting that, of the current mineral phases, it was

formed first. Magnetite can be the metamorphic by-product of hematite and siderite, at temperatures ranging from 480°C to 650°C and pressures of 5-12 kbars according to the following equation (Koziol, 2004):

$$3FeCO_{3(siderite)} + Fe_2O_{3(hematite)} \rightarrow Fe_3O_{4(magnetite)} + CO_2$$

The metamorphic grade of the Nuvvuagittuq belt would have been sufficient for this reaction to take place (Cates and Mojzsis, 2009). Ohmoto (2003) suggested that magnetite can also be formed through the reaction between pre-existing hematite and Fe(II)-rich hydrothermal fluids at <200°C, resulting in the massive transformation of hematite to magnetite. However this scenario seems unlikely in this case, due to the lack of evidence for the supergene enrichment which would likely accompany such a flux of hydrothermal fluids. The production of biogenic magnetite *via* the reduction of ferric oxyhydroxides through dissimilatory iron reduction (DIR; Lovley, 1993) is also an unlikely source for the magnetite in the Nuvvuagittuq chemical sediments. Whereas DIR typically produces magnetite with $\delta^{56}Fe<0‰$ (Johnson et al., 2008), the heavy Fe isotope composition (up to 0.97‰ – Dauphas et al., 2007a; O'Neil et al., 2007) of these sediments led Dauphas et al., (2007a) to suggest that this signature was a product of the binary mixing between more primary Fe-oxides and carbonate deposits. It seems likely therefore, that the magnetite in these chemical sediments formed as a metamorphic by-product of hematite and siderite.

Quartz in iron formations is generally thought to be the stable end product of an initially amorphous silica precipitate that was recrystallized to chert and then to

quartz at greenschist-facies conditions, as denoted by the 120° triple junctions that characterize the granoblastic texture of the quartz (Klein, 2005; Trendall and Morris, 1983; Young, 1976). In the BSF and BIF units of the Nuvvuagittuq belt, quartz can be found as inclusions within grunerite and actinolite, while magnetite can be found as inclusions within the quartz, suggesting that the latter was the second phase, after magnetite, to crystallize.

Metamorphic Fe-bearing silicate minerals are commonly thought of as the products of metamorphic dehydration of pre-existing silicate and carbonate phases (Mel'nik, 1982). Grunerite can be produced in the reaction between quartz and siderite or the conversion from minnesotaite (Klein, 2005; Trendall and Morris, 1983):

$$8(Fe, Mg)CO_{3\ (siderte)} + 8SiO_{2\ (quartz)} + H_2O \rightarrow (Fe,Mg)_7Si_8O_{22}(OH)_{2\ (grunerite)} + 7CO_2$$

or

$$7Fe_2Si_4O_{10}(OH)_{2\ (minnesotaite)} \rightarrow 3Fe_7Si_8O_{22}(OH)_{2\ (grunerite)} + 4SiO_{2\ (quartz)} + 4SiO_2 + 4H_2O$$

The occurrence of actinolite as exsolution lamellae in grunerite is thought to be a result of selective crystallization from a homogeneous amphibole as a consequence of slow-cooling from amphibolite-facies peak metamorphic temperature (Ross et al., 1969). Clinopyroxene is a characteristic granulite-facies mineral, and

occurs in BIF due to the decarbonation reaction between ankerite and quartz according to the following reaction (Klein, 2005):

$$Ca(Fe,Mg)(CO_3)_{2(ankerite)} + SiO_{2(quartz)} \rightarrow Ca(Fe,Mg)Si_2O_{6(clinopyroxene)} + 2CO_2$$

That augite as well as actinolite is present in Nuvvuagittuq chemical sediments suggests that some of the primary precipitates were Ca-bearing. Indeed, Dauphas et al. (2007a) concluded that in order to produce the range of Fe isotope compositions in the Nuvvuagittuq chemical sediments, binary mixing between Fe-oxides and some type of carbonate precursor was necessary. The precursors to the Fe-carbonates in most BIF are considered to have been very fine-grained carbonate oozes (Klein, 2005), however, the possibility that the source of Ca and Mg in the Nuvvuagittuq chemical sediments came from a Ca-Mg-Fe bearing silicate precursor cannot be ruled out.

2.5.2 Geochemistry

The composition of Archean chemical sediments ought to reflect input of solutes from both crustal weathering and hydrothermal emissions. Detrital input can also occur in shallow water facies iron formations, and such clastic particles tend to obscure the seawater signal.

Identification of a detrital component in BIF was done mainly through elevated concentrations of Al_2O_3, TiO_2 and high field strength elements - HFSE (e.g.,

Zr, Hf, Ta, Th) as well as through co-variations between HFSE and REE+Y ratios (La/La*, Y/Ho, Pr/Yb, Ce/Ce* - Bau, 1993; Bolhar et al., 2004; Ewers and Morris, 1981; McLennan et al., 1993). Despite being sandwiched in between high-Ti amphibolites below, and high-Al amphibolites above, both BIF and BSF units have low absolute Al and Ti concentrations (Al_2O_3: generally <0.5 wt%; TiO_2: <0.03 wt%). Concentrations of both REE+Y and HFSE are low in iron formations because dissolved REE+Y in the water column are normally scavenged by particulate matter before being adsorbed by Fe and Si gels on the seafloor, and input from a detrital source would commonly generate co-variations between HFSE and REE+Y in BIF (Bau, 1993). With the exception of samples 090710-13 (BSF) and 090710-12 (BIF), low concentrations of Zr, Hf, Ta and Th (<2.5 ppm) in the Nuvvuagittuq chemical sediments suggest little to no detrital input (Figure 2.7C,D; Appendix B). The two aforementioned samples have slightly higher Zr, Hf, Ta and Th concentrations, low Y/Ho ratios and flatter REE+Y profiles (Figure 2.6). However, even these concentrations are relatively low when compared to BIF with a recognized detrital component (e.g., Dales Gorge BIF).

The REE+Y profile of modern seawater is distinctive; the purest BIF and marine carbonates share certain seawater-like characteristics including (i) positive La and Eu anomalies; (ii) negative Ce anomalies (except for Eoarchean BIF); (iii) a relative depletion of LREE and MREE compared to HREE, and (iv) superchondritic Y/Ho ratios (i.e., >26) (Bau and Dulski, 1996; Bolhar et al., 2004). The reasons why these chemical sediments retain seawater-like REE+Y patterns is poorly understood,

but the similarity of REE+Y profiles in BIF units spanning the Mesoarchean (Alexander et al., 2008) through the Proterozoic (e.g., Derry and Jacobsen, 1990 and references therein) demonstrates that reflect the seawater from which they precipitated. Apart from the negative Ce anomaly, all the aforementioned seawater-like anomalies are observed in the REE+Y profiles for both the Nuvvuagittuq BSF and BIF. In oxic seawater, soluble Ce(III) is converted to insoluble Ce(IV) and thus, the lack of Ce anomalies in Archean BIF has been used to infer prevailing anoxic conditions (e.g. Derry and Jacobsen, 1990; Kato et al., 1998). Although superchondritic Y/Ho ratios are a characteristic shared by both Archean BIF and modern ferromanganese crusts, shale-normalized Y anomalies are positive in the former and negative in the latter. It has been suggested that this could be related to the rate of deposition of ferric-oxyhydroxide particles (e.g., Bau and Dulski, 1996). The REE+Y in BIF are fairly immobile even at amphibolite facies metamorphism, and their mobility depends on high water/rock ratios (w/r > 100) which are seldom achieved (Bau, 1991; Grauch, 1989). Of all the REE+Y, Eu is especially mobile due to the larger difference between its ionic radius and that of Fe^{2+}. Negative Eu anomalies, or inconsistent positive and negative Eu anomalies between samples, occur (Bau, 1993). The consistently positive Eu in all Nuvvuagittuq bulk samples suggests that there has been little REE+Y mobility.

It is possible to put a few constraints on the sources of REE+Y in the Nuvvuagittuq BSF and BIF. First, the strong positive Eu anomalies are distinctive of high-temperature (>350°C) hydrothermal fluids. A conservative, two component

mixing model between modern seawater and high-temperature hydrothermal fluids using Sm/Yb as a function of Eu/Sm implies that, like in the Isua BIF, a surprisingly small proportion of high-temperature hydrothermal fluids (< 0.1%) were enough to cause such high Eu anomalies in the Nuvvuagittuq BSF and BIF (Figure 2.8). Second, the Sm/Yb ratios of samples 0907010-13 (BSF), 090709-3 (BSF) and 090710-12 (BIF) are higher than the others and also display a subsequent decrease in Eu/Sm (Figure 2.8), a signature which can be produced upon the addition of clastic material (e.g., Bau, 1993). No BIF is completely devoid of some detrital component, and although these samples also have the highest Zr, Hf, Ta, Th and REE+Y concentrations of all the samples, they still have seawater-like La/La* and Eu/Eu* anomalies, and no Ce/Ce* anomalies (Figure 2.7A,B) which indicates that detrital inputs were minimal during chemical precipitation and the BSF and BIF units of the Nuvvuagittuq belt are relatively pure chemical sediments.

2.5.3 Comparing the Nuvvuagittuq Chemical Sediments with the Isua iron formations

Few Eoarchean-aged BIFs are known, and the recent discovery of the Nuvvuagittuq chemical sediments permits comparisons to be made with BIF from the Itsaq Gneiss Complex in West Greenland. Previous studies established that the chemical sediments from the Isua and Nuvvuagittuq belts have heavy δ^{56}Fe values (0.31-1.1 and 0.37-0.97‰, respectively), and these compositions are most parsimoniously explained through the partial oxidation of Fe via oxygenic or anoxygenic photosynthetic pathways (Dauphas et al., 2007a,b). These chemical sediments hold

important implications for preserving not only the composition of Earth's earliest oceans, but also evidence of the earliest potential biosignatures.

From the perspective of mineralogy and metamorphic histories the amphibolite-facies Isua BIF and the upper-amphibolite/lower granulite facies Nuvvuagittuq chemical sediments show similarities in terms of relative trace element abundances, where Zn and Ni occur in the highest concentrations. Regarding absolute abundances however, Ni (Nuvvuagittuq median: 57 ppm; Isua median: 24 ppm) and Zn (Nuvvuagittuq median: 50 ppm; Isua median: 21 ppm) occur in slightly higher concentrations in the former (Appel, 1979; Bolhar et al., 2004; Dymek and Klein, 1988; Frei and Polat, 2007, Polat and Frei, 2005; Shimizu et al., 1990). Detrital indicators (Al_2O_3, TiO_2, HFSE) at both locations are low, which suggests that both locations are relatively detritus free. Their REE+Y profiles show seawater-like anomalies with a relative depletion in LREE compared to MREE and HREE, consistently positive La and Eu anomalies, negative Y/Ho ratios, and overall, similar REE+Y concentrations (e.g., Dymek and Klein, 1988; Bolhar et al., 2004). Moreover, ratios of Sm/Yb and Eu/Sm suggest that both the Isua and Nuvvuagittuq chemical sediments had similar contributions (~0.1%) by high-temperature hydrothermal sources (Figure 2.8; Alexander et al., 2008). The similarities in the characteristics of the iron formations at Isua and Nuvvuagittuq suggests that they were deposited under comparable environmental conditions, input sources and *via* the

similar processes. This is the expected result for rocks of similar age and overall depositional setting.

2.5.4 Implications for the composition of the Eoarchean oceans

It is widely held, though unsubstantiated due to the scarcity of an Eoarchean rock record, that metal requirements in microbes co-evolved with seawater metal availability through time (Da Silva and Williams, 1991). As such, a key step in understanding the early evolution of life on Earth is to better understand the evolution of seawater composition. Studies that have sought to place quantitative constraints on the composition of the earliest oceans point to ferruginous waters (Holland, 1984) that were siliceous (Maliva et al., 2005), possibly mildly sulphidic (Saito et al., 2003), and likely contained an abundance of mafic-volcanic associated trace transition elements, such as Ni (Konhauser et al., 2009). Most BIF older than ~2.0 Ga years also possess chemical characteristics which suggest significant hydrothermal input into the oceans during their deposition, including positive Eu anomalies, a relative depletion of LREE in REE+Y profiles, and mantle-like Nd signatures (Beukes and Klein, 1990; Derry and Jacobsen, 1990; Jacobsen and Pimentel-Klose, 1988). Moreover, Isley (1995) estimated that, due to larger mantle heat flow during the Archean, rates of hydrothermal cycling were up to three times greater than at present, which provides an intimate link between the composition of solutes in seawater and

the composition of oceanic crust, and by extension, mantle activity. Indeed, Isley and Abbott (1999) show a strong correlation between mantle plume activity and BIF occurrence through time.

With experimentally derived partitioning coefficients (K_D), it is possible to derive the concentration of specific metal ion in the seawater from which chemical sediments precipitated. K_D values for Ni and Zn to ferric oxyhydroxides were calculated in the laboratory using the methodology of Konhauser et al., (2007, 2009), and were then applied to bulk (i.e., XRF and ICP-MS) values of Ni, Zn and Fe in BIF; BSF rocks were not used as they contain sulphide grains that may imply secondary Zn enrichment (see Supplementary Data). Our calculations indicate that Ni values in the ocean at the time of the deposition of the Nuvvuagittuq BIF reached up to ~ 300 nM as compared to ~ 12 nM of modern seawater, while Zn concentrations appeared to have only reached up to ~ 20 nM as compared to ~9 nM in today's oceans (Bruland and Lohan, 2004) .

It was recently proposed that the enhanced mantle partial-melting regime for peridotites in the Eo- and Mesoarchean and the related extrusion of Ni-rich ultra(mafic) volcanic rocks on the seafloor promoted high dissolved Ni concentrations in seawater. Archean-aged komatiite, tholeiites and basalts contain preferentially higher abundances of siderophile elements (e.g., Ni, Co, Cr, Fe) than their younger Proterozoic counterparts (e.g., Arndt, 1991; Taylor and McLennan, 1985) which could then become incorporated into BIF (Konhauser et al., 2009).

Therefore, Ni-enrichment in the Nuvvuagittuq BIF is to be expected. Crucially, Ni is a key component in several enzymes of methane-producing bacteria (methanogens), and thus, its abundance would have facilitated increased methane production on the early Earth (Kida et al., 2001).

Zinc is also ultimately sourced from (ultra)mafic volcanics (Le Roux et al., 2010), and accordingly, one would predict high Zn concentrations in the Nuvvuagittuq BIF. However, translating Zn concentrations in BIF to seawater concentrations is complicated by the fact that a number of dissolved species and mineral phases have high sorptive capacities for Zn, and therefore Zn may not have accumulated in seawater. For instance, experimental data has shown that both ferric oxyhydroxides and amorphous silica (Balistrieri et al., 2008; Pivovarov, 2008) can also sequester Zn, and thereby reduce its dissolved concentrations. In this regard, our application of K_D values for both Fe-only and silica-rich oceans both yield relatively low dissolved Zn concentrations. Planavsky et al., (2010) found that, based on the Zn composition of black shales through time, dissolved Zn concentrations in the Archean did not change significantly contrary to some suggestions (e.g., Dupont et al., 2010). Correspondingly, Zn concentrations in the Nuvvuagittuq BIF are comparable to Zn compositions in the Neoarchean (e.g., 2.75 Ga year old Carájas Formation; Dymek and Klein, 1988), Paleoproterozoic (e.g., 2.3 Ga year old Hotazel Formation BIF; Tsikos and Moore, 1997), and Neoproterozoic (590 Ma year old Yerbal formation; Pecoits et al., 2008).

Our results provide additional support for high Archean seawater Ni concentrations, and have important implications on Zn availability for early microbial metalloenzymes. Eukaryotes have a much more significant Zn requirement than prokaryotes, and previous studies have attributed the small number of ancient zinc enzymes (e.g., Dupont et al., 2006, 2010) to the non-bioavailability of Zn sulphide complexes, which dissociate slowly in seawater (Saito et al., 2003). Geochemical modeling results by Saito et al., (2003) suggest that even at dissolved sulphide levels on the order of 0.05 mM, enough sulphide exists in solution, following the formation of $FeHS^{+}$, to completely complex trace metals such as Cu, Cd and Zn. However, results from geochemical modelling experiments generated using Visual MINTEQ 3.0 (Gustafsson, 2011 - at 1 mM HS-; 10 mM each of Ni and Zn alongside other trace metals; 50 μM Fe2+, a conservative estimate after Holland, 1984; and under similar experimental parameters as in Saito et al., 2003), alternatively suggest that ~0.7 nM of Zn^{2+} and ~1.8 nM of Ni^{2+} would remain as free ions. When Fe is increased towards an upper limit for the Archean oceans (1.8 mM, Edmond et al., 1982), these values increase to ~6 and 7.9 nM for Zn^{2+} and Ni^{2+} respectively, that remain uncomplexed by sulphides (Table 2.2; see Appendix C for full modelling results and parameters). Although some of the Zn present in the Nuvvuagittuq BIFs likely sorbed onto ferric-oxyhydroxide particles in the form of Zn sulphide complexes, our findings suggest that a biologically significant fraction of Zn and Ni is likely to have been in a bioavailable form (e.g., chloro-, hydroxyl-, or uncomplexed). This is similar to

previous findings suggesting the utilization, and thereby bioavailable nature, of Ni in the metalloenzymes of methanogens (Kida et al., 2001; Konhauser et al., 2009).

2.6 Conclusions

Petrographic and geochemical analyses of chemical sediments in the Nuvvuagittuq Supracrustal Belt in northern Québec (Canada) lead us to conclude that:

1. There are two distinct chemical sedimentary units in the Nuvvuagittuq belt, a BIF unit consisting of alternating microbands of magnetite, Fe-Mg-Ca silicates and quartz, and a more silicate rich unit consisting of alternating microbands of quartz and Fe-Mg-Ca silicates (BSF).

2. The primary precipitates to these units were Fe-Mg-Ca-bearing silicate and/or carbonate minerals, chert, siderite and hematite. The precursor deposits were made up of layered amorphous silica and ferric oxyhydroxides, fine grained carbonate oozes and/or Fe-Mg-Ca rich silicate gels.

3. Low Al_2O_3, TiO_2, Zr, Hf, Ta and Th concentrations in most of the BSF and BIF samples suggest detritus-free chemical sediments; REE+Y profiles with distinctive seawater-like signatures. Furthermore, consistently positive Eu anomalies suggest that these units have preserved much of their seawater-like composition despite

metamorphic overprinting, with a ~0.1% contribution by high-temperature hydrothermal fluids, similar to the Isua BIF.

4. The most significant trace elements in the Nuvvuagittuq chemical sediments are Ni and Zn, with relative depletions (<15 ppm) in all other trace elements. In the BSF, Ni and Zn are particularly abundant in grunerite and actinolite. In the BIF, Ni is particularly abundant in magnetite, while Zn is abundant in grunerite and actinolite. The application of experimentally-derived partitioning coefficients to absolute concentrations in the BIF show that, compared to modern seawater, Earth's earliest oceans had relatively high dissolved Ni concentrations (up to ~300 nM), but somewhat similar Zn concentrations (up to ~20 nM). A biologically significant portion of the zinc was likely to have occurred as Zn^{2+} and able to form bioavailable complexes.

5. The petrographic and compositional similarities between the chemical sediments in the Nuvvuagittuq and Isua Supracrustal Belts suggest very similar depositional environments in terms of seawater composition, as well as relative input sources.

References

Alexander, B.W., Bau, M., Andersson, P., Dulski, P., 2008. Continentally-derived solutes shallow Archean seawater: rare earth element and Nd isotope evidence in iron formation from the 2.9 Ga Pongola Supergroup, South Africa. Geochimica et Cosmochimica Acta 72:378-394.

Alibo, D.S., Nozaki, Y., 1999. Rare earth elements in seawater: particle association, shale-normalization, and Ce oxidation. Geochimica et Cosmochimica Acta 63:363-372.

Appel, P.W.U., 1979. Cosmic grains in an iron-formation from the early Precambrian Isua Supracrustal Belt, West Greenland. The Journal of Geology 87:573-578.

Arndt, N.T., 1991. High Ni in Archean tholeiites. Tectonophysics 187:411-419.

Ayres, D.E., 1972. Genesis of Iron-bearing Minerals in banded iron formation mesobands in the Dales Gorge Member, Hamersley Group, Western Australia. Economic Geology 67:1214-1233.

Balistrieri, L.S., Borrok, D.M., Wanty, R.B., Ridley, W.I., 2008. Fractionation of Cu and Zn isotopes during adsorption onto amorphous Fe(III) oxyhydroxide:

Experimental mixing of acid rock drainage and ambient river water. Geochimica et Cosmochimica Acta 72:311-328.

Bau, M., 1991. Rare-earth element mobility during hydrothermal and metamorphic fluid-rock interaction and the significance of the oxidation state of europium. Chemical Geology 93:219-230.

Bau, M., 1993. Effects of syn- and post-depositional processes on the rare-earth element distribution in Precambrian iron-formations. European Journal of Mineralogy 5:257-267.

Bau, M., Dulski, P., 1996. Distribution of yttrium and rare-earth elements in the Penge and Kuruman iron-formations, Transvaal Supergroup, South Africa. Precambrian Research 79:37-55.

Bau, M., Dulski, P., 1999. Comparing yttrium and rare earths in hydrothermal fluids from the Mid-Atlantic Ridge: implications for Y and REE behaviour during near-vent mixing and for the Y/Ho ratio of Proterozoic seawater. Chemical Geology 155:77-90.

Beukes, N.J., Klein, C., 1990. Geochemistry and sedimentology of a facies transition -- from microbanded to granular iron-formation -- in the early Proterozoic Transvaal Supergroup, South Africa. Precambrian Research 47:99-139.

Bjerrum, C.J., Canfield, D.E., 2002. Ocean productivity before about 1.9 Gyr ago limited by phosphorus adsorption onto iron oxides. Nature 417:159-162.

Boily, M., Leclair, A., Maurice, C., Bédard, J.H., David, J., 2009. Paleo- to Mesoarchean basement recycling and terrane definition in the Northeastern Superior Province, Québec, Canada. Precambrian Research 168:23-44.

Bolhar, R., Kamber, B.S., Moorbath, S., Fedo, C.M., Whitehouse, M.J., 2004. Characterisation of early Archaean chemical sediments by trace element signatures. Earth and Planetary Science Letters 222:43-60.

Bolhar, R., Van Kranendonk, M.J., Kamber, B.S., 2005. A trace element study of siderite-jasper banded iron formation in the 3.45 Ga Warrawoona Group, Pilbara Craton--Formation from hydrothermal fluids and shallow seawater. Precambrian Research 137:93-114.

Bruland, K.W., Lohan, M.C., 2004. The Control of trace metals in seawater. In: Elderfield, H., Ed. The Oceans and Marine Geochemistry. The Treatise of Geochemistry p. 33 to 47.

Cates, N.L., Mojzsis, S.J., 2006. Chemical and isotopic evidence for widespread Eoarchean metasedimentary enclaves in southern West Greenland. Geochimica et Cosmochimica Acta 70:4229-4257.

Cates, N.L., Mojzsis, S.J., 2007. Pre-3750 Ma supracrustal rocks from the Nuvvuagittuq supracrustal belt, northern Québec. Earth and Planetary Science Letters 255:9-21.

Cates, N.L., Mojzsis, S.J., 2009. Metamorphic zircon, trace elements and Neoarchean metamorphism in the ca. 3.75 Ga Nuvvuagittuq supracrustal belt, Québec (Canada). Chemical Geology 261:99-114.

Da Silva, J.J.R.F., Williams, R.J.P., 1991. The biological chemistry of the elements: the inorganic chemistry of life, 2nd Ed. Oxford University Press, Oxford.

Dauphas, N., van Zuilen, M., Wadhwa, M., Davis, A.M., Marty, B., Janney, P.E., 2004. Clues from Fe isotope variations on the origin of early Archean BIFs from Greenland. Science 306:2077-2080.

Dauphas, N., Cates, N.L., Mojzsis, S.J., Busigny, V., 2007a. Identification of chemical sedimentary protoliths using iron isotopes in the > 3750 Ma Nuvvuagittuq supracrustal belt, Canada. Earth and Planetary Science Letters 254:358-376.

Dauphas, N., van Zuilen, M., Busigny, V., Lepland, A., Wadhwa, M., Janney, P.E., 2007b. Iron isotope, major and trace element characterization of early Archean supracrustal rocks from SW Greenland: Protolith identification and metamorphic overprint. Geochimica et Cosmochimica Acta 71:4745-4770.

David, J., Godin, L., Stevenson, R., O'Neil, J., Francis, D., 2009. U-Pb ages (3.8–2.7 Ga) and Nd isotope data from the newly identified Eoarchean Nuvvuagittuq supracrustal belt, Superior Craton, Canada. Geological Society of America Bulletin 121:150-163.

Deer, W.A., Howie, R.A., Zussman, J., 1992. An introduction to the rock forming minerals. Prentice Hall.

Derry, L.A., Jacobsen, S.B., 1990. The chemical evolution of Precambrian seawater: Evidence from REEs in banded iron formations. Geochimica et Cosmochimica Acta 54:2965-2977.

Dupont, C.L., Butcher, A., Valas, R.E., Bourne, P.E., Caetano-Anollés, G., 2010. History of biological metal utilization inferred through phylogenomic analysis of protein structures. Proceedings of the National Academy of Sciences 107:10567-10572.

Dupont, C.L., Yang, S., Palenik, B., Bourne, P.E., 2006. Modern proteomes contain putative imprints of ancient shifts in trace metal geochemistry. Proceedings of the National Academy of Sciences 103:17822-17827.

Dymek, R.F., Klein, C., 1988. Chemistry, petrology and origin of banded iron-formation lithologies from the 3800 Ma isua supracrustal belt, West Greenland. Precambrian Research 39:247-302.

Edmond, J.M., Von Damm, K.L., McDuff, R.E., Measures, C.I., 1982. Chemistry of hot springs on the East Pacific Rise and their effluent dispersal. Nature 297:187-191.

Ewers, W.E., Morris, R.C., 1981. Studies of the Dales Gorge Member of the Brockman Iron Formation, Western Australia. Econ Geol 76, 1929-1953.

Frei, R., Polat, A., 2007. Source heterogeneity for the major components of ~ 3.7 Ga Banded Iron Formations (Isua Greenstone Belt, Western Greenland): Tracing the nature of interacting water masses in BIF formation. Earth and Planetary Science Letters 253:266-281.

Grauch, R.I., 1989. Rare earth elements in metamorphic rocks. Reviews in Mineralogy and Geochemistry 21:147-167.

Gustafsson, J.P., 2011. Visual Minteq, 3.0 Ed. http://www.lwr.kth.se/English/OurSoftware/vminteq (Stockholm, Sweden).

Holland, H.D., 1984. The Cchemical evolution of the atmosphere and oceans. Princeton University Press, Princeton, NJ.

Isley, A.E., 1995. Hydrothermal plumes and the delivery of iron to banded iron formation. The Journal of Geology 103:169-185.

Isley, A.E., Abbott, D.H., 1999. Plume-related mafic volcanism and the deposition of banded iron formation. Journal of Geophysical Researcg 104:15461-15477.

Jacobsen, S.B., Pimentel-Klose, M.R., 1988. A Nd isotopic study of the Hamersley and Michipicoten banded iron formations: the source of REE and Fe in Archean oceans. Earth and Planetary Science Letters 87:29-44.

Johnson, C.M., Beard, B.L., Klein, C., Beukes, N.J., Roden, E.E., 2008. Iron isotopes constrain biologic and abiologic processes in banded iron formation genesis. Geochimica et Cosmochimica Acta 72:151-169.

Kato, Y., Ohta, I., Tsunematsu, T., Watanabe, Y., Isozaki, Y., Maruyama, S., Imai, N., 1998. Rare earth element variations in mid-Archean banded iron formations:

implications for the chemistry of ocean and continent and plate tectonics. Geochimica et Cosmochimica Acta 62:3475-3497.

Kida, K., Shigematsu, T., Kijima, J., Numaguchi, M., Mochinaga, Y., Abe, N., Morimura, S., 2001. Influence of Ni^{2+} and Co^{2+} on methanogenic activity and the amounts of coenzymes involved in methanogenesis. Journal of Bioscience and Bioengineering 91:590-595.

Klein, C., 2005. Some Precambrian banded iron-formations (BIFs) from around the world: Their age, geologic setting, mineralogy, metamorphism, geochemistry, and origins. American Mineralogist 90:1473-1499.

Konhauser, K.O., Hamade, T., Raiswell, R., Morris, R.C., Ferris, F.G., Southam, G., Canfield, D.E., 2002. Could bacteria have formed the Precambrian banded iron formations? Geology 30:1079-1082.

Konhauser, K.O., Lalonde, S.V., Amskold, L., Holland, H.D., 2007. Was there Really an Archean phosphate crisis? Science 315:1234.

Konhauser, K.O., Pecoits, E., Lalonde, S.V., Papineau, D., Nisbet, E.G., Barley, M.E., Arndt, N.T., Zahnle, K., Kamber, B.S., 2009. Oceanic nickel depletion and a methanogen famine before the Great Oxidation Event. Nature 458:750-753.

Koziol, A.M., 2004. Experimental determination of siderite stability and application to Martian Meteorite ALH84001. American Mineralogist 89:294-300.

Le Roux, V., Lee, C.T.A., Turner, S.J., 2010. Zn/Fe systematics in mafic and ultramafic systems: Implications for detecting major element heterogeneities in the Earth's mantle. Geochimica et Cosmochimica Acta 74:2779-2796.

Lovley, D.R., 1993. Dissimilatory metal reduction. Annual Review of Microbiology 47:263-290.

Maliva, R.G., Knoll, A.H., Simonson, B.M., 2005. Secular change in the Precambrian silica cycle: insights from chert petrology. Geological Society of America Bulletin 117:835-845.

Manning, C.E., Mojzsis, S.J., Harrison, T.M., 2006. Geology, age and origin of supracrustal rocks at Akilia, West Greenland. American Journal of Science 306:303-366.

McLennan, S.M., Hemming, S., McDaniel, D.K., Hanson, G.N., 1993. Geochemical approaches to sedimentation, provenance, and tectonics. Special Papers - Geological Society of America, 21-40.

Mel'nik, Y.P., 1982. Precambrian iron formations: physiochemical conditions of formation. Elsevier Scientific Publishing Company.

Nutman, A.P., McGregor, V.R., Friend, C.R.L., Bennett, V.C., Kinny, P.D., 1996. The Itsaq Gneiss Complex of southern West Greenland; the world's most extensive record of early crustal evolution (3900-3600 Ma). Precambrian Research 78:1-39.

O'Neil, J., Carlson, R.W., Francis, D., Stevenson, R.K., 2008. Neodymium-142 Evidence for Hadean Mafic Crust. Science 321:1828-1831.

O'Neil, J., Francis, D., Carlson, R., 2011. Implications of the Nuvvuagittuq Greenstone Belt for the formation of Earth's carly crust. Journal of Petrology. 52:985-1009.

Ohmoto, H., 2003. Nonredox transformations of magnetite-hematite in Hydrothermal Systems. Economic Geology 98:157-161.

Pecoits, E., Gingras, M.K., Aubet, N.R., Konhauser, K.O., in press. Ediacaran in Uruguay: palaeoclimatic and palaeobiolobical implications. Sedimentology 55:689-719.

Pivovarov, S., 2008. Adsorption of ions onto amorphous silica: ion exchange model. Journal of Colloid and Interface Science 319:374-376.

Planavsky, N.J., Scott, C., Bekker, A., Lyons, T.W., 2010. Tracking Zn Bioavailability Through Time: New Insights from Sulfidic Black Shales. American Geophysical Union, Fall Meeting, 2010, Abstract #OS33E-1510.

Polat, A., Frei, R., 2005. The origin of early Archean banded iron formations and of continental crust, Isua, southern West Greenland. Precambrian Research 138:151-175.

Ross, M., Papike, J.J., Shaw, K.W., 1969. Exsolution textures in amphiboles as indicators of subsolidus thermal histories. Mineralogical Society of Amberica Special Paper 2:275-299.

Saito, M.A., Sigman, D.M., Morel, F.M.M., 2003. The bioinorganic chemistry of the ancient ocean: the co-evolution of cyanobacterial metal requirements and

biogeochemical cycles at the Archean-Proterozoic boundary? Inorganica Chimica Acta 356:308-318.

Shimizu, H., Umemoto, N., Masuda, A., Appel, P.W.U., 1990. Sources of iron-formations in the archean isua and malene supracrustals, West Greenland: evidence from La-Ce and sm-nd isotopic data and REE abundances. Geochimica et Cosmochimica Acta 54:1147-1154.

Stevenson, R.K., David, J., Parent, M., 2006. Crustal evolution of the western Minto Block, northern Superior Province, Canada. Precambrian Research 145:229-242.

Taylor, S.R., McLennan, S.M., 1985. The continental crust: its composition and evolution. Blackwell, Oxford. 312 p.

Trendall, A.F., Morris, R.C., 1983. Iron fgormations: facts and problems. Elsevier Scientific Publishers Inc.

Tsikos, H., Moore, J.M., 1997. Petrography and geochemistry of the Paleoproterozoic Hotazel Iron-Formation, Kalahari manganese field, South Africa; implications for Precambrian manganese metallogenesis. Economic Geology 92:87-97.

Whitehouse, M.J., Fedo, C.M., 2007. Microscale heterogeneity of Fe isotopes in >3.71 Ga banded iron formation from the Isua Greenstone Belt, southwest Greenland. Geology 35:719-722.

Young, S.W., 1976. Petrographic textures of detrital polycrystalline quartz as an aid to interpreting crystalline source rocks. Journal of Sedimentary Research 46:595-603.

Figure 2.1 Map of the Nuvvuagittuq Supracrustal Belt (Northern Québec) showing the main rock units and sampling sites, and the stratigraphy of the chemical sediments on the western side of the belt (David et al., 2009; O'Neil et al., 2007, 2011).

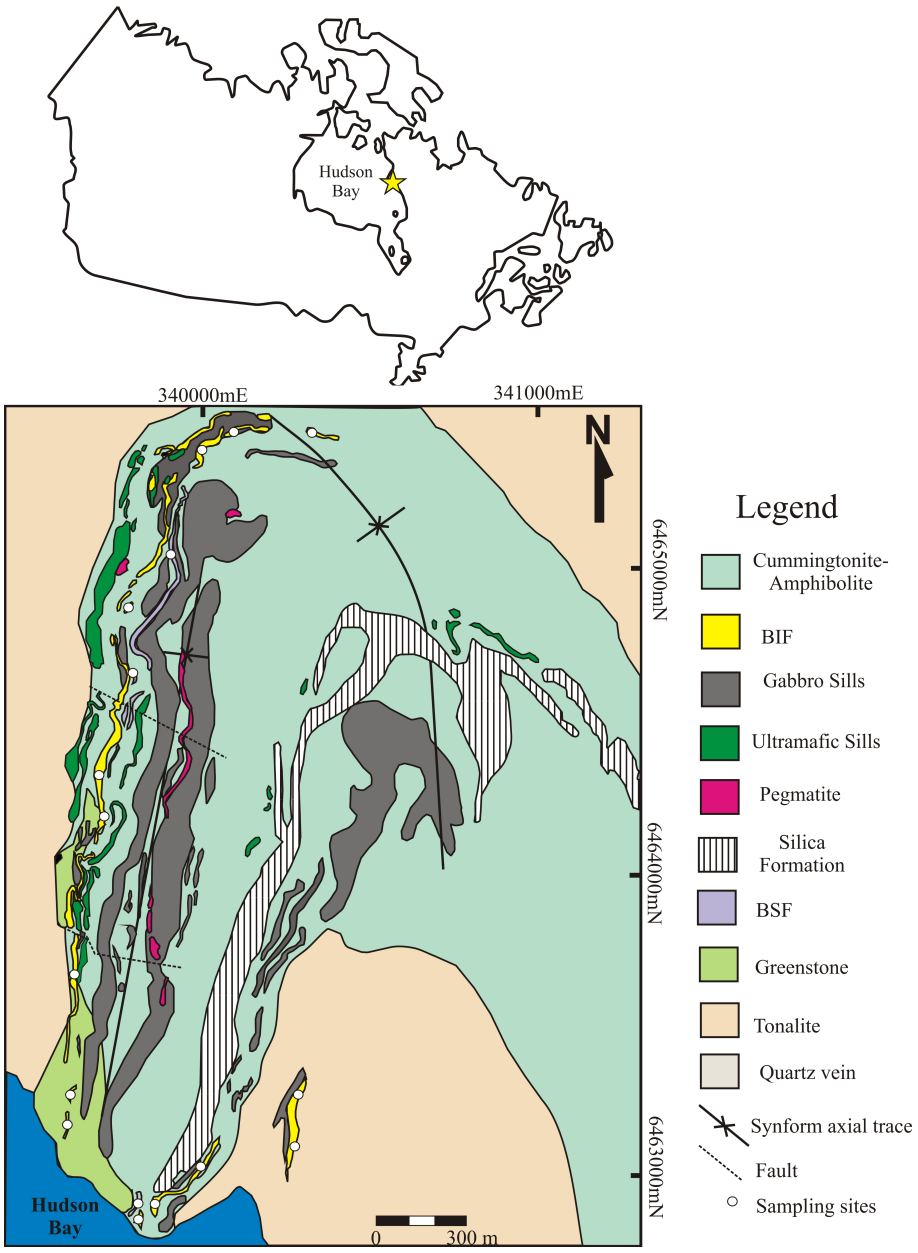
Hudson
Bay
340000mE
341000mE
N
6465000mN
6464000mN
6463000mN
Hudson
Bay
0
300 m
Legend
Cummingtonite-
Amphibolite
BIF
Gabbro Sills
Ultramafic Sills
Pegmatite
Silica
Formation
BSF
Greenstone
Tonalite
Quartz vein
Synform axial trace
Fault
Sampling sites

Figure 2.2 Photomicrographs and EMP maps showing representative textures and petrographic relationships between the main mineral phases in the BSF (090710-13) and BIF (090709-4b; 090709-5) units. A) BSF consisting of alternating Fe-silicate (grunerite, actinolite, augite) and quartz bands, and magnetite (black grains) associated with Fe-silicate bands (scale: 1000 μm). B) BIF consisting of alternating Fe-oxide (magnetite), Fe-silicate (grunerite, augite) and quartz bands (scale: 1000 μm). C) BIF consisting of alternating Fe-oxide and Fe-silicate bands; quartz and augite are associated with both types of bands (scale is 1000 μm). D) Fe-silicate band in a BSF showing mineral grains relationships between magnetite, quartz and grunerite (scale: 100 μm). E) A magnetite and Fe-silicate band in a BIF showing mineral phase relationships between quartz, magnetite and grunerite grains (scale: 100 μm). F) EMP map (Ca) of an Fe-silicate band in BSF showing lamellae of actinolite hosted by grunerite (scale: 200 μm).

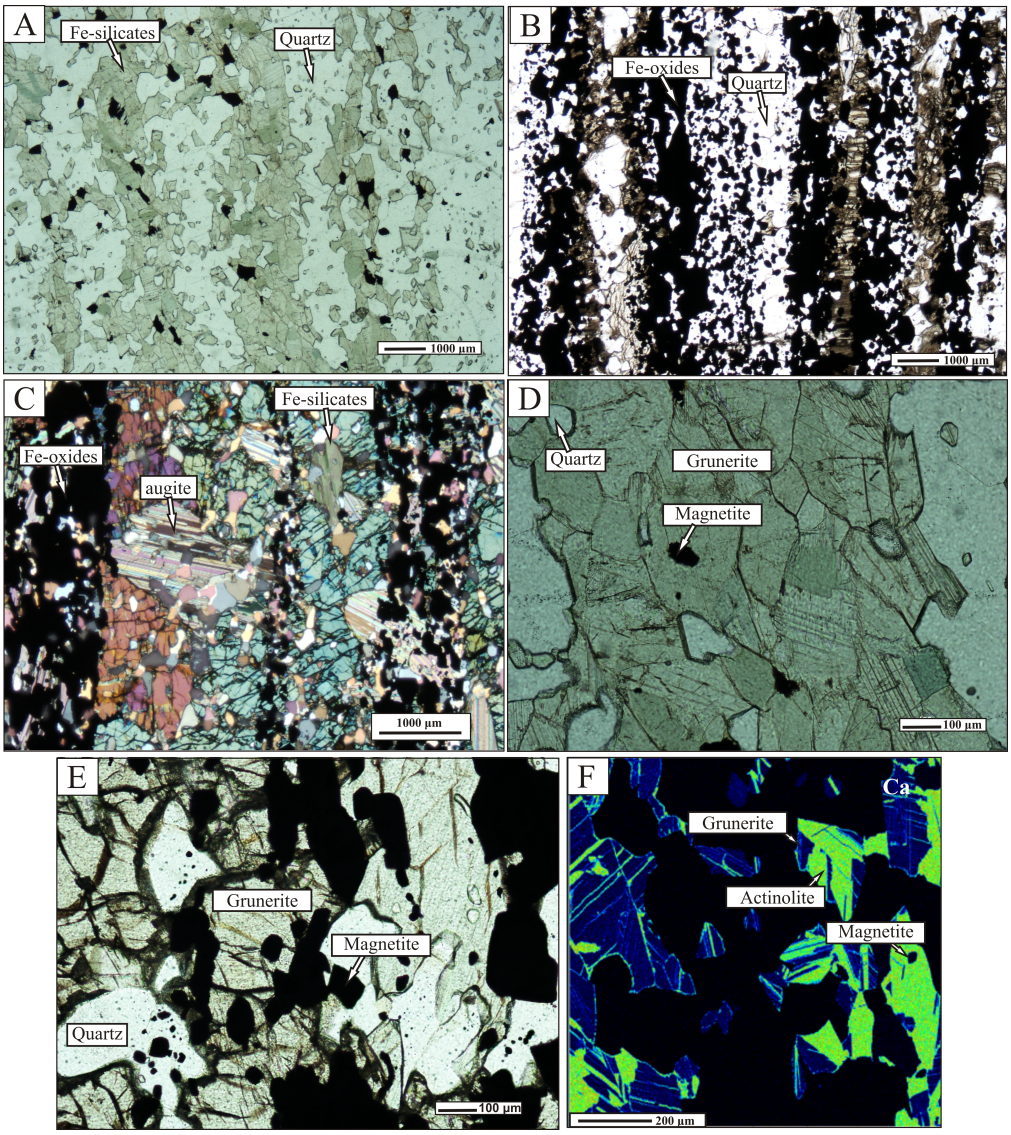
A
Fe-silicates
Quartz
1000 µm
B
Fe-oxides
Quartz
1000 µm
C
Fe-silicates
Fe-oxides
augite
1000 µm
D
Quartz
Grunerite
Magnetite
100 µm
E
Grunerite
Magnetite
Quartz
100 µm
F
Ca
Grunerite
Actinolite
Magnetite
200 µm

Figure 2.3 Plots showing selected trace element chemistry of the main mineral phases (magnetite, quartz, grunerite, augite and actinolite) in the BSF units on the right, and BIF units on the left.

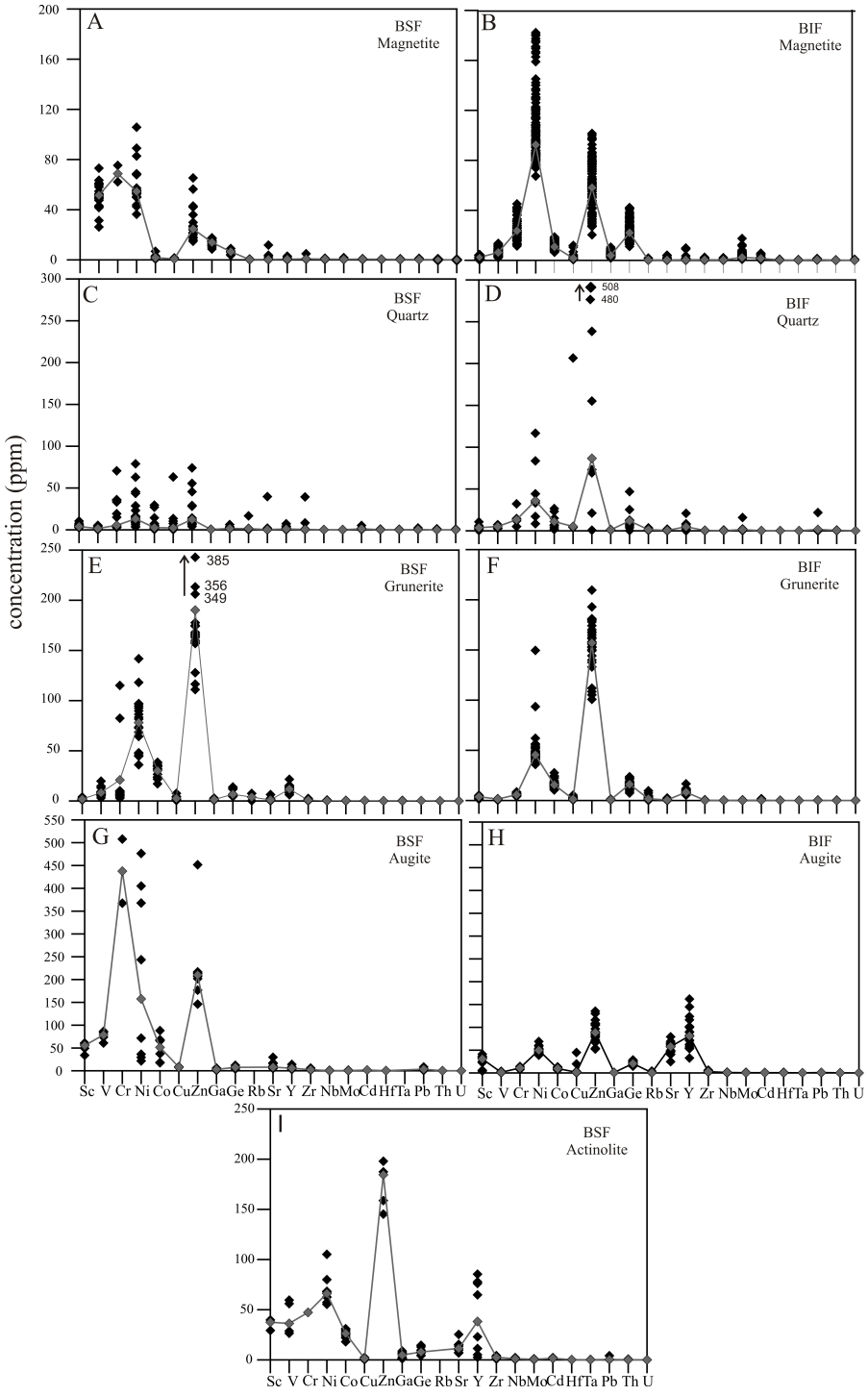
A
BSF
Magnetite
B
BIF
Magnetite
C
BSF
Quartz
D
508
480
BIF
Quartz
E
385
356
349
BSF
Grunerite
F
BIF
Grunerite
G
BSF
Augite
H
BIF
Augite
I
BSF
Actinolite
concentration (ppm)
Sc V Cr Ni Co Cu Zn Ga Ge Rb Sr Y Zr Nb Mo Cd Hf Ta Pb Th U

Figure 2.4 Plots showing the bulk composition of the major elements in: A) the BSF, and B) the BIF.

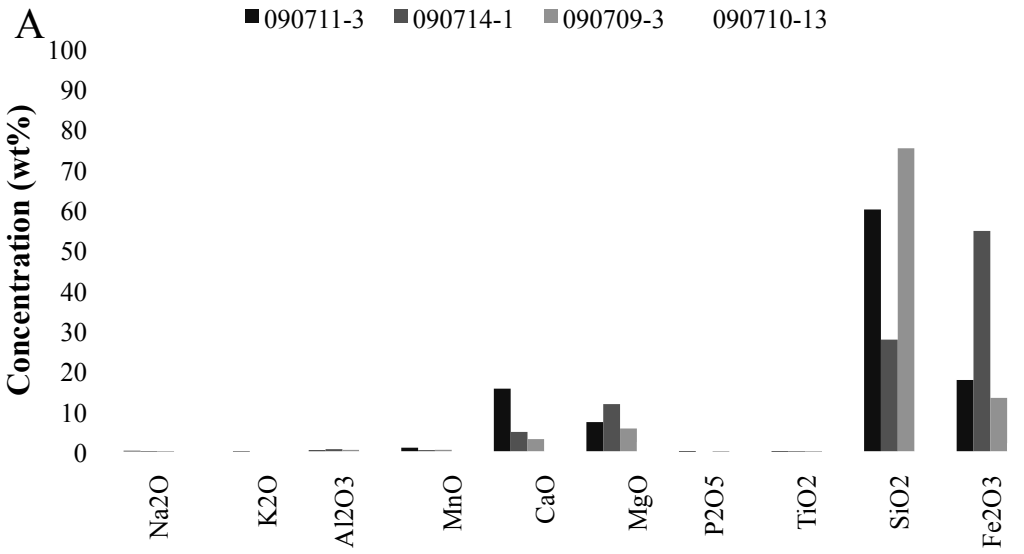
A
090711-3
090714-1
090709-3
090710-13
Concentration (wt%)
100
90
80
70
60
50
40
30
20
10
0
Na2O
K2O
Al2O3
MnO
CaO
MgO
P2O5
TiO2
SiO2
Fe2O3

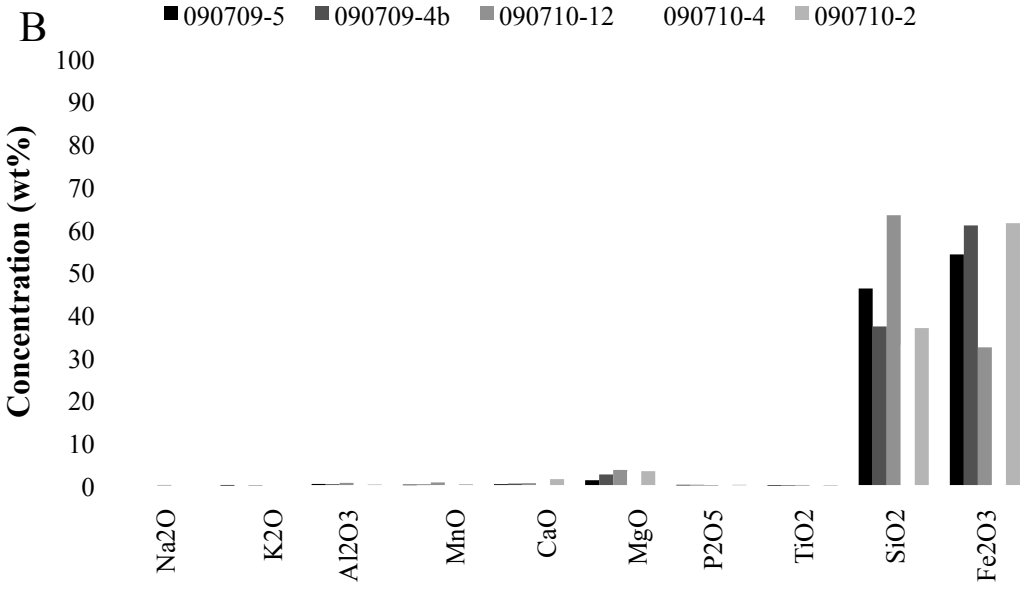
B
090709-5
090709-4b
090710-12
090710-4
090710-2
Concentration (wt%)
100
90
80
70
60
50
40
30
20
10
0
Na2O
K2O
Al2O3
MnO
CaO
MgO
P2O5
TiO2
SiO2
Fe2O3

Figure 2.5 Bulk major element composition of: A) the BSF, and B) the BIF. Median values are represented by the grey line.

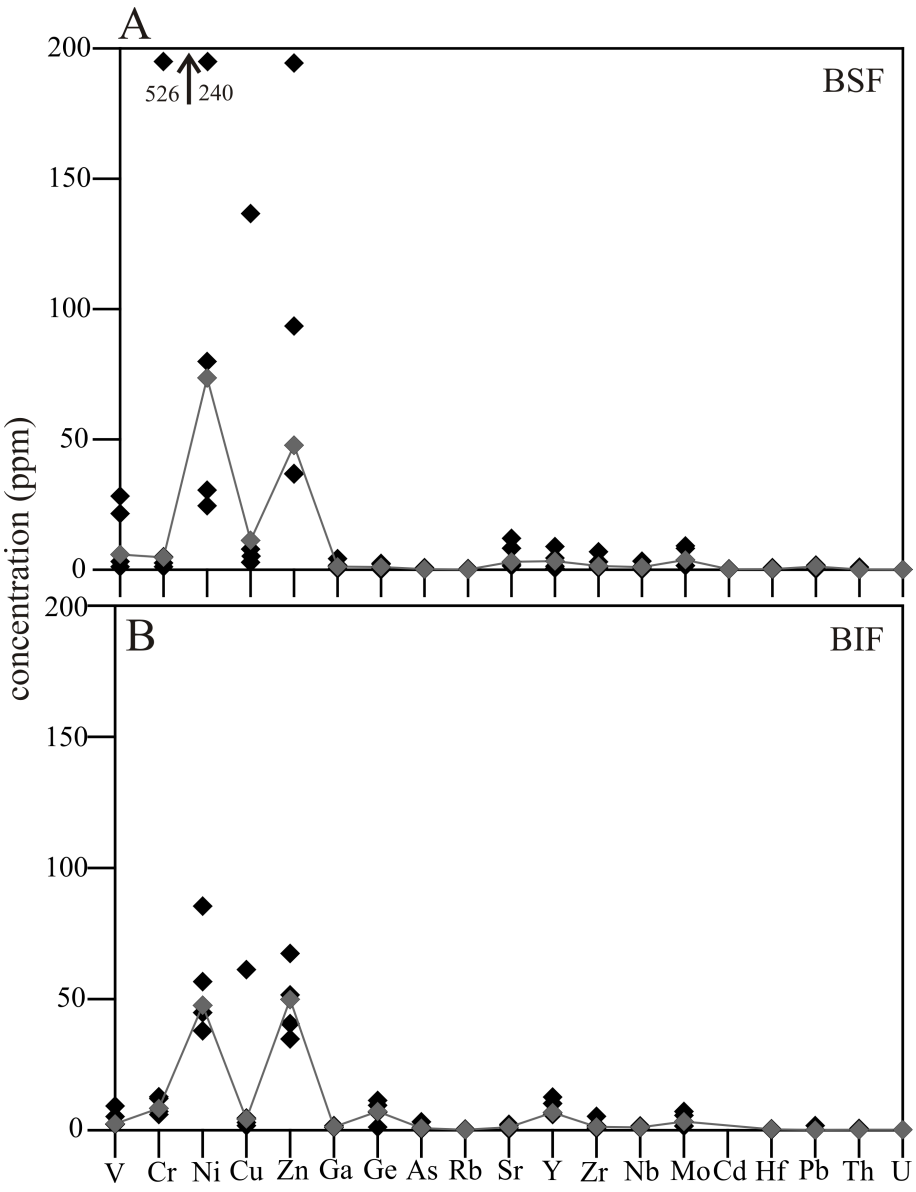
A
B
BSF
BIF
526
240
concentration (ppm)
200
150
100
50
0
V Cr Ni Cu Zn Ga Ge As Rb Sr Y Zr Nb Mo Cd Hf Pb Th U

Figure 2.6 Shale-normalized bulk REE+Y profiles for: A) the BSF, and B) the BIF, with REE+Y profile of Pacific seawater (Alibo and Nozaki, 1999) for comparison, and range of REE+Y profiles for Isua BIF (Bolhar et al., 2004). Sample 090710-13 (BSF) has the highest REE+Y abundances of all the BSF samples and flattest profile, whereas sample 090710-12 (BIF) has the highest REE+Y concentrations and flattest profile of the BIF samples.

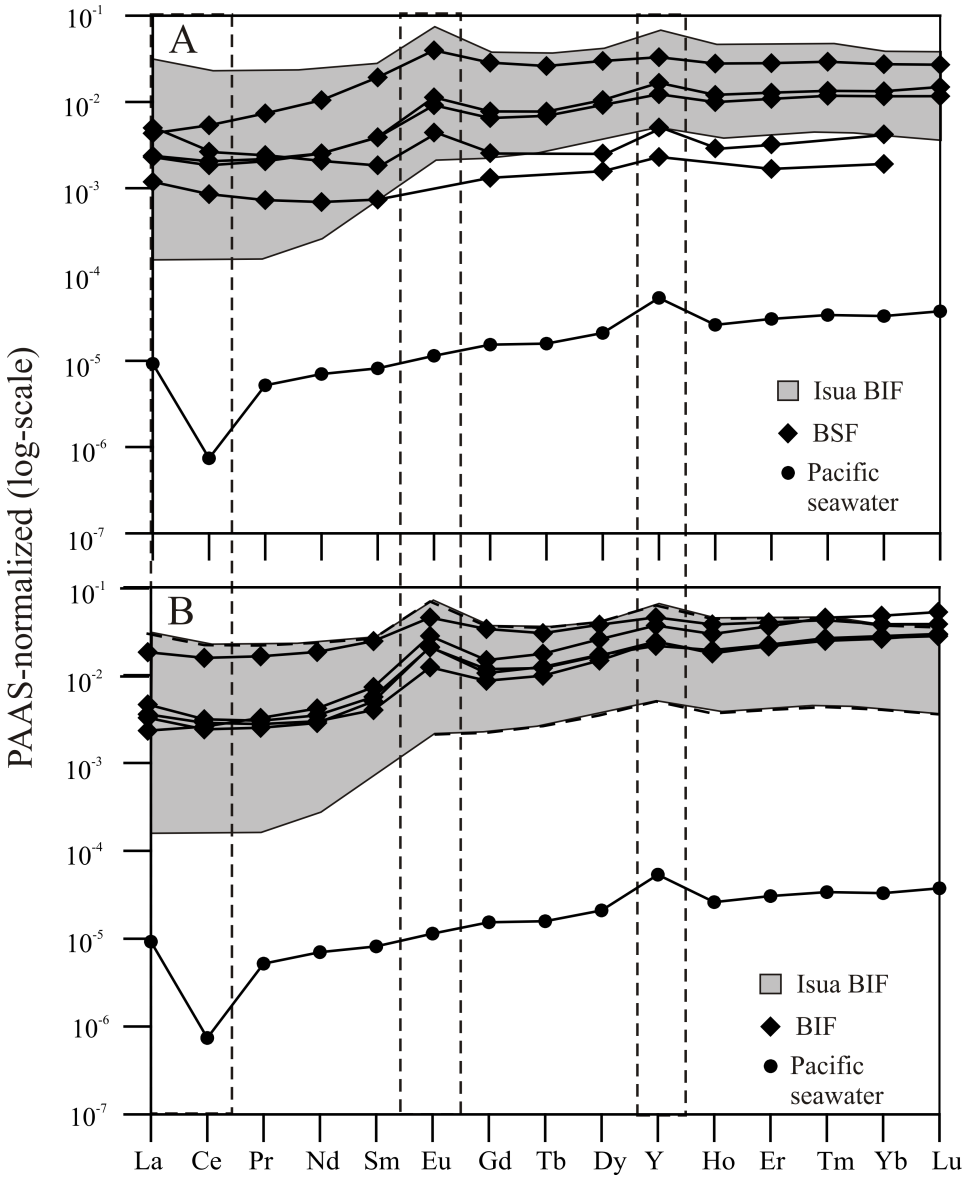
A
B
PAAS-normalized (log-scale)
10^{-1}
10^{-2}
10^{-3}
10^{-4}
10^{-5}
10^{-6}
10^{-7}
Isua BIF
BSF
Pacific seawater
Isua BIF
BIF
Pacific seawater
La Ce Pr Nd Sm Eu Gd Tb Dy Y Ho Er Tm Yb Lu

Figure 2.7 A) Positive La anomalies and negative Ce anomalies persist in all sample. B) Eu anomalies persist in all BSF and BIF samples. Calculations for La, Eu and Ce anomaly verifications from Bolhar et al., (2004). C) Plot comparing Zr over Th, and D) Plot comparing Zr over Y/Ho.

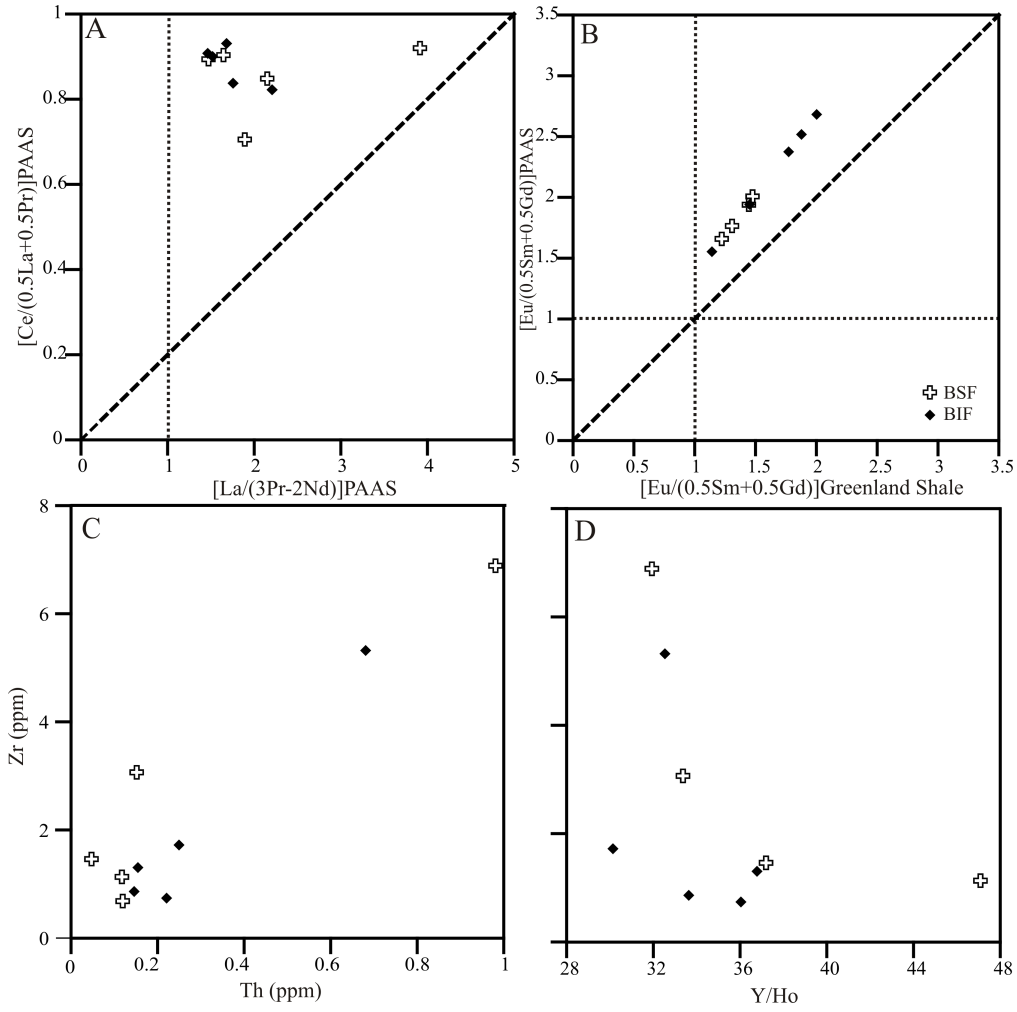
A
[Ce/(0.5La+0.5Pr)]PAAS
[La/(3Pr-2Nd)]PAAS
B
[Eu/(0.5Sm+0.5Gd)]PAAS
[Eu/(0.5Sm+0.5Gd)]Greenland Shale
BSF
BIF
C
Zr (ppm)
Th (ppm)
D
Y/Ho

Figure 2.8 Conservative, two-component mixing model of Sm/Yb vs. Eu/Sm ratios (after Alexander et al., 2008) for the Nuvvuagittuq BSF and BIF, Isua IF (Bolhar et al., 2004), high-temperature (> 350°C) hydrothermal fluids (Bau and Dulski, 1999), Pacific seawater (Alibo and Nozaki, 1999), and average Greenland shale (Bolhar et al., 2005).

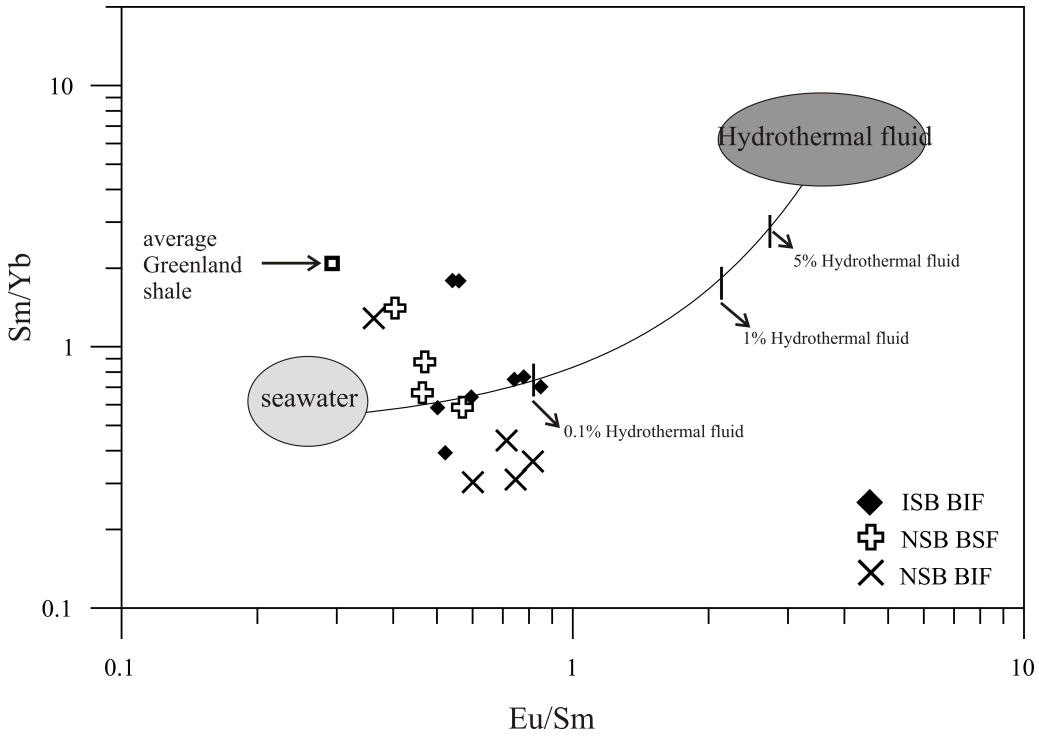
10
1
0.1
Sm/Yb
0.1
1
10
Eu/Sm
Hydrothermal fluid
average
Greenland
shale
seawater
5% Hydrothermal fluid
1% Hydrothermal fluid
0.1% Hydrothermal fluid
ISB BIF
NSB BSF
NSB BIF

Table 2.1 Summary of geochemical analyses of selected minerals. <D.L is below detection limit. Reported data are median values. See Appendix A for full analyses.

	Magnetite		Quartz		Grunerite		Augite		Actionlite
Wt.%*	**BIF**	**BSF**	**BIF**	**BSF**	**BIF**	**BSF**	**BIF**	**BSF**	**BSF**
SiO_2	0.16	0.06	101.23	99.59	49.04	52.38	50.47	51.37	52.73
Al_2O_3	0.46	0.01	0.03	0.01	0.14	0.22	0.11	0.28	1.52
TiO_2	0.02	0.01	0.00	0.00	0.04	0.02	0.02	0.00	0.03
FeO_{total}	92.73	93.93	0.36	0.01	46.79	30.17	21.46	11.92	18.70
MgO	0.02	0.01	0.01	0.01	4.97	12.72	6.73	10.76	12.51
MnO	0.02	0.08	< D.L	<D.L	0.48	0.99	0.23	0.96	0.43
CaO	0.00	0.03	< D.L	<D.L	0.63	0.85	21.44	23.33	11.58
K_2O	0.00	0.00	0.00	0.00	0.01	0.11	0.00	0.00	0.02
P_2O_5	0.00	0.01	0.00	0.00	0.05	0.05	0.00	0.00	0.01
ppm									
Sc	2.35	<D.L	3.64	3.97	3.72	1.78	30.66	55.42	37.57
V	6.50	51.56	5.16	1.55	1.46	7.23	1.34	78.77	36.34
Cr	25.67	68.78	13.27	8.09	5.78	7.09	10.92	699.69	47.33
Ni	93.61	54.58	36.01	13.25	45.48	81.56	49.79	157.58	66.10
Co	11.27	1.80	11.05	2.72	15.70	32.04	9.57	51.41	26.35
Cu	1.62	0.76	5.18	3.32	1.40	1.33	1.57	8.15	1.46
Zn	63.63	25.58	86.61	15.27	157.08	166.09	88.61	210.11	197.91
Ga	4.08	13.93	1.18	0.51	0.80	1.38	0.93	3.09	4.85
Ge	22.39	6.52	11.87	1.62	16.16	5.58	20.69	7.52	7.85
Rb	0.32	0.31	1.32	1.74	1.69	3.85	0.49	<D.L	<D.L
Sr	0.29	0.34	0.57	0.34	0.58	0.50	57.76	7.95	11.43
Y	0.39	0.54	4.77	1.08	8.26	11.49	81.28	5.70	38.24
Zr	0.43	0.81	0.48	0.52	0.27	0.60	2.88	2.47	2.55
Nb	0.36	0.67	0.33	0.18	0.19	0.27	0.95	0.40	1.16
Mo	2.31	0.51	1.42	0.17	0.25	0.26	0.49	0.61	0.66
Cd	1.57	0.60	0.21	1.19	0.34	0.35	0.61	1.61	1.61
Hf	0.32	0.49	0.12	0.16	0.09	0.07	0.54	0.33	0.19
Ta	0.22	0.31	0.10	0.12	0.03	0.03	0.21	<D.L	0.21
Pb	0.51	0.33	1.64	0.37	0.21	0.01	0.78	3.54	0.44
Th	0.16	0.14	0.62	0.04	0.08	0.29	0.22	0.08	0.20
U	0.11	<D.L	0.16	0.07	0.05	0.03	0.04	0.07	0.05

Table 2.2 Model output results examining the effect of sulphide and increasing iron on Zn and Ni speciation in Archean seawater. See Appendix C for modeling parameters.

Component	Species name	0.05 mM Fe^{2+} %Total Concentration	1.8 mM Fe^{2+} %Total Concentration
Sulphide	HS^{-1}	47.632	0.525
	$H_2S_{(aq)}$	10.227	0.113
	$FeHS^{+}$	42.09	99.346
Zinc	Zn^{+2}	7.402	59.658
	$ZnOH^{+}$	0.094	0.757
	$Zn(OH)_{2\,(aq)}$	0.024	0.197
	$ZnCl^{+}$	2.509	20.24
	$ZnCl_4^{-2}$	0.089	0.718
	$ZnCl^{3-}$	0.24	1.934
	$ZnCl_{2\,(aq)}$	0.469	3.784
	$Zn_2S_3^{-2}$	9.779	
	$ZnS_{(aq)}$	78.683	6.998
	$ZnCO_{3\,(aq)}$	0.451	3.623
	$ZnHCO^{3+}$	0.258	2.072
	$Zn(CO_3)_2^{-2}$		0.02
Nickel	Ni^{+2}	18.074	78.874
	$NiOH^{+}$	0.029	0.126
	NiCl+	0.789	3.447
	$NiCl_{2\,(aq)}$		0.023
	$NiHS^{+}$	77.935	3.755
	$NiCO_{3\,(aq)}$	0.711	3.092
	$NiHCO^{3+}$	2.456	10.681

Chapter 3. A detailed geochemical and petrographic study of chemical sedimentary rocks from the ≥3.77 Ga Nulliak Supracrustal Association (Labrador, Canada).

3.1 Introduction

Archean seawater differed significantly from modern oceans, and its compositional evolution through time is preserved in the pre-2.5 Ga metasedimentary rock record. It is well established that the Archean ocean was anoxic, with significant Fe(II) concentrations (Ewers, 1980; Ewers and Morris, 1981; Morris and Horowitz, 1983; Czaja et al., 2012), and was close to supersaturation with respect to amorphous silica (Maliva et al., 2005). The presence of high-Mg ultramafic volcanic rocks (komatiites) and a seemingly greater production of mafic rocks during the Archean eon suggests that mantle heat flow was higher then than at any later time in Earth's history (Arndt, 1991; Arndt et al., 2008; Berry et al., 2008). Consequently, the contribution of hydrothermal fluids to ocean composition was also higher, leading to greater abundances of trace metals in Archean seawater relative to Proterozoic and Phanerozoic seawater (e.g., Konhauser et al., 2009).

Banded iron formations (BIF) are among the best lithologies to study ancient seawater composition. These chemical sedimentary rocks precipitated directly out of seawater, and as such, they provide an invaluable, though intermittent, 3.0 Ga long

record of seawater evolution through time (see Bekker et al., 2010 for review). However, the dearth of pre-3.6 Ga (Eoarchean) BIF with well-established ages significantly constrains the availability of information on the earliest seawater. Importantly, the high grade, poly-metamorphic histories that characterize the few existing occurrences may have modified their primary compositions in ways significant to their value as early seawater proxies. This premise underlines the importance of distinguishing the typical, primary depositional compositions of BIF with metamorphic overprints.

All BIF characteristically have between 20-40 wt% FeO, between 40-60 wt% SiO_2, and low concentrations of trace metals (e.g., Sc, V, Cr, Co, Ni, Cu, Zn < 80 ppm). Detritus-poor BIF contain less than 1.8 wt% Al_2O_3, and low incompatible element (e.g., Zr, Th, Hf, Sc) abundances (Bau, 1993; Dymek and Klein, 1988; Klein, 2005). They also have certain rare-earth element and yttrium (REE+Y) profile features relative to shale that distinguish them from other rock types. For example, a typically concave-upward slope relative to the light rare earth elements (LREE), with a positive slope toward the heave rare earth elements (HREE) (Bolhar et al., 2004; Frei and Polat, 2007). This is due to increasing solution complexation of REE with increasing atomic number, so that HREE are more strongly complexed in solution relative to LREE (Cantrell and Byrne, 1987; Byrne and Kim, 1990). Exceptions to this are La and Y (Archean BIF have Y/Ho > 36; Bolhar et al., 2004) which are enriched in modern seawater relative to their neighbours, and their positive anomalies

in BIF further testify to marine depositional settings (Bau, 1999). One significant geochemical difference between pre-3.6 Ga BIF and their younger counterparts is a distinct hydrothermal overprint. Eoarchean BIF have strong, positive Eu anomalies, which are thought to be due to a greater input of high-temperature hydrothermal fluids relative to younger BIF (Dymek and Klein, 1988; Danielson et al., 1992). They also contain distinct iron isotope signatures relative to igneous rocks (spanning +0.5 ‰ to -1 ‰ /amu), which can reveal important information pertaining to iron cycling in the ancient oceans. Indeed, the ^{56}Fe isotope signature in BIF is typcially consistent with the oxidation and precipitation of ferrous iron in the water column (Rouxel et al., 2005) and/or dissimilatory iron reduction in the sedimentary pile (e.g., Johnson et al., 2008).

The scarcity of well-established, Eoarchean-aged, BIF localities emphasizes the importance of exploiting any known occurrence. Indeed, banded quartz-pyroxene rocks belonging to the ca. 3.85 Ga Akilia Association of South Greenland have received much attention due to the ongoing debate as to whether they chemical sedimentary in origin, or a product of high-grade metarmophic processes (Mojzsis et al., 1996; Fedo and Whitehouse, 2002; Fedo et al., 2006; Manning et al., 2006; Lepland et al., 2011). BIF from the ca. 3.7-3.8 Ga Isua Supracrustal Belt (ISB) have been relatively well-studied for well over two decades (e.g., Appel, 1980; Nutman, 1986; Frei and Polat, 2007), and the recent discovery of ≥3.75 Ga year old BIF and BIF-like sediments in the Nuvvuagittuq Supracrustal Belt (NSB, northern Québec;

Simard et al., 2003) has opened up the possibility of building a more global picture of early seawater composition.

Iron-rich units of chemical sedimentary origin have been known to exist in the ≥3.77 Ga Nulliak Supracrustal Association in northern Labrador, Canada (e.g., Nutman et al., 1989), but significantly less is available on them. These rocks represent a rare additional source of information to further our understanding of the chemical composition of Eoarchean seawater. In this work, we determine whether the Nulliak chemical sedimentary rocks can be used as seawater proxies by examining the degree of post-depositional disturbance that they have undergone. We present new, detailed petrographic and geochemical data (trace element as well as Fe isotope analyses) on these rare rock units, integrating mineral and whole-rock compositions, thereby creating a framework for better understanding the bulk and microscale variations.

3.2 Geological Setting

The Nulliak Supracrustal Association (referred to as 'Nulliak' herein) is a volcano-sedimentary sequence located in the Saglek area of Northern Labrador. It is part of the Nain Province of the North Atlantic Craton (NAC) which also hosts the Nuuk region of Southwest Greenland (Friend et al., 1988; Hoffman, 1989; Nutman et al., 1989; Schiøtte et al., 1990). The NAC is a triangular-shaped block bounded by the Makkovik-Ketilidian orogen to the southeast, the Torngat orogen to the west, and the

Naggsugtoqidian orogen to the northeast (Bridgewater et al., 1973; Hoffman, 1989). The Nain Province comprises the dominantly Eoarchean-aged Saglek Block and dominantly Mesoarchean-aged Hopdale Block which were juxtaposed ca. 2.55 Ga years ago (Schiøtte et al., 1993; James et al., 2002), and were separated by the intrusion of the Nain Plutonic Suite between 1305 Ma and 1312 Ma (Wasteneys et al., 1992, 1995, 1996; Connelly and Ryan, 1996).

Nulliak itself is thought to be at least 3776±8 Ma years old (U-Pb zircon age of a metavolcanic rock in the sequence, Schiotte et al., 1989a), and occurs as a few disseminated outcrops within the 3800 to 3600 Ma year old Uivak Gneisses (Schiøtte et al., 1989b).The most voluminous unit in the association is banded to homogeneous amphibolites with compositional affinities toward tholeiitic to komatiitic basalt. They are found in association with a metperidotite- and clinopyroxinite-layered amphibolite unit, interpreted as possibly representing differentiated flows or sills (Nutman et al., 1989). Two other important units, although volumetrically less important than the amphibolites, are compositionally-layered quartzofeldspathic gneiss, and sillimanite+garnet+biotite+quartz±plagioclase gneiss of probable sedimentary origin, Also present, though less common, are leucogabbros and anorhthosites. Interlayered and locally gradational with the amphibolites and quartzfeldspathic gneisses are quartz+magnetite±pyroxene±garnet±amphibole BIF (Nutman et al., 1989). The BIF units are generally <5m thick, though locally up to 100 m thick, and are associated with quartz-pyroxene rich rocks and olivine-diopside

rich marble of chemical sedimentary origin, which form units <2 m thick and locally up to 20 m thick. These three units are randomly layered on a 1 m scale (Nutman et al., 1989).

The geology and timing of geological events in the Saglek area has been likened to that of the Akulleq terrane in West Greenland, which is thought to be an ancient crustal accretion complex (Nutman and Collerson, 1991). The main component of the tonalitic to granodioritic Uivak Gneisses (thought to correlated with the early Amitsoq Gneisses of southern West Greenland) intruded into the Nulliak rocks 3732±6 Ma ago, resulting in an early granulite-facies metamorphic event (Baadsgaard et al., 1986). They are suggested to originate from the reworking of pre-existing TTG suites (Schiøtte et al., 1989a,b; 1993), and contain zircons with 3.85 to 3.9 Ga cores which may have belonged to an older sialic crust upon which the Nulliak Supracrustal Assemblage formed (Schiotte et al., 1989b; Nutman et al., 1989). At 3620 Ma years ago, the Saglek area underwent granulite-facies metamorphism, where injection of pegmatites and alkali-rich fluids reset Rb-Sr/Pb-Pb/Sm-Nd isotopic systems in the area (Bridgewater and Collerson, 1976; Schiotte et al., 1989b). Subsequently these pegmatites were intruded by the 3.24 Ga to 3.62 Ga old mafic Saglek dykes (Bridgewater and Shiøtte, 1991; Schiøtte et al., 1990). It has been suggested that this dyke swarm, along with the multi-generation Ameralik Dykes (3.5 Ga to 3.26 Ga) in the Itsaq Gneiss Complex (Akulleq Terrane, Southwest Greenland), represent the rifting of an older block of Eoarchean crustal material, and

would help to explain the various NAC terranes with similar Eoarchean histories, and differing Meso- and Neoarchean histories (Nutman et al., 1993; Friend and Nutman, 1994). The Saglek area was again intruded at ca. 3.0 Ga by the Upernavik Supracrustals which are found interleaved with the Uivak Gneisses (Schiotte et al., 1986). A second granulite-facies metamorphic event at ca. 2.9 Ga ago caused migmatization and partial melting of pre-existing mafic and ultramafic lithologies. mobilizing U, Th, Rb and Pb on a regional scale (Schiotte et al., 1986). This complex Archean metamorphic history ended with the intrusion of the Igukshuak granite at ca. 2.5 Ga (Nutman et al., 1989), which is when the geological histories of the various NAC terranes converge, suggesting their juxtaposition by this time (Friend et al., 1988; McGregor et al., 1991; Friend and Nutman, 2005, 2007).

3.3 Methods

Six samples of the Nulliak chemical sediments were made into polished thin sections, including three BIF samples, two quartz pyroxene rock samples, and one metacarbonate sample (Table 3.1). Petrography and mineralogy were established using reflected and transmission light microscopy, as well as elemental mapping using a JEOL 8900 electron probe microanalyzer at the University of Alberta. Samples were broken and sub-sampled to avoid veined and strongly recrystallized areas, and crushed in an agate mill. Powders were submitted for whole rock major

element XRF analysis at Activation Laboratories (Ontario, Canada) and for whole-rock trace element analysis after HNO_3-HF digestion using a PerkinElmer Elan6000 quadruple inductively coupled plasma mass spectrometer (ICP-MS) at the University of Alberta (Edmonton, Canada). Mineral phase and major element compositions were determined using the JEOL8900 under the following conditions: beam diameter (3 μm); voltage (20 kV); current (20 nA); and concentrations were calculated using ZAF matrix correction. All REE anomalies were calculated according to Bolhar et al., (2004).

Trace element compositions of individual mineral grains were analysed using the quadrupole ICP-MS attached to a New Wave UP213 laser ablation system (213 nm) under the following conditions: PR power (1200 W); peak hopping acquisition (50 ms dwell time); spot diameter (between 60 μm and 100 μm depending on grain size); repetition rate (5 Hz); and energy density (~13 J/cm^2). The international glass standard NIST610 was used for instrument calibration purposes, while Fe was used as an internal standard for each analysis. Data reduction was accomplished using GLITTER© (XP version, New Wave Research).

Whole rock Fe isotope compositions were analysed at the French oceanographic institution IFREMER, Brest campus, following previously published methods (Rouxel et al., 2005; 2008; Planavsky et al,. 2012). Briefly, 50-100 mg of sample powder was digested overnight at 80 °C in 4ml 1:1 HF-HNO_3 followed by 4 ml aqua regia, with complete evaporation in between. Samples were then taken up in

4ml 6N HCl, from which Fe was purified on Bio-Rad AG1X8 anion resin (2 ml wet resin bed) using 6N HCl for matrix elution followed by 0.24N HCl for Fe elution. Fe isotope compositions were determined using a Thermo Scientific Neptune multicollector inductively coupled plasma mass spectrometer operating at medium resolution to resolve isobaric interferences such as $^{40}Ar^{14}N$ on ^{54}Fe, $^{40}Ar^{16}O$ on ^{56}Fe, and $^{40}Ar^{16}O^{1}H$ on ^{57}Fe. Solutions were doped with Ni for mass bias correction, introduced to the instrument using an Apex Q desolvating nebuliser (Elemental Scientific, Omaha, NE, USA), and 'sample-standard bracketing' was used for data normalization to a Fe isotope standard solution of IRMM-14 run before and after each unknown. Geostandards BHVO-2 and IF-G yielded $\delta^{56}Fe$ values of 0.09±0.09 ‰ and 0.65±0.14‰, respectively, consistent with previous work (e.g., Planavsky et al., 2012), and repeated measurements of IRMM-14 (n=30) constrained average internal precision over the analytical session to better than ±0.08 (2 standard deviations).

3.4 Results

3.4.1 Petrography

The Nulliak chemical sedimentary rocks consist of three stratigraphically-related lithologies: a (1) BIF facies (Figure 3.1A); (2) quartz-pyroxene facies (Figure 3.2A); and (3) metacarbonate facies (Figure 3.3D,G). The principal BIF mineralogy consists

of quartz (35-45%), magnetite (25-35%), Fe-hornblende and actinolite (20-25%), clinopyroxene (5-20%), and accessory phases of garnet, biotite and apatite, each occurring as <5% of sample. While mesobanding is sometimes preserved (0.5-1 cm scale), no relict microbanding (<1 mm) is evident as the major mineral phases (quartz, magnetite, Fe-hornblende, actinolite and clinopyroxene) appear to be randomly intermixed (Figure 3.1). Quartz grains exist as irregularly-shaped crystals that vary in size from 0.01-3 mm, often showing intense undulatory extinction with occasional parallel lamellar structures within individual sub-grains, presumably a result of lattice defects as a response to a high and constant strain rate. Similarly, the magnetite grains are irregularly shaped and vary in size from 0.1-6 mm. Two amphibole phases occur, an iron-rich hornblende (Figure 3.1B-C) and a less defined actinolite phase that stems from alteration of clinopyroxene (Figure 3.1D-E). The former shows an interlinked network of light brown to dark green, subhedral crystals (0.01-5 mm), often with well-developed 120°/60° cleavages. The latter amphibole phase is pseudomorph after clinopyroxene where the original texture is progressively transformed into randomly oriented, occasionally radiating, acicular actinolite.

The majority of the pale-green clinopyroxene shows exsolution lamellae of another pyroxene of more orthorhombic symmetry (Figure 3.1D,E). These compositionally-zoned pyroxenes likely stem from the inversion of pigeonite, a low-Ca, ultra-high temperature pyroxene that upon slow cooling exsolve into lamellae of orthopyroxene and clinopyroxene, here, approximately parallel to the {001} plane.

The fine single lamellae throughout the grains and orthorhombic symmetry as patchy blebs in many of the clinopyroxene grains can be seen in Figure 3.1 (D,E). Anhedral, pale reddish-brown garnet porpyroblasts (2-5 mm) occur in certain samples, which are often poikiloblastic with quartz inclusions (Figure 3.1F,G). Flakes of dark-brown biotite can be found along cracks in the magnetite and along the actinolite rims. Elongated, colourless grains of apatite occur in contact with the latter.

The quartz-pyroxene rocks are poorly banded, and consist of quartz (60-70%), clinopyroxene (20-35%), as well as secondary actinolite, talc and calcite (each making up <10% of sample). Accessory phases of plagioclase, magnetite, olivine, zircon and disseminated pyrite/chalcopyrite occurring along cracks and rims of quartz and clinopyroxene (in sample YM82-72) occur each making up <5% of the rocks. Quartz and augite appear to be randomly inter-distributed, however, some layering is observed, mostly as a single-crystal thick, 3-4 mm-long clinopyroxene chains (Figure 3.2A). The quartz is irregularly shaped, ranging from 1-8 mm in size with sub-grains showing different extinction angles as a result of intense lattice strain. Similar to the quartz, the pale yellow to green, subhedral clinopyroxene varies in size from 1-5 mm and, although some may have minor talc-alteration along their rims, they are relatively unaltered (Figure 3.2B,C). In some of the samples, a minor, more colorless to pale brown pyroxene phase occurs, presumably as a result of higher Mg content. The majority of these are altered to a fine-grained mosaic of talc along their rims and have exsolution lamellae of amphibole parallel to {100}. Accessory phases of pale-

brown zircons, coarse-grained (up to 2.5mm) plagioclase showing well-developed poly-crystalline twins with minor sericite alteration also occur (Figure 3.2A). Occasionally, secondary biotite appears along the cracks and rims of the pyroxene and amphibole.

The metacarbonate rock is weakly banded, consisting of carbonate (40- 60%), magnetite (10-20%), diopside (10-15%), scapolite (5-10%), tremolite (<5%), talc (<5%) and accessory chlorite, titanite and olivine. It shows weakly developed, wavy microbands of carbonate interlayered with magnetite bands (Figure 3.2D-G). The pale brown carbonate is largely microcrystalline (<0.1 mm), while a few euhedral grains are up to 1 mm in size. The magnetite appears to have a bimodal size distribution, with a relatively unaltered, fine grained (≤0.1 mm) group, and a coarser grained (5-6 mm) group partly altered to chlorite, and oriented parallel to the direction of foliation. Similarly, two diopside phases occur (Figure 3.2D,E), a fine-grained (0.05-0.2 mm), anhedral group with well-rounded grain boundaries adjacent to the carbonate, and a coarser-grained (0.5-2 mm) group. While the finer grained diopside is especially associated with the carbonate layers, the coarser grained group is dispersed randomly throughout the rock. A portion of the coarse-grained diopside is surrounded by fine-grained diopside, talc and thin, colourless prismatic tremolite. Reaction zones along the contact between the large diopside grains and the fine-grained carbonate occur locally. Well-defined, compositionally-distinct, cm-thick bands of diopside, scapolite, ± altered olivine occur (Figure 3.2F,G).

3.4.2 Major and trace element whole rock composition

Selected major and trace elements are presented in Table 3.2. The BIF are made up dominantly of Fe (38-51 wt% $Fe_2O_{3\ Total}$) and Si (39-57 wt% SiO_2), and secondarily of Mg (1.7-3.4 wt% MgO), Ca (2.1-2.9 wt% CaO), and Al (0.8-2.7 wt% Al_2O_3). The most abundant trace elements in the BIF are Zn (32-108 ppm), Ba (26-146 ppm), Ni (13-58 ppm), Cr (22-101 ppm), and Sr (9-34 ppm) (Table 3.2). Some prevalent trends occur, namely, transition metals (Mo, V, Co and Cr) are positively correlated with Al_2O_3 (r^2>0.7), and Ge is positively correlated with $Fe_2O_{3\ Total}$ (Figure 3.3). In terms of REE+Y profiles, the BIF have very small, positive La anomalies (La/La*=1.09-1.15), slight positive to strong positive Eu anomalies (Eu/Eu*=1.03-2.4), superchondritic Y/Ho ratios (Y/Ho=35.72-39.55), and variable LREE-MREE-HREE relationships (Pr/Yb_{SN}=0.63-1.15; Sm/Yb_{SN}=0.76-1.53). Note that samples BR-82-26b and PI-1 (see Table 3.1) all have seawater-like REE+Y anomalies according to Bolhar et al., (2004), that is, La/La*>1, Eu/Eu*>1, superchondritic Y/Ho ratios, and LREE<MREE<HREE, while sample BR-82-94a has La/La* and Eu/Eu* closer to unity, and LREE>MREE>HREE (Figure 3.4).

The quartz-pyroxene rocks are mainly Si (85-87 wt% SiO_2), are iron-poor (4-7 wt% $Fe_2O_{3\ Total}$), and are comparable in Ca (~4 wt% CaO), Mg (2-3 wt% MgO) and Al (<2.5 wt% Al_2O_3) to the BIF samples. In terms of trace elements, Zn (9-302 ppm), Sr (12-33 ppm) and Ba (6-52 ppm) occur in the highest overall abundances of the rocks (Table 3.2). Like in the BIF, high V, Ni, Cr, and Co are associated with higher

Al, and both the BIF and the quartz-pyroxene samples show for chemical sediments relatively high levels of Th (up to 0.95 ppm), Hf (up to 0.64 ppm), and Zr (up to 20.4 ppm) (Table 3.2; Figure 3.3). Quartz-pyroxene sample YM82-72 is richer in trace metals (Cu=346 ppm; Ni=119 ppm) than BR-82-93, and has a higher sulphur abundance (0.4 wt% S), which is likely associated with sulphide minerals (see also section 3.4.1). Its REE+Y profile shows slight positive La anomaly (La/La*=1.15), slight positive Eu anomaly (Eu/Eu*=1.11), superchondritic Y/Ho ratio (32.72), LREE<HREE and MREE~HREE (Pr/Yb_{SN}=0.46; Sm/Yb_{SN}=0.95). While sample BR-82-93 has a REE+Y profile and anomalies more reminiscent of seawater, sample YM-82-72 has a strongly concave downward profile unlike typical Eoarchean BIF (Figure 3.4; Bolhar et al. al., 2004). As this sample likely contained sulphide minerals which that may have skewed the its REE+Y budget, we will take this into consideration when assessing its geochemical signature (Table 3.1). While sample BR82-93 shows a non-positive La anomaly (La/La*=0.98), it has a strong positive Eu anomaly (Eu/Eu*=3.03), superchondritic Y/Ho ratio (48.64), LREE<MREE<HREE (Pr/Yb_{SN}=0.44 Sm/Yb_{SN}=0.52).

Apart from Ca (27 wt% CaO) and Si (26 wt% SiO_2), the metacarbonate contains ~8 wt% each of MgO and $Fe_2O_{3\ Total.,}$ The most abundant trace elements are Zn (50 ppm) and Sr (22 ppm), while the rest are <15 ppm (Table 3.2), and its REE+Y profile shows La anomaly close to unity (La/La*=0.97), negative Eu anomaly (Eu/Eu*=0.89), strongly superchondritic Y/Ho ratio (57.73), and

LREE>MREE>HREE (Pr/Yb_{SN}=1.76; Sm/Yb_{SN}=1.36). Of all the rock samples analyzed here (apart from BR-82-94a), the REE+Y profile of metacarbonate PI-3 has the most extreme discrepancies from modern seawater.

3.4.3 Fe Isotopes

Fe isotope data for the Nulliak chemical sediments are presented in Table 3.3. The $\delta^{56}Fe$ values of the Nulliak chemical sediments (expressed in conventional delta notation as the ratio of $^{56}Fe/^{54}Fe$ in the sample relative to the igneous rock standard IRMM-14) range from -0.44‰ to 0.84‰, with an average precision of ±0.07‰ (2 standard deviations). No distinctive trend between these values and major or trace element concentrations is observed. The quartz-pyroxene and metacarbonate rocks have negative values (-0.02‰ to -0.44‰), while BIF have both positive and negative values (-0.30‰ to 0.84%).

3.4.4 Major mineral phase composition

Full analyses of mineral compositional data is available in Appendix E.

Magnetite

Apart from being dominantly Fe (92 wt% FeO), the prevailing trace elements in magnetite are Cr (164 ppm), Ni (86 ppm), V (62 ppm), and Zn (51 ppm), which tends

to be variable in some grains, ranging from ~400 ppm to 30 ppm. Co also occurs in notable concentrations (20 ppm), as does Ge (14 ppm).

Clinopyroxene

The major element composition of the clinopyroxene in the Nulliak rocks tends to vary: SiO_2 (60-41 wt%); FeO (16-27 wt%); CaO (1-12 wt%); and Al_2O_3 (0.6-12 wt%), with a bimodal compositional classification as either calcic clinopyroxene (augite) or pigeonite on a Ca-Mg-Fe diagram (Figure 3.5). Both of these groups show similar overall trends in terms of trace elements where the most abundant is Zn (155 ppm), Ni (62 ppm), Ge (22 ppm), Ba (17 ppm) and Sc (15 ppm). Notably, the calcic clinopyroxene tends to have significantly higher abundances of Zr and Cr than the pigeonite, and contains the majority of the Ba which occurs among the highest trace elements in both the BIF and quartz-pyroxene unit

3.5 Discussion

3.5.1 High temperature metamorphism of the Nulliak chemical sedimentary rocks

Rocks belonging to the ≥3.77 Ga Nulliak Supracrustal Association were metamorphosed to granulite facies (e.g.. Bridgewater and Collerson, 1976), as evidenced in this study by the presence of the two clinopyroxenes, augite and pigeonite. The latter is especially indicative of high temperature metamorphism with temperatures reaching 800-1000°C (depending on the Mg-Fe content of the

pyroxene), which is the theoretically-calculated solvus between lower temperature augite and higher temperature pigeonite (e.g., Gole and Klein, 1981; Fonarev et al., 2006). The crustal depth at which this thermal event took place is currently unknown, although Fonarev et al., (2006) reported a range of 5 to 11 kbar (<50 km crustal depth) using detailed barometric calculations on fluid inclusion data from similar ultrahigh temperature metamorphosed BIF within the East European craton. After the high-temperature peak in the Saglek area, slow cooling formed inverted (orthorhombic) pigeonite as evident from the exsolution lamellae mostly on the {100} surfaces of the original pigeonite. At these relatively high peak temperatures, the chert in the original BIF may have temporarily undergone phase changes, and as such, lost important information on its original composition. Aside from the Nain complex (Berg, 1977), pigeonite and exsolution textural pyroxene have only been reported from a few Archean BIF occurrences worldwide: the ultra-high temperature, metamorphosed BIF from the East European craton (Fonarev et al., 2006); the Biwabik BIF in Minnesota (Bonnichsen, 1975); the Stillwater BIF in Montana (Vaniman et al., 1980); and the BIF from the Napier complex, Enderby Land, Antarctica (Sandiford and Powell, 1986).

Clinopyroxene is the dominant silicate mineral left over from the original granulite-facies metamorphic assemblage in both the BIF and the quartz-pyroxene facies, as evidenced by a few relatively unaltered specimens in some samples. In BIF,

clinopyroxene is thought to be the result of ankerite decarbonation according to the following reaction (Klein, 2005):

$$Ca(Fe, Mg)(CO_3)_{2\ (Ankerite)} + 2SiO_{2\ (Quartz)} \Rightarrow Ca(Fe,Mg)Si_2O_6 + 2CO_{2\ (Clinopyroxene)}$$

The existence of both well-shaped and fibrous actinolite crystals also shows that the BIF have undergone retrograde metamorphism. Given that these amphiboles and pyroxenes together make up greater than 20% of the modal mineral content in the BIF, and up to 35% in the quartz-pyroxene samples (Table 3.1), this suggests that the primary Nulliak chemical sediment assemblage contained a significant carbonate fraction.

The unaltered condition of the clinopyroxene and plagioclase suggest an equilibrium prograde granulite-facies metamorphic assemblage, whereas the pseudomorphic amphiboles, calcite and talc may be the result of later, pervasive solutions that affected the pyroxenes. Strong similarities between these quartz-pyroxene rocks and those found at Akilia in Southwest Greenland are evident. The debate on their origin is ongoing with respect to whether they were chemical sediments containing the first evidence of bacterial carbon fractionation (Mojzsis et al., 2002) or whterh they were derived by the metasomatic alteration of an ultramafic precursor (Fedo and Whitehouse, 2002; Fedo et al., 2006).

Magnetite in high-grade assemblages is the recrystallization product of earlier, finer-grained magnetite (Klein, 2005) and shows no reaction features with other

mineral phases. While the original precursor to magnetite in BIF is not very well defined, it is thought that the original precipitates were ferric oxyhydroxides such as ferrihydrite [$Fe(OH)_3$], hydro magnetite ($Fe_3O_4 \cdot nH_2O$) or perhaps even a very magnetite-like mineral precipitate (Klein, 2005). In the hydrous precursors, the H_2O would have been lost during diagenesis due to compaction.

In terms of the metacarbonate unit, the origin of the calc-silicate mineral phases most likely stems from an impure limestone precursor as a result of carbonate precipitation mixed with siliciclastic input. The existence of minor scapolite indicates that sodium- and chlorine-rich fluids have influenced the sediments possible during the high activities of granitoid intrusions in the area.

3.5.2 Provenance of the Nulliak BIF, quartz-pyroxene and metacarbonate rocks

Evidence from major and trace elements

The composition of the Nulliak samples suggest that they contain a higher detrital contribution relative to pure chemical sediments. Certain elements (e.g., Ti, Al, Zr, Cr, Y, Th) are deemed able to withstand metamorphic and metasomatic processes. However, it is preferable to examine the ratios of elements with comparable chemical behaviour rather than single elements in applying provenance studies of high-grade metamorphosed rocks. Various ratios can be used to detect sources of detrital contamination, element mobility within rock units, as well as metmorphic protoliths (e.g., Sun and Nesbitt, 1979; McLennan et al., 1993; Arndt, 1994). While aluminum

values in BIF are typically low when compared to associated igneous and pelitic lithologies (Al_2O_3 <1.8 wt%; Klein, 2005), the Nulliak chemical sedimentary rocks contain as much as 2.73 wt% Al_2O_3, suggesting that they could be described as "contaminated BIF" (e.g., Nutman et al.,1989). Correspondingly, samples with higher Fe/Ti ratios appear to contain lower Al, as well as lower abundances of Th, Hf and Zr. The latter are trace elements generally regarded as immobile in seawater (Table 3.2), and for which the abundances of Th <0.09 ppm, Hf <0.04 ppm and Zr <1.1ppm are typical for uncontaminated BIF (Bolhar et al., 2004).

A few of the trace metals (e.g., V, Co, Cr, Mo) exhibit a marked positive correlation with Al, indicating that they were hosted within the detrital fraction. Relative to the Isua BIF, the Nulliak chemical sediments have higher TiO_2, Cr, and Y as seen on a plot of Cr/Y vs. TiO_2/P_2O_5 (Figure 3.6). Most of the Nulliak sediments plot close to the region of mafic Archean rocks, and coincide with a mixing ratio of between 10-20% detrital input of igneous material (Figure 3.6; see also Fedo and Whitehouse, 2002, and Figure 22 of Manning et al., 2006).

In BIF, Ni can be associated with detrital contamination by mafic to ultramafic lithologies (e.g., McGregor and Mason, 1977). Unlike the aforementioned metals, Ni does not correlate with detritally-sourced major elements (e.g., Al and Ti), suggesting instead that it was not derived from the same source as V, Co, Cr, Mo. If Ni concentrations are reflective of seawater Ni concentrations at the time of

deposition, then its concentration in BIF can be used to derive early seawater Ni concentrations (e.g., Konhauser et al., 2009).

Rare earth element and yttrium profiles

The robustness of REE up to upper-amphibolite facies metamorphism, their predictable behaviour, and relative immobility make them an invaluable tool for examining a rock's origins, and the post-depositional changes that it has been subjected to. The REE+Y profiles of the Nulliak BIF have patterns that suggest a seawater provenance: (1) concave-upward profile shapes showing HREE enrichment ($Pr/Yb_{SN}<1$ and $Sm/Yb_{SN}>1$); (2) positive La and Eu anomalies ($La/La^*>1$ and $Eu/Eu>1$); and (3) superchondritic Y/Ho ratios (Figure 3.4; Bolhar et al., 2004).

Quartz-pyroxene (BR82-93 and YM-82-72) and metacarbonate (PI-3) samples show no significant positive La anomaly ($La/La^*\leq1$). Nulliak samples show a positive correlation between ∑REE and Al suggesting that detrital contribution may be responsible for their rather flat REE+Y profiles (Figure 3.4 Bau 1993). No significant Ce anomalies are observed.

While BIF samples PI-1 and BR-82-26B appear to have preserved multiple seawater REE+Y signatures despite high-temperature metamorphism, sample BR-82-94, which has the lowest Al_2O_3 abundance of all the BIF samples, shows an atypical concave-downward shape caused by elevated LREE and MREE values relative to HREE, and a poorly developed Eu anomaly relative to the other samples ($Eu/Eu^*\sim1$

vs. ~2.4, respectively), implying some degree of post-depositional disturbance. A considerable water to rock ratio is required to remobilize rare earth elements in BIF (e.g., at least 100:1; Bau, 1991), and this is thought to be a rather unlikely scenario in most metamorphic environments (Bau, 1993). In general, REE with larger ionic radii are easier to remobilize than heavier REE. In particular, Eu has the highest mobility due to its comparatively larger ionic radius, and can be remobilized under high metamorphic temperatures (Bau and Dulski, 1996). There is also little evidence of significant post-depositional hydrothermal alteration, such as sulfides and gold hydrothermal mineral deposits. Indeed, the pigeonite in these rocks likely formed as a result of high temperature metamorphism through exsolution and recrystallization during cooling. Thus, the presence of inverted pigeonite suggests that metamorphic temperatures affecting the Nulliak chemical sedimentary rocks might have reached as high as ~ 800°C (Simmons et al., 1974).

The metacarbonate exhibits a non-seawater like REE+Y profile despite having similar absolute concentrations relative to the BIF samples. The absence of a La anomaly (La/La*~1), the slight negative Eu anomaly, and strong LREE and MREE enrichements relative to HREE suggest an origin other than direct precipitation from Eoarchean seawater. In comparison with the Nulliak ultramafic lithologies, Ca/Fe, Mg/Fe and Mn/Fe ratios in the metacarbonates are noticeably higher, similar to the metacarbonate rocks from Akilia Island in southern Greenland and in parts of the Isua Supracrustal Belt, and may have formed by the decarbonation

and desilicification of ultramafic rocks under granulite facies conditions (Nutman and Friend, 2006; Manning et al., 2006; Dauphas et al., 2007b).

Evidence from Fe isotopes

Unlike other more volatile isotopic systems (e.g., C and O), Fe isotopes are geochemically robust, and may preferentially retain pre-metamorphic signatures making them a useful tool in deciphering the provenance of highly deformed and metamorphosed rocks (e.g., Mojzsis et al., 2003; Anbar, 2004). Many natural materials tend to have distinctively narrow δ^{56}Fe ranges, where most terrestrial/plutonic igneous rocks fall within the 0.00±0.05‰ range (Beard et al., 2003a), as do fluvial and marine sediments, Proterozoic shale units, and modern wind-blown sediments. Therefore, any detrital component in a chemical sediment would reflect those of its source region (Beard et al., 2003b). Hydrothermal fluids from modern mid-ocean ridges comprise one of the only sources of negative δ^{56}Fe (-0.3‰ to -0.77‰; Sharma et al., 2001). However, Johnson et al. (2008) estimated that Archean equivalent fluids had a δ^{56}Fe ~ 0 (approaching that of the igneous rocks through which it flowed during its ascent to the Earth's surface), given hotter mantle temperatures and higher hydrothermal fluxes occurring at that time (e.g., Nisbet et al., 1993). In contrast, chemical sediments have characteristically large variations in δ^{56}Fe that are demonstrably preserved in metamorphosed Precambrian BIF (e.g., Dauphas et al., 2004; 2007a,b). BIF from the Kaapvaaal Craton have δ^{56}Fe values

ranging -2.5‰ to 1.0‰ (Johnson et al., 2003; 2008); this large variation is interpreted to have been caused by a combination of factors, for example, mineral-specific equilibrium isotope fractionation, the original iron isotope composition of the fluids from which these minerals precipitated, and the bacterial metabolic processes which might have influenced their formation (Johnson et al., 2003; 2008). Furthermore, metabolically-processed iron may also retain a 'vital effect' due to the redox-related changes driving iron isotope fractionation during microbially-influenced iron mineral precipitation (Johnson et al., 2002).

The Nulliak chemical sedimentary rocks display a wide range of Fe isotope compositions ($\delta^{56}Fe$ = -0.44 to +0.84‰), of which the BIF samples have both light and heavy values, while the quartz-pyroxene and calc-silicate rocks have light $\delta^{56}Fe$ values. Despite the evidence of a detrital component in these chemical sediments, the non-zero Fe isotope signatures of these rocks affirms the authigenic sedimentary nature of iron deposition. Ferric oxyhydroxides were likely formed in the water column through the oxidation of aqueous ferrous Fe – $Fe(II)_{aq}$, where overall fractionation appears to be independent of the oxidative pathway, whether by molecular oxygen, anaerobic photoferrotrophy, or UV photooxidation (e.g., Bullen et al., 2001; Croal et al., 2004; Balci et al., 2006). While complete oxidation of a $Fe(II)_{aq}$ pool will result in ferric oxyhydroxides with the pool's initial $\delta^{56}Fe$ composition, partial oxidation will result in ferric oxyhydroxides that are up to +4‰ higher (e.g., Wu et al., 2012). Reactions between these ferric oxyhydroxide precipitates and

various $Fe(II)_{aq}$ pools as they descend through the water column and their diagenesis upon burial result in their conversion to important BIF forming minerals (e.g., magnetite, siderite, ankerite).

The Fe isotope signatures of individual mineral phases weren't analyzed in this study. Previous studies of upper amphibolite to granulite facies BIF (e.g., Isua Supracrustal Belt and Akilia Island; Dauphas et al., 2004) as well as high temperature (>790°C) igneous and metamorphic rocks (Beard and Johnson, 2004) show that equilibrium Fe isotope fractionation between individual mineral phases is null at such high temperatures. In these cases, $\delta^{56}Fe$ of magnetite and silicates (the major phases in the Nulliak chemical sedimentary rocks) resembled those of the bulk rock.

The main Fe-bearing mineral of the BIF and metacarbonate is magnetite (up to 90 wt% FeO_{total}), and is augite (FeO_{total} = 16-27 wt%) in the quartz-pyroxene rocks. The precursors to these minerals, fine-grained (hydro)magnetite, and ankerite, respectively (Klein, 2005), form via the interaction between ferric oxyhydroxides and various $Fe(II)_{aq}$ pools, either during their descent through the water column, or after deposition in the sediment (Johnson et al., 2008). Positive $\delta^{56}Fe$ signatures in magnetite are thought to occur via the interaction of ferric oxyhydroxides formed by partial oxidation of hydrothermally-sourced $Fe(II)_{aq}$ (heavy $\delta^{56}Fe$ values) with more pristine pools of hydrothermally-sourced $Fe(II)_{aq}$ possessing near-zero $\delta^{56}Fe$ values. Such a scenario is easily envisioned for oxidative mechanisms restricted to the upper water column, where isotopically heavy precipitates formed a the zone of partial

oxidation would rain into a deeper, isotopically unaffected hydrothermal $Fe(II)_{aq}$ pool. Alternately, positive signatures may be generated in magnetite via the partial or near-complete reduction of ferric oxyhydroxides of nearly any initial isotope composition. Dissimilatory iron reduction (DIR) by iron reducing bacteria releases isotopically light $Fe(II)_{aq}$ and leaves the residual oxide isotopically heavy (in our case, for eventual reaction to magnetite); the relevance of this pathway is debated (Planavsky et al., 2012). By either scenario, the two BIF samples with positive $\delta^{56}Fe$ values in this study (DL-82-26B and BR-82-94A) testify to partial or complete Fe oxidation during sedimentation, most likely in the ancient water column.

The other BIF sample (PI-1) is characterized by a negative $\delta^{56}Fe$ composition (-0.30‰; Table 3.3); this is a first for Eoarchean BIF, and requires a $Fe(II)_{aq}$ pool with very low $\delta^{56}Fe$. One potential source is DIR (Johnson et al., 2008), although Raleigh distillation of water column Fe during ferric hydroxide precipitation can also eventually yield isotopically light ferric oxyhydroxides (and in turn, magnetite) without DIR. While magnetite with negative $\delta^{56}Fe$ could potentially occur as result of mineral precipitation from a metasomatic fluid, sample PI-1 has a high Fe/Ti ratio, comparable to Isua BIF (Fe/Ti mol-mol ratios of ~771 vs 250-1000, respectively; Dauphas et al., 2004), suggesting no significant Fe loss due to metasomatic alteration. Low sulphur abundances as well as petrographic observations in thin section confirm the absence of metasomatic sulphide minerals that might shift the whole-rock $\delta^{56}Fe$ composition toward lighter values. While heavily carbonated chemical sediments

(due to post-depositional processes) may have negative $\delta^{56}Fe$ compositions (e.g., the 3.7-3.8 Ga Isua Supracrustal Belt, Dauphas et al., 2007b), CaO abundances in this sample are low (~3 wt%). Importantly, sample P-1 has a seawater-like REE+Y profile with associated positive La and Eu anomalies as well as superchondritic Y/Ho ratios which suggests that the negative $\delta^{56}Fe$ in sample PI-1 may be a primary signature. More extensive sampling of this unique local is warranted to determine whether these BIF may provide evidence for Eoarchean DIR, or if their Fe isotope compositions may be entirely accounted for by oxidative processes.

The quartz-pyroxene facies unit represented by sample BR-82-93 has a $\delta^{56}Fe$ composition of -0.02‰, which is similar to igneous rocks, however it also has a strong seawater-like REE+Y profile, with related positive La and Eu anomalies as well as superchondritic Y/Ho ratios (Figure 3.4) suggestive of a chemical sedimentary origin with a minimal detrital influence (Al_2O_3=0.07 wt%). Similar to a Quebec Eoarchean quartz-pyroxene sample of near-zero $\delta^{56}Fe$ composition (IN05048) measured by Dauphas et al., (2007b), sample BR-82-93 has a high Fe/Ti ratio (~2100 mol/mol) such that admixture of igneous material is unlikely account for its near-zero $\delta^{56}Fe$ composition, making it more likely a sedimentary feature. Chemical sedimentary Fe-rich carbonate minerals such as siderite and ankerite (the likely precursors of the calcic clinopyroxenes in this sample) possess compositions near zero when formed by equilibrium precipitation from an unfractionated seawater $Fe(II)_{aq}$ pool, although they may also form via the complete reduction of near-zero

ferric oxyhydroxide precursors via DIR (Johnson et al., 2008). The data for sample YM82-72 has been purposely overlooked. The REE+Y profile strongly deviates from a seawater-like signature (Figure 3.5), while higher S contents and post-depositional pyrite and chalcopyrite grains seen in thin section deposited along mineral grain boundaries and fractures alerts us to potential sulphide contamination, which might account for its isotopically light (-0.44‰) composition.

The metacarbonate unit, represented by sample PI-3, has a negative δ^{56}Fe composition of -0.19‰, which is typical of Fe-rich carbonates from metasomatic, metamorphic, or sedimentary settings (e.g., Johnson et al., 2003; Frost et al., 2007; Dauphas et al., 2007b). Had these metacarbonates been of chemical sedimentary origin, they would have not only had a seawater-like REE+Y profile, but also likely $\delta^{56}Fe \leq 0$, such as the Fe-rich metacarbonates in the 3.7-3.8 Ga Isua Supracrustal Belt (Dauphas et al., 2007b). Together with a REE+Y profile that strongly deviates from a seawater-like signature, the light Fe isotope signature of the metacarbonate sample supports the idea of a metasomatic origin.

3.6 Conclusions

Along with the ca. 3.8 Ga year old Isua Supracrustal Belt, Akilia Island and the Nuvvuagittuq Supracrustal Belt, the Nulliak Supracrustal Association presents one of the few chemical sedimentary occurrences of confirmed Eoarchean age. This preliminary study suggests that despite the high degree of metamorphism, there still

exist pockets of chemical sedimentary rocks in the Nulliak Supracrustal Association that retain signatures of their formation from ancient seawater. These rocks consist of three field-related lithologies (Nutman et al., 1989), a BIF rich unit and a quartz-pyroxene rich unit both of chemical sedimentary origin, and a calc-silicate rich unit of metasomatic origin. Granulite facies metamorphic conditions are evident in the detailed petrology of the BIF and quartz-pyroxene rocks, which also show the effects of subsequent retrograde metamorphism. Their primary mineral assemblages are thought to have included a significant carbonate component, and were comprised mainly of chert + magnetite + ankerite and/or siderite. The chemical composition of the BIF appears to have been influenced to varying degrees by detrital input, likely mafic or ultramafic volcaniclastic debris, which is evident in their higher Al_2O_3, Th, Hf, and Zr values compared to more pure chemical sediments. Some of the quartz-pyroxene facies are remarkably well-preserved despite the high grade metamorphism, and relatively free of detrital input.

The whole-rock Fe isotope signatures of these chemical sediments range from heavy δ^{56}Fe values to near-zero and light δ^{56}Fe values. The near-zero and light Fe isotope signatures reported here are atypical of other ca. 3.8 Ga BIF (e.g, Dauphas et al., 2007a,b), but despite the granulite-facies metamorphism involved, seawater-like REE+Y profiles and strong Fe enrichments in these samples suggest that their Fe isotope compositions reflect primary signatures. The iron isotope data reported here reflects partial to complete oxidation of hydrothermal aqueous Fe(II) in the Nulliak

depositional basin ca. 3.8 Ga, and one sample may record evidence of dissimilatory iron reduction (DIR). More samples from the Nulliak Supracrustal Association should be examined in order to elaborate on the extent of these processes in the early Fe cycle.

References

Appel, P.W.U., 1980. On the early Archean Isua iron-formation, West Greenland. Precambrian Research 11:73-87.

Anbar, A.D., 2004. Iron stable isotopes: beyond biosignatures. Earth and Planetary Science Letters 217:223-236.

Arndt, N.T., 1991. High Ni in Archean tholeiites. Tectonophysics 187:411-419.

Arndt, N.T., 1994. Archean komatiites. Developments in Precambrian Geology 11:11-44.

Arndt, N.T., Coltice, N., Helmstaed, H., Gregoire, M., 2008. Origin of Archean subcontinental lithospheric mantle: some petrological constraints. Lithos. 109:61-71.

Baadsgaard H., Nutman A.P., Bridgewater D., 1986. Geochronology and isotopic variation of the early Archean Amitsoq gneisses of the Isukasia Area, southern West-Greenland. Geochimica et Cosmochimica Acta 50: 2173-2183.

Balci, N., Bullen, T.D., Witte-Lien, K., Shanks, W.C., Motelica, M., Mandernack, K.W., 2006. Iron isotope fractionation during microbially-stimulated Fe(II) oxidation and Fe(III) precipitation. Geochimica et Cosmochimica Acta 70:622-639.

Bau, M., 1991. Rare-earth element mobility during hydrothermal and metamorphic fluid-rock interaction and the significance of the oxidation state of Europium. Chemical Geology, 93:219-230.

Bau, M., 1993. Effects of syn- and post-depositional processes on the rare-earth element distribution in Precambrian iron-formations. European Journal of Mineralogy 5:257-267.

Bau, M., Dulski, P., 1996. Distribution of yttrium and rare-earth elements in the Penge and Kuruman iron-formations, Transvaal Supergroup, South Africa. Precambrian Research 79:37-55.

Bau, M., 1999. Scavenging of dissolved yttrium and rare earths by precipitating iron oxyhydroxide: Experimental evidence for Ce oxidation, Y-Ho fractionation, and lanthanide tetrad effect. Geochimica et Cosmochimica Acta 63:67-77.

Beard, B.L., Johnson, C.M., Skulan, J.L., Nealson, K.H., Cox, L., Sun, H., 2003a. Application of Fe isotopes to tracing the geochemical and biological cycling of Fe. Chemical Geology 195:87-117.

Beard, B.L., Johnson, C.M., Von Damm, K.L., Poulson, R.L., 2003b. Iron isotope constraints on Fe cycling and mass balance in oxygenated Earth oceans. Geology 31:629-632.

Beard, B.L., Johnson, C.M., 2004. Inter-mineral Fe isotope variations in mantle-derived rocks and implications for the Fe geochemical cycle. Geochimica et Cosmochimica Acta 68: 4727-4743.

Bekker, A., Slack, J.F., Planavsky, N.J., Krapez, B., Hofmann, A., Konhauser K.O., Rouxel, O.J., 2010. Iron formation: the sedimentary product of a complex interplay among mantle, tectonic, oceanic and biosphere processes. Economic Geology 105:467-508.

Berg, J., 1977. Regional geobarometry in the contact aureoles of the anorthositic Nain Complex, Labrador. Journal of Petrology 18:399-430.

Berry, A.J., Danyushevsky, L.V., O'Neill, H., Newville, M., Sutton, S.R., 2008. Oxidation state of iron in komatitic melt inclusions indicates hot Archean mantle. Nature. 455:960-963.

Bjerrum, C.J., Canfield, D.E., 2002. Ocean productivity before about 1.9 Gyr ago limited by phosphorus adsorption onto iron oxides. Nature 417:159-162.

Bolhar, R., Kamber, B.S., Moorbath, S., Fedo, C.M., Whitehouse, M.J., 2004. Characterisation of early Archaean chemical sediments by trace element signatures. Earth and Planetary Science Letters 222:43-60.

Bonnichsen, B., 1975. Geology of the Biwabik iron formation, Dunka River area, Minnesota. Economic Geology, 70:319-340.

Bridgewater, D., Watson, J., Windley, B.F., 1973. The Archean craton of the North Atlantic region. Philosophical Transactions of the Royal Society of London Proceedings A 273:493-512.

Bridgewater D., Collerson K.D., 1976. The Major petrological and geochemical characters of the 3600 M.Y Uivak gneisses from Labrador. Contributions to Mineralogy and Petrology 54:43-59.

Bridgewater D., Schiøtte L., 1991. The Archean Gneiss Complex of Northern Labrador: a review of current results, ideas and problems. Bulletin of the Geological Society of Denmark. 39:155-166.

Bullen, T.D., White, A.F., Childs, C.W., Vivit, D.V., Schulz, M.S., 2001. Demonstration of significant abiotic iron isotope fractionation in nature. Geology 29:699-702.

Byrne, R.H., Kim, K-H., 1990. Rare earth element scavening in seawater. Geochimica et Cosmochimica Acta 54:2645-2656.

Cantrell, K.J., Byrne, R.H., 1987. Rare earth element complexation by carbonate and oxalate ions. Geochimica et Cosmochimica Acta 51:597-605.

Croal, L.R., Johnson, C.M., Beard, B.L., Newmann, D.K., 2004. Iron isotope fractionation by Fe(II)-oxidizing photoautotrophic bacteria. Geochimica et Cosmochimica Acta 68:1227-1242.

Czaja, A.D., Johnson C.M., Roden, E.E., Beard, B.L., Voegelin A.R., Nagler, T.F., Beukes, N.J., Wille M., 2012. Evidence for free oxygen in the Neoarchean ocean based on coupled iron-molybdenum isotope fractionation. Geochimica et Cosmochimica Acta 86:118-137.

Danielson, A., Moller, P., Dulski, P., 1992. Chemical Geology 97:89-100.

Dauphas, N., van Zuilen, M., Wadhwa, M., Davis, A.M., Marty, B., Janney, P.E., 2004. Clues from Fe Isotope Variations on the Origin of Early Archean BIFs from Greenland. Science 306:2077-2080.

Dauphas, N., Cates, N.L., Mojzsis, S.J., Busigny, V., 2007a. Identification of chemical sedimentary protoliths using iron isotopes in the > 3750 Ma Nuvvuagittuq supracrustal belt, Canada. Earth and Planetary Science Letters 254:358-376.

Dauphas, N., van Zuilen, M., Busigny, V., Lepland, A., Wadhwa, M., Janney, P.E., 2007b. Iron isotope, major and trace element characterization of early Archean supracrustal rocks from SW Greenland: Protolith identification and metamorphic overprint. Geochimica et Cosmochimica Acta 71:4745-4770.

Dupont, C.l., Yang, S., Bourne, P.E., 2006. Proteomes contain putative imprints of ancient shifts in trace metal geochemistry. PNAS 103:17822-17827.

Dupont, C.L., Butcher, A., Valas, R.E., Bourne, P.E., Caetano-Anolles, G., 2010. History of biological metal utilization inferred through proteomic analysis of protein stuctures. PNAS 107:10567-10572.

Dymek, R.F., Klein, C., 1988. Chemistry, petrology and origin of banded iron-formation lithologies from the 3800 MA isua supracrustal belt, West Greenland. Precambrian Research 39:247-302.

Ewers, W.E., 1980. Chemical conditions for the precipitation of banded iron formations. *In*: Truedinger, P.A., Walter, M.R., Ralph, B.J., Eds. Biogeochemistry of Ancient and Modern Environments, Springer Berlin Heidelberg, p.83-92.

Ewers, W.E., Morris, R.C., 1981. Studies of the Dales Gorge Member of the Brockman iron formation, Western Australia. Economic Geology 76:1929-1953.

Fedo, C.M., Whitehouse, M.J., 2002. Metasomatic origin of quarz-pyroxene rock, Akilia, Greenland, and implications for Earth's earliest life. Science 296:1448-1452.

Fedo, C.M., Whitehouse, M.J., Kamber, B.S., 2006. Geological constraints on detecting the earliest life on Earth: a perspective from the Early Archean (older than 3.7 Gyr) of southwest Greenland. Philosophical Transactions of the Royal Society B 361:851-867.

Fonarev, V.I., Pilugin, S.M., Savko., K.A., Novikova, M.A., 2006. Exsolution textures of orthopyroxene and clinopyroxene in high-grade BIF of the Voronezh Cristalline Massif: evidence of ultrahigh-temperature metamorphism. Journal of Metamorphic Geology 24:135-151.

Frei, R., Polat, A., 2007. Source heterogeneity for the major components of ~ 3.7 Ga Banded Iron Formations (Isua Greenstone Belt, Western Greenland): tracing the nature of interacting water masses in BIF formation. Earth and Planetary Science Letters 253:266-281.

Frost, C.D., Von Blanckenburg, F., Schoenberg, R., Frost, B.R., Swapp, S.M., 2007. Preservation of Fe isotope heterogeneities during diagenesis and metamorphism of banded iron formation. Contribution to Mineralogy and Petrology 153:211-235.

Friend C.R.L., Nutman A.P., McGregor V.R., 1988. Late Archean terrane accretion in the Godthab region, southern West Greenland. Nature 335:535-538.

Friend C.R.L., Nutman A.P., 1994. 2 Archean granulite-facies metamorphic events in the Nuuk -Maanitsoq region, southern West Greenland: correlation with the Saglek Block, Labrador. Journal of the Geological Society 151: 421-424.

Friend C.R.L., Nutman A.P., 2005. New pieces to the Archean terrane jigsaw puzzle in the Nuuk region, southern West Greenland: steps in transforming a simple insight into a complex regional tectonothermal model. Journal of the Geological Society of London 162:147-162.

Friend C.R.L., Nutman A.P., 2007. Adjacent terranes with ca. 2715 and 2650 Ma high-pressure metamorphic assemblages in the Nuuk region of the North Atlantic Craton, southern West Greenland: complexities of Neoarchean collisional orogeny. Precambrian Research 155:159-203.

Gole, M.J., Klein, C., 1981. High-grade metamorphic banded iron formations, Western Australia: assemblages with coexisting pyroxene±fayalite. American Mineralogist 66:87-99.

Hamade, T., Konhauser, K.O., Raiswell, R., Goldsmith, S., Morris, R.C., 2003. Using Ge/Si ratios to decouple iron and silica fluxes in Precambrian banded iron formation. Geology 31:35-38.

Haugaard, R., Frei, R., Stendal, H., Konhauser, K.O., 2013. Petrology and geochemistry of the ~2.9 Ga Itilliarsuk banded iron formation and associated

supracrustal rocks, West Greenland: source characteristics and depositional environment. Precambrian Research 229:150-176.

Hoffman, P.F., 1989. Precambrian geology and tectonic history of North America. In: The geology of North America - an overview. The Geological Society of America. Chapter 16. pp. 447-512.

Isley, A.E., 1995. Hydrothermal plumes and the delivery of iron to banded iron formation. The Journal of Geology 103:169-185.

Jacobsen, S.B., Pimentel-Klose, M.R., 1988. A Nd isotopic study of the Hamersley and Michipicoten banded iron formations: the source of REE and Fe in Archean oceans. Earth and Planetary Science Letters 87:29-44.

James D.T., Kamo S., Krogh T., 2002. Evolution of 3.1 and 3.0 Ga volcanic belts and a new thermotectonic model for the Hopedale Block, North Atlantic Craton (Canada). Canadian Journal of Earth Sciences 39: 687-710.

Johnson, C.M., Skulan, J.L., Beard, B.L., Sun, H., Nealson, K.H., Braterman, P.S., 2002. Isotopic fractionation between Fe(III) and Fe(II) in aqueous solutions. Earth and Planetary Science Letters 195:141-153.

Johnson, C.M., Beard, B.L., Beukes, N.J., Klein, C., O'Leary, J.M., 2003. Ancient geochemical cycling in the Earth as inferred from Fe isotope studies of banded iron formations from the Transvaal Craton. Contributions to Mineralogy and Petrology 144:523-547.

Johnson, C.M., Beard, B.L., Klein, C., Beukes, N.J., Roden, E.E., 2008. Iron isotopes constrain biologic and abiologic processes in banded iron formation genesis. Geochimica et Cosmochimica Acta 72:151-169.

Klein, C., 2005. Some Precambrian banded iron-formations (BIFs) from around the world: Their age, geologic setting, mineralogy, metamorphism, geochemistry, and origins. American Mineralogist 90:1473-1499.

Konhauser, K.O., Pecoits, E., Lalonde, S.V., Papineau, D., Nisbet, E.G., Barley, M.E., Arndt, N.T., Zahnle, K., Kamber, B.S., 2009. Oceanic nickel depletion and a methanogen famine before the Great Oxidation Event. Nature 458:750-753.

Lepland, A., Van Zuilen, M.A., Philippot, P., 2011. Fluid deposited graphite and its geobiological implications in early Archean gneiss from Akilia, Greenland. Geobiology 9:2-9.

Maliva, R.G., Knoll, A.H., Simonson, B.M., 2005. Secular change in the Precambrian silica cycle: Insights from chert petrology. Geological Society of America Bulletin 117:835-845.

Manning, C.E., Mojzsis, S.J., Harrison, T.M., 2006. Geology, age and origin of supracrustal rocks at Akilia,West Greenland. American Journal of Science 306:303-366.

McGregor, V.R., Mason, B., 1977. Petrogenesis and geochemistry of metabasaltic and metasedimentary enclaves of the Amîtsoq gneisses, West Greenland. American Mineralogist 62:887-904.

McGregor V.R., Friend C.R.L., Nutman A.P., 1991. The late Archean mobile belt through Godthabsfjord, southern West Greenland: a continent-continent collision zone? Bulletin of the Geological Society of Denmark 39: 179-197.

McLennan, S.M., Hemming, S., McDaniel, D.K., Hanson, G.N., 1993. Geochemical approaches to sedimentation, provenance and tectonics. GSA Special Papers 284:21-40.

Mojzsis, S.J., Arrhenius, G., McKeegan, K.D., Harrison, T.M., Nutman, A.P., Friend, C.R.L., 1996. Evidence for life on Earth before 3,800 million years ago. Nature 387:55-59.

Mojzsis, S.J., Harrison, T.M., 2002. Establishment of a 3.83 Ga magmatic age for the Akilia tonialite (southern West Greenland). Earth and Planetary Science Letters 202:563-576.

Mojzsis, S.J., Coath, C.D., Greenwood, J.P., McKeegan, K.D., Harrison, T.M., 2003. Mass-independent isotope effects in Archean (2.5 to 3.8 Ga) sedimentary sulfides determined by ion microprobe analysis. Geochimica et Cosmochimica Acta 67:1635-1658.

Monster, J., Appel, P.W.U., Thode, H.G., Schidlowski, M., Carmichael, C.M., 1979. Sulfur isotope studies in early Archean sediments from Isua, West Greenland: implications for the antiquity of bacterial sulfate. Geochimica et Cosmochimica Acta 43:405-413.

Morris, R.C., Horowitz, R.C., 1983. The origin of the iron-formation-rich Hamersley Group of Western Australia – deposition on a platform. Precambrian Research 21:273-297.

Nisbet, E.G., Cheadle, M.J., Arndt, N.T., Bickle, M.J., 1993. Constraining the potential temperature of the Archean mantle: a review of the evidence of komatiites. Lithos 30: 291-307.

Nisbet, E.G., Fowler, C.M.R., 1996. The hydrothermal imprint of life: did heat-shock proteins, metalloproteins and photosynthesis begin around hydrothermal vents? Geological Society Special Publications 118:239-251.

Nutman, A.P., 1986. The early Archean to Proterozoic history of the Isukasia area, southern West Greenland. Bulletin Gronlands Geological Undersurvey 154:80.

Nutman, A.P., Fryer, B.J., Bridgewater, D., 1989. The early Archean Nulliak (supracrustal) assemblage, northern Labrador. Canadian Journal of Earth Sceinces 26:2159-2168.

Nutman, A.P., Collerson K.D., 1991. Very early Archean crustal accretion complexes preserved in the North Atlantic Craton. Geology 19:791-794.

Nutman A.P., Friend C.R.L., Kinny P.D., McGregor V.R., 1993. Anatomy of an early Archean gneiss complex: 3900 to 3600 Ma crustal evolution in southern West Greenland. Geology 21: 415-418.

Nutman, A.P., Friend, C.R.L., 2006. Petrography and geochemistry of apatites in banded iron formation, Akilia, W. Greenland: consequences for oldest life evidence. Precambrian Research 147:100-106.

Papineau, D., Mojzsis, S.J., 2006. Mass-independent fractionation of sulfur isotopes in sulfides from the pre-3770 Ma Isua Supracrustal Belt, West Greenland. Geobiology 4:227-238.

Papineau, D., De Gregorio, B.T., Cody, G.D., O'neil, J., Steele, A., Stroud, R.M., Fogel, M.L., 2011. Young poorly crystalline graphite in >3.8 Gyr-old Nuvvuagittuq banded iron formation. Nature Geosciences 4:376-379.

Planavsky, N.J., Rouxel, O.J., Bekker, A., Hofmann, A., Little, C.T.S., Lyons, T.W., 2012. Iron isotope composition of some Archean and Proterozoic iron formations. Geochemica et Cosmochimica Acta 80:158-169.

Robbins, L.J., Lalonde, S.V., Saito, M.A., Planavsky, N.J., Mloszewska, A.M., Pecoits, E., Scott, C., Dupont, C.L., Kappler, A., Konhauser, K.O., 2013. Authigenic iron oxide proxies for marine zinc over geological time and implications for eukaryotic metallome evolution. Geobiology 11:295-306.

Rosing, M.T., 1999. 13C-depleted carbon microparticles in >3700 Ma sea floor sedimentary rocks from West Greenland. Science 283:674-676.

Rouxel, O.J., Bekker, A., Edwards, K.J., 2005. Iron isotope constraints on the Archean and Paleoproterozoic ocean redox state. Science 307**:**1088–1091.

Saito, M.A., Sigman, D.M., Morel, F.M.M., 2003. The bioinorganic chemistry of the ancient ocean: the co-evolution of cyanobacterial metal requirements and biogeochemical cycles at the Archean-Proterozoic boundary? Inorganica Chimica Acta 356:308-318.

Sandiford, M., Powell, R., 1986. Deep crustal metamorphism during continental extension: modern and ancient examples. Earth and Planetary Science Letters 1986:151-158.

Sharma, M., Polizzotto, M., Anbar, A.D., 2001. Iron isotopes in hot springs along the Juan de Fuca Ridge. Earth and Planetary Science Letters 194:39-51.

Shimizu, H., Umemoto, N., Masuda, A., Appel, P.W.U., 1990. Sources of iron-formations in the archean isua and malene supracrustals, West Greenland: evidence from La-Ce and sm-nd isotopic data and REE abundances. Geochimica et Cosmochimica Acta 54:1147-1154.

Schiøtte L., Bridgewater, D., Collerson, K.D., Nutman, A.P., Ryan, A.B., 1986. Chemical and isotopic effects of late Archean high-grade metamorphism and granite injection on early Archean gneisses, Saglek-Hebron, northern Labrador. Geological Society London Special Publications 24:261-273.

Schiøtte L., Compston W., Bridgwater D., 1989a. Ion probe U-Th-Pb zircon dating of polymetamorphic orthogneisses from Northern Labrador, Canada. Canadian Journal of Earth Sciences 26:1533-1556.

Schiøtte L., Compston W., and Bridgwater D., 1989b. U-Th-Pb ages of single zircons in Archean supracrustals from Nain Province, Labrador Canada. Canadian Journal of Earth Sciences 26:2636-2644.

Schiøtte L., Noble S., Bridgewater D., 1990. U-Pb mineral age from northern Labrador: possible evidence for interlayering of early and middle Archean tectonic slices. Geoscience Canada 17:227-231.

Schiøtte L., Hansen, B.T., Shirey S.B., Bridgewater D., 1993. Petrological and whole rock isotopic characteristics of tectonically juxtaposed Archean Gnisses in the Okak Area of the Nain Province, Labrador: relevance for terrane models. Precambrian Research 63:293-323.

Simard, M., Parent, M., David, J., Sharma, K.N.M. 2003. Géologie de la région de la rivière Innuksuac (34K et 34L). Ministère des Resouces Naturelles, Québec: RG 2002-10:46p.

Simmons, E.C., Lindsley, D.H., Papike, J.J., 1974. Phase relations and crystallization sequence in a contact-metamorphosed rock from the Gunflint Iron Formation, Minnesota. Journal of Petrology 15:539-565.

Sun, S-S., Nesbitt, R.W., 1979. Geochemical characteristics of mid-ocean ridge basalts. Earth and Planetary Science Letters 44:119-138.

Vaniman, D.T., Papike, J.J., 1980. Lunar highland melt rocks: chemistry, petrology and silicate mineralogy. Proceedings of the Conference of the Lunar Highlands Crust 271-337.

Van Zuilen, M.A., Lepland, A., Arrhenius, G., 2002. Reassessing the evidence for the earliest traces of life. Nature 418:627-630.

Van Zuilen, M.A., Lepland, A., Terranes, J., Finarelli, J., Wahlen, M., Arrhenius, G., 2003. Graphite and carbonates in the 3.8 Ga old Isua Supracrustal Belt, southern West Greenland. Precambrian Research 126:331-348.

Van Zuilen, M.A., Matthew, K., Wopenka, B., Lepland, A., Marti, K.,Arrhenius, G., 2005. Geochimica et Cosmochimica Acta 69:1241-1252.

Wu, L., Percak-Dennett, E.M., Beard. B.L., Roden, E.E., Johnson, C.M., 2012. Stable iron isotope fractionation between aquious Fe(II) and moden Archean ocean Fe-Si coprecipitates and implications for iron isotope variations in the ancient rock record. Geochemica et Cosmochimca Acta 84:14-28.

Zerkle, A.L., House, C.H., Brantley, S.L., 2005. Biogeochemical signatures through time as inferred from whole microbial genomes. American Journal of Science 305:467-502.

Table 3.1 Nulliak banded iron formation (BIF), quartz-pyroxene (QP) and metacarbonate (MC) samples and associated mineralogies.

Sample	Rock Type	Mineralogy	Notes
DL-82-26B BR-82-94A Pl-1	BIF BIF BIF	quartz + magnetite + actinolite + inverted pigeonite ±garnet ± biotite ± apatite	no relict microbanding or compositional layering preserved
YM-82-72 BR-82-93	QP QP	quartz + augite ± talc ± calcite ± accessory phases	
PI-3	MC	carbonate + magnetite + diopside + scapolite ± tremolite ± talc ± accessory phases	Reaction zones occur between some of the dopside and carbonate grains.

Figure 3.1 Photomicrographs showing representative textures and petrographic relationships between the main mineral phases in the Nulliak BIF. A) Whole thin section image of sample DL82-26B. Note the weak banding and garnet porphyroblasts in the lower left corner. The main mineral phases are quartz, magnetite, Fe-hornblende (B-C), actinolite (D-E) and clinopyroxene. (D-E). The majority of the actionlite occurs as a tight network of acicular, sometimes radiating grains. Relict clinopyroxene grains often shows exsolution lamellae (D-F). Note the intense recrystallisation of the quartz grains in F and G.

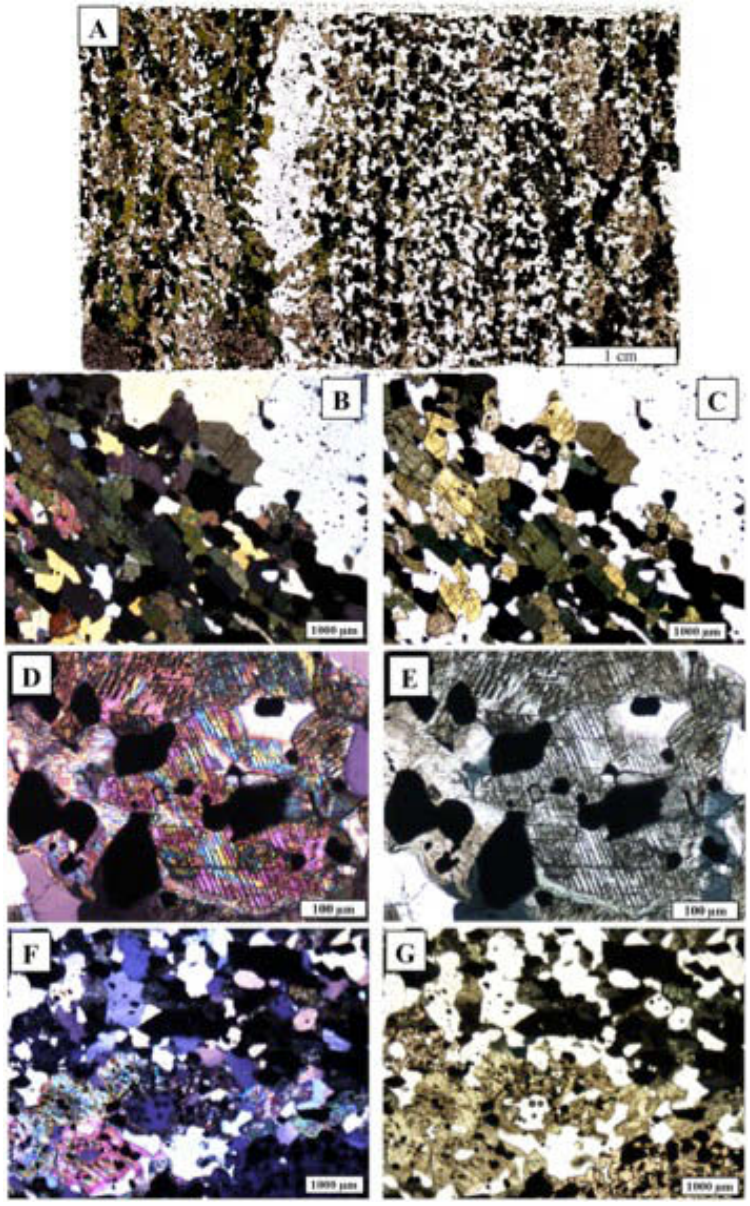
A
1 cm
B
1000 µm
C
1000 µm
D
100 µm
E
100 µm
F
1000 µm
G
1000 µm

Figure 3.2 Photomicrographs showing representative textures and petrographic relationships between the main mineral phases in the Nulliak quartz-pyroxene rocks and metacarbonates. A) Sample YM82-72 showing largely un-banded rock consisting of quartz (red arrows), augite (sometimes forming chains) and secondary actinolite. B) The augite occurs as subhedral, relatively unaltered grains. C) A few grains have minor talc alteration along their rims. D) Metacarbonate sample PI-3 consisting large of carbonate, magnetite, diopside, scapolite, tremolite and accessory chlorite, titanite and olivine. E) The carbonate is largely microcristalline with magnetite occurring largely as very fine-grained and relatively unaltered. F,G) Well-defined, centimeter-thick bands of diopside, scapolite and latered olivine occur.

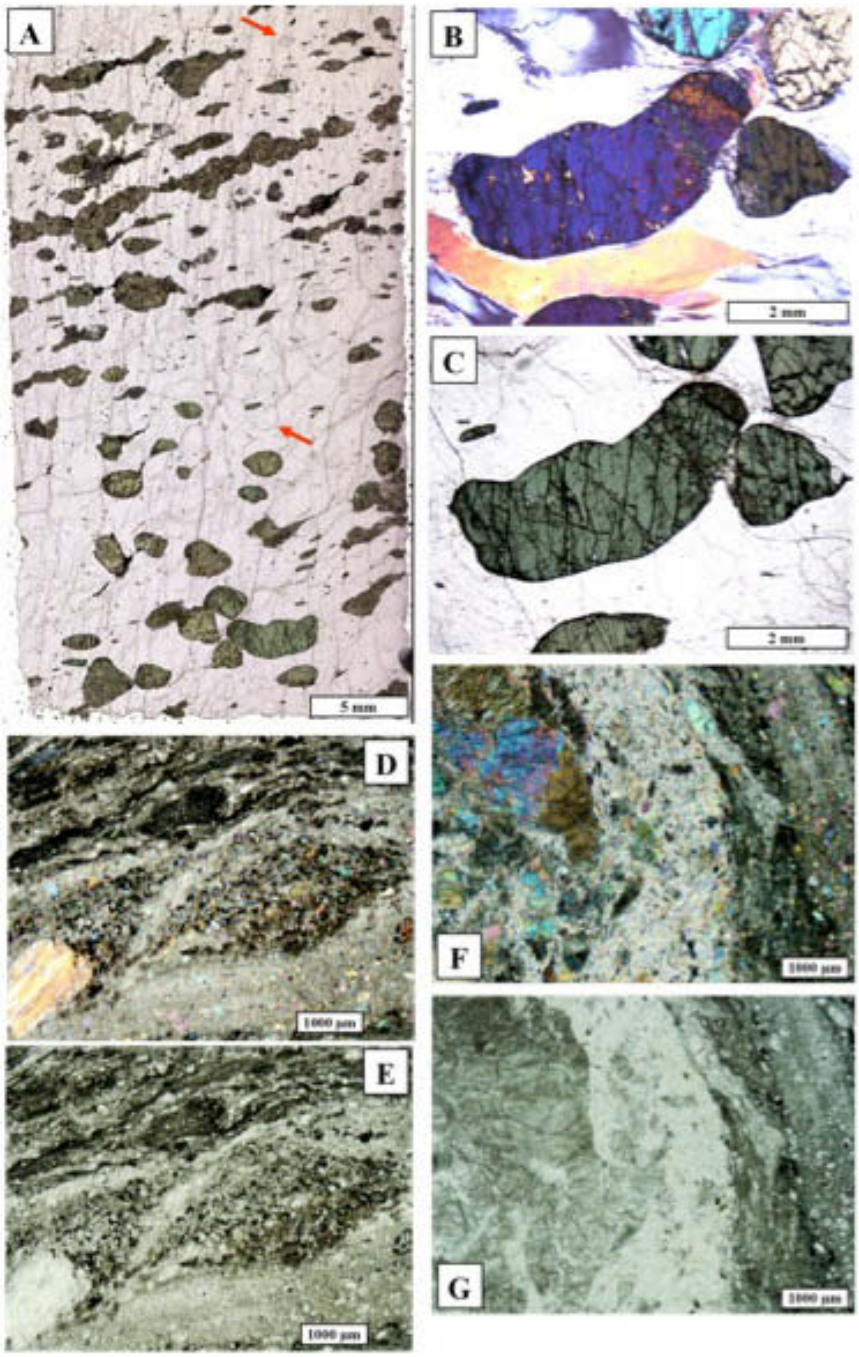
A
5 mm
B
2 mm
C
2 mm
D
1000 µm
E
1000 µm
F
1000 µm
G
1000 µm

Table 3.2 Summary of whole-rock geochemical analyses of the Nulliak banded iron formation (BIF), quartz-pyroxene rocks (QP) and metacarbonate (MC). See supplementary data for full analyses.

Element	DL-82-26B BIF	BR-82-94A BIF	PI-1 BIF	YM-82-72 QP	BR-82-93 QP	PI-3 MC
SiO_2 (wt%)	39.45	44.24	57.16	86.55	85.28	25.75
Al_2O_3	2.73	0.82	1.16	2.44	0.07	0.26
Fe_2O_{3total}	50.29	50.64	37.76	4.11	6.93	8.17
MnO	1.09	0.11	0.20	0.24	0.30	0.51
MgO	3.39	1.74	2.03	1.76	2.56	15.86
CaO	2.85	2.13	2.93	3.99	4.38	27.16
Na_2O	0.17	0.08	0.10	0.37	0.10	0.05
K_2O	0.24	0.21	0.07	0.09	< D.L	0.02
TiO_2	0.15	0.21	0.05	0.07	< D.L	0.01
P_2O_5	0.06	0.11	0.01	0.02	< D.L	< D.L
S	0.006	0.002	0.001	0.439	0.032	0.008
Total	99.66	98.70	100.70	100.40	99.78	99.50
Li (ppm)	3.20	3.11	8.44	0.74	11.03	1.26
Be	1.22	0.83	1.72	0.58	0.34	1.04
V	32.56	6.89	7.62	24.67	0.86	2.07
Cr	100.57	29.17	22.42	44.54	5.20	4.94
Co	18.47	3.67	6.08	8.01	1.10	4.37
Ni	58.48	12.80	42.09	118.93	6.95	8.96
Cu	34.07	8.11	4.84	345.75	7.55	2.74
Zn	77.52	107.95	31.78	302.30	8.69	49.47
Ga	4.43	17.93	4.33	5.14	0.24	1.99
Ge	11.88	12.51	5.23	0.21	0.27	0.82
As	0.95	0.62	0.39	0.22	0.18	0.51
Rb	8.16	15.10	2.66	1.75	0.11	1.55
Sr	33.50	9.43	29.77	33.31	11.55	21.90
Y	9.56	5.45	4.32	9.20	2.19	9.23
Zr	20.40	2.87	3.84	7.64	1.42	4.96
Nb	1.46	1.18	0.59	1.35	0.10	0.29
Mo	1.29	0.50	0.19	1.19	0.18	0.15
Ag	0.06	0.03	0.03	0.19	0.03	0.02
Cd	0.08	<DL	<DL	0.84	<DL	0.06
Cs	0.30	0.11	0.03	0.03	0.01	0.08
Ba	146.45	26.44	63.86	25.22	51.48	6.40
La	6.12	4.47	2.70	2.88	0.68	10.65
Ce	12.77	9.58	5.37	7.15	1.30	20.65
Pr	1.57	1.14	0.60	0.97	0.18	2.09
Nd	6.23	4.44	2.25	4.18	0.66	6.65
Sm	1.26	0.96	0.45	1.25	0.13	1.02
Eu	0.54	0.17	0.20	0.33	0.10	0.19
Gd	1.45	0.97	0.55	1.51	0.18	1.09
Tb	0.20	0.12	0.08	0.24	0.03	0.12
Dy	1.22	0.70	0.49	1.41	0.18	0.70
Ho	0.27	0.14	0.11	0.28	0.04	0.16
Er	0.81	0.38	0.35	0.78	0.15	0.49
Tm	0.11	0.05	0.05	0.11	0.02	0.06
Yb	0.68	0.31	0.30	0.66	0.12	0.37
Lu	0.10	0.05	0.04	0.09	<DL	0.06
Hf	0.64	0.16	0.24	0.32	<DL	0.28
Ta	0.22	0.08	0.16	0.28	<DL	0.32
W	0.31	0.06	0.08	<DL	0.14	0.17
Au	0.15	0.34	0.14	0.03	0.03	0.05
Pb	2.18	1.69	2.25	3.41	1.07	1.49
Th	0.95	0.43	0.50	0.31	0.08	1.22
U	0.25	0.09	0.04	0.27	0.06	0.18

Figure 3.3 Plots showing the relationships between a selection of trace elements, Al and Fe in banded iron formation (BIF) from this study and from Nutman et al., (1989), quartz-pyroxene rocks (QP), and metacarbonate (MC).

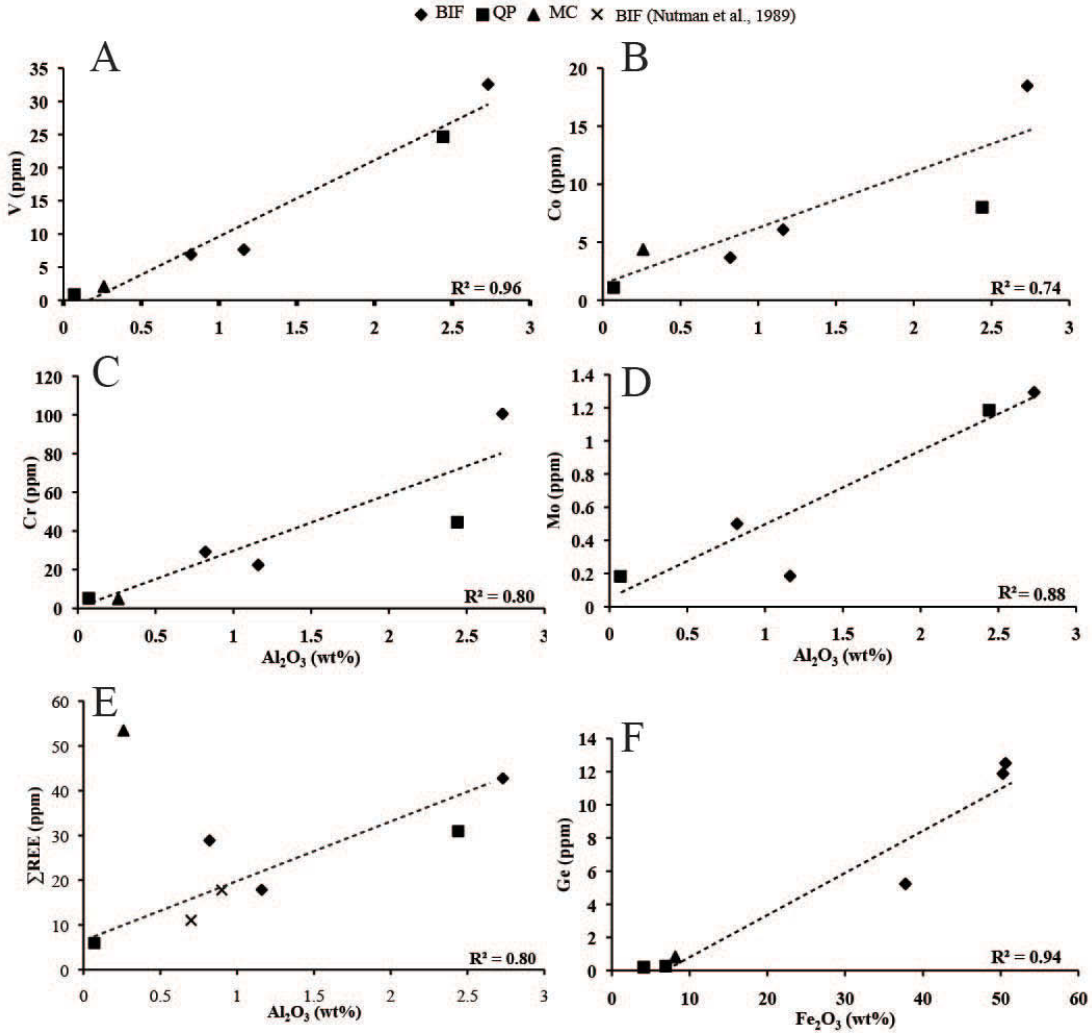
◆ BIF ■ QP ▲ MC × BIF (Nutman et al., 1989)
A
V (ppm)
R² = 0.96
B
Co (ppm)
R² = 0.74
C
Cr (ppm)
R² = 0.80
Al2O3 (wt%)
D
Mo (ppm)
R² = 0.88
Al2O3 (wt%)
E
∑REE (ppm)
R² = 0.80
Al2O3 (wt%)
F
Ge (ppm)
R² = 0.94
Fe2O3 (wt%)

Figure 3.4 REE+Y profiles and associated anomalies of the Nulliak BIF, quartz-pyroxene rocks, and metacarbonate: A) Comparing REE+Y profiles of Nulliak BIF with Pacific seawater (Alibo and Nozaki, 1999). B) Comparing REE+Y profiles of Nulliak quartz-pyroxene rocks (YM82-72 and BR82-93) and metacarbonate (PI-3) with that of Pacific seawater (Alibo and Nozaki, 1999). C) Plot after Bolhar et al., (2004) showing La/La* anomalies for the Nulliak samples. D) Plot comparing Eu/Eu* anomalies normalized to post-Archean Australian Shale (PAAS) with those normalized to Greenland Shale (GS, Bolhar et al., 2005).

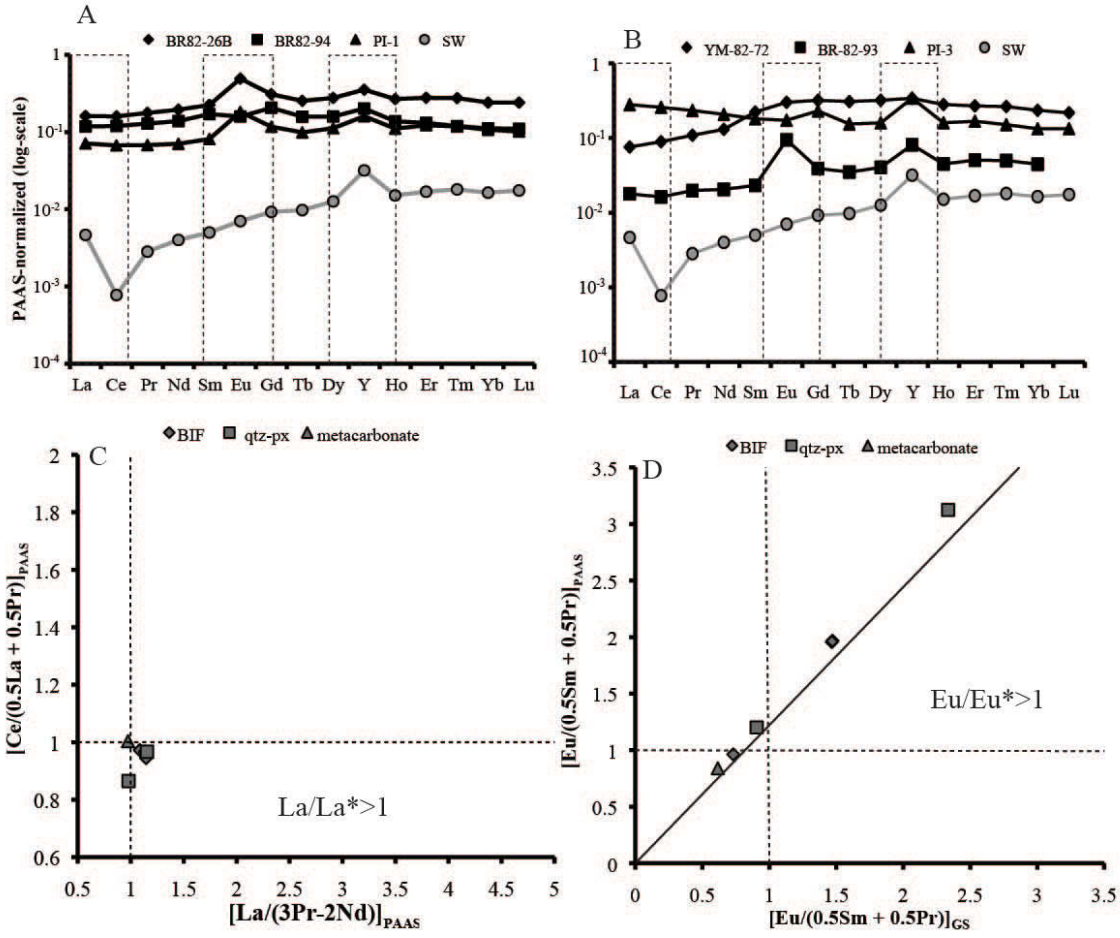
A
BR82-26B
BR82-94
PI-1
SW
PAAS-normalized (log-scale)
La Ce Pr Nd Sm Eu Gd Tb Dy Y Ho Er Tm Yb Lu
B
YM-82-72
BR-82-93
PI-3
SW
C
BIF
qtz-px
metacarbonate
[Ce/(0.5La + 0.5Pr)]PAAS
[La/(3Pr-2Nd)]PAAS
La/La*>1
D
[Eu/(0.5Sm + 0.5Pr)]PAAS
[Eu/(0.5Sm + 0.5Pr)]GS
Eu/Eu*>1

Table 3.3 Fe isotopic compositions of whole-rock banded iron formation (BIF), quartz-pyroxene (QP) and metacarbonate (MC) from the Nulliak Supracrustal Assocation.

Sample	Rock Type	Fe (mol g-1)	Fe/Ti (mol/mol)	δ^{56}Fe (‰, ± 2 SD)
DL-82-26B	BIF	6.30E-03	344.55	0.44± 0.09
BR-82-94A	BIF	6.34E-03	240.07	0.84± 0.09
Pl-1	BIF	4.73E-03	770.83	-0.30± 0.07
YM-82-72	QP	5.15E-04	62.29	-0.44± 0.06
BR-82-93	QP	8.68E-04	2108.93	-0.02± 0.04
PI-3	MC	1.02E-03	817.23	-0.19± 0.05

Figure 3.5 Ternary diagram displaying the chemical composition of clinopyroxenes in the Nulliak banded iron formation (BIF) and quartz-pyroxene rock (qtz-px), in terms of molecular percentages of Wollastonite (Ca), Enstatite (Mg), Ferrosilite (Fe) end members.

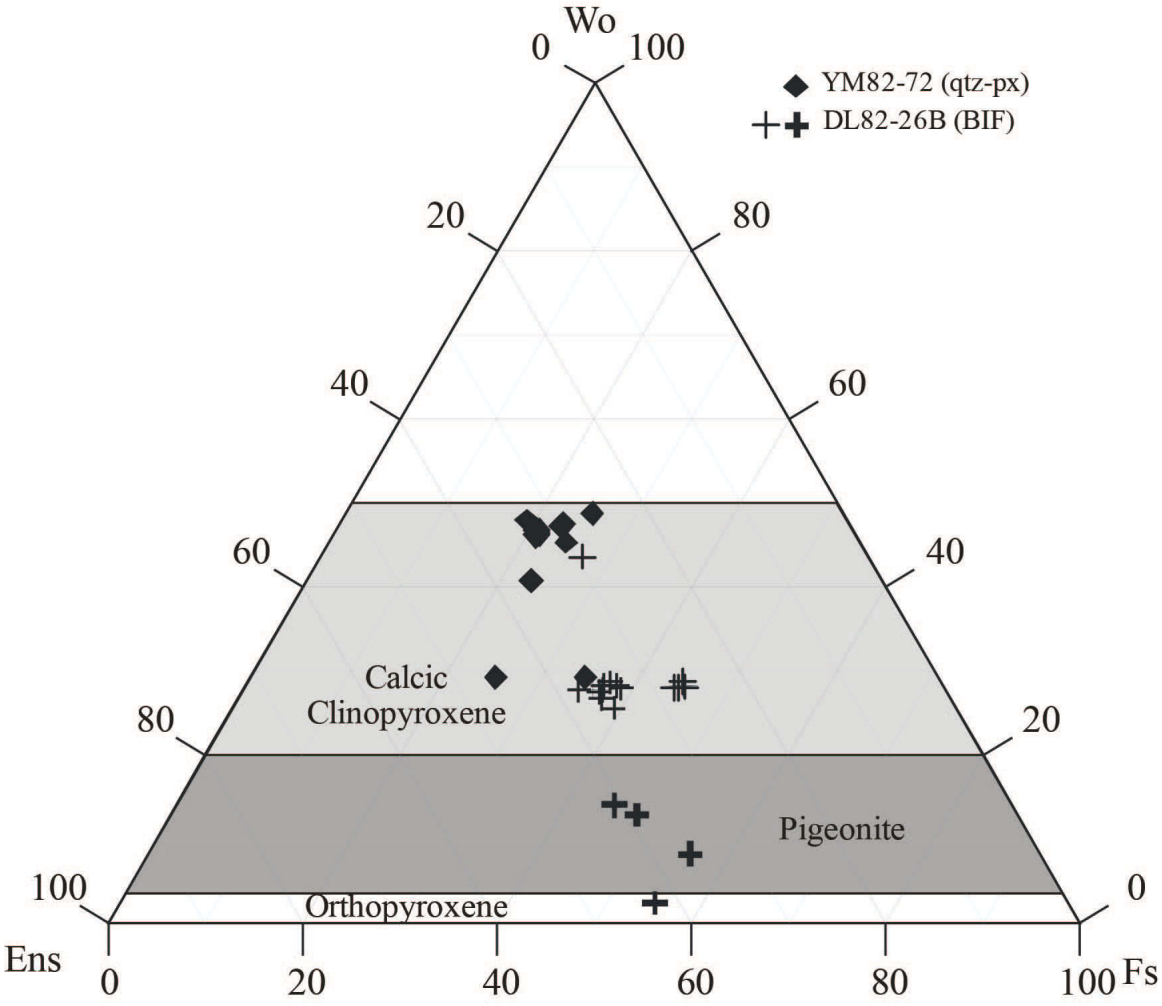
Wo
0
100
YM82-72 (qtz-px)
DL82-26B (BIF)
20
80
40
60
60
40
Calcic
Clinopyroxene
80
20
Pigeonite
100
0
Orthopyroxene
Ens
0
20
40
60
80
100
Fs

Figure 3.6 Two-component mixing model comparing immobile element ratios TiO_2/P_2O_5 vs Cr/Y of BIF from the Isua Supracrustal Belt (Dymek and Klein, 1988; Frei and Polat, 2007; Friend et al., 2008), Nuvvuagittuq Supracrustal Belt (Mloszewska et al., 2012), and Akilia Island (Friend et al., 2008), Barberton tholeiites (Venneman, 1999), Nulliak amphibolites (Nutman et al., 1989), Barberton and Nulliak komatiitic rocks (ultramafic) – Venneman, 1999 and Nutman et al., 1989 respectively, and Nulliak chemical sedimentary rock samples (BIF: DL82-26B, BR82-94, PI-1; quartz-pyroxene: BR82-93). The mixing model shows that the Nulliak chemical sedimentary rocks require between 10-20% Nulliak mafic rocks in order to account for their TiO_2/P_2O_5 and Cr/Y composition. After Manning et al., (2006) and Fedo and Whitehouse (2002).

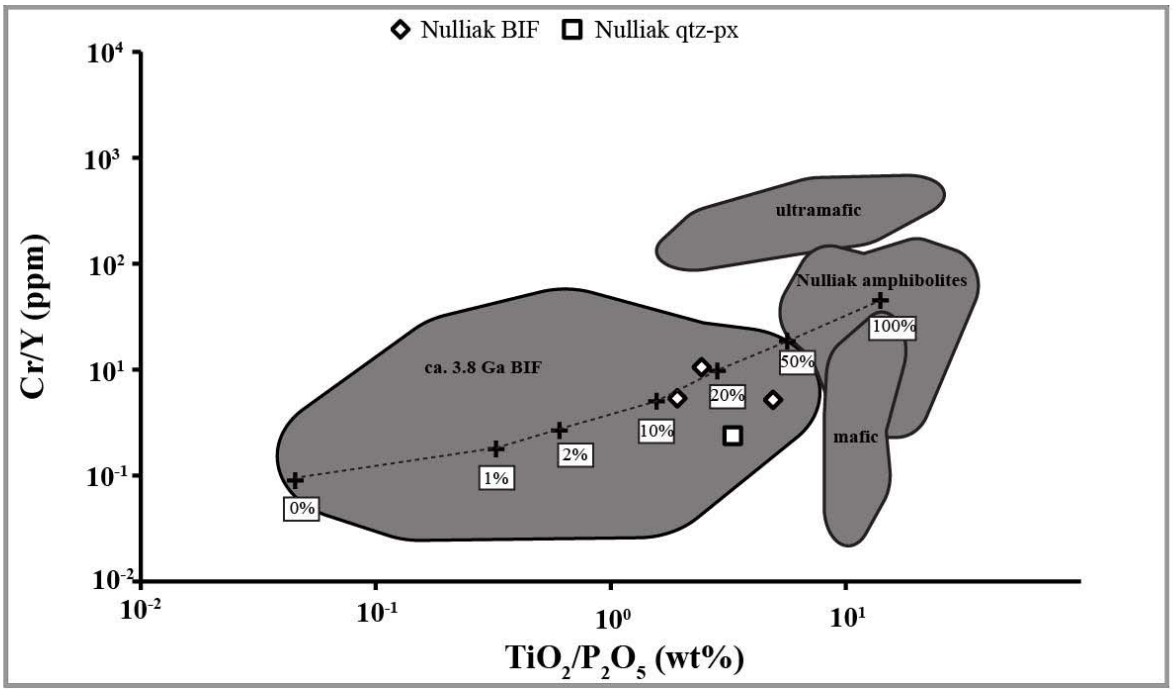
Nulliak BIF
Nulliak qtz-px
ultramafic
Nulliak amphibolites
ca. 3.8 Ga BIF
mafic
0%
1%
2%
10%
20%
50%
100%
Cr/Y (ppm)
TiO2/P2O5 (wt%)

Chapter 4. A geochemical and microbiological study assessing the UV attenuating effects of Fe and Si on the survival of early plantkonic cyanobacteria in Archean seawater

4.1 Introduction

How did free-floating bacteria survive in Archean littoral marine environments in the presence of high-intensity UV radiation? The oldest fossil evidence for life on Earth points to shallow marine environments hosting the earliest photosynthetic microbial ecosystems (Hoffman et al., 1999). With no protective ozone layer to act as a filter (Kasting et al., 1987), these habitats would have been bathed in high-intensity UV radiation. Indeed, UV-B radiation was thought to have been up to 11 times higher in the Archean (Segura et al., 2003). Also, a significant amount of UV-C radiation reached the Archean Earth's surface, whereas virtually none penetrates the ozone layer today (Segura et al., 2003). Incidentally, UV-C radiation is the most harmful to living organisms, by targeting DNA through the production of lesions that distort the double helix structure. This causes critical errors during the translation of genetic material resulting in serious metabolic defects (see review by Sinha and Hader, 2002 and references therein). Due to their mandatory light requirement, photosynthetic bacteria are especially sensitive to the effects of UV damage, yet fossil evidence

suggests that they survived to prosper in ancient high light environments, nevertheless.

Photosynthetic organisms are thought to have ancient origins. Anoxygenic photosynthesis is commonly thought to predate oxygenic photosynthesis, and uses reductants such as H_2S, Fe^{2+}, H_2, SO_3^{2-}, S^0 or S_2O_3 as electron donors instead of H_2O (Nisbet et al., 1995). Fossilized organo-sedimentary structures such as stromatolites are among the earliest forms of geological evidence for photosynthesis. These examples include fossils from the ca. 3.45 Ga Warrawoona Group (Pilbara Craton, Western Australia, Hoffman et al., 1999), as well as from the ca. 3.3 Ga Fig Tree Group (Swaziland Supergroup, South Africa, Byerly et al., 1989). In addition, microbially induced sedimentary structures (MISS), which are formed by microbial mats of filamentous, photosynthetic bacteria, have been characterized in rocks as old as 3.2 Ga in age (Moodies Group, South Africa; Noffke et al., 2006; Heubeck, 2009) and 2.9 Ga (Pongola Supergroup, South Africa, Noffke et al., 2003).

Although the idea that MISS were formed by cyanobacteria remains ambiguous (Noffke et al., 2006; Heubeck, 2009), the suggestion is consistent with evidence from the rock record of oxygenic photosynthesis occurring a few hundred million years prior to the Great Oxidation Event. Excess redox-sensitive Mo and Re isotopes in the ca. 2.5 Ga Mt. McRae Shale (Pilbara Craton), along with consistent, mass-independent, moderately negative $\Delta^{33}S_{sulphide}$ levels from microbial sulphate reduction, imply oxidative weathering of terrestrial sulphides (Kaufman et al., 2007). Stromatolites from the 2.72 Ga year old Tumbiana Formation (Pilbara Craton) that

formed in saline Archean lakes are thought to have been constructed by cyanobacteria. This is evidenced by a deficit in reduced compounds such as Fe^{2+} and SO_4^{2-}, implying oxygenic photosynthesis as the main mechanism for microbial growth (Buick, 1992). Similarly, sulphur and iron depleted kerogenous shales of the 3.2 Ga Gorge Creek Group (northwestern Australia) is consistent with an oxygenic photosynthetic source for the kerogen that they contain (Buick, 2008). Furthermore, recent evidence for extensive mobilization of the redox-sensitive Cr (Ijzermyn iron formation and Nsuze paleosol) and Mo (Sinqeni Formation) from the Pongola Supergroup (South Africa) push the evolution of cyanobacteria back to at least ca 3.0 Ga.

Nevertheless, oxygen levels were still considered to be below the concentrations required for a protective ozone layer (Farquhar et al., 2001; Pavlov and Kasting, 2002). Although microorganisms have inbuilt repair mechanisms to reverse the damage caused by UV radiation (photoreactivation, excision repair, lesion bypass, recombination repair), these systems can become overwhelmed (Singh et al., 2010). Compared with mat-forming bacteria, planktonic (free-floating) bacteria are more susceptible to UV damage as they lack the screening effect provided by extracellular layers or an aggregate lifestyle. Moreover, all mat-forming bacteria have a free-floating, motile stage in their life cycle that enables them to populate new environments (Stoodley et al., 2002). Thus, the means by which bacteria survived to first colonize early littoral (photic) marine environments, perhaps as early as 3.7 Ga, remains uncertain (Dauphas et al., 2007; Rosing and Frei, 2004).

Previous work has demonstrated that Fe(III)-Si gels and crusts overlying microbial mats effectively protect against UV radiation while still allowing enough photosynthetically-active radiation through (Pearson et al., 1993; Phoenix et al., 2001). Furthermore, the abundance of Fe-silicate minerals in Archean-aged banded iron formations, Fe- and Si-rich chemical sedimentary rocks, suggests that Fe has a high affinity for Si and readily complexed in the Archean water column (Klein, 2005). Therefore, could Fe-Si complexes have provided an effective shield planktonic photosynthesizers from incoming UV radiation?

We address this question by growing the planktonic marine cyanobacterium *Synechococcus* sp. PCC 7002 in iron- and silica-rich growth media simulating Archean seawater conditions (Czaja et al., 2012; Maliva et al., 2005). We subsequently irradiate these experimental cultures with UV-C fluxes (254 nm) that were conservatively set to an order of magnitude higher than those predicted for the Archean (3 mW/cm^2 compared with 0.4 mW/cm^2, Segura et al., 2003). Growth media was supplemented with Fe(III) (0.03 to 0.55 mM, Holland, 1984; Ewers, 1980; Morris and Horowitz, 1983, Czaja et al., 2012) and Si, where concentrations varied from 0.6 mM to 2 mM which are, approximately, the saturation with respect to the mineral cristobalite (0.67 mM), to nearing saturation with respect to amorphous silica (2.2 mM) (Maliva et al., 2005). The composition of the Fe(III) and Si supplements was based on studies of BIF composition (Holland, 1984; Ewers, 1980; Morris and Horowitz, 1983; Maliva et al., 2005; Czaja et al., 2012). By using a combination of microbiological techniques, biological and geochemical modeling, we are able to

make accurate predictions as to how the abundant Fe and Si in Archean seawater may have contributed to the survival and thus, earliest microbial colonization of coastal and open marine littoral zones.

4.2 Methods

4.2.1 Culturing

Synechococcus species PCC 7002 (previously known as *Agmenellum quadruplicatum*) is a unicellular, euryhaline marine cyanobacterium that is able to tolerate high light intensities (Nomura et al., 2006). The laboratory wild type strain used in this study was originally obtained from Dr. Donald Bryant (Pennsylvania State University).

Axenic cultures were grown in medium A (Stevens and van Baalen, 1973): 0.3 M NaCl; 8 mM KCl; 20 M $MgSO_4*7H_2O$; 0.37 mM KH_2PO_4; 2.4 mM $CaCl_2$; 0.08 mM Na_2EDTA; 0.01mM $FeCl_3*6H_2O$; P-1 metals (0.6 mM H_3BO_4; 21 mM $MnCl_2*4H_2O$; 2.3 µM ZnCl; 0.2 µM MoO_3; 0.02 µM $CoSO_4*5H_2O$; 0.06 µM $CoCl_2*6H_2O$); 4 µg L^{-1} of vitamin B_{12}, Tris buffered to pH 8.2, and supplemented with 0.01 M $NaNO_3$ (designated A+ media; Stevens and Porter, 1980), per litre of MilliQ water (Nanopure). Axenic stock populations were maintained on 1.5% (w/v) A+ agar plates at 30ºC under constant illumination (~50 µE/m^2/s). Sufficient biomass for UV experiments was obtained by growing large (300 mL) cultures at 30ºC, with shaking at 150 rpm for proper aeration and bubbled with air to ensure sufficient CO_2.

This was used to inoculate experimental cultures (50 mL) at 10% (v/v), in A+ supplemented with silica as Na_2SiO_3 and iron as $FeCl_2*6H_2O$ (as a 14.4 mM ferric iron stock solution in 0.1 N HCl). Pre-existing iron in A+ was taken into account when adding supplemental iron stock to achieve experimental iron concentrations.

4.2.2 UV irradiation experiments

To ascertain the effects of Si and Fe during the UV irradiation of live cells, cultures were irradiated in a Stratalinker UV Crosslinker 1800 containing 5x 254 nm bulbs collectively emitting radiation at 3 W/cm^2. Experimental cultures were grown in media supplemented with: (i) 0.2 mM, 0.6 mM, and 2.0 mM silica and no iron; (ii) 0.6 mM silica and 0.15 mM, 0.35 mM and 0.55 mM iron, (iv) 2.0 mM silica and 0.15 mM, 0.35 mM and 0.55 mM iron, and (v) no iron or silica. Ten milliliters of culture (~$4x10^7$ cells/mL) were poured into sterile plastic Petri dishes, so that a thin veneer of liquid covered the entire surface. Cultures were irradiated at 500 and 1000 J/m^2, where the former were incubated for 8 days, and the latter for 19 days. This was done so as to ascertain patterns of immediate recovery as well as long-term viability and growth. UV dosages were determined by similarly irradiating cultures in baseline A+ media at dosages ranging from 100 to 1000 J/m^2 and assessing growth rate post irradiation using optical density at 750 nm as a proxy for culture growth (Figure 4.1). The UV dosage was chosen based on degree of growth suppression post-irradiation (Figugre 4.1). The irradiated 10 mL cultures were poured into pre-prepared flasks

containing 40 mL of appropriately supplemented A+. After UV irradiation treatments, great care was taken not to expose cultures to wavelengths <520 nm at which they could photoreactivate. To this end, cultures were incubated in the dark for up to 6 hours immediately after UV treatment, after which PAR light was filtered through Roscolux Supergel filter plastic (#15).

4.2.3 Determination of cell viability post-irradiation

Growth rate was monitored via total chlorophyll a concentrations as a proxy for culture viability post-irradiation. A description of the chlorophyll a extraction methods can be found in Sakamoto and Bryant (1998). Immediately upon irradiation, the 10 mL experimental culture was poured into a pre-prepared 250 mL Erlenmyer flask containing 40 mL of A+ treated with appropriate amounts of iron and silica, incubated at 30ºC, and shaken at 150 rpm. Flasks were dark-incubated for the first 6 hours post-irradiation in order to prevent photoreactivation. Subsequently, aliquots were taken in duplicate every day or every third day for chlorophyll a analysis and optical density measurements at 750 nm (OD_{750}). The ratio of live to dead cells was determined indirectly, by way of counting the number of colony forming units (CFU) growing in samples plated on agar post-irradiation (an estimate of viability). Aliquots (100 uL) of each sample were streaked on agar plates, and incubated for ~10 days at 30ºC, and wavelengths <520 nm were filtered from the incoming fluorescent light. The number of initial cells in each culture, determined by way of their OD_{750}

measurements, was then subtracted from the number of CFU counted in each plate assuming that one CFU was formed by one viable cell.

4.2.4 UV attenuation and colloid size characterization

UV attenuation by the various media solutions supplemented with iron and/or silica was evaluated by measuring the % transmission of UV radiation at 254 nm with an ultraviolet spectrophotometer in quartz cuvettes with 1 cm path lengths. In order to ascertain a size range for the particulate matter causing the UV attenuation, solutions were filtered twice, firstly to 0.2 μm, whereupon UV attenuation at 254 nm was measured. The filtrate was subsequently filtered to 0.025 μm and measurement of UV attenuation at 254 nm was repeated. We had originally attempted to measure colloid particle size on a Malvern Zetasizer, however, however the media was deemed to polydisperse to yield accurate results. Therefore, the above methodology was used instead.

4.2.5 Geochemical Modeling

Equilibrium solution compositions were calculated using Visual MINTEQ version 3.0 (Gustafsson, 2011) where the thermodynamic database was updated to include stability constants for aqueous Fe^{+3}-Si complexes. Modeling parameters included (i) standard room temperature (25ºC) in order to facilitate comparison between geochemical models in the literature, (ii) supersaturated minerals were permitted to

precipitate, (iii) salinity was determined by the ionic strength of the solution, and (iv) activity coefficients were calculated using the Davis Equation.

4.3 Results

Figure 4.2 shows that *Synechococcus* cultures exposed to UV-C in supplemented media grew faster than un-supplemented irradiated cultures. Growth rates increased steadily as initial Fe-Si concentrations in the media approached the conservative theoretical upper limits for Archean seawater (Fe(III)=0.55 mM; Si=2.0 mM). This suggests that the elevated levels of Fe and Si present in Archean seawater protected cellular life from the harmful effects of the high-intensity UV radiation reaching Earth surface at the time. Si alone, even at the highest concentration, protects cells less efficiently from UV radiation than Fe and Si combined, suggesting that both supplements are required for a synergistic protective effect. Importantly, this protection extends to environments estimated to have had much lower background Fe concentrations (0.03 mM; Holland et al., 1984), habitats beyond the reach of upwelling Fe-rich waters, such as isolated lagoons (Figure 4.3). While UV-irradiation trials brought cell numbers down to less than 3% of the initial bacterial population, Figure 4.2A (inset) suggests that those surviving individuals were able to seed a population increase back to pre-exponential phase in UV-free cultures after only 6 days. Cell viability assays that reveal a positive correlation between initial Fe(III)-Si concentration and bacterial survival rate, from 0.13% viable cells in un-supplemented

media to 2.76% at the highest initial Fe(III)-Si concentrations. Collectively, these results suggest that Fe(III) and Si jointly provide effective protection against incoming UV-C radiation that is observable on a cellular level.

Transmission electron microscopy was used to ascertain the means by which the Fe(III) and Si were facilitating the UV protection. Transmission electron micrographs of Fe- and Si-supplemented cultures show fine-grained precipitates surrounding (but not directly attached to) the cell masses, with particle sizes in the tens of nanometer range (Figure 4.4). This suggests that particulate Fe(III)-Si complexes, instead of biomineralized coatings, were shielding the cells from incoming UV-C radiation. Chemical equilibrium modeling of the iron and silica supplemented growth media shows that it becomes mildly supersaturated with respect to ferrihydrite - [$Fe(OH)_3$], while the remainder of the ferric iron is partitioned as either soluble organic Fe(III)-EDTA or inorganic Fe species, such as Fe(III) (Figure 4.5). UV attenuation assays on supplemented growth media in the absence of bacteria concur with the growth analyses. These assays indicate that the Fe(III)-Si supplements differentially and progressively attenuate UV-C by ~21% in Si-only media; by ~62% in the lowest Fe(III)-Si end-members (0.15 mM Fe(III), 0.6 mM Si), and by ~73% in the highest Fe(III)-Si end-members (0.55 mM Fe(III), 2.0 mM Si) (Figure 4.6). Filtration analyses indicated that solid Fe(III)-Si particles between 0.025 and 0.22 um in size absorb ~27% of incoming UV-C while the soluble Fe(III)-Si colloidal species provide up to 40% of the UV-C attenuation (Figure 4.6). These filtration analyses suggest that while solid ferrihydrite in the growth media may

absorb a significant proportion of the incoming UV. However, these particles would presumably settled out of the water column, thereby playing a lesser role in UV attenuation in the long run. In contrast, the nanometer-sized Fe(III)-Si colloids that were observed would remain in suspension for longer time periods. The absence of equilibrium constants for polymeric Fe(III)-Si complexes precludes accurate equilibrium models of natural Fe(III)-Si rich aqueous systems at circum-neutral pH, however, their formation has been characterized spectroscopically (Pokrovsky et al., 2003). Nonetheless, our collective results suggest that the formation of colloidal Fe(III)-Si complexes in the simulated Archean growth media are responsible for the observed UV attenuation patterns.

4.4 Discussion

How did the earliest photosynthetic microorganisms survive high incident levels of UV radiation to first colonize early marine littoral zones? The earliest fossil evidence for life has been recovered from ancient littoral environments, such as restricted lagoonal settings (observed for example in stromatolites from the ca. 3.45 Ga Strelly Pool Chert, Pilbara Craton, Australia; Allwood et al., 2006) and zones of high sedimentation, such as tidal flats and estuaries (the MISS of the 3.48 Ga Dresser Formation, also in the Pilbara, for instance; Noffke et al., 2013). The benthic lifestyle depicted by these fossils provides significant protection against UV radiation, and has been invoked by some as a prerequisite for surviving the high levels of incident UV

radiation during the Archean (Knoll, 1979). Indeed, exopolysaccharides (EPS) and extracellular sheaths produced by mat-forming bacteria would have provided a substrate for UV-absorbing substances, such as microsporine amino acids and scytonemin (Ehling-Shultz et al., 1997; Quesada et al., 1999), while the mineralized coating of bacteria living an aggregate lifestyle would serve as physical barriers against UV radiation (Phoenix et al., 2006). However, the microorganisms that formed MISS are not thought to have had the benefit of a mineralized cover (Heubeck, 2009), and would have been at a distinct disadvantage to the microbes that formed ancient stromatolites. Most importantly, however, all mat-forming bacteria spread to new environments via a free-living motile stage (Stoodley et al., 2002).

The results presented in this study suggest that the Fe(III)-Si colloids forming in Fe- and Si- rich Archean water column would have provided effective protection against incoming UV radiation. Indeed, Fe(II) and Fe(III) are known to be efficient absorbers of UV radiation especially at the shorter wavelengths (Olson and Pierson, 1986). The additive nature of the UV absorbance curves for Fe(III)-Si and Fe(III)-only media solutions and their comparable slopes (Figure 4.3B) indicate that Fe(III) is controlling the attenuation of UV-C in these experiments. Importantly however, aqueous silica inhibits the transformation of aqueous Fe(III) polymers into ferrihydrite particles at pH>3 (Pokrovsky et al., 2003). Si disrupts the corner-linkages between the Fe-octahedra of the polymer and substitutes itself into the second coordination-shell around the iron ion (Cismeau et al., 2014). Thus, aqueous silica plays a major role in this protective mechanism by maintaining the solubility of

Fe(III), enabling it to function as a UV-C sunscreen. From a cellular standpoint, this mechanism likely occurred since at least 3.8 Ga (Klein, 2005), the age of the oldest BIF. Although the means of Fe(II) oxidation in anoxic Archean seawater are still debated (Bekker et al., 2010), it has been argued that photoferrotrophs metabolically oxidizing Fe(II) was the most plausible source of Fe(III) at the time. Photooxidation, albeit a significantly slower and less productive process, was another potential oxidation mechanism (Konhauser et al., 2002).

Although a planktonic cyanobacterium was used in this study, our model equally extends to the anoxygenic photosynthesizers that inhabited the Archean water column. Moreover, recent evidence suggests that oxygenic photosynthesis may have evolved by ca. 3.0 Ga (Crowe et al., 2013; Planavsky et al., 2014). Fossil evidence suggests that cyanobacteria had become part of Archean benthic communities by 2.7 Ga (stromatolites of the Tumbiana Formation, Pilbara Craton, Western Australia; Bosak et al., 2009) and perhaps even by 3.2 Ga (black shales of the Gorge Creek Group, northwestern Australia; Buick, 2008). Furthermore, the laminated textures found in some MISS occurrences can preserve filament-like fabrics that strongly resemble those of modern filamentous, mat-forming bacteria in both size and shape (e.g., phototrophic cyanobacteria of the class Oscillatoriacea and chemotrophic sulfur oxidizing bacteria such as *Beggiatoa*; Noffke et al., 2003).

Photosynthetic planktonic bacteria living in photic zone offshore were equally susceptible to UV radiation. A radiative transfer model of the Neoarchean water column suggests that only at a depth of 30 m would DNA damage rate to organisms

have reached levels at the modern ocean surface (Cockell, 2000). In this mixed layer, phytoplankton would have been at high risk of being transported to the surface (Neale et al., 1998). Despite the intracellular mechanisms that bacteria might have evolved at that time to overcome the effects of UV radiation (photoreactivation, excision repair, mutagenic repair/lesion bypass, recombination repair) (Sinha and Hader, 2002), by Archean standards, extant planktonic bacteria can only tolerate significantly lower levels of UV irradiation (Joux et al., 1999). A fundamental question that has until now remained unanswered is how these exposed organisms overcame detrimental UV stresses in order to propagate and colonize the earliest microbial ecosystems. The Fe(III)-Si protective model that we provide evidence for, holds for any microorganism growing in the Archean photic zone, and would almost certainly be valid for those growing at depth.

4.5 Conclusions

UV radiation is thought to have been one of the main obstacles facing the successful propagation of early life (Knoll, 1979). In modern seawater environments, the UV radiation in the upper few meters of the water column presents a considerable challenge to extant microorganisms (Joux et al., 1999). The absence of an ozone layer during the Archean eon meant that UV radiation reaching the ancient Earth's surface was several times higher than it is today (Segura et al., 2003). The initial colonization of early littoral marine environments and the subsequent success of early

photosynthetic life depended on the successful protection of free-floating microorganisms.

The model presented in this study suggests that the high Fe(III) and Si contents of Archean seawater acted as an effective sunscreen against incident UV-radiation, thus enabling the survival of the earliest free-floating bacteria. The Fe(III)-Si colloids in Archean seawater facilitated the propagation of early microogranisms throughout the Archean marine littoral zones, as evidenced by the Mesorchean fossil record (Hoffman et al., 1999; Allwood et al., 2006; Heubeck, 2009). Furthermore, both mat-forming and free-floating cyanobacteria could have flourished in the presence of high UV fluxes, allowing the production of the low levels of free oxygen that have been observed in the rock record as early as 2.95 Ga (Planavsky et al., 2014). The shielding role of Archean seawater implies that phototrophic bacteria could have been free to be carried by currents to colonize the photic zone across the planet, and ultimately allowed early cyanobacteria to produce the O_2 required for the Great Oxidation Event.

References

Allwood, A.C., Walter, M.R., Kamber, B.S., Marshall, C.P., Burch, I.W., 2006. Stromatolite reef from the early Archean era of Australia. Nature 44:714-718.

Bekker, A., Slack, J.F., Planavsky, N., Krapez, B., Hofmann, A., Konhauser, K.O., Rouxel, O.J., 2010. Iron formation: the sedimentary product of a complex interplay among mantle, tectonic, ocean and biospheric processes. Economic Geology 105:467-508.

Bosak, T., Liang, B., Sim, M.S., 2009. Petroff, A.P. Morphological record of oxygenic photosynthesis in conical stromatolites. PNAS 106:10939-10943.

Buick, R., 1992. The antiquity of oxygenic photosynthesis: evidence from stromatolites in sulphate-deficient Archean lakes. Science 255:74-77.

Buick, R. 2008. When did oxygenic photosynthesis evolve? Philosophical Transactions of the Royal Society B 363:2731-2743.

Byerly, G.R., Lower, D.R., Walsh, M.M., 1989. Stromatolites from the 3,300-3,500 Myr Swaziland Supergroup, Barberton Mountain Land, South Africa. Nature 319:489-491.

Cismeau, A.C., Michel, F.M., Tcaciuc, A.P., Brown, G.E. Jr., 2014. Properties of impurity-bearing ferrihydrite III. Effects of Si on the structure of 2-line ferrihydrite. Geochim. Cosmochim. Acta 133:168-185.

Cockell, C.S., 2000. Ultraviolet radiation and the photobiology of Earth's early oceans. Origin of Life and Evolution of the Biosphere 30:467-499.

Crowe, S.A., Dossing, L.N., Beukes, N.J., Bau, M., Kruger, S.J.., Frei, R., Canfield, D.E., 2013. Atmospheric oxygenation three billion years ago. Nature 501:535-538.

Czaja, A.D., Johnson C.M., Roden, E.E., Beard, B.L., Voegelin A.R., Nagler, T.F., Beukes, N.J., Wille M., 2012. Evidence for free oxygen in the Neoarchean ocean based on coupled iron-molybdenum isotope fractionation. Geochimica et Cosmochimica Acta 86:118-137.

Dauphas, N., Cates, N.L., Mojzsis S.J., Busigny, V., 2007. Identification of chemical sedimentary protoliths using iron isotopes in the >3.75 Ga Nuvvuagittuq Supracrustal Belt, Canada. Earth and Planetary Science Letters 254:358-376.

Ehling-Shultz, M., Bilger, W., Scherer, S., 1997. UV-B-induced synthesis of photoprotective pigments and extracellular polysaccharides in the terrestrial cyanobacterium Nostoc commune. Journal of Bacteriology 179:1940-1945.

Ewers, W.E.,1980. Chemical conditions for the precipitation of banded iron formations. In Biogeochemistry of Ancient and Modern Environments, Springer Berlin Heidelberg, p.83-92.

Farquhar, J., Savarino, J., Airibeau, S., Thiemens, M.H., 2001. Observation of wavelength-sensitive mass-independent sulfur isotope effects during SO_2 photolysis: implications for the early atmosphere. Journal of Geophysical Research 106:32829-32839.

Grotzinger, J.P., Knoll, A.H., 1999. Stromatolites in Precambrian carbonates: evolutionary mileposts or environmental dipsticks? Annual Reviews in Earth and Planetary Science 27:313-358.

Gustafsson, J.P. 2011. Visual Minteq 3.0: http: //www2.lwr.kth.se/English/OurSoftware/vminteq.

Heubeck, C., 2009. An early ecosystem of Archean tidal microbial mats (Moodies Group, South Africa, ca. 3.2 Ga). Geology 37:931-934.

Hoffman, H.J., Grey, K., Hickmann, A.H., Thorpe, R.I., 1999. Origin of 3.45 Ga coniform stromatolites in Warrawoona Group, Western Australia. GSA Bulletin 111:1256-1262.

Holland, H.D., 1984. The chemical evolution of the atmosphere and oceans. Princeton University Press. 582p.

Joux, F., Jeffrey, W.H., Lebaron, P., Mitchell, D.L., 1999. Marine bacterial isolates display diverse responses to UV-B radiation. Applied and Environmental Microbiology 65:3820-3827.

Kasting, J.F., 1987. Theorectical constraints on oxygen and carbon dioxide concentrations in the Precambrian atmosphere. Precambrian Research 34:205-229.

Kaufman, A.J., Johnston, D.T., Farquhar, J., Masterson, A.L., Lyons, T.W., Bates, S., Anbar, A.D., Arnold, G.L., Garvin, J., Buick, R.. 2007. Late Archean biospheric oxygenation and atmospheric evolution. Science 317:1900-1903.

Klein, C., 2005. Some Precambrian banded iron formations (BIFs) from around the world: their age, geological setting, mineralogy, metamorphism, geochemistry and origin. American Mineralogist 90:1473-1499.

Knoll, A.H., 1979. Archean photoautotrophy: some alternatives and limits. Origins of life. 9:313-327.

Konhauser, K.O., Hamade, T., Raiswell, R., Morris, R.C., Ferris, F.G., Southam, G., Canfield, D.E., 2002. Could bacteria have formed the Precambrian banded iron formations? Geology 30:1079-1082.

Konhauser, K.O., Amskold, L. Lalonde, S.V., Posth, N.R., Kappler, A., Anbar, A., 2007. Decoupling photochemical Fe(II) oxidation from shallow-water BIF deposition. Earth and Planetary Science Letters 258:87-100.

Konhauser, K.O., Lalonde, S.V., Planavsky, N.J., Pecoits, E., Lyons , T.W., Mojzsis, S.J., Rouxel, O.J., Barley, M.E., Rosiere, C., Fralick, P.W., Kump, L.R., Bekker, A., 2011. Aerobic bacterial pyrite oxidation and acid rock drainage during the Great Oxidation Event. Nature 478:369-373.

Maliva, R.G., Knoll, A.H., Simonson, B.M., 2005. Secular change in the Precambrian silica cycle: insight from chert petrology. GSA Bulletin 117:835-845.

Morris, R.C., Horowitz, R.C., 1983. The origin of the iron formation rich Hamersley Group of Western Australia - deposition on a platform. Precambr. Res., 21:273-297.

Neale, P.J., Davis, R.F., Cullen, J.J., 1998. Interactive effects of ozone depletion and vertical mixing on the photosynthesis of Antarctic phytoplankton. Nature 392:585-589.

Nisbet, E.G., Cann, J.R., Van Dover, C.L., 1995. Origin of photosynthesis. Nature 373:479.

Noffke, N., Hazen, R., Nhelko, N., 2003. Earth's earliest microbial mats in a siliciclastic marine environment (2.9 Ga Mozaan Group, South Africa). Geology 31:673-676.

Noffke, N., Eriksson, K.A., Hazen, R.M., Simpson, E.L., 2006. A new window into early Archean life: microbial mats in Earth's oldest siliciclastic tidal depost (3.2 Ga Moddies Group, South Africa). Geology 34:253-256.

Noffke, N., Christian, D., Wacey, D., Hazen, R.H., 2013. Microbially induced sedimentary structures recording an ancient ecosystem in the ca. 3.48 billion-year-old Dresser Formation, Pilbara, Western Australia. Astrobiology 13:1103-1124.

Nomura, C.T., Persson, S., Shen, G., Inoue-Sakamoto, K., Bryant, D.A., 2006. Characterization of two cytochrome oxidase operons in the marine cyanobacterium Synechococcus sp. PCC 7002: Inactivation of ctaDI affects the PS I:PS II ratio. Photosythesis Research 87:215-228.

Olson, J.M., Pierson, B.K., 1986. Photosynthesis 3.5 thousand million years ago. Photosynthesis Research 9:251-259.

Pavlov, A.A., Kasting, J.F., 2002. Mass-independent fractionation of sulfur isotopes in Archean sediments: strong evidence for an anoxic Archean atmosphere. *Astrobiology* 2:27-41.

Phoenix, V.R., Konhauser, K.O., Adams, D.G., Bottrell S.H., 2001. Role of biominiralization as an ultraviolet shield: implications for Archean life. Geology 29:823-826.

Phoenix, V.R., Bennett, P.C., Engel, A.S., Tyler, S.W., Ferris, F.G., 2006. Chilean high-altitude hot-spring scinters: a model system for UV screening mechanisms by early Precambrian cyanobacteria. Geobiology 4:15-28.

Pierson, B.K., Mitchell, H.K., Ruff-Roberts, A.L., 1993. Chloroflexus aurantiacus and ultraviolet radiation: implications for Archean shallow-water stromatolites. Origins of Life and Evolution of the Biosphere 23:243-260.

Planavsky, N.J., Asael, D., Hofmann, A., Reinhard, C.T., Lalonde, S.V., Knudsen, A., Wang, X., Ossa Ossa, F., Pecoits, E., Smith, A.J.B., Beaukes, N.J., Bekker, A., Johnson, T.M, Konhauser, K.O., Lyons, T.W., Rouxel, O.J., 2014. Evidence for oxygenic photosynthesis half a billion years before the great oxidation event. Nature Geoscience 7:283-286.

Pokrovski, G.S., Schott J., Farges, F., Hazemann J-L., 2003. Iron(III)-silica interactions in aqueous solutions: insight from x-ray absorption fine structure spectroscopy. Geochimica et Cosmochimica Acta 19:3559-3573.

Quesada, A., Vincent, W.F., Lean, D.R.S., 1999. Community and pigment structure of Arctic cyanobacterial assemblages: the occurrence and distribution of UV-absorbing compounds. FEMS Microbiology Ecology 28:315-323.

Rosing, M.T., Frei, R., 2004. U-rich Archaean sea-floor sediments from Greenland: indications of 3700 Ma oxygenic photosynthesis. Earth and Planetary Science Letters 217:237–244.

Sakamoto, T., Bryant, D.A., 1998. Growth at low temperature causes nitrogen limitation in the cyanobacterium Synechococcus sp. PCC 7002. Archives of Microbiology 196:10-19.

Segura, A., Krelove, K., Kasting, J.F., Sommerlatt, D., Meadows, V., Crisp, D., Cohen, M., Mlawir, E., 2003. Ozone concentrations and ultraviolet fluxes on Earth-like planets around other stars. Astrobiology 3:689-708.

Singh, S.P., Hader, D-P., Sinha, R.P., 2010. Cyanobacterial and ultraviolet radiation (UVR) stress: mitigation strategies. Ageing Research Reviews 9:79-90.

Sinha, R.P., Hader D-P., 2002 UV-induced DNA damage and repair: a review. Photochemical and Photobiological Sciences 1:225-236.\

Stevens, S.E Jr., Van Baalen, C., 1973. Characteristics of nitrate reduction in a mutant of the blue-green alga Agmenellum quadruplicatum. Plant Physiology 51:350-356.

Stevens, S.E & Porter, R.D., 1980. Transformation in Agmenellum quadruplicatum. Proeedings to the National Acadademy of Science 77, 6052-6056.

Stoodley, P., Sauer, K., Davies, D.G., Costerton, J.W., 2002. Biofilms as complex differentiated communities. Annual Reviews in Microbiology 56, 187-209.

Figure 4.1 Growth trials for *Synechococcus* sp. PCC 7002 grown in unsupplemented A+ media, for UV doses ranging from 100 J/m^2 to 1000 J/m^2. The optical density at 750 nm represents cellular growth rates over the number of days post incubation. The UV doses chosen for the UV experiments in this study (500 J/m^2, 1000 J/m^2) were based on the maximum depression of cellular growth rates on unsupplemented cultures.

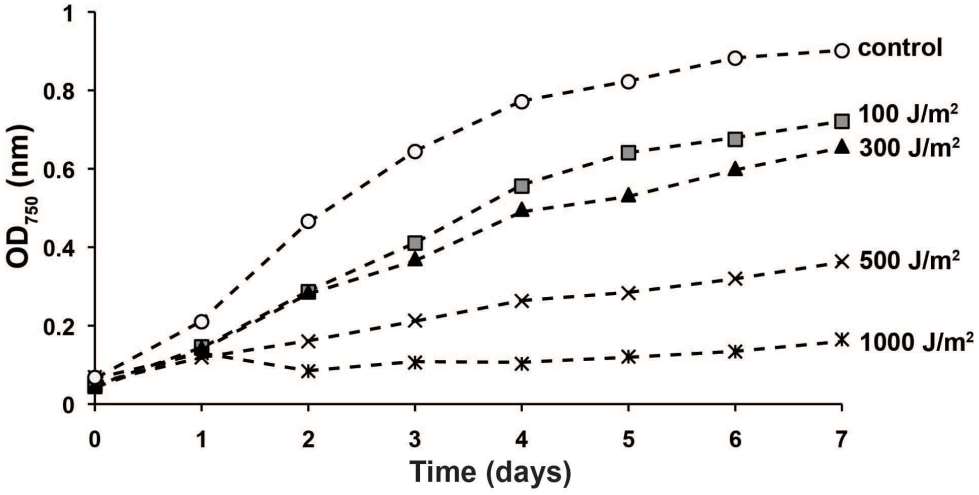
1
0.8
0.6
0.4
0.2
0
OD750 (nm)
0
1
2
3
4
5
6
7
Time (days)
control
100 J/m²
300 J/m²
500 J/m²
1000 J/m²

Figure 4.2 Growth rates of *Synechococcus* sp. PCC 7002 using the concentration of the pigment chlorophyll *a* measured over a number of days. Growth rates of UV irradiated cultures grown in unsupplemented A+ growth media ('control UV'), low Fe(III)/Si (0.15 mM/0.6 mM), high Fe/Si (0.55 mM/2.0 mM), and Si only (2.0 mM), are compared with non-irradiated cultures grown in unsupplemented A+ media ('control no UV'). These Fe(III) concentrations represent Archean environments exposed to Fe upwelling. A) Cultures irradiated at a UV dose of 500 J/m^2, and subsequently grown for 19 days; the inset shows the viability of these irradiated cultures where % survival was derived from colony forming unit (CFU) counts of plated cultures post-irradiation. B) Cultures irradiated at 1000 J/m^2 and subsequently grown for 8 days are most effectively protected by the highest Fe(III)-Si supplements, while Si alone does not appear to have a significant protective effect at such high UV doses.

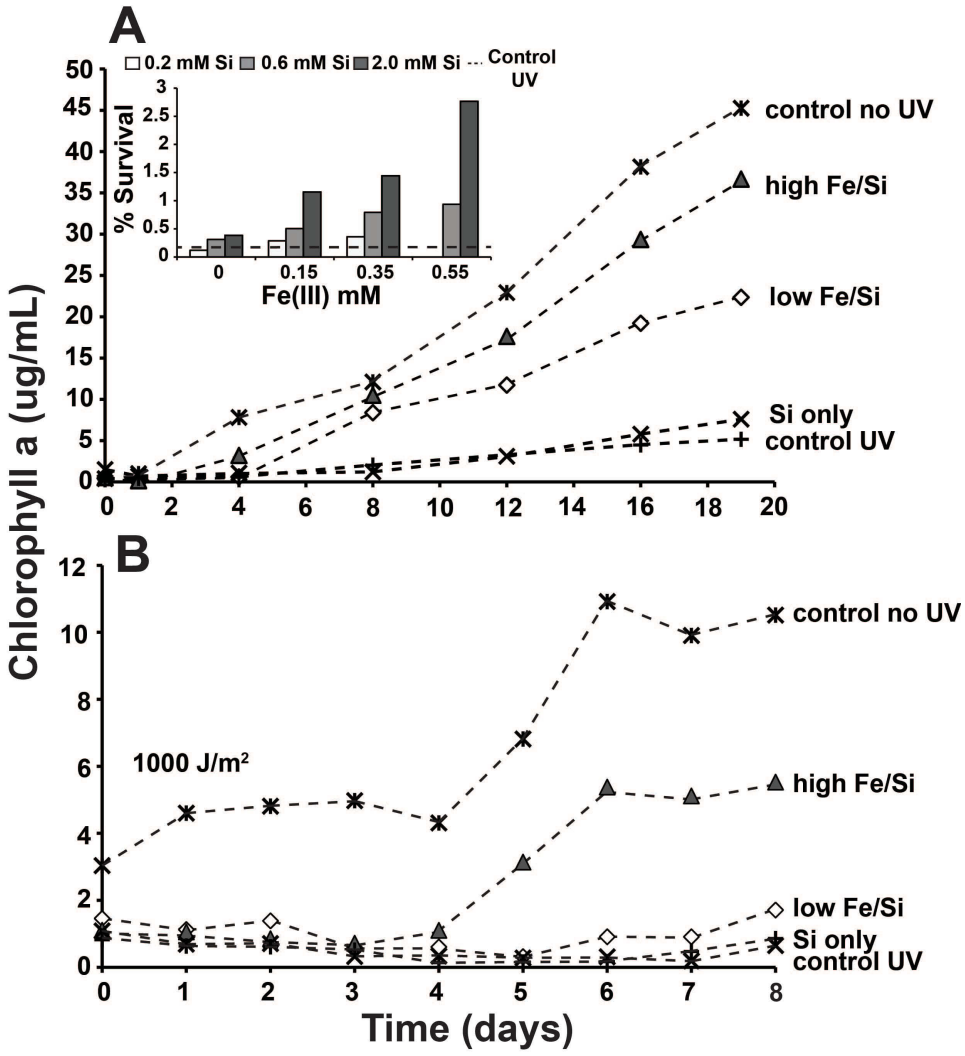
A
0.2 mM Si
0.6 mM Si
2.0 mM Si
Control UV
% Survival
Fe(III) mM
control no UV
high Fe/Si
low Fe/Si
Si only
control UV
Chlorophyll a (ug/mL)
B
1000 J/m²
control no UV
high Fe/Si
low Fe/Si
Si only
control UV
Time (days)

Figure 4.3 Growth rates of *Synechococcus* sp. PCC 7002 using the concentration of the pigment chlorophyll *a* measured over a number of days. Growth rates of UV irradiated cultures grown in unsupplemented A+ growth media ('control UV'), 0.03 mM Fe(III)/0.6 mM Si at 500 J/m^2 and at 1000 J/m^2 ('background Fe/Si') are compared with non-irradiated cultures grown in unsupplemented A+ media ('control no UV'). These Fe(III)and Si concentrations represent background Fe concentrations in Archean seawater environments beyond the reach of Fe upwelling (Holland, 1984; Maliva et al., 2005). Results show that even at the background Fe and Si concentrations estimated for Archean seawater, cyanobacteria are noticeably protected from UV-C radiation, when compared with irradiated bacteria grown in unsupplemented A+ media.

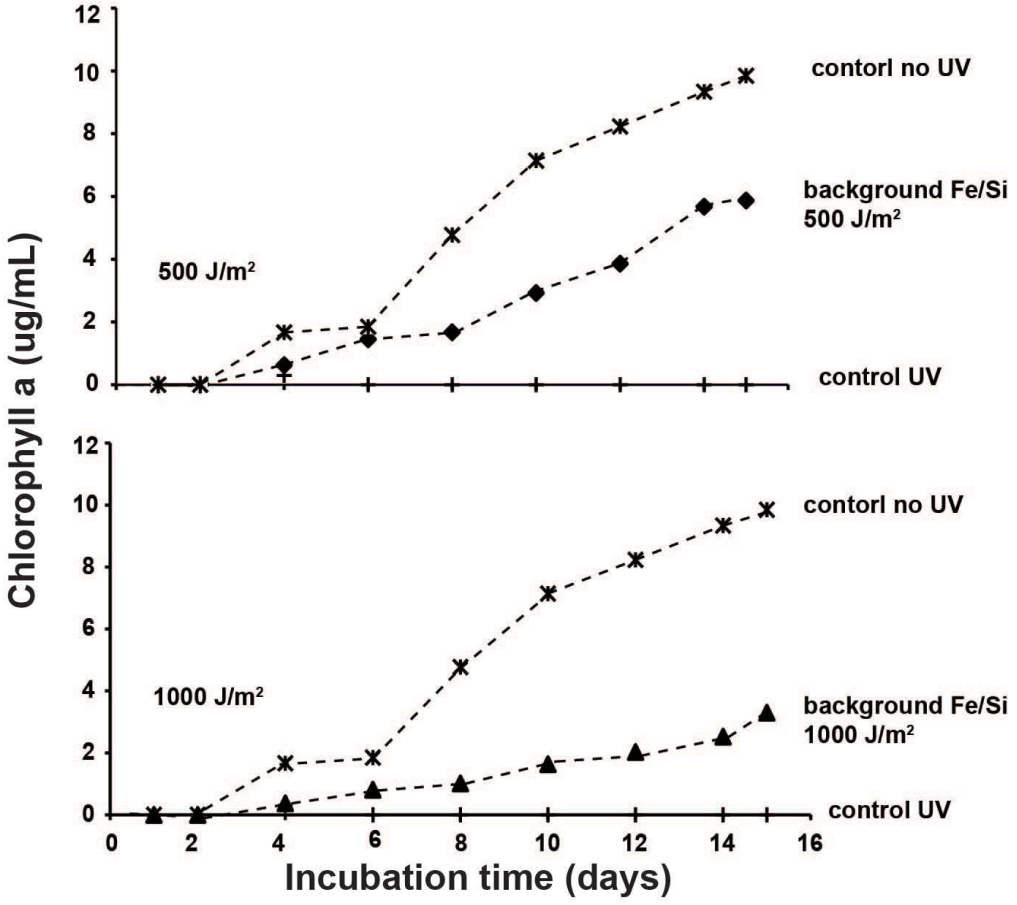
Chlorophyll a (ug/mL)
12
10
8
6
4
2
0
500 J/m²
contorl no UV
background Fe/Si
500 J/m²
control UV
1000 J/m²
contorl no UV
background Fe/Si
1000 J/m²
control UV
0
2
4
6
8
10
12
14
16
Incubation time (days)

Figure 4.4 Photomicrographs showing the ultrastructure of *Synechococcus* sp. PCC 7002. A) Scanning electron microscope (SEM) image of cultures grown in baseline A+ growth media, fixed with 2% gluteraldehyde-2.5% paraformaldehyde. B) Transmission electron microscope (TEM) image of cells stained with OsO_4 and Uranyl acetate, showing fine-grained precipitates tens of nanometer in size surrounding cells grown in 0.55 mM Fe(III) and 2.0 mM Si. C) TEM image showing the lack of actual biomineralization on *Synechococcus* cell wall. D) TEM image showing dark, Fe(III)-rich precipitates in comparison with the lighter salt precipitates that surround fixed cells grown in 0.55 mM Fe(III) and 2.0 mM Si.

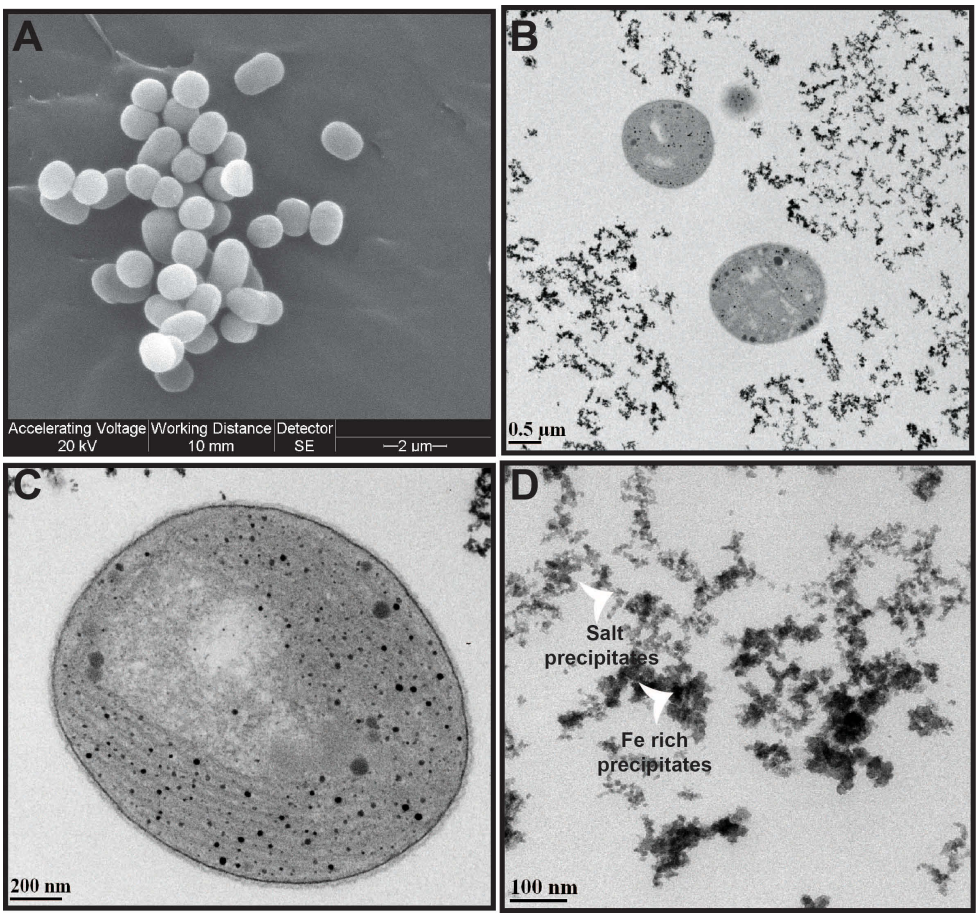
A
Accelerating Voltage
20 kV
Working Distance
10 mm
Detector
SE
—2 µm—
B
0.5 µm
C
200 nm
D
Salt precipitates
Fe rich precipitates
100 nm

Figure 4.5 Modeled chemical equilibrium concentrations for regular A+ growth media and mineral saturation indices (IAP/K_{sp}) as a function of silicic acid (H_4SiO_4) added to the media. Baseline A+ media is supersaturated with respect to ferrihydrite [$(Fe^{+3})_2O_3 \bullet 0.5H_2O$], while the remainder of the Fe(III) is found as soluble organic Fe(III)-EDTA and soluble inorganic Fe(III) complexes. According to the model, the addition of Fe(III) to the media simply increases the amount of ferrihydrite precipitate.

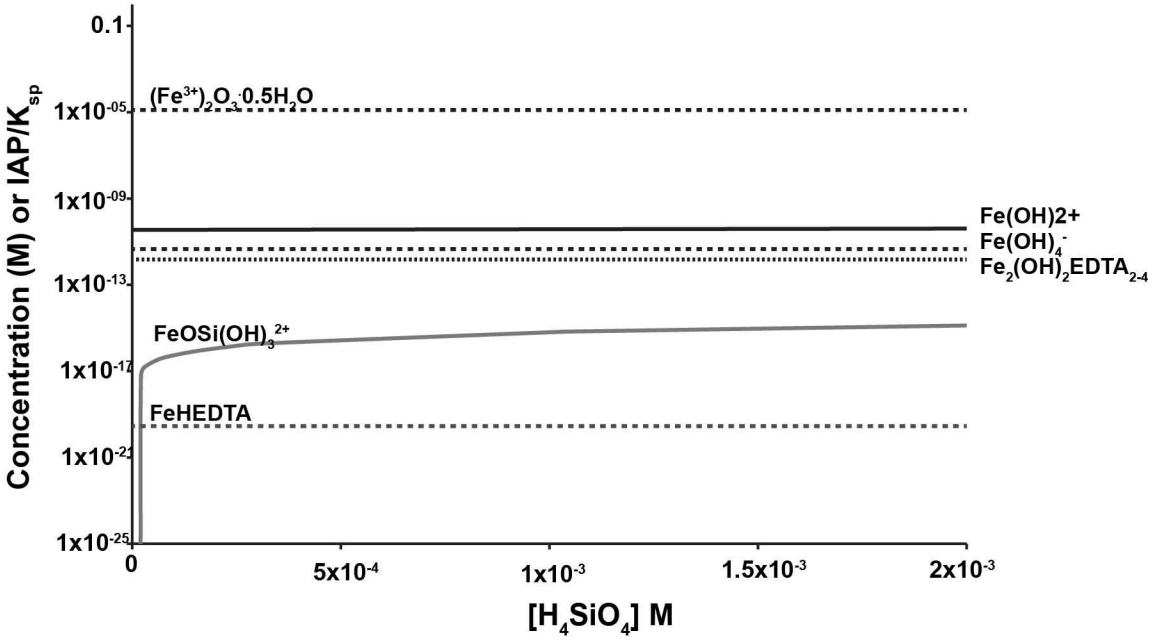
0.1
1x10-05
1x10-09
1x10-13
1x10-17
1x10-21
1x10-25
Concentration (M) or IAP/Ksp
(Fe3+)2O3·0.5H2O
Fe(OH)2+
Fe(OH)4-
Fe2(OH)2EDTA2-4
FeOSi(OH)32+
FeHEDTA
0
5x10-4
1x10-3
1.5x10-3
2x10-3
[H4SiO4] M

Figure 4.6 UV attenuation of A+ growth media supplemented with various concentrations of Fe(III) and Si, where the additive effect of the UV-C (254 nm) absorbance with increasing Si concentration suggests that Si is keeping Fe(III) in suspension. The similar slopes of the Fe(III)-Si curves (triangles and squares) to the Fe(III)-only curve (diamonds) suggests that the UV absorbance is mainly controlled by Fe(III).

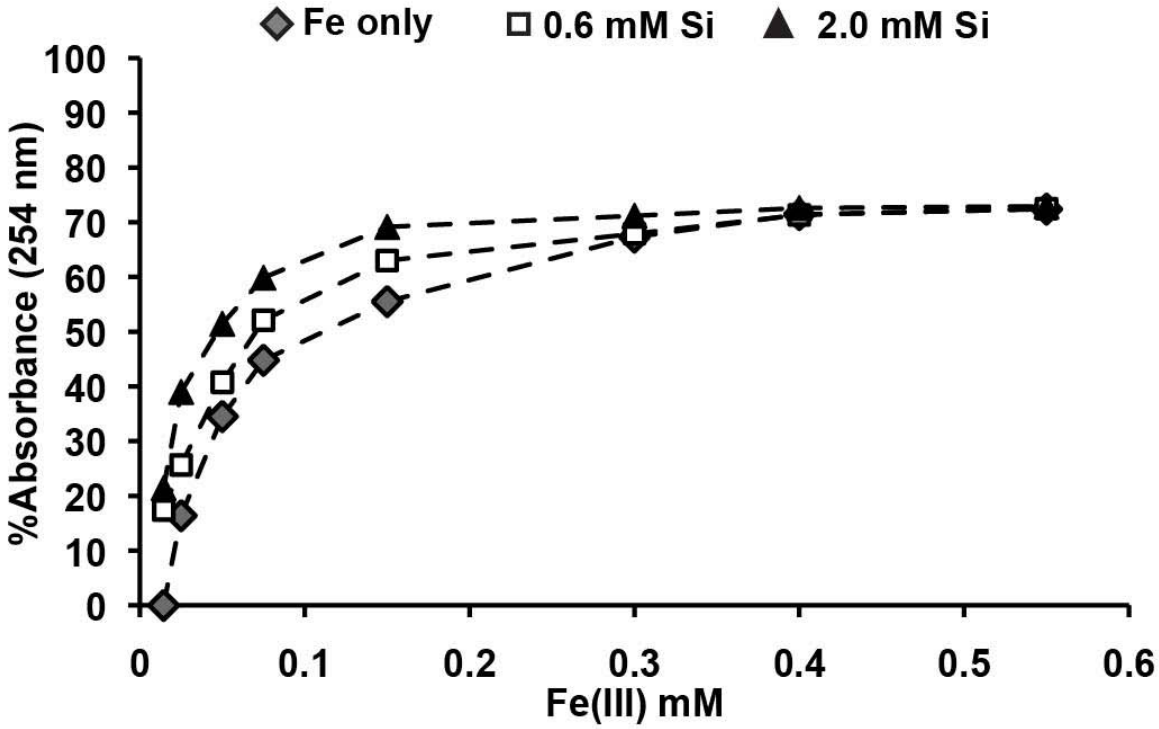
Fe only
0.6 mM Si
2.0 mM Si
%Absorbance (254 nm)
100
90
80
70
60
50
40
30
20
10
0
0
0.1
0.2
0.3
0.4
0.5
0.6
Fe(III) mM

Chapter 5. A geochemical and microbiological study assessing the effects of aqueous Si on Fe toxicity in Archean marine cyanobacteria.

5.1 Introduction

The changing redox state of seawater through geologic time has directed the evolution of early microbial life, acting as a selective pressure by depleting and/or enriching various trace metals and other nutrients. Take for example the initial production of oxygen once cyanobacteria had evolved. The timing for this event remains controversial, but the most accepted view is that cyanobacteria had already evolved by 2.7 Ga (see Buick, 2008), and perhaps earlier (Crowe et al., 2013; Planavsky et al., 2014). Before then, the oceans were anoxic, containing Fe(II) concentrations of at least 30 μM, and potentially up to several hundred μM during times of Fe upwelling (Holland, 1984; Ewers, 1980; Morris and Horowitz, 1983; Czaja et al., 2012). Because Si-secreting organisms, such as diatoms and coccolithophores, had not yet evolved, dissolved Si concentrations were also much higher than modern seawater levels, and estimated to be between 0.67 and 2.2 mM (Siever, 1992; Maliva et al., 2005).

A remarkably coherent ensemble of evidence then point to a significant accumulation of atmospheric oxygen for the first time in Earth's history beginning ca. 2.45 Ga, the so-called Great Oxidation Event (GOE). Briefly, this includes the

disappearance of detrital pyrite, uranitite and siderite from fluvial and deltaic deposits, an increase in the retention of iron in paleosols, an enrichment of Cr and U in iron formations, and perhaps most importantly, the disappearance of sedimentary sulfur isotope mass-independent (S-MIF) anomalies indicative of atmospheric SO_2 processing in the absence of appreciable ozone (see Session et al., 2009; Farquhar et al., 2011). With increased oxidative continental weathering, the flux of nutrients entering the oceans dramatically increased, resulting in a significant increase in cyanobacterial activity and O_2 generation (Konhauser et al., 2011; Bekker et al., 2012). This eventually enabled the proliferation of the more energy-demanding eukaryotes by introducing oxygen as a powerful electron acceptor into the electron transport chain (i.e., aerobic respiration).

The ehanced abundance of oxygen, however, created unique challenges for microorganisms that had evolved to live in anoxic conditions, including (1) the production of Fe-potentiated reactive oxygen species, toxic by-products of the breakdown of molecular oxygen (Fridovich, 1987, 1995; Imlay and Linn, 1988) and (2) a significant decrease in Fe bioavailability upon the oxidation of Fe(II) in seawater to insoluble Fe(III)-oxyhydroxides, such as ferrihydrite, $Fe(OH)_3$. It is interesting that those same oxygenic photosynthetic microorganisms (e.g., cyanobacteria) would have been particularly sensitive to these problems as they assimilate iron (as Fe-S clusters) as well as oxygen free radicals to participate in their electron transport chain. Ironically, while cyanobacteria were the key players in the

GOE, they would also have to develop means to rid themselves of the toxic by-products of their own metabolism.

In today's well-oxygenated oceans, free dissolved Fe is extremely rare (<2 nm; Bruland and Lohan, 2004). Indeed iron is one of the most limiting nutrients in marine environments, forcing phytoplankton to release organic metal chelators (siderophores) in order to meet their metabolic Fe demands (e.g., Trick, 1989). Yet, as introduced above, Fe can be a double-edge sword, and despite being a key nutrient with an important role in controlling primary productivity, it can also be toxic to cells. Reactive oxygen species (ROS, including; singlet oxygen - $^1O_2$; superoxide anion - O_2^-; hydrogen peroxide - H_2O_2; hydroxyl radical - $OH\cdot$) are produced when Fe(II) is oxidized. Fe(III) is reduced by superoxide (reaction 1) producing Fe(II), which is subsequently decomposed by hydrogen peroxide during the Fenton Reaction (reaction 2), where the sum of these two equations is called the Haber-Weiss reaction (reaction 3) as described in Touati et al., (2000):

$$(1)\ Fe^{3+} + O_2^- \rightharpoonup Fe^{2+}\ O_2$$

$$(2)\ Fe^{2+} + H_2O_2 \rightharpoonup Fe^{3+} + OH^- + OH\cdot$$

$$(3)\ O^{2-} + H_2O_2 \rightharpoonup O_2 + OH^- + OH\cdot$$

A small quantity of ROS is also produced in cells as a result of a diverse range of natural metabolic processes (e.g., photosynthesis, respiration). Despite the evolution of an extensive array of cellular mechanisms designed to manage this

unavoidable ROS, the combination of soluble Fe and free oxygen produce ROS in quantities that overwhelm the cell with significant metabolic consequences, such as damage to genetic material (DNA and RNA), as well as protein deterioration and lipid peroxidation, any of which can lead to cell death. In this regard, it has been suggested that Fe in concentrations greater than 100 μM are enough to diminish photosynthetic oxygen production and cause the several hundred million year delay between the first appearance of cyanobacteria and the GOE (Swanner et al., in review).

Before the GOE, various sources of bioavailable Fe may have existed in the oceans. In largely anoxic Archean seawater, hydrothermally-sourced Fe(II) would have remained in solution until it reached a localized area of shallow oxygenated seawater termed 'oxygen oases' (Anbar et al., 2007), upon which insoluble Fe(III) would form. The Precambrian ocean may have also contained significant levels of dissolved organic carbon as evidenced by the large fluctuations in the Precambrian carbon-isotope record (Logan et al., 1995; Rothman et al., 2003; Fike et al., 2006). As cells lysed in the upper water column, organic acids of low molecular weight known to chelate Fe(III) would have been released (Thurman, 1985). These postulated Meso- and Neoarchean 'oxygen oases' might, therefore, have featured a temporary pool of soluble Fe(III)-ligand complexes in the presence of free oxygen, creating another set of conditions toxic to life.

Conversely, silica has a high affinity for iron in natural environments (e.g., Carlson and Schwertmann, 1981; Konhauser and Ferris, 1996) and it readily complexed with Fe in ancient seawater, as evidenced by the abundant iron silicate minerals in Archean-aged banded iron formations (Fe- and Si- rich chemical sedimentary rocks that precipitated directly out of seawater; Klein, 2005; Bekker et al., 2010). Si disrupts the hydrolysis of Fe(III) polymers, and delays the formation of ferric oxyhydroxide precipitates, such as nanoparticulate ferrihydrite, at circum-neutral pH through the formation of Fe(III)-Si complexes (Pokrovsky et al., 2003). It has been reported that this delay occurs through aqueous Si complexing at free corner sites of Fe polymers and oligomers or sorbing onto ferrihydrite particle surfaces. In either case, the silica blocks reactive Fe surface sites and decreases Fe bioavailability to microorganisms. In highly siliceous environments, the end result may even be the incorporation of Fe by amorphous Si (Cismeau et al., 2014). The end result is that by complexing with Fe, aqueous Si might have reduced potentially toxic levels of bioavailable Fe in Archean seawater in the form of Fe(II) and organically chelated Fe(III).

We test this hypothesis by growing the marine planktonic cyanobacterium *Synechococcus* sp. PCC 7002 (henceforth referred to as *Synechococcus*) in Fe- and/or Si-rich growth media designed to mimic Archean seawater conditions (e.g., Morris and Horowitz, 1983; Holland et al., 1984; Maliva et al., 2005; Czaja et al., 2012). We assessed the status of experimental *Synechococcus* populations through changes in

chlorophyll *a* pigment levels as proxies for the rate of population growth, while intracellular ROS levels were measured as a source for metabolic stress. We modelled two Archean, Fe-rich seawater environments by growing *Synechococcus* (1) anoxically and supplementing Fe as Fe(II), and (2) under oxygenic conditions with Fe as Fe(III), using the synthetic metal chelators ethylenediaminetetraacetic acid (EDTA) or citric acid as proxies for natural organic ligands. We hypothesize that the abundant aqueous Si in Archean seawater would have complexed unbound Fe(III) and organic Fe(III) complexes, thereby lessening the potential for Fe toxicity, and thus allowing cyanobacteria to potentially thrive in the Archean oceans.

5.2 Methods

5.2.1 Culturing

Synechococcus species PCC 7002 (previously known as *Agmenellum quadruplicatum* PR-6) is a unicellular, euryhaline marine cyanobacterium able to tolerate high light intensities (Nomura et al., 2006). The laboratory wild type strain used here was obtained from Dr. Donald Bryant (Pennsylvania State University).

Axenic cultures were grown in medium A (Stevens and van Baalen, 1973): 0.3 M NaCl; 8 mM KCl; 12 mM $NaNO_3$; 20 M $MgSO_4 \cdot 7H_2O$; 0.37 mM KH_2PO_4; 2.4 mM $CaCl_2$; 0.08 mM Na_2EDTA; 0.01mM $FeCl_3 \cdot 6H_2O$; P-1 metals (0.6 mM H_3BO_4; 21 mM $MnCl_2 \cdot 4H_2O$; 2.3 uM ZnCl; 0.2 uM MoO_3; 0.02 uM $CoSO_4 \cdot 5H_2O$; 0.06 uM $CoCl_2 \cdot 6H_2O$); 4 ug L^{-1} vitamin B_{12} and 0.01 M $NaNO_3$ (designated medium A+; Stevens and Porter, 1980) per liter of MilliQ water (Nanopure), and Tris buffered to pH 8.2. Axenic stock populations were maintained on 1.5% (w/v) agar in A+ media in Petri dishes kept at 30ºC under constant illumination (~ 50 uE/m^2/s). Stock populations were maintained on A+ agar plates, and experimental cultures were maintained through successive transfers into 50 mL of media with 10% v/v inoculations. All liquid cultures were grown at 30ºC under constant illumination (~100 uE/m^2/s) with shaking at 150 rpm provided aeration for liquid cultures. In order to obtain sufficient biomass for Fe- and Si growth experiments. 300 mL cultures were grown in 1L Erlenmeyer flasks and bubbled with in air to enhance CO_2 supply. The 10% v/v inoculum used to establish these cultures was derived from a 50

mL liquid culture. This 300 mL culture was then used to inoculate 50 mL experimental cultures with A+ supplemented with the indicated concentrations of Si as Na_2SiO_3 (to final concentrations ranging from 0.2, 0.6 and 2.0 mM) and Fe as $FeCl_2 \cdot 6H_2O$ (to final concentrations ranging from 0.03 to 1 mM). Pre-existing Fe in A+ was taken into account when adding supplemental Fe(III) stock to achieve the indicated experimental concentrations. In some experiments, Na_2EDTA was replaced with citrate (as a 0.1M stock solution in ultra pure water) as the metal chelator in the growth media. In all experiments, cultures were harvested when optical density measurements at a wavelength of 750 nm (OD_{750}) indicated that they had reached ~$6x10^7$ cells/mL.

For anoxic experiments, Na_2EDTA was excluded from the A+ media, 0.22 mM $NaHCO_3$ was added as a carbon source and Fe(II) as $FeCl_2 \cdot 4H_2O$ (to final concentrations ranging from 0.03 to 1 mM) was used as an iron source. Growth media (50 mL cultures) and stock solutions were inoculated in 100 mL serum bottles (Schott AG, Mainz, Germany) with rubber septa crimped with aluminum caps. Extensive vacuum and degassing under an N_2 gas stream made the media and stock solutions anoxic. Cultures were shaken (~150 rpm) and incubated at 30°C under a low, steady stream of mixed gas (H_2:N_2:CO_2 = 5%:5%:90%) (Praxair, Edmonton, Alberta, Canada).

5.2.2 Growth Rate

Bacterial growth rates were determined using chlorophyll *a* contents determined by spectrophotometric analysis, according to the protocol of Sakamoto and Bryant (1998). The survival of a culture was determined by its appearance, where cultures were deemed dead if they were clear and transparent, and were deemed healthy if they were a clear, vibrant green. "Dead" cultures were plated on A+ agar plates and incubated at 30°C for 5-7 days in order to confirm their growth status.

5.2.3 Intracellular ROS

The effect of Fe and Si on the accumulation of reactive oxygen species in *Synechococcus* was determined using the fluorescent intracellular dye CH-H_2DCFDA (Life Technologies). The manufacturer's protocol was used with slight modifications (http://tools.lifetechnologies.com/content/sfs/manuals/mp36103.pdf). Samples were washed in 1 M phosphate buffer saline (PBS), and suspended in 1 mL of 1 M PBS. CH-H_2DCFDA was reconstituted immediately before use with molecular grade dimethyl sulfoxide (DMSO) to a stock solution of 0.5 mM. CH-H_2DCFDA (10 μM) was added to each sample. Samples were then incubated under normal growth conditions for 30 min. Post-incubation, samples were washed with 1 M PBS, and suspended in 1 mL 1 M PBS, after which samples were allowed to recover for ~10 h under normal growth conditions. Samples were loaded into a UV- transparent 96 well

flat-bottomed plate, (Corning Costar) and background fluorescence was ascertained on a fluorescent scanner (Horiba Fluoromax Compact Fluorospectrometer) prior to quantification. Samples were quantified for intracellular ROS on a fluorescence microplate reader (BioTek Flx800 Fluorescence Microplate Reader). Fluorescence in non-stained samples was also analyzed in order to remove background fluorescence from the sample readings. The following controls were also analyzed: PBS, PBS+dye, H_2O_2, H_2O_2+dye, a non-Fe- and Si-treated culture, and a non-Fe- and Si-treated culture+dye.

Most modern cyanobacterial lab strains, *Synechococcus* included, are pre-conditioned to low-Fe bioavailability and the exposure to high-Fe conditions, in the form of either chelated Fe(III) or Fe(II) under anoxic conditions, induces a cellular response to enhance Fe uptake and storage for times of low-Fe bioavailability (Wilhelm 1995). Thus, intracellular ROS assays were performed on both un-acclimated and pre-acclimated cells (grown under the specified Fe and Si conditions) for 2 days prior to the assay in order to assess both initial and acclimated responses to high Fe conditions.

5.2.4 Geochemical Modelling

Equilibrium solution compositions were calculated using Visual MINTEQ version 3.0 (Gustafson, 2011), where the thermodynamic database was updated to include

stability constants for aqueous Fe^{+3}-Si complexes (Pokrovski et al., 2003). Modeling parameters included standard room temperature (25ºC) in order to facilitate comparison with other models from the literature, supersaturated minerals were permitted to precipitate, salinity determined by the ionic strength of the solution, and activity coefficients were calculated using the Davis Equation.

5.3 Results

5.3.1 Fe tolerance of Synechococcus in the presence of Si

Figure 5.1 shows the effects of varying Fe(III) - 0.014 to 1 mM, and Si - 0.2 to 2.0 mM, on the survival of *Synechococcus* in the presence of a metal chelator under oxygenic conditions (1 PAL). In this model system, Fe(III) was kept in a soluble and bioavailable form as Fe(III)-EDTA or as Fe-citrate complexes in the growth media.

The curve in Figure 5.1a separates the zones of cell death and cell survival. In the presence Na_2EDTA, we observed a hyperbolic trend between Fe(III) concentration, Si concentration and cell survival. In the absence of Si, Fe(III) concentrations above 0.075 to 0.1 mM caused cell death within 3 hours of inoculation. Moreover, cultures harvested at Fe(III) levels above 0.05 mM showed signs of stress by growing in strands of up to 5 cells long (as compared with unstressed, single-celled cultures in unsupplemented A+, Figure 5.2). Upon the addition of Si at concentrations ranging from 0.025 to 0.4 mM, Fe tolerance increased

significantly (Figure 5.1B), reaching an upper threshold of ~0.75 mM [Fe(III)] at a Si concentration of ~0.4 mM.

Ligand to metal ratios of 10:1 were used for citrate replacement experiments in order for all the Fe to be bound by citrate (Engelmann et al., 2003). Similar to the results obtained with growth media containing Na_2EDTA, cultures grown in the presence of citrate died within hours of inoculation at Fe(III) levels above 0.075-0.1 mM, but could survive levels of up to 0.75 mM in the presence of Si above concentrations of ~0.4 mM (Figure 5.1A). In order to examine the effects of the Fe(III)-Si conditions within the 'live' zone of Figure 5.1A, *Synechococcus* growth rates were monitored in Fe(III) concentrations ranging from 0.03 to 1 mM and Si concentrations ranging from 0.2 to 2.0 mM (Figure 5.3). In general, a decrease in growth rate was observed with higher Fe(III) concentrations. It would also appear that overall, growth rates became suppressed as the Fe(III) levels increase, and improved as Si was added to the growth media (Figure 5.3A,C). In additon, we observed no noticeable effects of Si alone on cyanobacterial growth rates (Figure 5.3B). Cultures grown in Si concentrations ranging from 0.2 to 2 mM followed a similar growth trend as cultures grown in normal A+ media (Figure 5.3B). These trends were equally maintained in media where citrate replaced EDTA as the chelating agent (Figure 5.3C).

The iron tolerance of *Synechococcus* was significantly higher under anoxic conditions. In the absence of Si, cultures survived at concentrations of up to at least 1

mM, which approaches maximum estimates for Archean seawater (Morris and Horowitz, 1983; Holland, 1984; Czaja et al., 2012). Chlorophyll *a* levels were significantly higher under these growth conditions compared with oxygenic cultures. It is likely that this is due to having access to more CO_2 under the experimental anoxic conditions than they would by being bubbled with regular air. Cultures were being flushed at a constant rate with mixed CO_2 gas at a pressure of ~0.05 atm, which is within the range for estimates for the pressure of CO_2 in the Archean atmosphere, which ranges from current atmospheric levels of $3x10^{-4}$ atm up to 1000 times higher (Kasting et al., 2001). Indeed, cultures grown anoxically have noticeably higher iron tolerance levels than cultures grown under oxygenic conditions in the presence of EDTA or citrate. Cultures were able to withstand Fe(II) concentrations of up to 1 mM in the absence of Si. Nevertheless, cultures with Fe(II) supplemented without Si exhibited lower growth rates as compared with cultures containing both Fe(II) and Si supplements (Figure 5.4). This suggests that although the effects of Fe toxicity is reduced by the absence of free oxygen in the media, toxic effects still occur as a result of high Fe(II) levels. Moreover, the presence of Si under these conditions reduced the effects of Fe stress. The potential source of this stress is investigated in the following section.

5.3.2 Oxidative Stress in Synechococcus in the presence of Fe and Si

Intracellular levels of reactive oxygen species (ROS) were measured in Fe and Si supplemented media in order to ascertain a cause for the iron toxicity effects that we observed. Under both oxygenic and anoxic conditions, ROS was measured in cultures both acclimated and un-acclimated to iron stress. ROS in un-acclimated cultures were measured 2 hours after inoculating a culture grown in regular A+ media into iron-rich A+ media. ROS in acclimated cultures were measured after the culture had been growing in iron-rich A+ media for 2 days. ROS levels are reported as a fold change relative to a culture grown in un-supplemented media ('normal' levels). In cultures grown under both oxygenic and anoxic conditions, a positive correlation is observed between intracellular ROS levels and the Fe concentration added to the growth media (Figure 5.5). This is consistent with the growth data under both oxygenic and anoxic conditions. Cultures to which silica was added in addition to iron exhibit lower n-fold increases in ROS levels, as compared with cultures to which only iron was added. Cultures that remained alive after 2 days post-inoculation exhibited up to 27-fold increases in ROS at initial Fe(III) concentrations of 0.55 mM and 0.6 mM Si in EDTA media, and up to 33-fold increases in citrate media. In both EDTA- and citrate- containing media, cultures grown at 0.75 mM Fe(III) were chlorotic within 2 hours of inoculation (insufficient production of chlorophyll, as determined by the yellow-khaki color of a culture) and dead within 3 hours, regardless of Si content. In the presence of 0.6 mM Si, cells exhibited 39- and 46-fold increases in ROS contents

in EDTA and citrate media, respectively, and in the absence of Si, up to 32- and 110-fold increases, respectively. In contrast, cultures supplemented with Fe(III) between 0.15 and 0.55 mM died within 24 hours in the absence of Si. While their ROS levels were significantly lower in these treatments after 2 hours than in cultures exposed to 0.75 mM Fe(III), it is likely that their intracellular ROS levels increased steadily within this 24 hour time period. Importantly, we did not observe a noticeable difference between EDTA or citrate in the efficiency of binding Fe and causing the toxicity effects (depression of growth; intracellular ROS levels), at the concentrations used in the growth media.

Cultures which were pre-acclimated to high iron conditions for 2 days showed an overall decrease in the level of intracellular ROS (Figure 5.5). The most drastic difference occurred in the citrate media, where ROS levels in cultures exposed to 0.03 mM Fe in the absence of Si decreased from 18-fold to 4-fold after 2 days. This is to be expected, given that *Synechococcus* lab strains were adapted to the low iron levels present in bacterial growth media (14.4 μM in A+ media; Stevens and Porter, 1980), and were likely to be predisposed to take advantage of iron-replete conditions for the purpose of iron storage.

Cultures grown under oxygenic conditions in the presence of a EDTA or citrate showed noticeably higher increases in ROS (up to 39-fold and 110-fold the normal level in EDTA and citrate variations, respectively) compared with anoxic cultures in which ROS levels increased only 11-fold above the normal level. This

observation is in agreement with the higher iron tolerance of cultures grown anoxically, compared with cultures grown in oxygenic conditions inß the presence of a metal chelator.

In summary, in both chelated-oxygenic and anoxic growth conditions, a suppression in cellular growth rate was observed in relation to an increase in initial iron concentration. In contrast, growth rates increased upon the addition of Si. Correspondingly, we observed a greater production of intracellular ROS leves in increasingly iron-stressed cells, and a lower production of these stress agents upon the addition of Si. Moreover, the presence of soluble, EDTA or citrate chelated Fe(III) in the presence of oxygenic conditions appeared to cause a more toxic effect that the presence of soluble Fe(II) under anoxic growth conditions. The corresponding growth rate measurements and ROS results presented above suggest a link between: (1) the amount of iron stress exhibited by the cells and the production of oxidative stress agents; (2) the level of iron stress and silica concentrations initially added to the growth media; and (3) the level of iron stress in the presence of free oxygen and soluble, bioavailable iron. The overall decrease in intracellular ROS levels after 2 days of acclamation to high iron levels suggests that the cells have already started to adapt to these conditions.

5.3.3 Geochemical modelling

To examine the effects of Fe on cellular growth, geochemical modeling of Fe and Si supplemented A+ growth media under oxygenic and anoxic conditions were conducted (Figure 5.6). The presence of a metal chelator served to bind a significant proportion of the Fe(III), keeping it soluble and bioavailable (Figure 5.6A). In the absence of a chelator, A+ media containing 1 mM Fe(III) and aqueous Si would be strongly supersaturated with respect to ferrihydrite, $Fe(OH)_3$. The remainder occurs as inorganic iron hydroxide species (total inorganic iron species = $4.48x10^{-11}$ M). Under oxygenic conditions in media containing EDTA and 1 mM Fe(III) with varying Si concentration, modeled saturation indices at chemical equilibrium suggest that the solution becomes mildly supersaturated with respect to the mineral ferrihydrite; $9.94x10^{-4}$ M). The excess iron is partitioned as (soluble) organic Fe-EDTA complexes (for a total concentration of $6.04x10^{-6}$M), and as inorganic Fe species (total concentration of inorganic species $4.48x10^{-11}$ M) (Figure 5.6A).

In media using citrate as the metal chelator (in ratios of 10:1 ligand to metal), 1 mM Fe(III), and varying Si concentrations at chemical equilibrium (Figure 5.6B) our geochemical modeling results suggest that the solution is supersaturated with respect to ferrihydrite (total concentration of $1x10^{-3}$ M). According to our model, the excess the iron is partitioned as inorganic iron hydroxide species (total concentration of $4,48x10^{-11}$ M) and as organic Fe citrate species (total concentration of $6.57x10^{-13}$ M) (Figure 5.6C). Our modeling results also suggest that the Mg in the A+ media

binds much of the citrate. This is distinct from the study by Engelmann et al., (2003), which suggested that in aqueous solutions, all iron should be bound by citrate at a ligand to metal ratio of 10:1. Nevertheless, the biological data implies that much of the Fe is being bound by citrate, causing iron toxicity effects in *Synechococcus* cultures. These contrasting results between this geochemical model and the biological data may be explained by insufficient equilibrium constants existing for polymeric iron-silica constants at pH 7-8 with which to model iron-silica behaviour at circum-neutral pH. At a pH of 7-8, Si and Fe(III) form polymers in aqueous solutions (Pokrovsky et al., 2003). Unfortunately, the variable nature of these polymers precludes the calculations of equilibrium constants for polymeric Fe(III)-Si complexes, and prevents accurate equilibrium models of nature Fe-Si rich systems at pH 7-8 (Pokrovsky et al. 2003). It is possible that this lack of appropriate modelling parameters is contributing to the discrepancy between our geochemical and biological models. Under anoxic conditions in the absence of a metal chelator, most of the Fe(II) occurs as dissolved Fe(II) (5.88×10^{-4} M), while the rest is partitioned as inorganic iron hydroxide, iron carbonate, iron sulfide, iron phosphate and iron chloride species, for a total concentration of 4.12×10^{-12} M (Figure 5.6D). Overall, these modeling results suggests that under both oxygenated conditions in the presence of a chelator, and under anoxic conditions, a significant portion of iron supplemented to A+ media exists as soluble ions or complexes. With respect to our biological observations, it supports the observed correlation between the levels of soluble iron and the degree of iron stress expressed by experimental *Synechococcus* cultures.

5.4 Discussion

Cyanobacteria are major primary producers in the open ocean, driving global oxygen, nitrogen and carbon cycles since their evolution ~3.0 Ga years ago (Falkowski, 1997; Kaufman, 2014). In this capacity, the geochemical rock record indicates that cyanobacteria evolved in an environment in which the high iron concentrations should have been dangerous to them (Czaja et al., 2012). The metabolic iron demand of cyanobacteria is exceptionally high among prokaryotic photosynthesizers (Keren et al., 2004). It is a key component in heme and Fe-S complexes among other molecules, which play vital roles in photosynthesis, respiration, nitrogen acquisition and metabolism (Strauss, 1994). In modern seawater, Fe occurs in such low concentrations (<2 nM; Bruland and Lohan, 2004), that some cyanobacteria have adapted by developing specialized organic ligands to bind iron in order to meet their metabolic demands (Barbeau et al., 2001). In contrast, when iron is present in large quantities, it can become a toxin by catalyzing the formation of oxygen free radicals via Fenton chemistry (e.g., Linn, 1998). Oxygen free radicals cause damage to genetic material as well as lipid peroxidation and protein deterioration, any of which can often lead to cell death (Imlay, 2003).

The two Archean seawater environments modeled in our experiments both represent scenarios in which Fe would be predicted to be toxic to cyanobacteria. The tested model systems ranged from anoxic, open-ocean conditions with Fe as Fe(II), to the oxygenic conditions of shallow coastal oxygen oases where some Fe present as

Fe(III) was chelated by ligands (Fike, et al. 1996; Anbar et al., 2007). Our results show that under anoxic conditions, and at the predicted Archean seawater Fe(II) concentration of 0.03 to 1 mM (Ewers, 1980; Morris and Horowitz, 1983; Holland, 1984; Czaja et al., 2012), growth of ancient cyanobacteria would have been suppressed but would not have killed them. This decline in growth could have been a result of lower rates of photosynthesis, as shown by Swanner et al (in review). In contrast, under oxygenated conditions bioavailable Fe(III)-ligand complexes were observed to be lethal to cyanobacteria above Fe(III) concentrations of above 0.075 mM. In both scenarios, Archean silica concentrations (0.67 to 2.2 mM, Maliva et al., 2005) increased the iron tolerance of cyanobacteria under all conditions tested. Unexpectedly, the *Synechococcus* experiments and geochemical modeling results suggest that this protection is caused by a reduction in iron bioavailability through the complexation of iron by silica. The addition of Si to growth media not only resulted in a decrease in intracellular ROS accumulation, but a concomitant increase in cellular growth rates as compared with *Synechococcus* cultures grown under Fe-only conditions. Therefore, the results also highlight the crucial distinction between the presence of Fe and its bioavailability, with respect to Fe toxicity.

While it is well known that soluble Fe is most energetically favourable for uptake by microorganisms, not all soluble Fe is bioavailable. Fe bound to the fungal siderophore desferrioxamine is soluble but not bioavailable, and has actually been used experimentally to reduce Fe availability (Eldridge et al., 2004). Desferroxiamine

is a large molecule which binds to all 6 Fe coordination sites (Graf et al., 1984). In the case of EDTA binding to Fe(III), the EDTA molecule's small size causes a distortion of the Fe(III) atom and the subsequent formation of a seventh coordination sight loosely bound to an H_2O molecule (Graf et al., 1984). The H_2O molecule is only loosely bound implying that a cell can bind with the Fe(III)-EDTA complex when the H_2O unbinds from the iron coordinate site. Thus in order for the hexadentate Fe atom to be taken up by a cell, it must be in a catalytically-active form with a free or loosely-bound coordination site.

The lethal effects on experimental *Synechococcus* cultures grown at ~0.075 mM Fe(III) under oxygenated conditions in the presence of an organic metal ligand is supported by previous work (Dunford, 1987). Indeed, our biological results show that Fe(III)-ligand complexes, such as Fe(III)-EDTA and Fe(III)-citrate, trigger the production of intracellular ROS, and the redox potentials of both chelators are thermodynamically suitable for triggering the Fenton reaction (e.g., Aoki et al., 1988; Zhuang and Chen, 1993; Escot et al., 1989). Furthermore, citrate is an organic ligand that is naturally found in seawater, and has been experimentally shown to maintain the solubility of Fe(III) in natural seawater (Rose and Waite, 2003).

Geological evidence suggests that organic ligands such as citrate may have been abundant before the GOE. Abundances of ^{34}S and ^{13}C isotopes in hydrocarbons extracted from Proterozoic-aged sediments (2500 to 541 Ma) suggest extensive degradation and dispersal of organic matter throughout the water column (Logan et

al., 1995). The most parsimonious way of explaining the occurrence of hydrocarbons and contemporaneous sulphide minerals with enriched ^{13}C and ^{34}S isotopic signatures, respectively, is the relatively complete reworking of organic matter prior to burial by sulphate-reducing bacteria (Logan et al., 1995). Upon the evolution of planktonic metazoans at the beginning of the Cambrian period (541 to 584 Ma), this organic matter would have been rapidly consumed by heterotrophs in the upper water column and buried as faecal pellets, resulting in conditions similar to the relatively organic-carbon depleted conditions observed in modern seawater (Butterfield, 2009). Indeed, picoplankton (0.2 to 2 μm sized unicellular organisms), which are thought to have dominated the Precambrian oceans, exhibit significantly lower aggregation and sinking rates than their larger counterparts, due to their size and shape (Burd and Jackson, 2009; Butterfield, 2009). Organic acids such as citrate and other low-molecular weight species are commonly found in many biological systems, and are released during cell lysis upon a organism's death (Pierre and Gauthier-Luneau, 2000). This evidence suggests that the concentration of metal-binding organic acids may have been significantly higher in the Precambrian oceans.

The production of oxygen free radicals is initiated by soluble iron reacting with hydrogen peroxide, and therefore iron homeostasis is strictly controlled by the cell regardless of the Fe oxidation state (Touati et al., 2000). For example, the uptake of Fe-siderophores by modern cyanobacteria is often a species-specific (for a review see Hider and Kong, 2010). Cyanobacteria have evolved sophisticated systems to

manage Fe intake and sequestration in a non-toxic form (ferritins and bacterioferritins; Harrison and Arosio, 1996; Lewin et al., 2005; Shcolnick et al., 2009), as well as detoxification systems to neutralize any accumulated, intracellular ROS, including non-enzymatic ROS-scavenging molecules such as carotenoids and α-tocopherol (Cabiscol et al., 2000 and Imlay, 2003) and enzymatic ROS scavengers such as superoxide dismutase and catalase (Fridovich et al., 1997; Storz and Imlay, 1999; Latifi et al., 2008). Fe homeostasis in most Gram-negative bacteria is globally regulated by the *Fur* or ferric uptake regulator protein which controls the (i) induction of Fe(II) and Fe(III) uptake functions; (ii) expression of Fe-storage proteins and Fe utilizing enzymes, and (iii) expression of genes for siderophore synthesis (Hantke, 1987; Kammler et al., 1993; Hantke, 2003; Cartron et al., 2006; Lee and Helmann, 2007). Thus, the increases in intracellular oxidative stress observed in our *Synechococcus* cultures in both anoxic and oxygenic conditions is most likely due to a lapse in cellular control of the Fe uptake/storage systems or an imbalance in antioxidant levels (Touati et al., 1995; Ghassemian and Strauss, 1996; Katoh et al. 2001; Latifi et al., 2008). Furthermore, the observed decrease in intracellular ROS levels in cultures acclimated to high iron levels suggests that these systems have adapted to these conditions (Figure 5.5). Thus, the presence of high silica levels in the Archean oceans may have facilitated the survival of early cyanobacteria by allowing them to adapt to high iron conditions by lowering soluble iron to more manageable levels.

5.5 Conclusions

Cyanobacteria evolved by ~3.0 Ga years ago (Crowe et al., 2013; Planavsky et al., 2014), and perhaps as early as 3.5 Ga (Heubeck, 2009) under harsh, Fe-rich conditions that were likely not conducive to the survival of early life. In this study, we show that the survival of early cyanobacteria and presumably, other bacteria, was associated with the protection from Fe-induced toxicity provided by the high concentration of aqueous Si present in Archean seawater. Thus, the presence of Si enabled early cyanobacteria to thrive under these conditions, as evidenced by the Fe-heavy metabolic demands of modern cyanobacteria.

When they first evolved, much of the oxygen that cyanobacteria emitted would have quickly been depleted by reduced ion species in their immediate environment (Jamieson et al., 1986). Once free oxygen started to accumulate in the water column, organic ligands released from degrading organic matter into so-called 'oxygen oases' (e.g., Anbar et al., 2007), formed soluble but toxic Fe(III)-ligand complexes. Our data shows that Si would have lowered the toxicity of the Fe(III)-ligand complexes, allowing cyanobacteria to continue to thrive in these transition environments This would have facilitated the further expansion of oxygenated regions in early shallow seawater environments.

Under modern, fully oxygenated conditions, Fe is one of the two most limiting nutrients, along with phosphorous. One of the most valuable sources of

bioavailable Fe in modern seawater are Fe-ligand (siderophore) complexes, which increase soluble Fe levels (<2 nm; Bruland and Lohan, 2004) by as much as two orders of magnitude (Kuma et al., 1996). While the Great Oxygenation Event (ca. 2.32 Ga, Bekker et al., 2004) removed high iron levels. However, it also caused a new suite of issues given that the combination of iron and oxygen is toxic to organisms even at low iron levels. Microorganisms would eventually adapt to these low iron conditions by evolving systems to acquire, as well as maintain, intracellular Fe levels required for metabolic functions in a non-toxic form. The importance of Fe-storage and detoxification is emphasized by the ubiquitous distribution of ferritins and superoxide dismutases across all living species.

In terms of future work, the derivation of equilibrium constants for polymeric iron-silica complexes at circum-neutral pH will greatly enhance the information that can be gained from future geochemical modeling studies of Fe and Si in seawater. In the meantime, the amount of Fe bound to citrate and the amount of Fe and Si complexes in solution can be calculated indirectly by: (1) using the ferrozine assay (Viollier et al. 2003) and the heteropoly-molybdate blue technique (Fanning and Pilson, 1973) to calculate unbound Fe(III) and Si in the citrate media. We will then combine these results with (2) measurements from inductively coupled mass spectrometry of the total soluble silica and iron concentrations in the citrate media. By comparing these results with theoretical concentrations of Fe-Si complexes from

our geochemical modelling, we may be able to derive the various pools of bound iron in our media.

This study builds comprehensive model of some conditions likely experienced by ancient microbial life, through a combination of microbiological and molecular assays and geochemical modelling. While the composition of seawater during the early evolution of life contained Fe concentrations of up to ~1 mM that normally would not support life, the experiments presented here indicate that the high concentrations of Si in early seawater (up to 2.2 mM) protected early life from the harmful effects of Fe toxicity. This protective effect allowed cyanobacteria to flourish, producing oxygen that contributed to the precipitation of Fe(III) minerals such as ferrihydrite, resulting in the exceedingly low levels observed in the modern oceans. The latter condition facilitated the evolution of multicellular life as we know it today. These findings will have important implications for the ancient biosphere, the early Fe cycle and the survival and subsequent evolution of higher life forms.

References

Anbar, A.D., Duan, Y., Lyons, T.W., Arnold, G.L., Kendall, B., Creaser, R.A., Kaufman, A.J., Gordon, G.W., Scott, C., Garvin, J., Buick, R., 2007. A whiff of oxygen before the Great Oxidation Event? Science 317:1903-1906.

Aoki, K., Ishida, M., Tokuda, K., 1988. Voltammetry ad microcylinder electrodes part IV: second-order catalytic reaction or ethylenediamminetetraacetic acid with hydrogen peroxide. Journal of Electroanal Chemistry 245:39-50.

Barbeau, K., Rue, E.L., Bruland, K.W., Butler, A., 2001. Photochemical cycling of iron in the surface ocean mediated by microbial iron(III)-binding ligands. Nature 413:409-413.

Bekker, A., Holland, H.D., Wang, P-L., Rumble III, D., Stein, H.J., Hannah, J.L., Coetzee, L.L., Beukes, N.J., 2004. Dating the rise of atmospheric oxygen. Nature 427:117-120.

Bekker, A., Slack, J.F., Planavsky, N., Krapez, B., Hofmann, A., Konhauser, K.O., Rouxel, O.J., 2010. Iron formation: the sedimentary product of a complex interplay among mantle, tectonic, ocean and biospheric processes. Economic Geology 105:467-508.

Bekker, A., Holland, H.D., 2012. Oxygen overshoot and recovery during the early Proterozoic. Earth and Planetary Science Letters 317-318:295-304.

Bruland, K.W., Lohan, M.C., 2004. The Control of trace metals in seawater. In: Elderfield, H., Ed. The Oceans and Marine Geochemistry. The Treatise of Geochemistry p. 33 to 47.

Buick, R., 2008. When did oxygenic photosynthesis evolve? Philosophical Transactions of the Royal Society B 363:2731-2743.

Burd, A.B., Jackson, G.A., 2009. Particle aggregation. Annual Review of Marine Science 1:65-90.

Butterfield, N.J., 2009. Oxygen, animals and oceanic ventilation: an alternate view. Geobiology 7:1-7.

Cabiscol, E., Tamarit, J., Ros, J., 2000. Oxidative stress in bactria and protein damage by reactive oxygen species. International Microbiology 3:3-8.

Carlson, L., Schwertmann, U., 1981. Natural ferrihydrites in surface deposits from Finland and their association with silica. Geochimica et Cosmochimica Acta 45:421-425.

Cartron, M.L., Maddocks, S., Gillingham, P., Craven, C.J., Andrews, S.C., 2006. Feo-transport of ferrous iron into bacteria. Biometals 19:143-157.

Cismeau, A.C., Michel, F.M., Tcaciuc, A.P., Brown, G.E. Jr., 2014. Properties of impurity-bearing ferrihydrite III. Effects of Si on the structure of 2-line ferrihydrite. Geochim. Cosmochim. Acta 133:168-185.

Crowe, S.A., Dossing, L.N., Beukes, N.J., Bau, M., Kruger, S.J.., Frei, R., Canfield, D.E., 2013. Atmospheric oxygenation three billion years ago. Nature 501:535-538.

Czaja, A.D., Johnson C.M., Roden, E.E., Beard, B.L., Voegelin A.R., Nagler, T.F., Beukes, N.J., Wille M., 2012. Evidence for free oxygen in the Neoarchean ocean based on coupled iron-molybdenum isotope fractionation. Geochimica et Cosmochimica Acta 86:118-137.

Dunford, H.B., 1987.Free radicals in iron-containing systems. Free Radical Biology and Medicine 3:405-421.

Eldridge, M.L., Trick, C.G., Alm, M.B., DiTullio, G.R., Rue, E.L., Bruland, K.W., Hutchins, D.A., Wilhelm, S.W., 2004. Planktonic community response to a manipulation of iron in HNLC waters of the subtropical Pacific Ocean. Aquatic Microbial Ecology 35:79-91.

Engelmann, M.D., Bobier, R.T., Hiatt, T., Cheng, I.F., 2003. Variability of the Fenton reaction on characteristics of the EDTA, DPTA and citrate complexes of iron. Biometals 16:519-527.

Escot, M., Martre, A.M., Poillen, P., Martinet, P., 1989. Electrochemical study of iron(III) complextion by some model ligands of biological interest I. Acetohydroxamic acid, acetylacetone and citric acid. Bulletin de la Societe de Chimie France 3:316-320.

Ewers, W.E.,1980. Chemical conditions for the precipitation of banded iron formations. In Biogeochemistry of Ancient and Modern Environments, Springer Berlin Heidelberg, p.83-92.

Fanning, K.A., Pilson, M.E.Q., 1973. On the spectrophotometric determination of dissolved silica in natural waters. Analytical Chemistry 45:136-140.

Farquhar, J., Zerkle, A.L., Bekker, A., 2011. Geological constraints on the origin of oxygenic photosynthesis. Photosynthesis Research 107:11-36.

Fike, D.A., Grotzinger, J.P., Summons, R.E., 2006. Oxidation of the Ediacaran ocean. Nature 444:744-747.

Fridvovich, I., 1995. Superoxide radicals and superoxide dismutase. Annual Reviews in Biochemistry 64:97-112.

Fridovich, I., 1997. Superoxide anion radicals (O^{-}_{2}), superoxide dismutases and related matters. The Journal of Biological Chemistry 272:18515-18517.

Ghassemian, M., Straus, N.A., 1996. Fur regulates the expression of iron-stress genes in the cyanobacterium Synechococcus sp. PCC 7942. Microbiology 142:1469-1476.

Graf, E., Mahoney, J.R., Bryant, R.G., Eaton, J.W., 1984. The Journal of Biological Chemistry 259:3620-3624.

Gustafsson, J.P. 2011. Visual Minteq 3.0: http: //www2.lwr.kth.se/English/OurSoftware/vminteq.

Hantke, K., 1987. Negative control of iron uptake systems in Escherichia coli. FEMS Microbiology Letters 15:83-86.

Hantke, K., 2003. Is bacterial ferrous iron transporter FeoB a living fossil? Trends in Microbiology 11:192-195.

Harrison, P.M., Arosio, P., 1996. The ferritins: molecular properties, iron storage function, and cellular regulation. Biochimica et Biophysica Acta 1275:161-203.

Hider, R.C., Kong, H., Chemistry and Biology of Siderophores. Natural Product Reports 27:637-657.

Holland, H.D., 1984. The chemical evolution of the atmosphere and oceans. Princeton University Press. 582p.

Imlay, J.A., Linn, S., 1988. DNA damage and oxygen radical toxicity. Science 240:1302-1309.

Imlay, J.A., 2003. Pathways to oxidative damage. Annual Reviews in Microbiology 57:395-418.

Jamieson, D., Chance, B., Cadenas, E., Boveris, A., 1986. The relation of free radical production to hypoxia. Annual Reviews in Physiology 48:708-719.

Kammler, M., Schön, C., Hantke, K., 1993. Characterization of the ferrous iron uptake system of Escherichia coli. Journal of Bacteriology 175:6262-6218.

Kasting, J.F., Pavlov, A.A., Siefferto, J.L., 2001. A coupled ecosystem-climate model for predicting the methane concentration in the Archean atmosphere. Origins of Life and Evolution of the Biosphere 31:271-285.

Katoh, H., Hagino, N., Grossman, A.R., Ogawa, T., 2001. Genes essential to iron transport in the cyanobacterium Synechocystis sp. PCC 6803. Journal of Bacteriology 183:2779-2784.

Kaufman A., 2014. Early Earth: cyanobacteria at work. Nature Geoscience 7:253-254.

Keren, N., Aurora, R., Pakrasi, H.B., 2004. Critical roles of bacterioferritins in iron storage and proliferation of cyanobacteria. Plant Physiology 135:1666-1673.

Klein, C., 2005. Some Precambrian banded iron formations (BIFs) from around the world: their age, geological setting, mineralogy, metamorphism, geochemistry, and origin. American Mineralogist 90:1473-1499.

Konhauser, K.O., Ferris, F.G., 1996. Diversity of iron and silica precipitation by microbial mats in hydrothermal waters, Iceland: implications for Precambrian iron formations. Geology 24:323-326.

Konhauser, K.O., Lalonde, S.V., Planavsky, N.J., Pecoits, E., Lyons, T.W., Mojzsis, S.J., Rouxel, O.J., Barley, M.E., Rosière, C., Fralick, P.W., Kump, L.R., Bekker, A., 2011. Aerobic bacterial pyrite oxidation and acid rock drainage during the Great Oxidation Event. Nature 478:369-373.

Kuma, K., Nishioka, J., Matsunaga, K., 1996. Limnological Oceanography 41:396-407.

Latifi, A., Ruiz, M., Zhang, C-C., 2009. Oxidative stress in cyanobacteria. FEMS Microbiology Reviews 33:258-278.

Lee, J-W., Helmann, J.D., 2007. Functional speclization within the Fur family of metalloregulators. Biometals 20:485-499.

Lewin, A., Moore, G.R., Le Brun, N.E., 2005. Formation of protein-coated iron minerals. Dalton Transactions 22:3597-3610.

Linn, S., 1998. DNA damage by iron and hydrogen peroxide in vivo. Druge Metabolism Reviews 30:313-326.

Logan, G.A., Hayes, J.M., Hieshima, G.B., Summons, R.E., 1995. Terminal Proterozoic reorganization of biogeochemical cycles. Nature 376:53-56.

Maliva, R.G., Knoll, A.H., Simonson, B.M., 2005. Secular change in the Precambrian silica cycle: Insights from chert petrology. Geological Society of America Bulletin 117:835-845.

Morris, R.C., Horowitz, R.C., 1983. The origin of the iron-formation-rich Hamersley Group of Western Australia – deposition on a platform. Precambrian Research 21:273-297.

Nomura, C.T., Persson, S., Shen, G., Inoue-Sakamoto, K., Bryant, D.A., 2006. Characterization of two cytochrome oxidase operons in the marine cyanobacterium Synechococcus sp. PCC 7002: Inactivation of ctaDI affects the PS I:PS II ratio. Photosythesis Research 87:215-228.

Pierre, J.L., Gautier-Luneau, I., 2000. Iron and citric acid: a fuzzy chemistry of fuzzy biological relevance. Biometals 13:91-96.

Planavsky, N.J., Asael, D., Hofmann, A., Reinhard, C.T., Lalonde, S.V., Knudsen, A., Wang, X., Ossa Ossa, F., Pecoits, E., Smith, A.J.B., Beaukes, N.J., Bekker, A., Johnson, T.M, Konhauser, K.O., Lyons, T.W., Rouxel, O.J., 2014. Evidence for

oxygenic photosynthesis half a billion years before the great oxidation event. Nature Geoscience 7:283-286.

Pokrovski, G.S., Schott J., Farges, F., Hazemann J-L., 2003. Iron(III)-silica interactions in aqueous solutions: insight from x-ray absorption fine structure spectroscopy. Geochimica et Cosmochimica Acta 19:3559-3573.

Rose, A.L., Waite, T.D., 2003. Kinetics of iron complexation by dissolved natural organic matter in coastal waters. Marine Chemistry 84:85-103.

Rothman, D.H., Hayes, J.M., Summons, R.E., 2003. Dynamics of the Neoproterozoic carbon cycle. PNAS 100:8124-8129.

Sakamoto, T., Bryant, D.A., 1998. Growth at low temperature causes nitrogen limitation in the cyanobacterium Synechococcus sp. PCC 7002. Archives of Microbiology 196:10-19.

Shcolnick, S., Summerfield, T.C., Reytman, L., Sherman, L.A., Keren, N., 2009. The mechanism of iron homeostasis in the unicellular cyanobacterium Synechococystis sp. PCC 6803 and its relationship to oxidative stress. Plant Phyiology 150:2045-2056.

Sessions, A.L., Doughty, D.M., Welander, P.V., Summons, R.E., Newmann, D.K., 2009. The continuing puzzle of the Great Oxidation Event. Current Biology 19:567-574.

Siever, R., 1992. The silica cylce in the Precambrian. Geochimica et Cosmochimica Acta 56:3265-3272.

Stevens, S.E Jr., Van Baalen, C., 1973. Characteristics of nitrate reduction in a mutant of the blue-green alga Agmenellum quadruplicatum. Plant Physiology 51:350-356.

Stevens, S.E & Porter, R.D., 1980. Transformation in Agmenellum quadruplicatum. Proeedings to the National Acadademy of Science 77, 6052-6056.

Storz, G., Imlay, J.A., 1999. Oxidative stress. Current Opinion in Microbiology 2:188-194.

Strauss, N.A., 2004. Iron deprivation: physiology and gene regulation. The Molecular Biology of Cyanobacteria, Springer Netherlands, p. 731-750.

Swanner, E.D., Mloszewska, A.M., Cirpka, O., Schoenberg, R., Konhauser, K.O., Kappler A., in review. Toxic levels of Fe(II) in Archean seawater modulated oxygen producution. Nature Geoscienc.

Thurman, E. M., 1985. Organic chemistry of natural waters volume 2. Martinus Nihoff/Dr W. Junk Pubs. Springer.

Touati, D., Jacques, M., Tardat, B., Bouchard, L., Despeid, S., 1995. Lethal oxidative damage and mutagenesis are generated by iron in delta fur mutants of Escherichia coli: protective role of superoxide dismutase. Journal of Bacteriology 177:2305-2314.

Touati, D., 2000. Iron and oxidative stress in bacteria. Archives of biochemistry and biophysics 373:1-6.

Trick, C.G., Wilhelm, S.W., 1995. Physiological changes in the coastal marine cyanobacterium Synechococcus sp. PCC 7002 exposed to low ferric ion levels. Marine Chemistry 50:207-217.

Wilhelm, S.W., 1995. Ecology of iron-limited cyanobacteria: a review of physiological responses and implications for aquatic systems. Aquatic Microbial Ecology 9:295-303.

Zhuang, Q-K., Chen, H-Y., 1993. A theoretical analyses and its application of the second order EC reactions at microelectrodes under stead-state conditions. Chinese Journal of Chemistry 11:308-315.

Figure 5.1 Plot showing the relationship between Fe(III), Si, and cell survival under oxygenic conditions in the presence of a EDTA and citrate. A) The curve separates concentrations above which cultures died (crosses) and below which cultures lived (black circles for A+ media with EDTA; grey circles for A+ media with). B) The level of Fe(III) tolerance increases rapidly when Si is initially added to the media in quantities between 0.014 and 0.4 mM, and plateaus at 0.75 mM as Si concentrations reach ~0.4 mM.

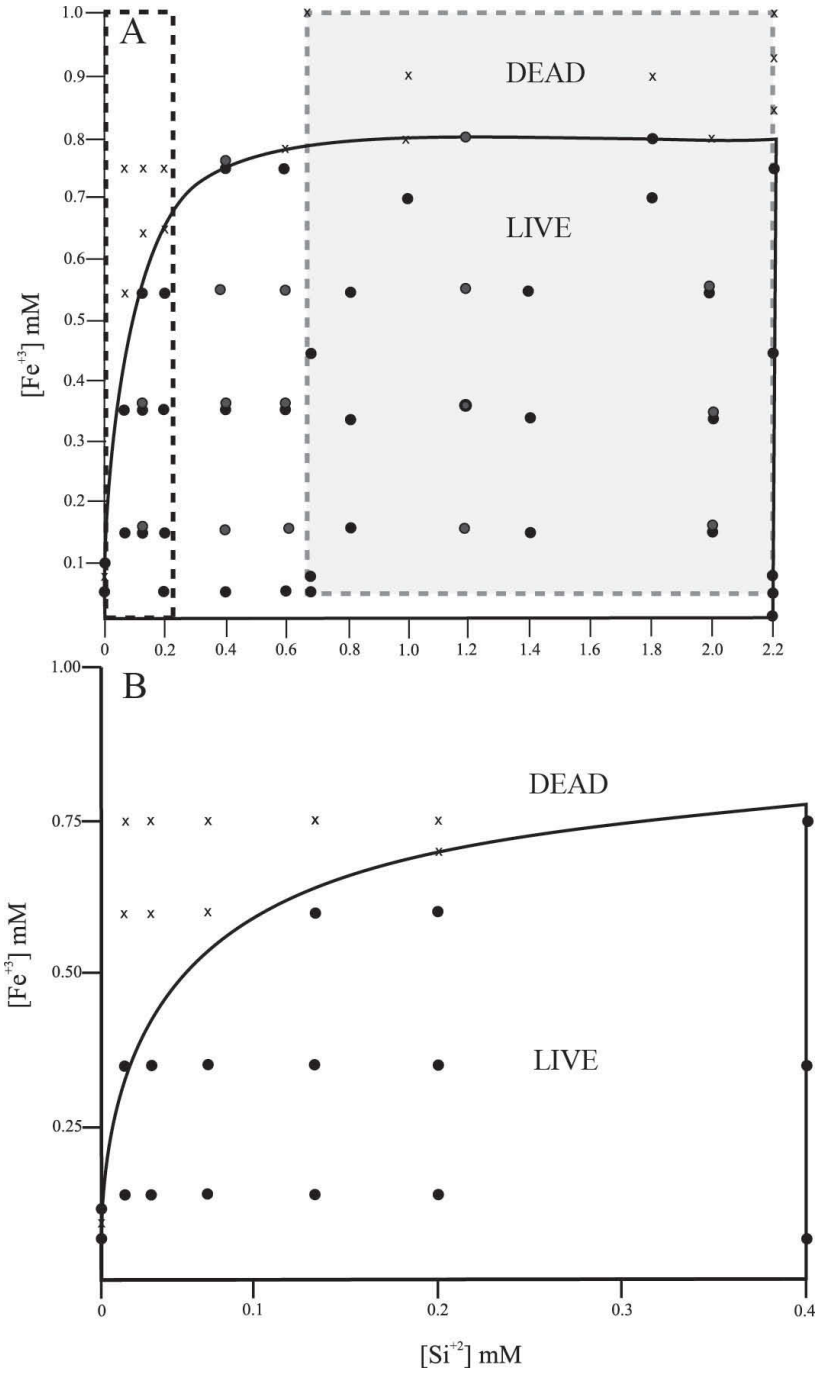
A
DEAD
LIVE
[Fe+3] mM
1.0
0.9
0.8
0.7
0.6
0.5
0.4
0.3
0.2
0.1
0
0.2
0.4
0.6
0.8
1.0
1.2
1.4
1.6
1.8
2.0
2.2
B
DEAD
LIVE
[Fe+3] mM
1.00
0.75
0.50
0.25
0
0.1
0.2
0.3
0.4
[Si+2] mM

Figure 5.2 A) Sample of *Synechococcus* sp. PCC 7002 liquid cultures in normal A+ media, grown under constant illumination at 30°C, shown here at various cell densities. B) Scanning electron micrograph of Synechococcus cells grown in normal A+ media and fixed with 2.5% gluteraldehyde and 2% paraformaldehyde. C) Transmission electron micrograph showing the intracellular ultrastructure of *Syenchococcus* cell at mid-log phase in normal A+ media: CW= cell wall; R= ribosome; C= carboxysome; N= nucleoide; TM= thylakoid membrane; CG= cyanophycin granule. D) Cells grown in A+ media containing EDTA and 1mM Fe(III) and 0.6 mM Si. Light-colored granules are salt crystals, while dark/black granules are Fe(III)-rich precipitates.

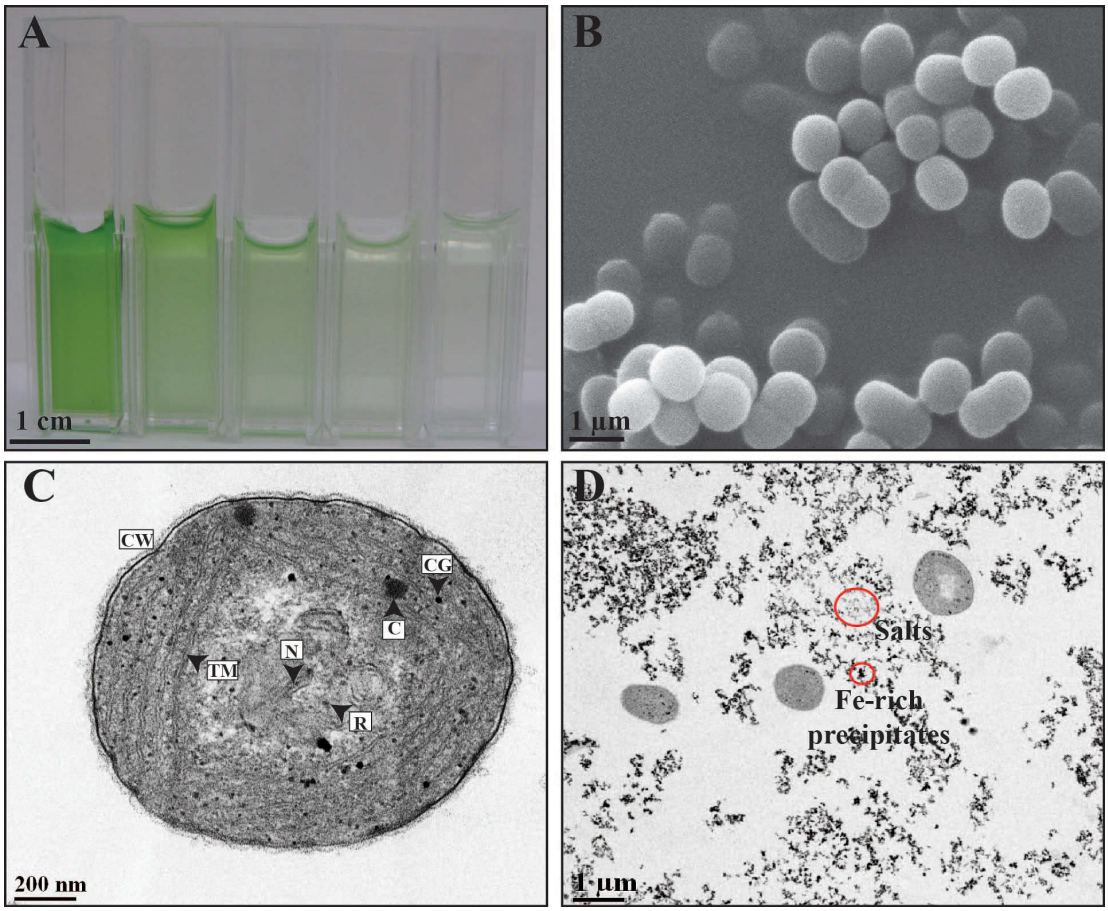
A
1 cm
B
1 µm
C
CW
CG
C
N
TM
R
200 nm
D
Salts
Fe-rich
precipitates
1 µm

Figure 5.3 Plots showing the effects of Fe(II), Fe(III) and Si on the growth rate of cyanobacteria. Changes in the concentration of the pigment chlorophyll a over time (as the number of days post inoculation) are used as a proxy for cellular growth rates. A) Changes in cellular growth rates of cultures grown in EDTA containing A+ media at Fe(III) concentrations of 0.03, 0.15, 0.35, 0.55 and 0.75 mM and 0.6 mM Si. Growth rates of cultures grown at 0.03 mM Fe(III) and 0 mM Si are shown for comparison, however culture grown at concentrations above 0.075-0.1 mM Fe(III) in the absence of Si are not plotted as they died within 24 hours. B) Changes in cellular growth rates with increasing Si concentrations: 0.2. 0.6 and 2 mM Si. C) Changes in cellular growth rates of cultures grown in A+ media where EDTA was replaced with citrate. Cultures were grown at Fe(III) concentrations of 0.03, 0.15, 0.35, 0.55 and 0.75 mM and 0.6 mM Si. Growth rates of cultures grown at 0.03 mM Fe(III) and 0 mM Si are shown for comparison, however culture grown at concentrations above 0.075-0.1 mM Fe(III) in the absence of Si are not plotted as they died within 24 hours.

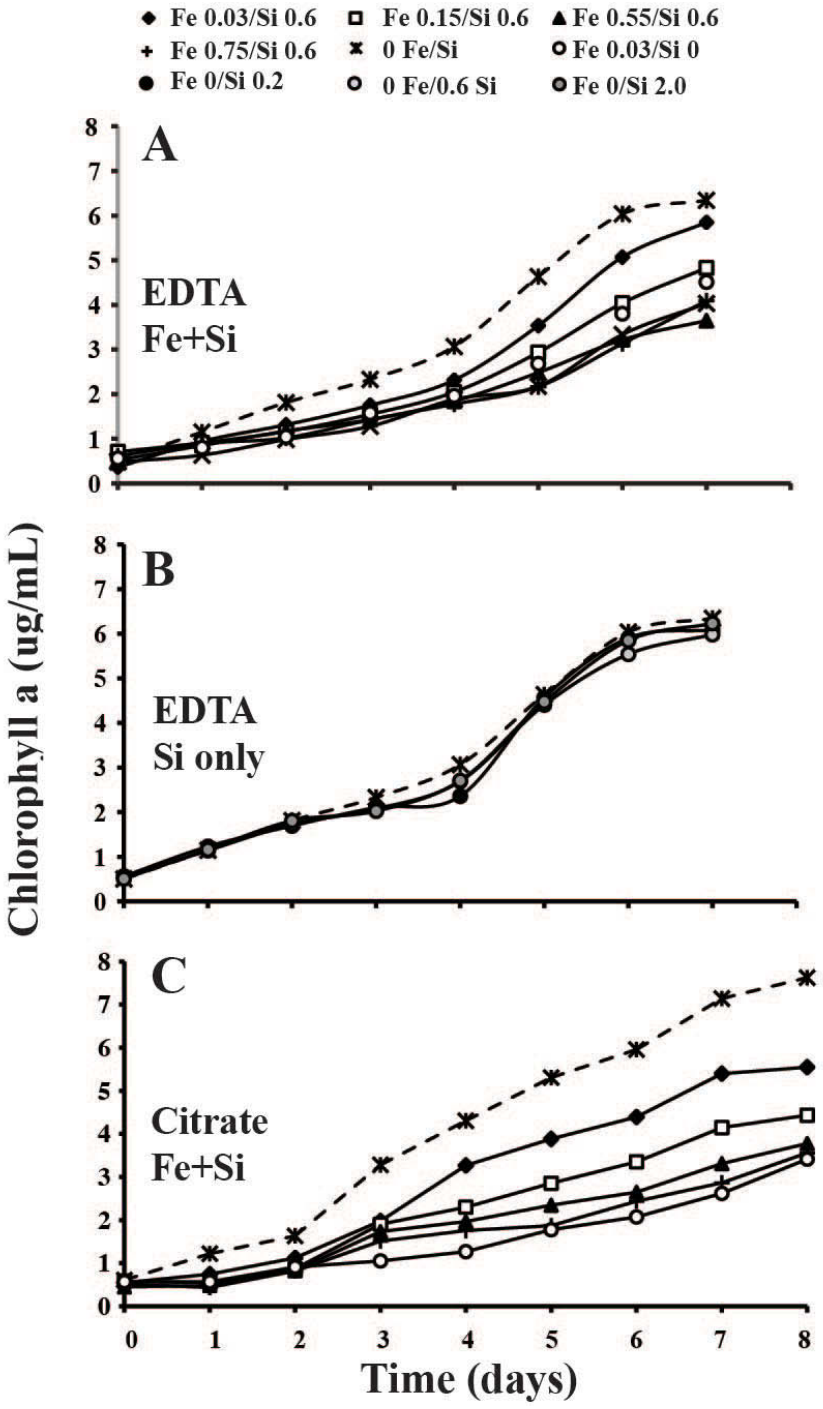
Fe 0.03/Si 0.6
Fe 0.15/Si 0.6
Fe 0.55/Si 0.6
Fe 0.75/Si 0.6
0 Fe/Si
Fe 0.03/Si 0
Fe 0/Si 0.2
0 Fe/0.6 Si
Fe 0/Si 2.0
A
EDTA
Fe+Si
B
EDTA
Si only
C
Citrate
Fe+Si
Chlorophyll a (ug/mL)
Time (days)
0
1
2
3
4
5
6
7
8

Figure 5.4 Plots comparing cellular growth rates of *Synechococcus* sp. PCC 7002 cultures grown under anoxic conditions in the absence of a metal chelator, at Fe(II) concentrations ranging from 0.03 to 1.0 mM, in the A) absence and B) presence of Si. Growth rates are represented by changes in the pigment chlorophyll a over the number of days post inoculation.

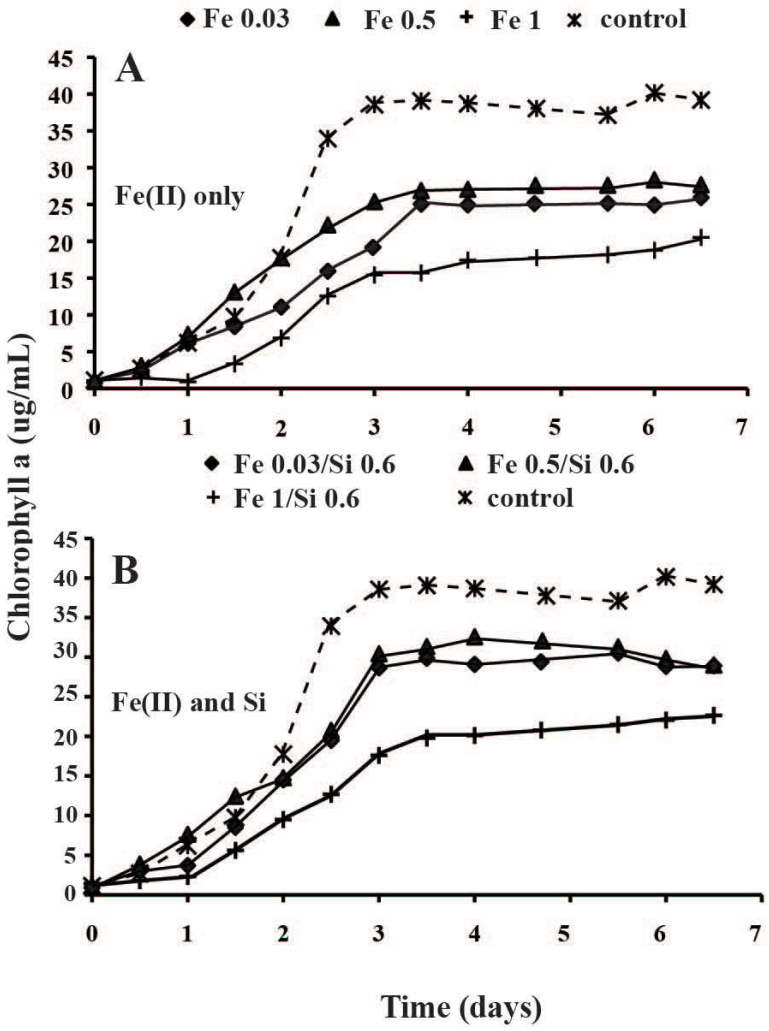
Fe 0.03
Fe 0.5
Fe 1
control
A
Fe(II) only
Fe 0.03/Si 0.6
Fe 0.5/Si 0.6
Fe 1/Si 0.6
control
B
Fe(II) and Si
Chlorophyll a (ug/mL)
Time (days)

Figure 5.5 Levels of intracellular reactive oxygen species (ROS) with increasing iron concentrations in *Synechococcus* cultures grown in: A) un-acclimated cells (measured 2 hours after inoculation) grown in A+ media with EDTA, under oxygenic conditions. B)in acclimated cells (measured after 2 days post-inoccluation) grown in A+ with EDTA under oxygenic conditions. C) In un-acclimated cells grown in A+ media where EDTA has been replaced with citrate, under oxygenic conditions. D) In acclimated cells grown in A+ media where EDTA has been replaced with citrate, under oxygenic conditions. E) In un-acclimated cells grown in A+ containing no metal chelator, under anoxic conditions, and F) In acclimated cells grown in A+ containing no metal chelaotr, under anoxic conditions.

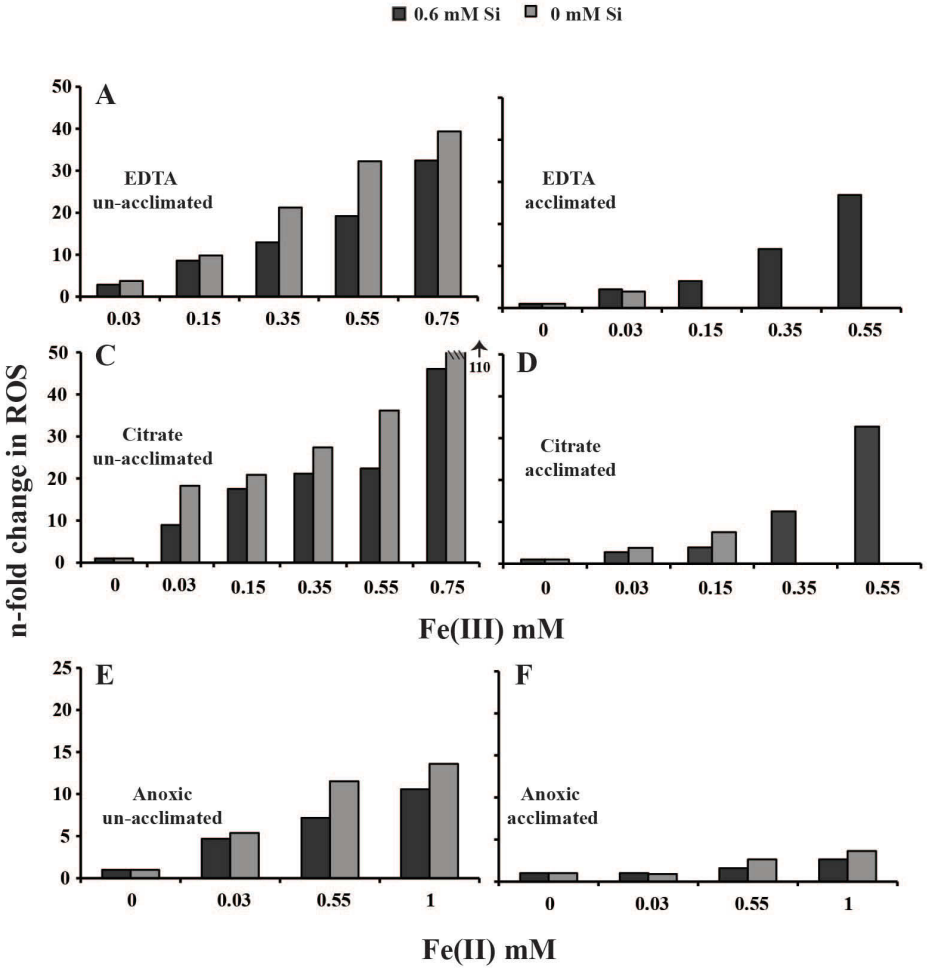
0.6 mM Si
0 mM Si
A
EDTA
un-acclimated
EDTA
acclimated
C
Citrate
un-acclimated
110
D
Citrate
acclimated
n-fold change in ROS
Fe(III) mM
E
Anoxic
un-acclimated
F
Anoxic
acclimated
Fe(II) mM

Figure 5.6 Modeled chemical equilibrium concentrations of iron species in A+ bacterial growth media supplemented with 1 mM Fe as either Fe(II) or Fe(III), and mineral saturation indices (IAP/K_{sp}) as a function of silicic acid (H_4SiO_4). A) Media containing no metal chelator. B) Media containing EDTA. C) Media where EDTA has been replaced by citrate, and D) Anoxic media containing no metal chelator.

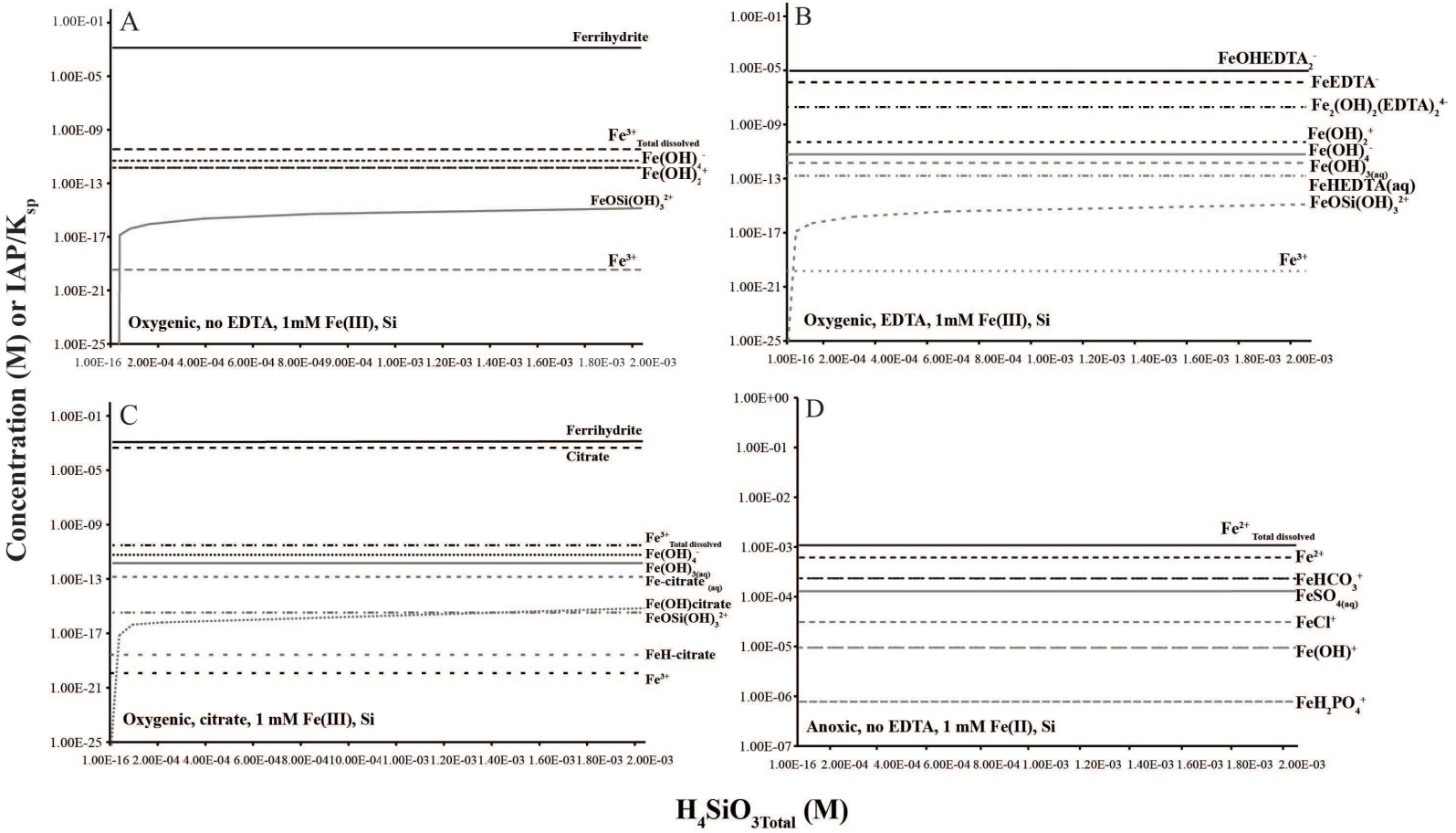
A
Ferrihydrite
Fe3+ Total dissolved
Fe(OH)4-
Fe(OH)2+
FeOSi(OH)32+
Fe3+
Oxygenic, no EDTA, 1mM Fe(III), Si
B
FeOHEDTA2-
FeEDTA-
Fe2(OH)2(EDTA)24-
Fe(OH)2+
Fe(OH)2-
Fe(OH)4
Fe(OH)3(aq)
FeHEDTA(aq)
FeOSi(OH)32+
Fe3+
Oxygenic, EDTA, 1mM Fe(III), Si
C
Ferrihydrite
Citrate
Fe3+ Total dissolved
Fe(OH)4-
Fe(OH)3(aq)
Fe-citrate(aq)
Fe(OH)citrate
FeOSi(OH)32+
FeH-citrate
Fe3+
Oxygenic, citrate, 1 mM Fe(III), Si
D
Fe2+ Total dissolved
Fe2+
FeHCO3+
FeSO4(aq)
FeCl+
Fe(OH)+
FeH2PO4+
Anoxic, no EDTA, 1 mM Fe(II), Si
Concentration (M) or IAP/Ksp
H4SiO3Total (M)

Chapter 6. Conclusions

The antiquity of bacterial life is well established, but the environmental conditions surrounding its evolution are still poorly understood. On one hand, Archean seawater was a nutrient-rich medium that provided early microorganisms with bioactive trace metals in abundances that met their metabolic requirements and facilitated growth. On the other hand, shallow marine habitats were inhospitable environments bathed in high intensity UV radiation with high iron levels toxic to life. Nevertheless, the Archean photic zone contained important habitats that hosted early photosynthetic microbial assemblages. Fossil evidence from ancient coastal marine settings suggest thriving benthic communities by at least ca. 3.5 Ga (Hoffman et al., 1999) and planktonic communities by perhaps as early as ca. 3.8 Ga (Rosing, 1999). This demonstrates that early microbes managed to overcome these environmental stresses. The work presented in this thesis provides evidence that the means by which they achieved this feat of survival is in the composition of Archean seawater itself.

6.1 The availability of bioactive trace metals in the Eoarchean oceans using the 3.8 Ga BIF rock record

There is a strong connection between seawater composition and the early evolution of life. Recent proteomic studies have used the trace metal requirements of ancient

microbes in an attempt to indirectly establish the bioavailability of trace metals in the earliest oceans (Saito et al., 2003; Zerkle et al., 2005; Dupont et al., 2006, 2010). However, the results of these studies are largely unsubstantiated due to the scarcity of an Eoarchean meta-sedimentary rock record. Exciting new opportunities are presented by BIF units in the recently discovered ≥3.75 Ga Nuvvuagittuq Supracrustal Belt, and rare BIF samples from the >3.77 Ga Nulliak Supracrustal Association. By using Eoarchean-aged BIF as proxies for the trace metal composition of pre-3.8 Ga seawater, we are able to supply a direct, physical context for the trends conserved in the proteomic imprints of extant microorganisms.

The classical overview by da Silva and William (1991) of how inorganic chemistry is used in biological systems shows that the selection of elements found in the active site of modern enzymes in extant biological systems diverges noticeably from the bioavailability of these elements in modern seawater. It famously suggests that they were selected perhaps billions of years ago under very different environmental conditions. The relative abundance of Ni and Zn in ca. 3.8 Ga seawater, as shown in our study of BIF from the Nuvvuagittuq Supracrustal Belt, has important implications. For instance, Ni plays an important nutritional role in a number of biological systems. It is a key metal co-factor in the enzymes of methanogens responsible for methane production: methyl-coenzyme M reductase and acetyl-CoA synthase (Ragsdale and Kumar, 1996). Methanogens are among the most ancient organisms (Ueno et al., 2006), and were responsible for much of the methane production during the Archean (Kasting et al., 2003). In other bacteria, Ni is found in

urease and hydrogenase enzymes, key components in cellular nitrogen and hydrogen uptake systems respectively, as well as in superoxide dismutase, which plays an important role in cellular detoxification (da Silva and Williams, 2001). The high abundances that we report in Eoarchean seawater (up to 300 nM; Mloszewska et al., 2012) contrast the relatively low Ni abundances in modern seawater (<12 nM, Bruland and Lohan). Thus, we can relate our findings to the importance of this metal in microbial metabolisms with ancient lineages, such as methanogenesis, as suggested by earlier proteomic studies (Zerkle et al., 2005). While modern methanogens are restricted to anaerobic habitats containing high trace element fluxes from degrading organic matter (Liu et al., 2012), the high Ni abundances in anoxic ca. 3.8 Ga seawater would have met their metabolic needs. In support of our findings, a recent study ties a decline in ocean Ni levels to a disruption of biogenic methane production at ca. 2.5Ga, just prior to the Great Oxidation Event (Konhauser et al., 2009). An abundance of seawater Ni allowed methanogens to thrive and maintain the anoxic state of the Archean atmosphere, at CH_4 levels up to 1000 times greater than modern levels (~1.8 parts per million; Catling et al., 2001; Kasting and Siefert, 2002). This case presents direct evidence for the link between early seawater composition, the state of the ca. 3.8 Ga atmosphere and the ancient biosphere.

In a second example, our findings regarding the relative abundance of Zn in Eoarchean seawater opens up new questions regarding the evolution of early eukaryotic life. Proteomic studies have attributed low Zn abundances in early seawater to the low number of ancient, Zn-binding microbial metallo-enzymes in

prokaryotes (Dupont et al., 2010). The relatively low Zn requirement of most modern cyanobacteria has been attributed to the depletion of Zn as non-bioavailable sulfide complexes, which dissociated slowly in seawater (Saito et al., 2003). These purported low Zn levels have even been linked to the delay in the evolution of eukaryotes (Saito et al., 2003; Dupont et al., 2010). However, our findings suggest that Zn levels in Eoarchean seawater may have been as high as 20 nM (modern Zn levels in seawater are <9nM; Bruland and Lohan, 2004). New geochemical modeling results suggest that a biologically significant fraction similar to that found in modern seawater (up to 6 nM as chloro- or hydroxyl-complexes, or alternately, uncomplexed Zn^{2+}) would have been available for uptake by microorganisms (Mloszewska et al., 2012). Recent complementary studies looking at of Zn abundances in BIF and black shale through time lend support to our findings. They suggest that marine Zn concentrations varied within an order of magnitude of modern values throughout geologic time (Robbins et al., 2013; Scott et al., 2013). Contrary to previous suggestions, our results decouple the geochemical evolution of Zn in seawater and the early biological evolution of eukaryotic organisms. Most Zn-binding proteins in eukaryotes are predominantly structural and exist in the nucleus (Dupont et al., 2010). Furthermore, the number of Zn-binding proteins is proportional to proteome size (Dupont et al., 2010). Thus, the greater abundance of these proteins in Eukarya may have to do with genome regulation and allometry, rather than Zn bioavailability (Robbins et al., 2013). In light of this new evidence, this hypothesis will have to be confirmed through future phylogenetic work on eukaryotic Zn binding domains.

Our results highlight the importance of using multidisciplinary research methodologies to build a more comprehensive picture of early microbial evolution. BIF provide a 3.0 Ga year archive of seawater composition. By comparing the proteomic records of extant microorganisms with ancient lineages with direct evidence of ancient seawater composition from the rock record, we can effectively tease apart the extrinsic factors that may have directed the early evolution of life on Earth.

6.2 A biogeochemical model for the 700 million year transition period preceding the GOE

While Archean seawater was rich in the trace metals required to support microbial metabolisms, it also contained toxic iron levels and high incident UV radiation levels that were detrimental to early life. The abundance of iron and silica characteristic of Archean seawater may have been just as important to the initial survival of the most ancient planktonic microorganisms, and to the early colonization of littoral marine environments, much as the rise of oxygen was important to the proliferation of eukaryotes.

UV radiation was a problem for microorganisms living in the upper water column until atmospheric oxygen levels reached values of around 10^{-1} PAL approximately 2.3 billion years ago (Kasting and Donahue, 1980; Kasting and Catling, 2003). As evidenced by the abundance of iron-silicate minerals in Archean-aged BIF, iron has a high affinity for silica and complexed readily in the Archean

water column (Klein, 2005). These complexes acted as UV shields in photic environments, effectively protecting planktonic microorganisms from harmful UV damage. By delaying the formation of ferric oxyhydroxide precipitates, Si bound to iron polymers keeping them in solution, thus maintaining the effectiveness of the iron as a UV shield in the Archean water column.

Silica also played a protective role, by reducing the levels of bioavailable iron in the water column. The abundance of soluble iron, either as Fe(II) in anoxic environments or as Fe(III)-ligand complexes in oxygen oases (Anbar et al., 2007), were toxic to microorganisms such as early cyanobacteria. By causing the toxic buildup of intracellular reactive oxygen species, iron reduces cell growth, and possibly even photosynthetic rates, as evidenced by lower rates of oxygen production in iron–stressed cyanobacteria (Swanner et al., in review). In the presence of aqueous Si, we observed the reduction of intracellular ROS levels in iron-stressed cells, under both oxygenic and anoxic conditions, and a concomitant increase in cellular growth rates. Importantly, the presence of Si enables cells to adapt to high iron conditions, resulting in a decrease in toxic, intracellular ROS build over time.

The ongoing debate on the origin of oxygenic photosynthesis has been brought to the forefront of scientific research by the recent discoveries of redox-sensitive Cr and Mo isotopes in 3.0 Ga year old metasedimentary rocks, suggesting the accumulation of free oxygen in the atmosphere and oceans perhaps as early as the Mesoarchean (Crowe et al., 2013; Planavsky et al., 2014). Direct fossil and biomarker evidence for the occurrence of Archean-aged cyanobacteria are not robust (Brocks

and Pearson, 2005; Buick, 2008), and therefore, we must rely on a combination of circumstantial evidence for the origins of oxygenic photosynthesis. The findings based on our biological models suggest that the survival of early cyanobacteria, both planktonic and mat-forming varieties (Pierson et al., 1993; Phoenix et al., 2001), would not have been deterred by the harsh environmental conditions of the Archean ocean. In this regard, there is no reason why they shouldn't have thrived in pre-2.5 Ga year old seawater, as implied by isotopic evidence from the rock record.

The transitional accumulation of free oxygen in the atmosphere irreversibly changed the redox state of the oceans and atmosphere. The level of soluble iron would have been reduced to less than 0.002 μM from the 1000 μM prior to the Great Oxidation Event (ca. 2.32 Ga; Bekker et al., 2004). However, the presence of soluble Fe(III)-organic chelator complexes may have continued to be a problem until the evolution of diatoms, radiolaria, silicoflagellates, sponges and other zooplankton, in the early Phanerozoic eon (Maliva et al., 1989; Butterfield, 2009). While diatoms and other silica-secreting organisms deplete oceanic silica levels by taking it up to build their frustules, the ingestion of organic carbon by zooplankton and subsequent burial of the fecal pellets lowers the supply of organic chelators *via* the depletion of oceanic organic carbon.

While the presence of free oxygen in the atmosphere and oceans may have eliminated high incident UV radiation levels and iron stress in the oceans, it introduced a set of new problems. Oxygen, the metabolic waste product of oxygenic

photosynthesis, is toxic to most organisms including to the ones that produce it. Organisms would have to rely on ways to rid themselves of reactive oxygen species (ROS), as well as evolve mechanisms for taking up and storing iron in a non-hazardous way (ferritins and bacterioferritins) (Barbeau et al., 2001; Lee and Helmann, 2007).

6.3 Future Work

Cyanobacteria were key players in the oxygenation of our planet. However, we still have much to learn about how these bacteria grow in anoxic, iron-rich conditions. Given that modern marine environments are oxygenic and depleted in iron, many studies exist on the metabolic effects of iron deficiency in cyanobacteria, as well as on gene expression, iron acquisition and storage. By contrast, only a few pioneering studies exist on the physiological ecology of mat-forming cyanobacteria living in the Fe(II)-rich Chocolate Pots Hot Springs in Yellowstone National Park (Pierson et al., 1999; Pierson and Parenteau, 2000). As a consequence, some questions remain: how do cyanobacteria take up Fe(II) versus Fe(III) under iron replete conditions? When intracellular ROS buildup occurs due to high iron levels, is it due to a breakdown in the iron storage system, or the detoxification system within the cell? Do iron uptake mechanisms change in cyanobacterial strains that have been acclimated to high iron conditions for several months/years? Getting a handle on these questions will enable us to better understand the mechanisms underpinning the initial accumulation of atmospheric free oxygen.

Geochemical modeling analyses are important for understanding the geochemistry behind high iron/high silica Archean seawater model systems. As most of them occur at circum-neutral pH, the absence of equilibrium constants for polymeric iron-silica complexes at pH 7-8 (Pokrovski et al., 2003) is a problem. Given the variable nature of these polymers, developing such constants is no small task. However, their development will unquestionably improve our understanding of Archean seawater systems.

In summary, studying the co-evolution of early life with changing seawater composition through geologic time is well documented and best done with a thorough knowledge not only of the rock and fossil records, but also of microbial systems and their chemical signatures. The multidisciplinary approach of this research has allowed us to elucidate some of the important interactions between the hydro-, litho- and atmosphere on early life. Much work has been done on the abiotic aspects and theoretical predictions of the relationship between early life and its environment. Therefore, the next logical step was to determine whether the proposed interactions between the earliest microorganisms and Archean seawater could be replicated in living bacterial systems. This is what I have strived to accomplish in this thesis.

References

Anbar, A.D., Duan, Y., Lyons, T.W., Arnold, G.L., Kendall, B., Creaser, R.A., Kaufman, A.J., Gordon, G.W., Scott, C., Garvin, J., Buick, R., 2007. A whiff of oxygen before the Great Oxidation Event? Science 317:1903-1906.

Barbeau, K., Rue, E.L., Bruland, K.W., Butler, A., 2001. Photochemical cycling of iron in the surface ocean mediated by microbial iron(III)-binding ligands. Nature 413:409-413.

Bekker, A., Holland, H.D., Wang, P-L., Rumble III, D., Stein, H.J., Hannah, J.L., Coetzee, L.L., Beukes, N.J., 2004. Dating the rise of atmospheric oxygen. Nature 427:117-120.

Brocks, J.J., Pearson A., 2005. Building the biomarker tree of life. Reviews in Mineral Geochemistry 59:233-258.

Bruland, K.W., Lohan, M.C., 2004. The Control of trace metals in seawater. In: Elderfield, H., Ed. The Oceans and Marine Geochemistry. The Treatise of Geochemistry p. 33 to 47.

Buick, R., 2008. When did oxygenic photosynthesis evolve? Philosophical Transactions of the Royal Society B. 363:2731-2743.

Butterfield, N.J., 2009. Oxygen, animals and oceanic ventilation: an alternate view. Geobiology 7:1-7.

Catling, D.C., Zahnle, K.J., McKay, C.P., 2001. Biogenic methane, hydrogen escape, and the irreversible oxygenation of early Earth. Science 293:839-843.

Crowe, S.A., Dossing, L.N., Beukes, N.J., Bau, M., Kruger, S.J.., Frei, R., Canfield, D.E., 2013. Atmospheric oxygenation three billion years ago. Nature 501:535-538.

Da Silva, J.J.R.F., Williams, R.J.P., 1991. The biological chemistry of the elements: the inorganic chemistry of life. New York, Oxford University Press 2nd Ed. 541p.

Da Silva, J.J.R.F, Williams, R.J.P., 2001. The biological chemistry of the elements. New York, Oxford University Press 3rd Ed., 575 p.

Dupont, C.l., Yang, S., Bourne, P.E., 2006. Proteomes contain putative imprints of ancient shifts in trace metal geochemistry. PNAS 103:17822-17827.

Dupont, C.L., Butcher, A., Valas, R.E., Bourne, P.E., Caetano-Anolles, G., 2010. History of biological metal utilization inferred through proteomic analysis of protein stuctures. PNAS 107:10567-10572.

Hoffman, H.J., Grey, K., Hickmann, A.H., Thorpe, R.I., 1999. Origin of 3.45 Ga coniform stromatolites in Warrawoona Group, Western Australia. GSA Bulletin 111:1256-1262.

Kasting, J.F., Donohue, T.M., 1980. The evolution of atmospheric ozone. Journal of Geophysical Research: Oceans 85:3255-3263.

Kasting, J.F., Siefert, J.L., 2002. Life and the evolution of Earth's atmosphere. Science 296:1066-1068.

Kasting, J.F., Catling, D., 2003. Evolution of a habitable planet. Annual Review of Astronomy and Astrophysics 41:429-463.

Klein, C., 2005. Some Precambrian banded iron formations (BIFs) from around the world: their age, geological setting, mineralogy, metamorphism, geochemistry, and origin. American Mineralogist 90:1473-1499.

Konhauser, K.O., Pecoits, E., Lalonde, S.V., Papineau, D., Nisbet, E.G., Barley, M.E., Arndt, N.T., Zahnle, K., Kamber, B.S., 2009. Nickel depletion and a methanogen famine before the Great Oxidation Event. Nature 458:750-753.

Lee, J-W., Helmann, J.D., 2007. Functional speclization within the Fur family of metalloregulators. Biometals 20:485-499.

Liu, Y., Beer, L.L., Whitman, W.B., 2012. Methanogens: a window into ancients sulfure metabolism. Trends in Microbiology. 20:251-258.

Maliva, R.G., Knoll, A.H., Siever, R., 1989. Secular changes in chert distribution: a reflection of evolving biological participation in the silica cycle. Palaios 4:519-532.

Mloszewska, A.M., Pecoits, E., Cates, N.L., Mojzsis, S.J., O'Neil, J., Robbins, L.J., 2012. The composition of the Earth's oldest iron formations: the Nuvvuagittuq Supracrustal Bet (Québec, Canada). Earth and Planetary Science Letters 317:331-342.

Pierson, B.K., Mitchell, H.K., Ruff-Roberts, A.L., 1993. *Chloroflexus aurantiacus* and ultraviolet radiation: implications for Archean shallow-water stromatolites. Origins of Life and Evolution of the Biosphere 23:243-260.

Pierson, B.K., Parenteau, M.N., Griffin, B.M., 1999. Phototrophs in high-iron-concentration microbial mats: physiological ecology of phototrophs in an iron-depositing hot spring. Applied Environmental Microbiology 65:5474-5483.

Pierson, B.K., Parenteau, M.N., 2000. Phototrophs in high-iron microbial mats; microstructure of mats in iron depositing hot springs. FEMS Microbioloy Ecology 32:181-196.

Phoenix, V.R., Konhauser, K.O., Adams, D.G., Bottrell S.H., 2001. Role of biominiralization as an ultraviolet shield: implications for Archean life. Geology 29:823-826.

Planavsky, N.J., Asael, D., Hofmann, A., Reinhard, C.T., Lalonde, S.V., Knudsen, A., Wang, X., Ossa Ossa, F., Pecoits, E., Smith, A.J.B., Beaukes, N.J., Bekker, A., Johnson, T.M, Konhauser, K.O., Lyons, T.W., Rouxel, O.J., 2014. Evidence for oxygenic photosynthesis half a billion years before the great oxidation event. Nature Geoscience 7:283-286.

Pokrovski, G.S., Schott J., Farges, F., Hazemann J-L., 2003. Iron(III)-silica interactions in aqueous solutions: insight from x-ray absorption fine structure spectroscopy. Geochimica et Cosmochimica Acta 19:3559-3573.

Ragsdale, S.W., Kumar, M., 1996. Nickel-containing carbon monoxide dehydrogenase/Acetyl Co-A synthase. Chemical Reviews 96:2515-1539.

Robbins, L.J., Lalonde, S.V., Saito, M.A., Planavsky, N.J., Mloszewska, A.M., Pecoits, E., Scott, C., Dupont, C.L., Kappler, A., Konhauser, K.O., 2013. Authigenic iron oxide proxies for marine zinc over geological time and implications for eukaryotic metallome evolution. Geobiology 11:295-306.

Rosing, M.T., 1999. 13C-depleted carbon microparticles in >3700 Ma sea floor sedimentary rocks from West Greenland. Science 283:674-676.

Saito, M.A., Sigman, D.M., Morel, F.M.M., 2003. The bioinorganic chemistry of the ancient ocean: the co-evolution of cyanobacterial metal requirements and biogeochemical cycles at the Archean-Proterozoic boundary? Inorganica Chimica Acta 356:308-318.

Scott, C., Planavsky, N.J., Dupont, C.L. Kendll, B., Gill, B.C., Robbins, L.J., Husband, K.,F., Arnold, G.L., Wing, B.A., Poulton, S.W., Bekker, A., Anbar, A.D., Konhauser, K.O., Lyons, T.W., 2013. Bioavailability of zinc in marine systems through time. Nature Geoscience 6:125-128.

Swanner, E.D., Mloszewska, A.M., Cirpka, O., Schoenberg, R., Konhauser, K.O., Kappler A., in review. Toxic levels of Fe(II) in Archean seawater modulated oxygen producution. Nature Geoscience.

Ueno, Y., Yamada, K., Yoshida, N., Maruyama, S., Isozaki, Y., 2009. Evidence from from fluid inclusions for microbial methanogenesis in the early Archean era. Nature 440:516-519.

Zerkle, A.L., House, C.H., Brantley, S.L., 2005. Biogeochemical signatures through time as inferred from whole microbial genomes. Americal Journal of Science 306:467-502.

References

Alexander, B.W., Bau, M., Andersson, P., Dulski, P., 2008. Continentally-derived solutes shallow Archean seawater: rare earth element and Nd isotope evidence in iron formation from the 2.9 Ga Pongola Supergroup, South Africa. Geochimica et Cosmochimica Acta 72:378-394.

Alibo, D.S., Nozaki, Y., 1999. Rare earth elements in seawater: particle association, shale-normalization, and Ce oxidation. Geochimica et Cosmochimica Acta 63:363-372.

Allwood, A.C., Walter, M.R., Kamber, B.S., Marshall, C.P., Burch, I.W., 2006. Stromatolite reef from the early Archean era of Australia. Nature 44:714-718.

Anbar, A.D., 2004. Iron stable isotopes: beyond biosignatures. Earth and Planetary Science Letters 217:223-236.

Anbar, A.D., Duan, Y., Lyons, T.W., Arnold, G.L., Kendall, B., Creaser, R.A., Kaufman, A.J., Gordon, G.W., Scott, C., Garvin, J., Buick, R., 2007. A whiff of oxygen before the Great Oxidation Event? Science 317:1903-1906.

Aoki, K., Ishida, M., Tokuda, K., 1988. Voltammetry ad microcylinder electrodes part IV: second-order catalytic reaction or ethylenediamminetetraacetic acid with hydrogen peroxide. Journal of Electroanal Chemistry 245:39-50.

Appel, P.W.U., 1979. Cosmic grains in an iron-formation from the early Precambrian Isua Supracrustal Belt, West Greenland. The Journal of Geology 87:573-578.

Appel, P.W.U., 1980. On the early Archean Isua iron-formation, West Greenland. Precambrian Research 11:73-87.

Arndt, N.T., 1991. High Ni in Archean tholeiites. Tectonophysics 187:411-419.

Arndt, N.T., 1994. Archean komatiites. Developments in Precambrian Geology 11:11-44.

Arndt, A., Ginibre, C., Chauvel, C., Albareded, F., Cheadle, M., Herzberg, C., Jenner, G., Lahaye, Y., 1998. Were komatiites wet? Geology 26:739-742.

Arndt, N.T., Coltice, N., Helmstaed, H., Gregoire, M., 2008. Origin of Archean subcontinental lithospheric mantle: some petrological constraints. Lithos. 109:61-71.

Ayres, D.E., 1972. Genesis of Iron-bearing Minerals in banded iron formation mesobands in the Dales Gorge Member, Hamersley Group, Western Australia. Economic Geology 67:1214-1233.

Baadsgaard H., Nutman A.P., Bridgewater D., 1986. Geochronology and isotopic variation of the early Archean Amitsoq gneisses of the Isukasia Area, southern West-Greenland. Geochimica et Cosmochimica Acta 50: 2173-2183.

Balci, N., Bullen, T.D., Witte-Lien, K., Shanks, W.C., Motelica, M., Mandernack, K.W., 2006. Iron isotope fractionation during microbially-stimulated Fe(II) oxidation and Fe(III) precipitation. Geochimica et Cosmochimica Acta 70:622-639.

Balistrieri, L.S., Borrok, D.M., Wanty, R.B., Ridley, W.I., 2008. Fractionation of Cu and Zn isotopes during adsorption onto amorphous Fe(III) oxyhydroxide: Experimental mixing of acid rock drainage and ambient river water. Geochimica et Cosmochimica Acta 72:311-328.

Barbeau, K., Rue, E.L., Bruland, K.W., Butler, A., 2001. Photochemical cycling of iron in the surface ocean mediated by microbial iron(III)-binding ligands. Nature 413:409-413.

Barley, M.E., Krapez, B., Groves, D.I., Kerrich, R., 1998. The Late Archean bonanza: metallogenic and environmental consequences of the interaction between mantle plumes, lithospheric tectonics and global cyclicity. Precambrian Research 91:65-90.

Bau, M., 1991. Rare-earth element mobility during hydrothermal and metamorphic fluid-rock interaction and the significance of the oxidation state of europium. Chemical Geology 93:219-230.

Bau, M., 1993. Effects of syn- and post-depositional processes on the rare-earth element distribution in Precambrian iron-formations. European Journal of Mineralogy 5:257-267.

Bau, M., Dulski, P., 1996. Distribution of yttrium and rare-earth elements in the Penge and Kuruman iron-formations, Transvaal Supergroup, South Africa. Precambrian Research 79:37-55.

Bau, M., Dulski, P., 1999. Comparing yttrium and rare earths in hydrothermal fluids from the Mid-Atlantic Ridge: implications for Y and REE behaviour during near-vent mixing and for the Y/Ho ratio of Proterozoic seawater. Chemical Geology 155:77-90.

Beard, B.L., Johnson, C.M., Skulan, J.L., Nealson, K.H., Cox, L., Sun, H., 2003a. Application of Fe isotopes to tracing the geochemical and biological cycling of Fe. Chemical Geology 195:87-117.

Beard, B.L., Johnson, C.M., Von Damm, K.L., Poulson, R.L., 2003b. Iron isotope constraints on Fe cycling and mass balance in oxygenated Earth oceans. Geology 31:629-632.

Beard, B.L., Johnson, C.M., 2004. Inter-mineral Fe isotope variations in mantle-derived rocks and implications for the Fe geochemical cycle. Geochimica et Cosmochimica Acta 68: 4727-4743.

Beukes, N.J., Klein, C., 1990. Geochemistry and sedimentology of a facies transition -- from microbanded to granular iron-formation -- in the early Proterozoic Transvaal Supergroup, South Africa. Precambrian Research 47:99-139.

Bekker, A., Holland, H.D., Wang, P-L., Rumble III, D., Stein, H.J., Hannah, J.L., Coetzee, L.L., Beukes, N.J., 2004. Dating the rise of atmospheric oxygen. Nature 427:117-120.

Bekker, A., Holland, H.D., Wang, P-L., Rumble III, D., Stein, H.J., Hannah, J.L., Coetzee, L.L., Beukes, N.J., 2004. Dating the rise of atmospheric oxygen. Nature 427: 117-120.

Bekker, A., Slack, J.F., Planavsky, N.J., Krapez, B., Hofmann, A., Konhauser K.O., Rouxel, O.J., 2010. Iron formation: the sedimentary product of a complex interplay among mantle, tectonic, oceanic and biosphere processes. Economic Geology 105:467-508.

Bekker, A., Holland, H.D., 2012. Oxygen overshoot and recovery during the early Proterozoic. Earth and Planetary Science Letters 317-318:295-304.

Berg, J., 1977. Regional geobarometry in the contact aureoles of the anorthositic Nain Complex, Labrador. Journal of Petrology 18:399-430.

Berry, A.J., Danyushevsky, L.V., O'Neill, H., Newville, M., Sutton, S.R., 2008. Oxidation state of iron in komatitic melt inclusions indicates hot Archean mantle. Nature. 455:960-963.

Bjerrum, C.J., Canfield, D.E., 2002 Ocean productivity before about 1.9 Gyr ago limited by phosphorus adsorption onto iron oxides. Nature 417:159-162.

Boily, M., Leclair, A., Maurice, C., Bédard, J.H., David, J., 2009. Paleo- to Mesoarchean basement recycling and terrane definition in the Northeastern Superior Province, Québec, Canada. Precambrian Research 168:23-44.

Bolhar, R., Kamber, B.S., Moorbath, S., Fedo, C.M., Whitehouse, M.J., 2004. Characterization of early Archean chemical sediments by trace element signatures. Earth and Planetary Science Letters 222:43-60.

Bolhar, R., Van Kranendonk, M.J., Kamber, B.S., 2005. A trace element study of siderite-jasper banded iron formation in the 3.45 Ga Warrawoona Group, Pilbara Craton--Formation from hydrothermal fluids and shallow seawater. Precambrian Research 137:93-114.

Bonnichsen, B., 1975. Geology of the Biwabik iron formation, Dunka River area, Minnesota. Economic Geology, 70:319-340.

Bosak, T., Liang, B., Sim, M.S., 2009. Petroff, A.P. Morphological record of oxygenic photosynthesis in conical stromatolites. PNAS 106:10939-10943.

Brasier, M.D., Green, O.R., Jephcoat, A.P., Kleppe, A.K., Van Kranendonk, M., Lindsay, J.F., Steele, A., Grassineau N., 2002. Questioning the evidence for Earth's oldest fossils. Nature 416:76-81.

Bridgewater, D., Watson, J., Windley, B.F., 1973. The Archean craton of the North Atlantic region. Philosophical Transactions of the Royal Society of London Proceedings A 273:493-512.

Bridgewater D., Collerson K.D., 1976. The Major petrological and geochemical characters of the 3600 M.Y Uivak gneisses from Labrador. Contributions to Mineralogy and Petrology 54:43-59.

Bridgewater D., Schiøtte L., 1991. The Archean Gneiss Complex of Northern Labrador: a review of current results, ideas and problems. Bulletin of the Geological Society of Denmark. 39:155-166.

Brocks, J.J., Logan, G.A., Buick, R., Summons, R.E.,1999. Archean molecular fossils and the early rise of eukaryotes. Science 285:1033-1036.

Brocks, J.J., 2001. Molecular fossils in Archean rocks. PhD thesis. University of Sidney.

Brocks, J.J., Pearson A., 2005. Building the biomarker tree of life. Reviews in Mineral Geochemistry 59:233-258.

Bruland, K.W., Lohan, M.C., 2004. The Control of trace metals in seawater. In: Elderfield, H., Ed. The Oceans and Marine Geochemistry. The Treatise of Geochemistry p. 33 to 47.

Buick, R., 1992. The antiquity of oxygenic photosynthesis: evidence from stromatolites in sulphate-deficient Archean lakes. Science 255:74-77.

Buick, R., 2008. When did oxygenic photosynthesis evolve? Philosophical Transactions of the Royal Society B. 363:2731-2743.

Bullen, T.D., White, A.F., Childs, C.W., Vivit, D.V., Schulz, M.S., 2001. Demonstration of significant abiotic iron isotope fractionation in nature. Geology 29:699-702.

Burd, A.B., Jackson, G.A., 2009. Particle aggregation. Annual Review of Marine Science 1:65-90.

Butterfield, N.J., 2009. Oxygen, animals and oceanic ventilation: an alternate view. Geobiology 7:1-7.

Byerly, G.R., Lower, D.R., Walsh, M.W., 1989. Stromatolites from the 3,300-3,500-Myr Swaziland Supergroup, Barberton Mountain Land, South Africa. Nature 319:489-491.

Byrne, R.H., Kim, K-H., 1990. Rare earth element scavening in seawater. Geochimica et Cosmochimica Acta 54:2645-2656.

Cabiscol, E., Tamarit, J., Ros, J., 2000. Oxidative stress in bactria and protein damage by reactive oxygen species. International Microbiology 3:3-8.

Cantrell, K.J., Byrne, R.H., 1987. Rare earth element complexation by carbonate and oxalate ions. Geochimica et Cosmochimica Acta 51:597-605.

Carlson, L., Schwertmann, U., 1981. Natural ferrihydrites in surface deposits from Finland and their association with silica. Geochimica et Cosmochimica Acta 45:421-425.

Cartron, M.L., Maddocks, S., Gillingham, P., Craven, C.J., Andrews, S.C., 2006. Feo-transport of ferrous iron into bacteria. Biometals 19:143-157.

Cates, N.L., Mojzsis, S.J., 2006. Chemical and isotopic evidence for widespread Eoarchean metasedimentary enclaves in southern West Greenland. Geochimica et Cosmochimica Acta 70:4229-4257.

Cates, N.L., Mojzsis, S.J., 2007. Pre-3750 Ma supracrustal rocks from the Nuvvuagittuq supracrustal belt, northern Québec. Earth and Planetary Science Letters 255:9-21.

Cates, N.L., Mojzsis, S.J., 2009. Metamorphic zircon, trace elements and Neoarchean metamorphism in the ca. 3.75 Ga Nuvvuagittuq supracrustal belt, Québec (Canada). Chemical Geology 261:99-114.

Catling, D.C., Zahnle, K.J., McKay, C.P., 2001. Biogenic methane, hydrogen escape, and the irreversible oxygenation of early Earth. Science 293:839-843.

Cismeau, A.C., Michel, F.M., Tcaciuc, A.P., Brown, G.E. Jr., 2014. Properties of impurity-bearing ferrihydrite III. Effects of Si on the structure of 2-line ferrihydrite. Geochim. Cosmochim. Acta 133:168-185.

Cockell, C.S., 2000. Ultraviolet radiation and the photobiology of Earth's early oceans. Origin of Life and Evolution of the Biosphere 30:467-499.

Condie, K.C., 1981. Archean Greenstone Belts. Elsevier Amsterdam, 434 p.

Condie, K.C., 2001. Mantle plumes and their record in Earth history. Cambridge University Press. 305 p.

Croal, L.R., Johnson, C.M., Beard, B.L., Newmann, D.K., 2004. Iron isotope fractionation by Fe(II)-oxidizing photoautotrophic bacteria. Geochimica et Cosmochimica Acta 68:1227-1242.

Crowe, S.A., Dossing, L.N., Beukes, N.J., Bau, M., Kruger, S.J.., Frei, R., Canfield, D.E., 2013. Atmospheric oxygenation three billion years ago. Nature 501:535-538.

Czaja, A.D., Johnson C.M., Roden, E.E., Beard, B.L., Voegelin A.R., Nagler, T.F., Beukes, N.J., Wille M., 2012. Evidence for free oxygen in the Neoarchean ocean based on coupled iron-molybdenum isotope fractionation. Geochimica et Cosmochimica Acta 86:118-137.

Cockell, C.S., 2000. Ultraviolet radiation and the photobiology of Earth's early oceans. Origin of Life and Evolution of the Biosphere 30:467-499.

Crowe, S.A., Dossing, L.N, Beukes, N.J., Bau, M., Kruger, S.J., Frei, R., Canfield, D.E., 2013. Atmospheric oxygenation three billion years ago. Nature 501:535-538.

Danielson, A., Moller, P., Dulski, P., 1992. Chemical Geology 97:89-100.

Da Silva, J.J.R.F., Williams, R.J.P., 1991. The biological chemistry of the elements: the inorganic chemistry of life. New York, Oxford University Press 2nd Ed. 541p.

Da Silva, J.J.R.F, Williams, R.J.P., 2001. The biological chemistry of the elements. New York, Oxford University Press, 575 p.

Dunford, H.B., 1987.Free radicals in iron-containing systems. Free Radical Biology and Medicine 3:405-421.

Dauphas, N., Van Zuilen, M., Wadhwa, M., Davis, A.M., Marty, B., Janney, P.E., 2004. Clues from Fe isotope variations on the origin of Early Archean BIFs from Greenland. Science 306:2077-2080.

Dauphas, N., Cates, N.L., Mojzsis, S.J., Busigny, V., 2007a. Identification of chemical sedimentary protoliths using iron isotopes in the > 3750 Ma Nuvvuagittuq supracrustal belt, Canada. Earth and Planetary Science Letters 254:358-376.

Dauphas, N., Van Zuilen, M., Busigny, V., Lepland, A., Wadhwa, M., Janney, P.E., 2007b. Iron isotope, major and trace element characterization of Early Archean

supracrustal rocks from SW Greenland: protolith identification and metamorphic overprint. Geochimica et Cosmochimica Acta 71:4745-4770.

David, J., Godin, L., Stevenson, R., O'Neil, J., Francis, D., 2009. U-Pb ages (3.8–2.7 Ga) and Nd isotope data from the newly identified Eoarchean Nuvvuagittuq supracrustal belt, Superior Craton, Canada. Geological Society of America Bulletin 121:150-163.

Deer, W.A., Howie, R.A., Zussman, J., 1992. An introduction to the rock forming minerals. Prentice Hall.

De Ronde, C.E.J., Channer, D.M.D., Faure K., Bray, C.J., Spooner, E.T.C., 1997. Fluid chemistry of Archean seafloor hydrothermal vents: implications for the composition of circa. 3.2 Ga seawater. Geochimica et Cosmochimica Acta 61:4025-4042.

Derry, L.A., Jacobsen, S.B., 1990. The chemical evolution of Precambrian seawater: Evidence from REEs in banded iron formations. Geochimica et Cosmochimica Acta 54:2965-2977.

Dupont, C.l., Yang, S., Bourne, P.E., 2006. Proteomes contain putative imprints of ancient shifts in trace metal geochemistry. PNAS 103:17822-17827.

Dupont, C.L., Butcher, A., Valas, R.E., Bourne, P.E., Caetano-Anolles, G., 2010. History of biological metal utilization inferred through proteomic analysis of protein stuctures. PNAS 107:10567-10572.

Dutkiewicz, A., Ridley, J., Buick, R., 2003. Oil-bearing CO2-CH4-H2O fluid inclusions: oil survival since the Palaeoproterozoic after high temperature entrapment. Chemical Geology 194:51-79.

Dutkiewicz, A., Volk, H., George, S.C., Ridley, J., Buick, R., 2006. Biomarkers from Huronian oil-bearing fluid inclusions: an uncontaminated record of life before the Great Oxidation Event. Geology 34:437-440.

Dymek, R.F., Klein, C., 1988. Chemistry, petrology and origin of banded iron-formation lithologies from the 3800 Ma Isua Supracrustal Belt, West Greenland. Precambrian Research 39:247-302.

Edmond, J.M., Von Damm, K.L., McDuff, R.E., Measures, C.I., 1982. Chemistry of hot springs on the East Pacific Rise and their effluent dispersal. Nature 297:187-191.

Ehling-Shultz, M., Bilger, W., Scherer, S., 1997. UV-B-induced synthesis of photoprotective pigments and extracellular polysaccharides in the terrestrial cyanobacterium Nostoc commune. Journal of Bacteriology 179:1940-1945.

Eldridge, M.L., Trick, C.G., Alm, M.B., DiTullio, G.R., Rue, E.L., Bruland, K.W., Hutchins, D.A., Wilhelm, S.W., 2004. Planktonic community response to a manipulation of iron in HNLC waters of the subtropical Pacific Ocean. Aquatic Microbial Ecology 35:79-91.

Engelmann, M.D., Bobier, R.T., Hiatt, T., Cheng, I.F., 2003. Variability of the Fenton reaction on characteristics of the EDTA, DPTA and citrate complexes of iron. Biometals 16:519-527.

Escot, M., Martre, A.M., Poillen, P., Martinet, P., 1989. Electrochemical study of iron(III) complextion by some model ligands of biological interest I. Acetohydroxamic acid, acetylacetone and citric acid. Bulletin de la Societe de Chimie France 3:316-320.

Ewers, W.E., Morris, R.C., 1981. Studies of the Dales Gorge Member of the Brockman Iron Formation, Western Australia. Econ Geol 76, 1929-1953.

Ewers, W.E., 1980. Chemical conditions for the precipitation of banded iron formations. *In*: Truedinger, P.A., Walter, M.R., Ralph, B.J., Eds. Biogeochemistry of Ancient and Modern Environments, Springer Berlin Heidelberg, p.83-92.

Ewers, W.E., Morris, R.C., 1981. Studies of the Dales Gorge Member of the Brockman iron formation, Western Australia. Economic Geology 76:1929-1953.

Falkowski, P.G., 1997. Evolution of the nitrogen cycle and its influence on the biological sequestration of CO_2 in the ocean. Nature 387:272-275.

Fanning, K.A., Pilson, M.E.Q., 1973. On the spectrophotometric determination of dissolved silica in natural waters. Analytical Chemistry 45:136-140.

Farquhar, J., Bao, H., Thiemens, M., 2000. Atmospheric influence of Earth's earliest sulfur cycle. Science 289:756-758.

Farquhar, J., Savarino, J., Airibeau, S., Thiemens, M.H., 2001. Observation of wavelength-sensitive mass-independent sulfur isotope effects during SO_2 photolysis: implications for the early atmosphere. Journal of Geophysical Research 106:32829-32839.

Farquhar, J., Wing, B.A., 2003. Multiple sulfur isotopes and the evolution of the atmosphere. Earth and Planetary Science Letters 213:1-13.

Farquhar, J., Zerkle, A.L., Bekker, A., 2011. Geological constraints on the origin of oxygenic photosynthesis. Photosynthesis Research 107:11-36.

Fedo, C.M., Whitehouse, M.J., 2002. Metasomatic origin of quarz-pyroxene rock, Akilia, Greenland, and implications for Earth's earliest life. Science 296:1448-1452.

Fedo, C.M., Whitehouse, M.J., Kamber, B.S., 2006. Geological constraints on detecting the earliest life on Earth: a perspective from the Early Archean (older than 3.7 Gyr) of southwest Greenland. Philosophical Transactions of the Royal Society B 361:851-867.

Fike, D.A., Grotzinger, J.P., Summons, R.E., 2006. Oxidation of the Ediacaran ocean. Nature 444:744-747.

Fonarev, V.I., Pilugin, S.M., Savko., K.A., Novikova, M.A., 2006. Exsolution textures of orthopyroxene and clinopyroxene in high-grade BIF of the Voronezh Cristalline Massif: evidence of ultrahigh-temperature metamorphism. Journal of Metamorphic Geology 24:135-151.

Frei, R., Polat, A., 2007. Source heterogeneity for the major components of ~ 3.7 Ga Banded Iron Formations (Isua Greenstone Belt, Western Greenland): Tracing the nature of interacting water masses in BIF formation. Earth and Planetary Science Letters 253:266-281.

Fridvovich, I., 1995. Superoxide radicals and superoxide dismutase. Annual Reviews in Biochemistry 64:97-112.

Fridovich, I., 1997. Superoxide anion radicals (O^{-}_{2}), superoxide dismutases and related matters. The Journal of Biological Chemistry 272:18515-18517.

Friend C.R.L., Nutman A.P., McGregor V.R., 1988. Late Archean terrane accretion in the Godthab region, southern West Greenland. Nature 335:535-538.

Friend C.R.L., Nutman A.P., 1994. 2 Archean granulite-facies metamorphic events in the Nuuk -Maanitsoq region, southern West Greenland: correlation with the Saglek Block, Labrador. Journal of the Geological Society 151: 421-424.

Friend C.R.L., Nutman A.P., 2005. New pieces to the Archean terrane jigsaw puzzle in the Nuuk region, southern West Greenland: steps in transforming a simple insight into a complex regional tectonothermal model. Journal of the Geological Society of London 162:147-162.

Friend C.R.L., Nutman A.P., 2007. Adjacent terranes with ca. 2715 and 2650 Ma high-pressure metamorphic assemblages in the Nuuk region of the North Atlantic Craton, southern West Greenland: complexities of Neoarchean collisional orogeny. Precambrian Research 155:159-203.

Froelich, P.N., Blanc, V., Mortlock, R.A., Chillrud, S.N., Dunstan, W., Udomkit, A., Peng, T-H., 1992. River fluxes of dissolved silica to the ocean were higher during glacials: Ge/Si in diatoms, rivers and oceans. Paleoceanography 7:739-767.

Frost, C.D., Von Blanckenburg, F., Schoenberg, R., Frost, B.R., Swapp, S.M., 2007. Preservation of Fe isotope heterogeneities during diagenesis and metamorphism of banded iron formation. Contribution to Mineralogy and Petrology 153:211-235.

Ghassemian, M., Straus, N.A., 1996. Fur regulates the expression of iron-stress genes in the cyanobacterium Synechococcus sp. PCC 7942. Microbiology 142:1469-1476.

Gole, M.J., Klein, C., 1981. High-grade metamorphic banded iron formations, Western Australia: assemblages with coexisting pyroxene±fayalite. American Mineralogist 66:87-99.

Graf, E., Mahoney, J.R., Bryant, R.G., Eaton, J.W., 1984. The Journal of Biological Chemistry 259:3620-3624.

Grauch, R.I., 1989. Rare earth elements in metamorphic rocks. Reviews in Mineralogy and Geochemistry 21:147-167.

Grotzinger, J.P., Kasting, J.F., 1993. New constraints on Precambrian ocean composition. Geology 101:235-243.

Grotzinger, J.P., Knoll, A.H., 1999. Stromatolites in Precambrian carbonates: evolutionary mileposts or environmental dipsticks? Annual Reviews in Earth and Planetary Science 27:313-358.

Gustafsson, J.P., 2011. Visual Minteq, 3.0 Ed. http://www.lwr.kth.se/English/OurSoftware/vminteq (Stockholm, Sweden).

Hamade, T., Konhauser, K.O., Raiswell, R., Goldsmight, S., Morris, R.C., 2003. Using Ge/Si ratios to decouple iron and silica fluxes in Precambrian banded iron formations. Geology 31:35-38.

Hantke, K., 1987. Negative control of iron uptake systems in Escherichia coli. FEMS Microbiology Letters 15:83-86.

Hantke, K., 2003. Is bacterial ferrous iron transporter FeoB a living fossil? Trends in Microbiology 11:192-195.

Harrison, P.M., Arosio, P., 1996. The ferritins: molecular properties, iron storage function, and cellular regulation. Biochimica et Biophysica Acta 1275:161-203.

Haugaard, R., Frei, R., Stendal, H., Konhauser, K.O., 2013. Petrology and geochemistry of the ~2.9 Ga Itilliarsuk banded iron formation and associated supracrustal rocks, West Greenland: source characteristics and depositional environment. Precambrian Research 229:150-176.

Heubeck, C., 2009. An early ecosystem of Archean tidal microbial mats (Moodies Group, South Africa, ca. 3.2 Ga). Geology 37:931-934.

Hider, R.C., Kong, H., Chemistry and Biology of Siderophores. Natural Product Reports 27:637-657.

Hoffman, P.F., 1989. Precambrian geology and tectonic history of North America. In: The geology of North America - an overview. The Geological Society of America. Chapter 16. pp. 447-512.

Hoffman, H.J., Grey, K., Hickmann, A.H., Thorpe, R.I., 1999. Origin of 3.45 Ga coniform stromatolites in Warrawoona Group, Western Australia. GSA Bulletin 111:1256-1262.

Holland, H.D., 1984. The chemical evolution of the atmosphere and oceans. Princeton NJ: Princeton Univesity Press. 582 p.

Holland, H.D., 2006. The oxygenation of the atmosphere and oceans. Transactions of the Royal Society B 361:903-915.

Imlay, J.A., Linn, S., 1988. DNA damage and oxygen radical toxicity. Science 240:1302-1309.

Imlay, J.A., 2003. Pathways to oxidative damage. Annual Reviews in Microbiology 57:395-418.

Isley, A.E., 1995. Hydrothermal plumes and the delivery of iron to banded iron formation. The Journal of Geology 103:169-185.

Isley, A.E., Abbott, D.H., 1999. Plume-related mafic volcanism and the deposition of banded iron formation. Journal of Geophysical Researcg 104:15461-15477.

Jacobsen, S.B., Pimentel-Klose, M.R., 1988. A Nd isotopic study of the Hamersley and Michipictoten banded iron formations: the souce of REE and Fe in Archean oceans. Earth and Planetary Science Letters 87:29-44.

James D.T., Kamo S., Krogh T., 2002. Evolution of 3.1 and 3.0 Ga volcanic belts and a new thermotectonic model for the Hopedale Block, North Atlantic Craton (Canada). Canadian Journal of Earth Sciences 39: 687-710.

Jamieson, D., Chance, B., Cadenas, E., Boveris, A., 1986. The relation of free radical production to hypoxia. Annual Reviews in Physiology 48:708-719.

Jaun, B., Thauer, R.K., 2007. Methyl-coenzyme M reductase and its nickel corphin coenzyme F430 in methanogenic archaea. Metal Ions in Life Sciences 2:323-356.

Johnson, C.M., Skulan, J.L., Beard, B.L., Sun, H., Nealson, K.H., Braterman, P.S., 2002. Isotopic fractionation between Fe(III) and Fe(II) in aqueous solutions. Earth and Planetary Science Letters 195:141-153.

Johnson, C.M., Beard, B.L., Beukes, N.J., Klein, C., O'Leary, J.M., 2003. Ancient geochemical cycling in the Earth as inferred from Fe isotope studies of banded iron formations from the Transvaal Craton. Contributions to Mineralogy and Petrology 144:523-547.

Johnson, C.M., Beard, B.L., Klein, C., Beukes, N.J., Roden, E.E., 2008. Iron isotopes constrain biologic and abiologic processes in banded iron formation genesis. Geochimica et Cosmochimica Acta 72:151-169.

Joux, F., Jeffrey, W.H., Lebaron, P., Mitchell, D.L., 1999. Marine bacterial isolates display diverse responses to UV-B radiation. Applied and Environmental Microbiology 65:3820-3827.

Kammler, M., Schön, C., Hantke, K., 1993. Characterization of the ferrous iron uptake system of Escherichia coli. Journal of Bacteriology 175:6262-6218.

Kasting, J.F., 1987. Theoretical constraints on oxygen and carbon dioxide concentrations in the Precambrian atmosphere. Precambrian Research 34:205-229.

Kasting, J.F., Donohue, T.M., 1980. The evolution of atmospheric ozone. Journal of Geophysical Research: Oceans 85:3255-3263.

Kasting, J.F., 1993. Earth's early atmosphere. Science 259:920-926.

Kasting, J.F., Pavlov, A.A., Sieffert, J.L., 2001. A coupled ecosystem-climate model for predicting the methane concentration in the Archean atmosphere. Origins of Life and Evolution of the Biosphere 31:271-285.

Kasting, J.F., Siefert, J.L., 2002. Life and the evolution of Earth's atmosphere. Science 296:1066-1068.

Kasting, J.F., Catling, D., 2003. Evolution of a habitable planet. Annual Review of Astronomy and Astrophysics 41:429-463.

Kasting, J.F., Howard, M.T., 2006. Atmospheric composition and climate on early Earth. Philosophical Transactions of the Royal Society B 361:1733-1742.

Kaufman, A.J., Johnston, D.T., Farquhar, J., Masterson, A.L., Lyons, T.W., Bates, S., Anbar, A.D., Arnold, G.L., Garvin, J., Buick, R,. 2007. Late Archean biospheric oxygenation and atmospheric evolution. Science 317:1900-1903.

Kato, Y., Ohta, I., Tsunematsu, T., Watanabe, Y., Isozaki, Y., Maruyama, S., Imai, N., 1998. Rare earth element variations in mid-Archean banded iron formations: implications for the chemistry of ocean and continent and plate tectonics. Geochimica et Cosmochimica Acta 62:3475-3497.

Katoh, H., Hagino, N., Grossman, A.R., Ogawa, T., 2001. Genes essential to iron transport in the cyanobacterium Synechocystis sp. PCC 6803. Journal of Bacteriology 183:2779-2784.

Kaufman A., 2014. Early Earth: cyanobacteria at work. Nature Geoscience 7:253-254.

Keren, N., Aurora, R., Pakrasi, H.B., 2004. Critical roles of bacterioferritins in iron storage and proliferation of cyanobacteria. Plant Physiology 135:1666-1673.

Kida, K., Shigematsu, T., Kijima, J., Numaguchi, M., Mochinaga, Y., Abe, N., Morimura, S., 2001. Influence of Ni^{2+} and Co^{2+} on methanogenic activity and the amounts of coenzymes involved in methanogenesis. Journal of Bioscience and Bioengineering 91:590-595.

Klein, C., 2005. Some Precambrian banded iron formations (BIFs) from around the world: their age, geological setting, mineralogy, metamorphism, geochemistry, and origin. American Mineralogist 90:1473-1499.

Knauth, L.P., Lowe, D.R., 2003. High Archean climatic temperature inferred from oxygen isotope geochemistry of cherts in 3.5 Ga Swaziland Supergroup, South Africa. GSA Bulletin 115:566-580.

Knoll, A.H., 1979. Archean photoautotrophy: some alternatives and limits. Origins of Life 9:313-327.

Konhauser, K.O., Ferris, F.G., 1996. Diversity of iron and silica precipitation by microbial mats in hydrothermal waters, Iceland: implications for Precambrian iron formations. Geology 24:323-326.

Konhauser, K.O., Hamade, T., Raiswell, R., Morris, R.C., Ferris, F.G., Southam, G., Canfield, D.E., 2002. Could bacteria have formed the Precambrian banded iron formations? Geology 30:1079-1082.

Konhauser, K.O., Lalonde, S.V., Arnskold, L., Holland, H.D., 2007. Was there really an Archean Phosphate crisis? Science 315:1234.

Konhauser, K.O., Pecoits, E., Lalonde, S.V., Papineau, D., Nisbet, E.G., Barley, M.E., Arndt, N.T., Zahnle, K., Kamber, B.S., 2009. Nickel depletion and a methanogen famine before the Great Oxidation Event. Nature 458:750-753.

Konhauser, K.O., Lalonde, S.V., Planavsky, N.J., Pecoits, E., Lyons, T.W., Mojzsis, S.J., Rouxel, O.J., Barley, M.E., Rosière, C., Fralick, P.W., Kump, L.R., Bekker, A.,

2011. Aerobic bacterial pyrite oxidation and acid rock drainage during the Great Oxidation Event. Nature 478:369-373.

Koziol, A.M., 2004. Experimental determination of siderite stability and application to Martian Meteorite ALH84001. American Mineralogist 89:294-300.

Kuma, K., Nishioka, J., Matsunaga, K., 1996. Limnological Oceanography 41:396-407.

Latifi, A., Ruiz, M., Zhang, C-C., 2009. Oxidative stress in cyanobacteria. FEMS Microbiology Reviews 33:258-278.

Lee, J-W., Helmann, J.D., 2007. Functional speclization within the Fur family of metalloregulators. Biometals 20:485-499.

Lepland, A., Van Zuilen, M.A., Philippot, P., 2011. Fluid deposited graphite and its geobiological implications in early Archean gneiss from Akilia, Greenland. Geobiology 9:2-9.

Le Roux, V., Lee, C.T.A., Turner, S.J., 2010. Zn/Fe systematics in mafic and ultramafic systems: Implications for detecting major element heterogeneities in the Earth's mantle. Geochimica et Cosmochimica Acta 74:2779-2796.

Lewin, A., Moore, G.R., Le Brun, N.E., 2005. Formation of protein-coated iron minerals. Dalton Transactions 22:3597-3610.

Linn, S., 1998. DNA damage by iron and hydrogen peroxide in vivo. Druge Metabolism Reviews 30:313-326.

Liu, Y., Beer, L.L., Whitman, W.B., 2012. Methanogens: a window into ancients sulfure metabolism. Trends in Microbiology. 20:251-258.

Logan, G.A., Hayes, J.M., Hieshima, G.B., Summons, R.E., 1995. Terminal Proterozoic reorganization of biogeochemical cycles. Nature 376:53-56.

Lovley, D.R., 1993. Dissimilatory metal reduction. Annual Review of Microbiology 47:263-290.

Lupton, J.E., 1995. Hydrothermal plumes: near and far field. *In*: Humphris, S.E., Zierenberg, R.A., Mullineau, L.S., Thomson, R.E Eds. Seafloor hydrothermal systems: Physical, chemical, biological, and geological interactions. Geophysical Monograph: 91. Washington, DC. American Geophysical Union, 317-346p.

Manning, C.E., Mojzsis, S.J., Harrison, T.M., 2006. Geology, age and origin of supracrustal rocks at Akilia,West Greenland. American Journal of Science 306:303-366.

Maliva, R.G., Knoll, A.H., Simmonson, B.M., 2005. Secular change in the Precambrian silica cycle: insights from chert petrology. GSA Bulletin 117:835-845.

Mallick, N. Cu-induced Oxidative stress in chlorophycean microalga Chlorella vulgaris. Journal of Plant Physiology 161:591-597.

McGregor, V.R., Mason, B., 1977. Petrogenesis and geochemistry of metabasaltic and metasedimentary enclaves of the Amîtsoq gneisses, West Greenland. American Mineralogist 62:887-904.

McGregor V.R., Friend C.R.L., Nutman A.P., 1991. The late Archean mobile belt through Godthabsfjord, southern West Greenland: a continent-continent collision zone? Bulletin of the Geological Society of Denmark 39: 179-197.

McLennan, S.M., Hemming, S., McDaniel, D.K., Hanson, G.N., 1993. Geochemical approaches to sedimentation, provenance, and tectonics. Special Papers - Geological Society of America, 21-40.

Mel'nik, Y.P., 1982. Precambrian iron formations: physiochemical conditions of formation. Elsevier Scientific Publishing Company.

Michard, A., 1986. The REE content of some hydrothermal fluids. Chemical Geology 55:51-60.

Mloszewska, A.M., Pecoits, E., Cates, N.L., Mojzsis, S.J., O'Neil, J., Robbins, L.J., 2012. The composition of the Earth's oldest iron formations: the Nuvvuagittuq Supracrustal Bet (Québec, Canada). Earth and Planetary Science Letters 317:331-342.

Mojzsis, S.J., Arrhenius, G., McKeegan, K.D., Harrison, T.M., Nutman, A.P., Friend, C.R.L., 1996. Evidence for life on Earth before 3,800 million years ago. Nature 387:55-59.

Mojzsis, S.J., Harrison, T.M., 2002. Establishment of a 3.83 Ga magmatic age for the Akilia tonialite (southern West Greenland). Earth and Planetary Science Letters 202:563-576.

Mojzsis, S.J., Coath, C.D., Greenwood, J.P., McKeegan, K.D., Harrison, T.M., 2003. Mass-independent isotope effects in Archean (2.5 to 3.8 Ga) sedimentary sulfides

determined by ion microprobe analysis. Geochimica et Cosmochimica Acta 67:1635-1658.

Monster, J., Appel, P.W.U., Thode, H.G., Schidlowski, M., Carmichael, C.M., 1979. Sulfur isotope studies in early Archean sediments from Isua, West Greenland: implications for the antiquity of bacterial sulfate. Geochimica et Cosmochimica Acta 43:405-413.

Morris, R.C., Horowitz, R.C., 1983. The origin of the iron-formation-rich Hamersley Group of Western Australia – deposition on a platform. Precambrian Research 21:273-297.

Mortlock, R.A., Froelich, P.N., Feely, R.A., Massoth ,G.J., Butterfield, D.A., Lutpon, J.E., 1993. Silica and germanium in Pacific Ocean hydrothermal vents and plumes. Earth and Planetary Science Letters 119:365-378.

Neale, P.J., Davis, R.F., Cullen, J.J., 1998. Interactive effects of ozone depletion and vertical mixing on the photosynthesis of Antarctic phytoplankton. Nature 392:585-589.

Nisbet, E.G., Cheadle, M.J., Arndt, N.T., Bickle, M.J., 1993. Constraining the potential temperature of the Archean mantle: a review of the evidence from komatiites. Lithos 30:291-307.

Nisbet, E.G., Cann, J.R., Van Dover, L., 1995. Origin of Photosynthesis. Nature 373:479.

Nisbet, E.G., Fowler, C.M.R., 1996. The hydrothermal imprint of life: did heat-shock proteins, metalloproteins and photosynthesis begin around hydrothermal vents? Geological Society Special Publications 118:239-251.

Noffke, N., Hazen, R., Nhelko, N., 2003. Earth's earliest microbial mats in a siliciclastic marine environment (2.9 Ga Mozaan Group, South Africa). Geology 31:673-676.

Noffke, N., Eriksson, K.A., Hazen, R.M., Simpson, E.L., 2006. A new window into early Archean life: microbial mats in Earth's oldest siliciclastic tidal depost (3.2 Ga Moddies Group, South Africa). Geology 34:253-256.

Noffke, N., Christian, D., Wacey, D., Hazen, R.H., 2013. Microbially induced sedimentary structures recording an ancient ecosystem in the ca. 3.48 billion-year-old Dresser Formation, Pilbara, Western Australia. Astrobiology 13:1103-1124.

Nomura, C.T., Persson, S., Shen, G., Inoue-Sakamoto, K., Bryant, D.A., 2006. Characterization of two cytochrome oxidase operons in the marine cyanobacterium Synechococcus sp. PCC 7002: Inactivation of ctaDI affects the PS I:PS II ratio. Photosythesis Research 87:215-228.

Nutman, A.P., 1986. The early Archean to Proterozoic history of the Isukasia area, southern West Greenland. Bulletin Gronlands Geological Undersurvey 154:80.

Nutman, A.P., Fryer, B.J., Bridgewater, D., 1989. The early Archean Nulliak (supracrustal) assemblage, northern Labrador. Canadian Journal of Earth Sceinces 26:2159-2168.

Nutman, A.P., Collerson K.D., 1991. Very early Archean crustal accretion complexes preserved in the North Atlantic Craton. Geology 19:791-794.

Nutman, A.P., McGregor, V.R., Friend, C.R.L., Bennett, V.C., Kinny, P.D., 1996. The Itsaq Gneiss Complex of southern West Greenland; the world's most extensive record of early crustal evolution (3900-3600 Ma). Precambrian Research 78:1-39.

Nutman, A.P., Friend, C.R.L., 2006. Petrography and geochemistry of apatites in banded iron formation, Akilia, W. Greenland: consequences for oldest life evidence. Precambrian Research 147:100-106.

O'Neil, J., Carlson, R.W., Francis, D., Stevenson, R.K., 2008. Neodymium-142 Evidence for Hadean Mafic Crust. Science 321:1828-1831.

O'Neil, J., Francis, D., Carlson, R., 2011. Implications of the Nuvvuagittuq Greenstone Belt for the formation of Earth's carly crust. Journal of Petrology. 52:985-1009.

Ohmoto, H., 2003. Nonredox transformations of magnetite-hematite in Hydrothermal Systems. Economic Geology 98:157-161.

Olson, J.M., Pierson, B.K., 1986. Photosynthesis 3.5 thousand million years ago. Photosynthesis Research 9:251-259.

Ourisson, G., Rohmer, M., Porella, K., 1987. Prokaryotic hopanoids and other ploylerpenoid stero surrogates. Annual Reviews in Microbiology 41:301-333.

Papineau, D., Mojzsis, S.J., 2006. Mass-independent fractionation of sulfur isotopes in sulfides from the pre-3770 Ma Isua Supracrustal Belt, West Greenland. Geobiology 4:227-238.

Papineau, D., De Gregorio, B.T., Cody, G.D., O'neil, J., Steele, A., Stroud, R.M., Fogel, M.L., 2011. Young poorly crystalline graphite in >3.8 Gyr-old Nuvvuagittuq banded iron formation. Nature Geosciences 4:376-379.

Pavlov, A.A., Kasting, J.F., 2002. Mass-independent fractionation of sulfur isotopes in Archean sediments: strong evidence for an anoxic Archean atmosphere. *Astrobiology* 2:27-41.

Partin, C.A., Bekker, A., Planavsky, N.J., Scott, C.T., Gill, B.C., Li, C., Podkoryrov, V., Maslov, A., Konhauser, K.O., Lalonde, S.V., Love, G.D., Poulton, S.W., Lyons, L.W., 2013. Large-scale fluctuations in Precambrian atmospheric and oceanic oxygen levels from the record of U in shales. Earth and Planetary Science Letters, 369-370:284-293.

Pavlov, A.A., Kasting, J.F., 2002. Mass-independent fractionation of sulfur isotopes in Archean sediments: strong evidence for an anoxic Archean atmosphere. Astrobiology 2: 27-41.

Pecoits, E., Gingras, M.K., Aubet, N.R., Konhauser, K.O., in press. Ediacaran in Uruguay: palaeoclimatic and palaeobiolobical implications. Sedimentology 55:689-719.

Phoenix, V.R., Konhauser, K.O., Adams, D.G., Bottrell S.H., 2001. Role of biominiralization as an ultraviolet shield: implications for Archean life. Geology 29:823-826.

Phoenix, V.R., Bennett, P.C., Engel, A.S., Tyler, S.W., Ferris, F.G., 2006. Chilean high-altitude hot-spring scinters: a model system for UV screening mechanisms by early Precambrian cyanobacteria. Geobiology 4:15-28.

Pierre, J.L., Gautier-Luneau, I., 2000. Iron and citric acid: a fuzzy chemistry of fuzzy biological relevance. Biometals 13:91-96.

Pierson, B.K., Mitchell, H.K., Ruff-Roberts, A.L., 1993. *Chloroflexus aurantiacus* and ultraviolet radiation: implications for Archean shallow-water stromatolites. Origins of Life and Evolution of the Biosphere 23:243-260.

Pierson, B.K., Parenteau, M.N., Griffin, B.M., 1999. Phototrophs in high-iron-concentration microbial mats: physiological ecology of phototrophs in an iron-depositing hot spring. Applied Environmental Microbiology 65:5474-5483.

Pierson, B.K., Parenteau, M.N., 2000. Phototrophs in high-iron microbial mats; microstructure of mats in iron depositing hot springs. FEMS Microbioloy Ecology 32:181-196.

Pivovarov, S., 2008. Adsorption of ions onto amorphous silica: ion exchange model. Journal of Colloid and Interface Science 319:374-376.

Planavsky, N.J., Rouxel, O.J., Bekker, A., Lalonde, S.V., Konhauser, K.O., Reinhard, C.T., Lyons, T.W., 2010. The evolution of the marine phosphate reservoir. Nature 467:1088-1090.

Planavsky, N.J., Rouxel, O.J., Bekker, A., Hofmann, A., Little, C.T.S., Lyons, T.W., 2012. Iron isotope composition of some Archean and Proterozoic iron formations. Geochemica et Cosmochimica Acta 80:158-169.

Planavsky, N.J., Asael, D., Hofmann, A., Reinhard, C.T., Lalonde, S.V., Knudsen, A., Wang, X., Ossa Ossa, F., Pecoits, E., Smith, A.J.B., Beaukes, N.J., Bekker, A., Johnson, T.M, Konhauser, K.O., Lyons, T.W. & Rouxel, O.J. 2014 Evidence for oxygenic photosynthesis half a billion years before the great oxidation event. Nature Geoscience 7:283-286.

Pokrovski, G.S., Schott J., Farges, F., Hazemann J-L., 2003. Iron(III)-silica interactions in aqueous solutions: insight from x-ray absorption fine structure spectroscopy. Geochimica et Cosmochimica Acta 19:3559-3573.

Polat, A., Frei, R., 2005. The origin of early Archean banded iron formations and of continental crust, Isua, southern West Greenland. Precambrian Research 138:151-175.

Quesada, A., Vincent, W.F., Lean, D.R.S., 1999. Community and pigment structure of Arctic cyanobacterial assemblages: the occurrence and distribution of UV-absorbing compounds. FEMS Microbiology Ecology 28:315-323.

Ragsdale, S.W., Kumar, M., 1996. Nickel-containing carbon monoxide dehydrogenase/Acetyl Co-A synthase. Chemical Reviews 96:2515-1539.

Rasmussen, B., Buick, R., 1999. Redox state of the Archean atmosphere: evidence from detrital heavy minerals in ca. 3250-2750 Ma sandstones from the Pilbara Craton, Australia. Geology 27:115-118.

Rastogi, R.P., Singh, S.P., Häder, D-P., Sinha, R.P., 2010. Detection of reactive oxygen species (ROS) by the oxidant-sensing probe 2', 7'-dichlorodihydrofluorecein

diacetate in the cyanobacterium Anabaena variabilis PCC 7937. Biochemical and Biophysical Research Communications 397:603-607.

Robbins, L.J., Lalonde, S.V., Saito, M.A., Planavsky, N.J., Mloszewska, A.M., Pecoits, E., Scott, C., Dupont, C.L., Kappler, A., Konhauser, K.O., 2013. Authigenic iron oxide proxies for marine zinc over geological time and implications for eukaryotic metallome evolution. Geobiology 11:295-306.

Robert, F., Chaussidon, M., 2006. A paleotemperature curve for the Precambrian oceans based on silicon isotopes in cherts. Nature 443:969-972.

Rose, A.L., Waite, T.D., 2003. Kinetics of iron complexation by dissolved natural organic matter in coastal waters. Marine Chemistry 84:85-103.

Rosing, M.T., 1999. 13C-depleted carbon microparticles in >3700 Ma sea floor sedimentary rocks from West Greenland. Science 283:674-676.

Rosing, M.T., Frei, R., 2004. U-rich Archaean sea-floor sediments from Greenland: indications of 3700 Ma oxygenic photosynthesis. Earth and Planetary Science Letters 217:237–244.

Ross, M., Papike, J.J., Shaw, K.W., 1969. Exsolution textures in amphiboles as indicators of subsolidus thermal histories. Mineralogical Society of Amberica Special Paper 2:275-299.

Rothman, D.H., Hayes, J.M., Summons, R.E., 2003. Dynamics of the Neoproterozoic carbon cycle. PNAS 100:8124-8129.

Rouxel, O.J., Bekker, A., Edwards, K.J., 2005. Iron isotope constraints on the Archean and Paleoproterozoic ocean redox state. Science 307**:**1088–1091.

Roy, S., 1997. Genetic diversity of manganese deposition in the terrestrial geological record. Geological Society of London Special Publications 119:5-27.

Rye, R., Holland, H.D., 1998. Paleosols and the evolution of atmospheric oxygen: a critical review. American Journal of Science 298:621-672.

Saito, M.A., Sigman, D.M., Morel, F.M.M., 2003. The bioinorganic chemistry of the ancient ocean: the co-evolution of cyanobacterial metal requirements and biogeochemical cycles at the Archean-Proterozoic boundary? Inorganica Chimica Acta 356:308-318.

Sakamoto, T., Bryant, D.A., 1998. Growth at low temperature causes nitrogen limitation in the cyanobacterium Synechococcus sp. PCC 7002. Archives of Microbiology 196:10-19.

Sandiford, M., Powell, R., 1986. Deep crustal metamorphism during continental extension: modern and ancient examples. Earth and Planetary Science Letters 1986:151-158.

Schiøtte L., Bridgewater, D., Collerson, K.D., Nutman, A.P., Ryan, A.B., 1986. Chemical and isotopic effects of late Archean high-grade metamorphism and granite injection on early Archean gneisses, Saglek-Hebron, northern Labrador. Geological Society London Special Publications 24:261-273.

Schiøtte L., Compston W., Bridgwater D., 1989a. Ion probe U-Th-Pb zircon dating of polymetamorphic orthogneisses from Northern Labrador, Canada. Canadian Journal of Earth Sciences 26:1533-1556.

Schiøtte L., Compston W., and Bridgwater D., 1989b. U-Th-Pb ages of single zircons in Archean supracrustals from Nain Province, Labrador Canada. Canadian Journal of Earth Sciences 26:2636-2644.

Schiøtte L., Noble S., Bridgewater D., 1990. U-Pb mineral age from northern Labrador: possible evidence for interlayering of early and middle Archean tectonic slices. Geoscience Canada 17:227-231.

Schiøtte L., Hansen, B.T., Shirey S.B., Bridgewater D., 1993. Petrological and whole rock isotopic characteristics of tectonically juxtaposed Archean Gnisses in the Okak Area of the Nain Province, Labrador: relevance for terrane models. Precambrian Research 63:293-323.

Schopf, J.W., 1993. Microfossils of the early Archean Apex chert: new evidence of the antiquity of life. Science 26:640-646.

Schopf, J.W., 2000. The fossil record: tracing the roots of the cyanobacterial lineage. In: Whitton, B.A., Potts, M., Eds. The ecology of cyanobacteria: their diversity in time and space. Kluwer Academic, p.13 to 35.

Schopf, J.W., Kudryavtsev, A.B., Sugitani, K., Water, M.R., 2010. Precambrian microbe-like pseudofossils: a promising solution to the problem. Precambrian Research 179:191-205.

Scott, C., Planavsky, N.J., Dupont, C.L. Kendll, B., Gill, B.C., Robbins, L.J., Husband, K.,F., Arnold, G.L., Wing, B.A., Poulton, S.W., Bekker, A., Anbar, A.D.,

Konhauser, K.O., Lyons, T.W., 2013. Bioavailability of zinc in marine systems through time. Nature Geoscience 6:125-128.

Segura, A., Krelove, K., Kasting, J.F., Sommerlatt, D., Meadows, V., Crisp, D., Cohen, M., Mlawer, E., 2003. Ozone concentrations and ultraviolet fluxes on Earth-like planets around other stars. Astrobiology 3:689-708.

Sessions, A.L., Doughty, D.M., Welander, P.V., Summons, R.E., Newmann, D.K., 2009. The continuing puzzle of the Great Oxidation Event. Current Biology 19:567-574.

Shcolnick, S., Summerfield, T.C., Reytman, L., Sherman, L.A., Keren, N., 2009. The mechanism of iron homeostasis in the unicellular cyanobacterium Synechococystis sp. PCC 6803 and its relationship to oxidative stress. Plant Phyiology 150:2045-2056.

Sharma, M., Polizzotto, M., Anbar, A.D., 2001. Iron isotopes in hot springs along the Juan de Fuca Ridge. Earth and Planetary Science Letters 194:39-51.

Shibuya, T., Komiya, T., Nakamura, K., Takai, K., Maruyama, S., 2010. Highly alkaline, high-temperature hydrothermal fluids in the early Archean ocean. Precambrian Research 182:230-238.

Shimizu, H., Umemoto, N., Masuda, A., Appel, P.W.U., 1990. Sources of iron-formations in the archean isua and malene supracrustals, West Greenland: evidence from La-Ce and sm-nd isotopic data and REE abundances. Geochimica et Cosmochimica Acta 54:1147-1154.

Siebert, C., Kramers, J.D., Meisel, T., Morel, P., Nägler, T.F., 2005. PGE, Re-Os, and Mo isotope systematics in Archean and early Proterozoic sedimentary systems as proxies for redox conditions of the early Earth. Geochimica et Cosmochimica Acta 69:1787-1801

Siever, R., 1992. The silica cycle in the Precambrian. Geochimica et Cosmochimica Acta. 56:3265-3272.

Simard, M., Parent, M., David, J., Sharma, K.N.M. 2003. Géologie de la région de la rivière Innuksuac (34K et 34L). Ministère des Resouces Naturelles, Québec: RG 2002-10:46p.

Simmons, E.C., Lindsley, D.H., Papike, J.J., 1974. Phase relations and crystallization sequence in a contact-metamorphosed rock from the Gunflint Iron Formation, Minnesota. Journal of Petrology 15:539-565.

Sinha, R.P., Hader D-P., 2002 UV-induced DNA damage and repair: a review. Photochemical and Photobiological Sciences 1:225-236.

Sinha, R.P., Häder, D-P., 2002. UV- induced DNA damage and repair: a review. Photochemical and Photobiological Science 1:225-236.

Sleep, N.H., Hessler, A.M., 2006. Weathering of quartz as an Archean climatic indicator. Earth and Planetary Science Letters 241:594-602.

Stevens, S.E Jr., Van Baalen, C., 1973. Characteristics of nitrate reduction in a mutant of the blue-green alga Agmenellum quadruplicatum. Plant Physiology 51:350-356.

Stevens, S.E & Porter, R.D., 1980. Transformation in Agmenellum quadruplicatum. Proeedings to the National Acadademy of Science 77, 6052-6056.

Stevenson, R.K., David, J., Parent, M., 2006. Crustal evolution of the western Minto Block, northern Superior Province, Canada. Precambrian Research 145:229-242.

Stoodley, P., Sauer, K., Davies, D.G., Costerton, J.W., 2002. Biofilms as complex differentiated communities. Annual Reviews in Microbiology 56:187-209.

Storz, G., Imlay, J.A., 1999. Oxidative stress. Current Opinion in Microbiology 2:188-194.

Strauss, N.A., 2004. Iron deprivation: physiology and gene regulation. The Molecular Biology of Cyanobacteria, Springer Netherlands, p. 731-750.

Stueken, E.E., Catling, D.C., Buick, R., 2012. Contributions to late Archean sulphur cycling by life on land. Nature Geoscience. 5:722-725.

Summons, R.E., Jahnke, L.L., Hope, J.M.M., Logan, G.A., 2-Methylhopanoids as biomarkers for cyanobacterail oxygenic photosynthesis. Nature 400:554-557.

Summons, R.E., Bradley, A.S., Jahnke, L.L., Waldbauer, J.R., 2006. Steroids, triterpenoids and molecular oxygen. Philosophical Transactions of the Royal Society B 361:951-968.

Sun, S-S., Nesbitt, R.W., 1979. Geochemical characteristics of mid-ocean ridge basalts. Earth and Planetary Science Letters 44:119-138.

Swanner, E.D., Mloszewska, A.M., Cirpka, O., Schoenberg, R., Konhauser, K.O., Kappler A., in review. Toxic levels of Fe(II) in Archean seawater modulated oxygen producution. Nature Geoscienc.

Taylor, S.R., McLennan, S.M., 1985. The continental crust: its composition and evolution. Blackwell, Oxford. 312 p.

Thurman, E. M., 1985. Organic chemistry of natural waters volume 2. Martinus Nihoff/Dr W. Junk Pubs. Springer.

Touati, D., Jacques, M., Tardat, B., Bouchard, L., Despeid, S., 1995. Lethal oxidative damage and mutagenesis are generated by iron in delta fur mutants of Escherichia coli: protective role of superoxide dismutase. Journal of Bacteriology 177:2305-2314.

Touati, D., 2000. Iron and oxidative stress in bacteria. Archives of biochemistry and biophysics 373:1-6.

Trendall, A.F., Blockley, J.G., 1970. The iron formations of the Hamersley Group, Western Australia with special references to the associated crocodilite. Western Australia Geological Survey Bulletin 119:353p.

Trendall, A.F., Morris, R.C., 1983. Iron fgormations: facts and problems. Elsevier Scientific Publishers Inc.

Trendall, A.F., 2002. The significance of iron-formation in the Precambrian stratigraphic record. In: Altermann, W., Corcorane, P.L. Eds. Precambrian sedimentary environments: a modern approach to depositional systems. Internationa Association of Sedimentologists Special Publication 44:22-66.

Trick, C.G., Wilhelm, S.W., 1995. Physiological changes in the coastal marine cyanobacterium Synechococcus sp. PCC 7002 exposed to low ferric ion levels. Marine Chemistry 50:207-217.

Tsikos, H., Moore, J.M., 1997. Petrography and geochemistry of the Paleoproterozoic Hotazel Iron-Formation, Kalahari manganese field, South Africa; implications for Precambrian manganese metallogenesis. Economic Geology 92:87-97.

Ueno, Y., Yamada, K., Yoshida, N., Maruyama, S., Isozaki, Y., 2009. Evidence from from fluid inclusions for microbial methanogenesis in the early Archean era. Nature 440:516-519.

Van den Boorne, S.H.J.M., Van Bergen, M.J., Nijman, W., Vroon, P.Z., 2007. Dual role of seawater and hydrothermal fluids in Early Archean chert formation: evidence from silicon isotopes. Geology 35:939-942.

Vaniman, D.T., Papike, J.J., 1980. Lunar highland melt rocks: chemistry, petrology and silicate mineralogy. Proceedings of the Conference of the Lunar Highlands Crust 271-337.

Van Zuilen, M.A., Lepland, A., Arrhenius, G., 2002. Reassessing the evidence for the earliest traces of life. Nature 418:627-630.

Van Zuilen, M.A., Lepland, A., Terranes, J., Finarelli, J., Wahlen, M., Arrhenius, G., 2003. Graphite and carbonates in the 3.8 Ga old Isua Supracrustal Belt, southern West Greenland. Precambrian Research 126:331-348.

Van Zuilen, M.A., Matthew, K., Wopenka, B., Lepland, A., Marti, K.,Arrhenius, G., 2005. Geochimica et Cosmochimica Acta 69:1241-1252.

Viollier E., Inglett, P.W., Roychoudhury, N., Van Cappellan, P., The ferrozine method revisited: Fe(II)/Fe(III) determination in natural waters. Applied Geochemistry 15:785-790.

Whitehouse, M.J., Fedo, C.M., 2007. Microscale heterogeneity of Fe isotopes in >3.71 Ga banded iron formation from the Isua Greenstone Belt, southwest Greenland. Geology 35:719-722.

Wilhelm, S.W., 1995. Ecology of iron-limited cyanobacteria: a review of physiological responses and implications for aquatic systems. Aquatic Microbial Ecology 9:295-303.

Winterbourne, C.C., 1995. Toxicity of iron and hydrogen peroxide: the Fenton reaction. Toxicology letters. 82/83: 969-974.

Wille, M., Kramers, J.D., Nägler, T.F., Beukes, N.J., Shröder, S., Meisel, T., Lacassie, J.P., Voegelin, A.R., 2007. Evidence for a gradual rise of oxygen between 2.6 and 2.5 Ga from Mo isotopes and Re-PGE signatures in shales. Geochimica et Cosmochimica Acta. 71:2417-2435.

Wu, L., Percak-Dennett, E.M., Beard. B.L., Roden, E.E., Johnson, C.M., 2012. Stable iron isotope fractionation between aquious Fe(II) and moden Archean ocean Fe-Si coprecipitates and implications for iron isotope variations in the ancient rock record. Geochemica et Cosmochimca Acta 84:14-28.

Young, S.W., 1976. Petrographic textures of detrital polycrystalline quartz as an aid to interpreting crystalline source rocks. Journal of Sedimentary Research 46:595-603.

Zerkle, A.L., House, C.H., Brantley, S.L., 2005. Biogeochemical signatures through time as inferred from whole microbial genomes. Americal Journal of Science 306:467-502.

Zhuang, Q-K., Chen, H-Y., 1993. A theoretical analyses and its application of the second order EC reactions at microelectrodes under stead-state conditions. Chinese Journal of Chemistry 11:308-315.

Appendix A. Major and trace element data for the main mineral phases in the banded silicate and iron formations (BSF, BIF) in selected samples from the Nuvvuagittuq Supracrustal Belt.

Oxides in weight percent (wt%), while trace elements are in parts per million (ppm)

Major element data obtained from electron microprobe (EMP), and trace element data from laser ablation inductively couple mass spectrometry (LA-ICP-MS) in facilities at the University of Alberta's Earth and Atmospheric Science Department.

Mineral phases in the BSF are in grey, while mineral phases in the BIF are in white.

Table A1. Major and trace element compositions of the major mineral phases in selected chemical sedimentary rock samples from the Nuvvuagittuq Supracrustal Belt.

	Magnetite						Grunerite						Actinolite		
	median		max		min		median		max		min		median	max	min
wt %	n=177	n=22					n=35	n=24					n=9		
SiO_2	0.16	0.06	0.24	0.07	0.10	0.06	49.04	52.38	52.81	53.03	47.90	51.18	52.73	54.00	52.27
Al_2O_3	0.46	0.01	6.08	0.01	0.28	0.00	0.14	0.22	0.29	0.55	0.07	0.17	1.52	1.60	0.47
TiO_2	0.01	0.02	0.05	0.02	0.00	0.01	0.00	0.00	0.02	0.04	0.00	0.00	0.03	0.06	0.00
FeOtotal	92.73	93.93	93.28	93.94	87.43	93.92	46.79	30.17	47.56	30.42	37.81	28.62	18.70	25.51	18.01
MgO	0.02	0.01	0.19	0.01	0.00	0.01	4.97	12.72	8.05	13.27	3.42	12.44	12.51	13.11	7.16
MnO	0.02	0.08	0.07	0.09	0.00	0.07	0.48	0.99	0.73	1.18	0.28	0.84	0.43	0.96	0.37
CaO	0.00	0.03	0.03	0.04	0.00	0.03	0.63	0.85	0.67	2.29	0.00	0.66	11.58	12.15	10.63
Na_2O	0.02	0.05	0.12	0.06	0.00	0.04	0.01	0.04	0.08	0.09	0.00	0.02	0.16	0.18	0.11
K_2O	0.00	0.00	0.02	0.00	0.00	0.00	0.00	0.00	0.11	0.01	0.00	0.00	0.02	0.04	0.01
P_2O_5	0.01	0.00	0.07	0.00	0.00	0.00	0.01	0.00	0.05	0.05	0.00	0.00	0.01	0.03	0.00
Total	93.53	94.21	96.67	94.24	92.44	94.18	100.61	97.12	101.49	98.84	99.50	95.73	97.66	100.01	96.27
ppm															
Sc	2.35	<D.L	4.05	<D.L	0.83	<D.L	3.72	1.78	5.23	24.97	1.31	0.94	37.57	39.84	29.30
V	6.50	51.56	27.26	73.09	2.04	26.25	1.46	7.23	1.77	19.74	0.34	3.09	36.34	59.58	26.48
Cr	25.67	68.78	81.16	75.37	11.47	62.18	5.78	7.09	8.59	115.10	4.06	2.79	47.33	47.33	47.33
Ni	93.61	54.58	248.33	105.74	64.38	36.36	45.48	81.56	149.55	141.77	35.92	36.07	66.10	105.21	55.40
Co	11.27	1.80	48.32	6.85	4.59	0.69	15.70	32.04	27.64	55.53	10.53	17.12	26.35	31.05	18.07
Cu	1.62	0.76	11.92	1.59	0.45	0.74	1.40	1.33	5.30	7.54	0.54	0.48	1.46	2.45	0.28
Zn	63.63	25.58	207.33	65.36	18.60	14.87	157.08	166.09	275.51	385.33	100.80	110.97	197.91	637.90	145.25
Ga	4.08	13.93	21.57	17.61	1.81	8.66	0.80	1.38	1.43	2.89	0.44	0.76	4.85	8.89	1.12
Ge	22.39	6.52	116.63	9.06	11.06	3.66	16.16	5.58	23.69	13.95	7.46	4.52	7.85	14.55	4.28
Rb	0.32	0.31	1.81	0.72	0.10	0.08	1.69	3.85	9.70	7.53	0.15	0.17	<D.L	<D.L	<D.L
Sr	0.29	0.34	369.37	11.82	0.02	0.08	0.58	0.50	2.75	6.35	0.08	0.21	11.43	25.35	6.85
Y	0.39	0.54	588.18	2.93	0.05	0.15	8.26	11.49	17.01	37.45	5.34	6.16	38.24	85.41	2.50
Zr	0.43	0.81	2.42	4.91	0.10	0.48	0.27	0.60	0.74	2.47	0.19	0.26	2.55	4.26	0.88
Nb	0.36	0.67	2.09	1.37	0.07	0.22	0.19	0.27	0.39	0.99	0.02	0.17	1.16	2.27	0.54
Mo	2.31	0.51	17.46	1.82	0.75	0.28	0.25	0.26	0.62	0.57	0.05	0.07	0.66	1.10	0.22
Cd	1.57	0.60	5.64	0.98	0.37	0.25	0.34	0.35	1.80	0.48	0.16	0.22	1.61	2.22	1.39
La	0.14	0.57	196.39	1.02	0.02	0.24	0.47	0.17	3.92	1.51	0.07	0.02	3.43	6.76	0.51
Ce	0.14	0.27	237.55	1.52	0.01	0.13	0.61	0.22	4.81	5.89	0.06	0.08	12.40	36.86	0.59
Pr	0.10	0.10	32.01	0.52	0.02	0.05	0.13	0.15	0.43	1.38	0.03	0.05	3.36	4.85	0.56
Nd	0.30	0.55	177.22	1.74	0.06	0.28	0.58	0.36	2.87	10.56	0.23	0.16	17.96	27.38	0.37
Sm	0.36	0.33	25.05	0.61	0.02	0.17	0.31	0.51	1.03	4.29	0.06	0.22	7.30	11.79	0.16
Eu	0.21	0.13	12.76	0.41	0.01	0.08	0.17	0.18	0.65	1.48	0.09	0.08	2.50	3.53	0.06
Gd	0.51	0.65	41.49	1.14	0.03	0.20	0.46	0.92	1.59	6.01	0.09	0.17	6.32	15.38	0.37
Tb	0.13	0.12	6.88	0.29	0.02	0.06	0.09	0.17	0.38	1.00	0.06	0.08	1.90	2.18	0.05
Dy	0.40	0.22	66.22	1.57	0.07	0.12	0.85	1.46	2.82	6.20	0.37	0.74	9.81	12.64	0.58
Ho	0.18	0.16	15.05	0.26	0.03	0.05	0.22	0.34	0.74	1.34	0.11	0.20	1.55	2.78	0.10
Er	0.54	0.36	55.90	0.74	0.04	0.13	1.28	1.14	2.53	3.51	0.55	0.74	3.85	6.45	0.47
Tm	0.13	0.16	7.00	0.48	0.02	0.08	0.29	0.20	0.58	0.42	0.10	0.13	0.57	0.99	0.07
Yb	0.70	0.51	41.38	1.79	0.07	0.21	2.89	1.47	5.93	3.05	1.15	1.04	3.96	8.17	0.32
Lu	0.14	0.15	5.88	0.60	0.03	0.05	0.62	0.24	1.18	0.46	0.18	0.14	0.44	0.92	0.18
Hf	0.32	0.49	1.09	0.66	0.07	0.14	0.09	0.07	0.24	0.11	0.02	0.06	0.19	0.28	0.10
Ta	0.22	0.31	0.57	0.88	0.03	0.09	0.03	0.03	0.21	0.54	0.01	0.02	0.21	0.45	0.12
Pb	0.51	0.33	1.46	1.23	0.19	0.17	0.21	0.01	0.53	0.14	0.09	0.01	0.44	4.21	0.22
Th	0.16	0.14	0.66	0.38	0.02	0.05	0.08	0.29	0.45	0.29	0.01	0.29	0.20	0.76	0.07
U	0.11	<D.L	0.81	<D.L	0.00	<D.L	0.05	0.03	0.18	0.06	0.01	0.01	0.05	0.12	0.01

Continued on next page

	Augite						Quartz					
	median		max		min		median		max		min	
wt %	n=24	n=8					n=10	n=37				
SiO_2	50.47	51.37	51.68	51.99	49.12	50.88	101.22	99.67	101.54	100.39	101.10	98.01
Al_2O_3	0.11	0.28	0.28	0.54	0.10	0.15	0.03	0.01	0.04	0.03	0.02	0.00
TiO_2	0.00	0.02	0.01	0.04	0.00	0.00	0.00	0.00	0.01	0.03	0.00	0.00
FeOtotal	21.46	11.92	22.97	14.51	20.88	9.73	0.51	0.02	0.71	0.17	0.05	0.00
MgO	6.73	10.76	7.36	11.47	6.62	9.42	0.02	0.01	0.02	0.02	0.00	0.00
MnO	0.23	0.96	0.27	1.34	0.20	0.65	0.00	0.01	0.03	0.03	0.00	0.00
CaO	21.44	23.33	21.90	23.67	18.11	22.71	0.00	0.00	0.01	0.02	0.00	0.00
Na_2O	0.11	0.15	0.12	0.22	0.09	0.14	0.01	0.00	0.03	0.04	0.00	0.00
K_2O	0.00	0.00	0.04	0.01	0.00	0.00	0.00	0.00	0.01	0.01	0.00	0.00
P_2O_5	0.00	0.00	0.02	0.01	0.00	0.00	0.00	0.00	0.03	0.03	0.00	0.00
Total	100.38	98.88	101.89	99.85	99.44	97.43	100.84	99.84	101.29	100.45	99.23	99.04
ppm												
Sc	30.66	55.42	41.23	61.05	4.18	34.01	3.64	3.97	10.72	10.47	0.31	2.44
V	1.34	78.77	3.58	86.42	0.38	60.86	5.16	1.55	7.37	5.34	2.62	0.29
Cr	10.92	699.69	14.17	1196.58	7.66	367.37	13.27	8.09	32.25	70.56	5.12	2.62
Ni	49.79	157.58	68.82	476.48	38.94	21.56	36.01	13.25	188.29	378.07	8.49	3.39
Co	9.57	51.41	13.34	88.16	6.32	17.62	11.05	2.72	41.38	62.92	1.50	0.46
Cu	1.57	8.15	44.84	8.90	0.40	7.39	5.18	3.32	206.65	1794.71	4.08	0.30
Zn	88.61	210.11	135.41	451.68	52.41	146.11	86.61	15.27	507.95	151.33	0.75	4.01
Ga	0.93	3.09	1.38	5.86	0.73	1.12	1.18	0.51	5.46	0.72	0.83	0.36
Ge	20.69	7.52	28.49	12.15	14.85	3.83	11.87	1.62	68.69	6.31	0.31	1.08
Rb	0.49	<D.L	4.05	<D.L	0.32	<D.L	1.32	1.74	5.47	16.74	0.57	0.18
Sr	57.76	7.95	79.18	29.76	24.78	4.91	0.57	0.34	2.46	39.77	0.15	0.08
Y	81.28	5.70	161.97	13.99	32.75	3.09	4.77	1.08	20.93	7.24	0.02	0.09
Zr	2.88	2.47	6.21	6.02	1.97	1.49	0.48	0.52	0.72	39.37	0.05	0.10
Nb	0.95	0.40	1.84	1.17	0.26	0.14	0.33	0.18	1.86	0.33	0.01	0.04
Mo	0.49	0.61	1.34	1.56	0.36	0.20	1.42	0.17	15.92	0.82	0.21	0.02
Cd	0.61	1.61	1.10	1.61	0.33	1.61	0.21	1.19	0.30	5.26	0.13	0.41
La	11.25	0.49	36.42	0.84	5.44	0.13	0.57	0.12	1.68	11.84	0.13	0.02
Ce	27.97	1.00	75.70	3.94	11.12	0.41	0.78	0.29	2.93	20.89	0.16	0.08
Pr	3.61	0.19	8.71	0.43	1.69	0.12	0.50	0.40	4.81	1.84	0.02	0.04
Nd	18.46	0.88	55.48	3.39	7.92	0.55	1.91	23.61	359.92	112.93	0.24	0.24
Sm	4.34	0.39	9.76	0.76	1.52	0.26	0.65	0.54	8.82	1.93	0.27	0.15
Eu	2.86	0.29	6.71	0.49	0.76	0.05	0.47	0.14	0.79	0.37	0.01	0.05
Gd	5.51	1.16	17.43	1.36	2.38	0.96	0.62	0.31	1.82	1.71	0.15	0.08
Tb	1.65	0.21	2.63	0.76	0.56	0.04	0.20	0.13	0.30	0.21	0.10	0.01
Dy	9.56	1.07	19.63	1.82	3.92	0.46	0.78	0.29	3.43	1.41	0.10	0.09
Ho	2.04	0.60	5.26	0.66	1.26	0.54	0.24	0.13	0.74	0.28	0.04	0.02
Er	6.53	0.75	10.60	1.00	2.33	0.43	1.10	0.30	2.05	0.92	0.07	0.04
Tm	0.81	0.16	1.75	0.23	0.23	0.12	0.28	0.10	0.55	0.18	0.13	0.01
Yb	5.43	1.16	10.19	2.03	2.99	0.46	2.86	0.60	4.69	2.46	0.56	0.09
Lu	1.25	0.33	1.71	0.44	0.76	0.19	0.76	0.12	1.14	0.26	0.20	0.01
Hf	0.54	0.33	1.40	0.43	0.10	0.22	0.12	0.16	0.21	0.90	0.04	0.02
Ta	0.21	<D.L	0.25	<D.L	0.11	<D.L	0.10	0.12	0.14	0.67	0.05	0.02
Pb	0.78	3.54	1.03	8.34	0.39	1.00	1.64	0.37	21.83	2.28	0.03	0.13
Th	0.22	0.08	0.44	0.25	0.03	0.05	0.62	0.04	0.90	1.31	0.12	0.01
U	0.04	0.07	0.12	0.15	0.01	0.04	0.16	0.07	0.27	0.87	0.06	0.01

Appendix B. Whole rock major and trace element data for selected banded silicate and iron formation (BSF, BIF) samples from the Nuvvuagittuq Supracrustal Belt

Major elements in weight percent (wt%), while trace elements are in parts per million (ppm).

Values below the detection limit of the instrument are denoted by '<D.L.'

Volatile loss during sample analysis is denoted by 'LOI' (loss on ignition).

Samples were prepared by crushing unweathered, freshly cut samples in a cleaned tungsten-carbide mill.

Oxide weights were analyzed via xray fluorescence (XRF) at Activation Laboratories (Ancaster, Ontario), on fused pellets. Trace elements were analyzed via quadrupole inductively couple mass spectrometry (quad ICP-MS) in facilities at the University of Alberta's Earth and Atmospheric Science Department.

Table B1. Whole rock major and trace element compositions of selected chemical sedimentary rock samples from the Nuvvuagittuq Supracrustal Belt.

element	090709-3	090710-13	090711-3	090714-1	090709-4B2	090709-5	090710-2	090710-4	090710-12
	BSF	BSF	BSF	BSF	BIF	BIF	BIF	BIF	BIF
Easting	339878	339632	340282	340214	339664	339546	339632	339632	339944
Northing	6464930	6464364	6463158	6463149	6464365	6463571	6464364	6464364	6462967
wt%									
SiO_2	89.87	75.12	59.94	27.67	37.14	46.03	36.76	32.89	63.19
Al_2O_3	1.38	0.33	0.23	0.51	0.21	0.26	0.14	0.35	0.51
TiO_2	0.028	0.012	0.008	0.01	0.007	0.008	0.005	0.012	0.018
Fe_2O_{3total}	2	13.22	17.66	54.62	60.8	54.01	61.33	66.1	32.25
MgO	2.26	5.63	7.22	11.68	2.48	1.13	3.25	2.96	3.54
MnO	0.12	0.34	0.87	0.28	0.14	0.11	0.22	0.25	0.61
CaO	3.25	3	15.51	4.78	0.34	0.2	1.39	0.9	0.45
Na_2O	0.08	0.03	0.11	0.04	< D.L	< D.L	< D.L	< D.L	0.03
K_2O	0.01	< D.L	< D.L	0.02	< D.L	0.02	< D.L	< D.L	0.01
P_2O_5	0.01	0.01	0.01	< D.L	0.06	0.06	0.08	0.09	0.01
LOI	1.21	1.86	-0.32	-0.17	-1.76	-1.49	-2.46	-3.48	-0.64
Total	100.2	99.57	>101.0	99.45	99.43	100.3	100.7	100.1	99.99
S	0.003	0.571	0.034	0.002	0.016	0.016	0.009	0.007	0.271
ppm									
Li	5.42	0.33	4.09	1.30	<D.L	<D.L	<D.L	0.38	0.67
Be	0.22	0.16	0.92	0.19	0.88	2.11	4.04	3.87	0.28
V	21.53	5.87	3.16	28.23	2.19	2.35	2.43	5.19	9.26
Cr	526.19	5.01	4.75	2.59	5.98	7.17	8.36	12.76	12.10
Ni	79.92	73.59	30.53	240.79	47.62	44.85	37.88	56.67	85.46
Cu	7.90	136.66	11.23	2.83	2.96	4.67	1.73	4.27	61.23
Zn	36.69	47.77	93.49	194.42	49.89	40.66	67.40	34.81	51.59
Ga	1.71	1.19	1.10	4.26	1.23	1.08	1.01	1.76	1.24
Ge	0.04	2.13	2.45	1.06	6.84	7.15	9.52	11.34	1.18
As	0.81	0.22	0.26	0.61	0.73	0.81	1.06	3.22	0.38
Rb	0.13	0.09	0.07	0.47	0.20	0.45	0.18	0.17	0.31
Sr	12.07	3.07	8.24	2.13	1.88	0.52	2.25	1.15	0.39
Y	3.32	8.89	4.50	1.37	6.73	6.00	6.73	10.22	12.65
Zr	3.07	6.89	1.46	1.13	1.30	1.72	0.74	0.86	5.32
Nb	3.32	1.02	0.38	1.25	1.66	0.91	1.13	1.10	1.03
Mo	8.20	9.13	1.54	1.59	5.63	7.16	1.65	1.56	3.29
Cd	0.08	<D.L	0.34	0.25	<D.L	<D.L	<D.L	<D.L	<D.L
Sn	0.25	0.39	0.16	4.21	0.73	0.66	0.53	0.68	0.94
Sb	0.05	0.04	0.06	0.03	0.03	0.03	0.06	0.06	0.02
Te	<D.L	0.04	0.02	<D.L	<D.L	<D.L	0.02	0.03	0.03
Cs	0.03	0.08	0.03	0.09	0.19	0.33	0.20	0.21	0.12
Ba	2.42	1.85	2.17	1.37	0.60	0.69	0.23	0.28	0.99
La	0.87	1.65	0.90	1.90	1.42	1.29	1.82	0.92	7.18
Ce	1.48	4.29	1.65	2.12	2.38	2.01	2.61	2.16	13.02
Pr	0.18	0.66	0.19	0.22	0.26	0.23	0.28	0.30	1.51
Nd	0.81	3.36	0.81	0.67	0.99	0.95	1.16	1.39	6.07

Continued on next page

element	090709-3 BSF	090710-13 BSF	090711-3 BSF	090714-1 BSF	090709-4B2 BIF	090709-5 BIF	090710-2 BIF	090710-4 BIF	090710-12 BIF
ppm									
Sm	0.22	1.08	0.22	0.10	0.23	0.29	0.33	0.42	1.41
Eu	0.10	0.44	0.12	0.05	0.14	0.24	0.23	0.32	0.51
Gd	0.31	1.34	0.37	0.12	0.42	0.51	0.57	0.72	1.63
Tb	0.05	0.20	0.06	<D.L	0.08	0.10	0.10	0.14	0.24
Dy	0.41	1.31	0.46	0.11	0.67	0.78	0.76	1.17	1.70
Ho	0.10	0.28	0.12	0.03	0.18	0.20	0.19	0.30	0.39
Er	0.31	0.82	0.37	0.09	0.65	0.67	0.64	1.08	1.20
Tm	0.05	0.12	0.05	<D.L	0.11	0.11	0.10	0.19	0.17
Yb	0.33	0.77	0.37	0.12	0.77	0.80	0.75	1.37	1.10
Lu	0.05	0.12	0.06	<D.L	0.12	0.13	0.13	0.23	0.17
Hf	0.36	0.78	0.08	0.10	0.38	0.55	0.35	0.15	0.19
Ta	0.53	0.43	0.50	1.38	3.13	1.84	2.42	1.90	1.47
Re	<D.L	<D.L	0.00	0.00	0.04	0.02	0.01	0.01	0.01
Pb	1.25	0.66	1.81	0.27	0.12	0.12	0.09	0.11	1.73
Th	0.15	0.98	0.05	0.12	0.15	0.25	0.22	0.15	0.68
U	0.11	0.05	<D.L	0.05	<D.L	<D.L	<D.L	<D.L	0.19

Appendix C. Geochemical modeling results as well as geochemical modeling parameters for species in seawater during the deposition of the Nuvvaugittuq chemical sediments, using Visual MINTEQ© for two Fe(II) conditions.

‘-‘ Designates no species generated

Table C1. Geochemical modeling results for species in Nuvvuagittuq seawater.

Component	Species name	**1** **0.05 mM Fe^{2+}** %Total Concentration	**2** **1.8 mM Fe^{2+}** %Total Concentration
Sulphide	HS^{-1}	47.632	0.525
	$H_2S_{(aq)}$	10.227	0.113
	$FeHS^{+}$	42.09	99.346
	$Cd(HS)_{2\ (aq)}$	0.02	0.014
Sodium	Na^{+1}	91.166	91.169
	$NaCl_{(aq)}$	8.745	8.742
	$NaHCO_{3\ (aq)}$	0.082	0.082
Chlorine	Cl^{-1}	85.732	85.709
	$CaCl^{+}$	0.491	0.491
	$FeCl^{+}$	-	0.025
	$MgCl^{+}$	3.593	3.595
	$NaCl_{(aq)}$	10.184	10.18
Calcium	Ca^{+2}	76.276	76.265
	$CaCl^{+}$	22.519	22.535
	$CaHCO_3^{+}$	1.07	1.067
	$CaCO_{3\ (aq)}$	0.134	0.134
Magnesium	Mg^{+2}	67.546	67.529
	Mg2CO3+2	0.023	0.023
	$MgCl^{+}$	31.605	31.625
	MgCO3 (aq)	0.06	0.059
	$MgHCO_3^{+}$	0.763	0.761
Iron	Fe^{+2}	14.472	86.407
	$FeOH^{+}$	0.073	0.437
	$FeCl^{+}$	1.073	6.413
	$FeHS^{+}$	84.181	5.548
	$FeHCO^{3+}$	0.201	1.195
Carbonate	CO_3^{-2}	0.28	0.279
	$Mg_2CO_3^{+2}$	0.121	0.12
	HCO_3^{-}	75.222	74.896
	$H2CO_3^{*}{}_{(aq)}$	3.469	3.453
	FeHCO3+	-	0.428
	$MgCO_{3\ (aq)}$	0.633	0.631
	$MgHCO^{3+}$	8.121	8.093
	$CaHCO^{3+}$	2.183	2.176
	$CaCO_{3\ (aq)}$	0.274	0.272
	$NaCO^{3-}$	0.759	0.756
	$NaHCO_{3\ (aq)}$	8.936	8.896

Continued on next page

Component	Species name	**1** **0.05 mM Fe^{2+}** %Total Concentration	**2** **1.8 mM Fe^{2+}** %Total Concentration
Manganese	Mn^{+2}	31.605	79.424
	$MnCO_{3\,(aq)}$	1.678	4.201
	$MnOH^{+}$	0.01	0.025
	MnCl3-	0.159	0.399
	$MnCl_{2\,(aq)}$	1.264	3.179
	$MnCl^{+}$	3.715	9.343
	$MnHS^{+}$	60.874	1.689
	$MnHCO^{3+}$	0.695	1.74
Cobalt	Co^{+2}	29.652	84.382
	$CoOH^{+}$	0.075	0.214
	$CoCl^{+}$	1.557	4.434
	$CoHS^{+}$	65.574	2.06
	$CoCO_{3\,(aq)}$	0.598	1.697
	$CoHCO^{3+}$	2.542	7.21
Cadmium	Cd^{+2}	-	0.863
	$CdCl^{+}$	-	9.7
	$CdCl_{2\,(aq)}$	-	7.737
	$CdHS^{+}$	0.219	13.61
	$Cd(HS)_{2\,(aq)}$	99.434	68.034
	$Cd(HS)^{3-}$	0.339	0.03
	$CdCO_{3\,(aq)}$	-	0.021
Copper (univalent)	$CuCl^{2-}$	85.54	85.55
	$CuCl_3^{-2}$	13.557	13.547
	$CuCl_{\,(aq)}$	0.899	0.899
Copper (divalent)	Cu^{+2}	11.504	12.171
	$CuOH^{+}$	4.612	4.884
	$Cu(OH)_{2\,(aq)}$	0.175	0.185
	$CuCl^{+}$	2.698	2.857
	$CuCl_{2\,(aq)}$	0.142	0.151
	$Cu_2S_3^{-2}$	0.037	
	$CuS_{(aq)}$	5.217	0.061
	$CuCO_{3\,(aq)}$	71.746	75.628
	$CuHCO^{3+}$	0.8	0.843
	$Cu(CO_3)_2^{-2}$	3.068	3.22

Continued on next page

Table C2. Geochemical modeling parameters for the speciation model of Nuvvuagittuq seawater.

Component	Species name	**1** **0.05 mM Fe^{2+}** %Total Concentration	**2** **1.8 mM Fe^{2+}** %Total Concentration
Zinc	Zn^{+2}	7.402	59.658
	$ZnOH^{+}$	0.094	0.757
	$Zn(OH)_{2\ (aq)}$	0.024	0.197
	$ZnCl^{+}$	2.509	20.24
	$ZnCl_4^{-2}$	0.089	0.718
	$ZnCl^{3-}$	0.24	1.934
	$ZnCl_{2\ (aq)}$	0.469	3.784
	$Zn_2S_3^{-2}$	9.779	
	$ZnS_{\ (aq)}$	78.683	6.998
	$ZnCO_{3\ (aq)}$	0.451	3.623
	$ZnHCO^{3+}$	0.258	2.072
	$Zn(CO_3)_2^{-2}$	-	0.02
Nickel	Ni^{+2}	18.074	78.874
	$NiOH^{+}$	0.029	0.126
	NiCl+	0.789	3.447
	$NiCl_{2\ (aq)}$		0.023
	$NiHS^{+}$	77.935	3.755
	$NiCO_{3\ (aq)}$	0.711	3.092
	$NiHCO^{3+}$	2.456	10.681

Geochemical modeling parameters:

(molal)	**1**	**2**
H^{+1}	0	0
Na^{+1}	0.545	0.545
Cl^{-1}	0.468	0.468
Ca^{+2}	0.0102	0.0102
Mg^{+2}	0.0532	0.0532
Fe^{+2}	0.00005	0.00179051
DIC	0.005	0.005
Mn^{+2}	0.00000001	0.00000001
Co^{+2}	0.00000001	0.00000001
Cd^{+2}	0.00000001	0.00000001
Cu^{+1}	0.00000001	0.00000001
Cu^{+2}	0.00000001	0.00000001
Zn^{+2}	0.00000001	0.00000001
Ni^{+2}	0.00000001	0.00000001
HS^{-1}	0.0001	0.0001
	pH=7.5	HS- = 0.1 mM

Appendix D. Whole rock major and trace element for selected chemical sedimentary rock samples from the Nulliak Supracrustal Association.

'BIF' designates banded iron formation, 'QP' designates quartz-pyroxene facies, and 'MC' designates 'metacarbonate facies'.

Major elements in weight percent (wt%), while trace elements are in parts per million (ppm).

Values below the detection limit of the instrument are denoted by '<D.L.'

Volatile loss during sample analysis is denoted by 'LOI' (loss on ignition).

Samples were prepared by crushing unweathered, freshly cut samples in a cleaned tungsten-carbide mill.

Oxide weights were analyzed via xray fluorescence (XRF) at Activation Laboratories (Ancaster, Ontario), on fused pellets. Trace elements were analyzed via quadrupole inductively couple mass spectrometry (quad ICP-MS) in facilities at the University of Alberta's Earth and Atmospheric Science Department.

Table D1. Whole rock major and trace element analyses for selected chemical sedimentary rock samples from the Nulliak Supracrustal Association

element	DL-82-26B BIF	BR-82-94A BIF	Pl-1 BIF	YM-82-72 SF	BR-82-93 SF	PI-3 CF
wt%						
SiO2	39.45	44.24	57.16	86.55	85.28	25.75
Al2O3	2.73	0.82	1.16	2.44	0.07	0.26
Fe2O3Total	50.29	50.64	37.76	4.11	6.93	8.17
MnO	1.09	0.11	0.2	0.24	0.3	0.51
MgO	3.39	1.74	2.03	1.76	2.56	15.86
CaO	2.85	2.13	2.93	3.99	4.38	27.16
Na2O	0.17	0.08	0.1		0.1	0.05
K2O	0.24	0.21	0.07	0.09	< D.L	0.02
TiO2	0.146	0.211	0.049	0.066		0.01
P2O5	0.06	0.11	0.01	0.02		
S	0.006	0.002	0.001	0.439	0.032	0.008
LOI	-0.77	-1.59	-0.8	0.74	0.14	21.7
Total	99.66	98.7	100.7	100.4	99.78	99.5
ppm						
Li	3.2	3.11	8.44	0.74	11	1.26
Be	1.2	0.8	1.7	0.6	0.3	1
V	32.6	6.89	7.62	24.7	0.86	2.07
Cr	101	29.2	22.4	44.5	5.2	4.94
Co	18.5	3.67	6.08	8.01	1.1	4.37
Ni	58.5	12.8	42.1	119	6.95	8.96
Cu	34.1	8.11	4.84	346	7.55	2.74
Zn	77.5	108	31.8	302	8.69	49.5
Ga	4.43	17.9	4.33	5.14	0.24	1.99
Ge	11.9	12.51	5.23	0.21	0.27	0.82
As	0.95	0.62	0.39	0.22	0.18	0.51
Rb	8.16	15.1	2.66	1.75	0.11	1.55
Sr	33.5	9.43	29.8	33.3	11.5	21.9
Y	9.56	5.45	4.32	9.2	2.19	9.23
Zr	20.4	2.87	3.84	7.64	1.42	4.96
Nb	1.46	1.18	0.59	1.35	0.1	0.29
Mo	1.29	0.5	0.19	1.19	0.18	0.15
Ag	0.06	0.03	0.03	0.19	0.03	0.02
Cd	0.08	<DL	<DL	0.84	<DL	0.06
Cs	0.3	0.11	0.03	0.03	0.01	0.08
Ba	146	26.4	63.9	25.2	51.5	6.4
La	6.12	4.47	2.7	2.88	0.68	10.6
Ce	12.8	9.58	5.37	7.15	1.3	20.7
Pr	1.57	1.14	0.6	0.97	0.18	2.09
Nd	6.23	4.44	2.25	4.18	0.66	6.65
Sm	1.26	0.96	0.45	1.25	0.13	1.02
Eu	0.54	0.17	0.2	0.33	0.1	0.19
Gd	1.45	0.97	0.55	1.51	0.18	1.09
Tb	0.2	0.12	0.08	0.24	0.03	0.12
Dy	1.22	0.7	0.49	1.41	0.18	0.7
Ho	0.27	0.14	0.11	0.28	0.04	0.16

Continued on next page

element	DL-82-26B BIF	BR-82-94A BIF	Pl-1 BIF	YM-82-72 SF	BR-82-93 SF	PI-3 CF
ppm						
Tb	0.2	0.12	0.08	0.24	0.03	0.12
Dy	1.22	0.7	0.49	1.41	0.18	0.7
Ho	0.27	0.14	0.11	0.28	0.04	0.16
Er	0.81	0.38	0.35	0.78	0.15	0.49
Tm	0.11	0.048	0.047	0.106	0.02	0.06
Yb	0.68	0.31	0.3	0.66	0.12	0.37
Lu	0.1	0.05	0.04	0.09	<DL	0.06
Hf	0.64	0.16	0.24	0.32	<DL	0.28
Ta	0.22	0.08	0.16	0.28	<DL	0.32
W	0.31	0.06	0.08	<DL	0.14	0.17
Au	0.15	0.34	0.14	0.03	0.03	0.05
Pb	2.18	1.69	2.25	3.41	1.07	1.49
Th	0.95	0.43	0.5	0.31	0.08	1.22
U	0.25	0.09	0.04	0.27	0.06	0.18

Appendix E. Major and trace element data for the main mineral phases in the BIF and quartz-pyroxene rocks from the Nulliak Supracrustal Association.

Oxides in weight percent (wt%), while trace elements are in parts per million (ppm) Major element data obtained from electron microprobe (EMP), and trace element data from laser ablation inductively couple mass spectrometry (LA-ICP-MS) in facilities at the University of Alberta's Earth and Atmospheric Science Department.

Table E1. Major and trace element analyses of the main mineral phases in chemical sedimentary rock samples from the Nulliak Supracrustal Association.

Min phase	Sample	TiO2	MgO	SiO2	FeO	K2O	Na2O	Al2O3	MnO	CaO
magnetite	YM82-26	0.07	0.01	0.13	91.89	0.00	0.10	0.27	0.10	0.01
magnetite	YM82-26	0.03	0.02	0.10	91.64	0.00	0.08	0.12	0.11	0.01
magnetite	YM82-26	0.32	0.03	0.11	91.53	0.00	0.03	0.14	0.16	0.01
magnetite	YM82-26	0.06	0.03	0.10	91.70	0.01	0.00	0.14	0.07	0.01
magnetite	YM82-26	0.08	0.03	0.08	91.80	0.02	0.08	0.27	0.14	0.02
magnetite	YM82-26	0.06	0.00	0.07	91.48	0.01	0.04	0.27	0.07	0.01
magnetite	YM82-26	0.06	0.01	0.08	91.52	0.01	0.02	0.24	0.11	0.02
magnetite	YM82-26	0.11	0.00	0.11	91.35	0.01	0.01	0.14	0.12	0.00
magnetite	YM82-26	0.04	0.00	0.09	91.77	0.00	0.06	0.11	0.08	0.00
magnetite	YM82-26	0.03	0.03	0.12	91.79	0.00	0.00	0.22	0.11	0.00
magnetite	YM82-26	0.02	0.00	0.07	91.76	0.00	0.00	0.11	0.02	0.01
magnetite	YM82-26	0.13	0.04	0.08	91.71	0.00	0.01	0.12	0.13	0.00
magnetite	YM82-26	0.06	0.17	0.39	90.49	0.04	0.01	0.59	0.08	0.01
magnetite	YM82-26	0.01	0.03	0.12	91.47	0.00	0.00	0.24	0.12	0.00
magnetite	YM82-26	0.04	0.00	0.09	91.69	0.00	0.00	0.23	0.13	0.01
magnetite	YM82-26	0.00	0.01	97.91	0.04	0.02	0.04	0.04	0.00	0.03
magnetite	YM82-26	0.05	0.05	0.12	91.57	0.02	0.20	0.09	0.11	0.00
magnetite	YM82-26	0.11	0.02	0.09	91.20	0.02	0.06	0.16	0.12	0.00
magnetite	YM82-26	0.06	0.00	0.10	91.22	0.00	0.09	0.20	0.10	0.01
magnetite	YM82-26	0.05	0.05	0.10	91.36	0.00	0.03	0.20	0.06	0.00
magnetite	YM82-26	0.08	0.05	0.13	91.12	0.04	0.07	0.18	0.11	0.02
magnetite	YM82-26	0.07	0.04	0.09	91.44	0.00	0.02	0.12	0.11	0.01
magnetite	YM82-26	0.04	0.01	0.08	90.81	0.00	0.00	0.10	0.04	0.02
magnetite	YM82-26	0.05	0.03	0.03	91.39	0.00	0.07	0.14	0.08	0.00
magnetite	YM82-26	0.11	0.03	0.11	92.16	0.00	0.00	0.19	0.01	0.00
magnetite	YM82-26	0.07	0.00	0.10	91.37	0.00	0.05	0.10	0.06	0.00
magnetite	YM82-26	0.06	0.00	0.09	91.94	0.00	0.00	0.08	0.05	0.02

Continued on next page

Min phase	Sample	P2O5	Total	Na23	Mg24	Al27	Si28	P31	K39	Ca44
magnetite	YM82-26	0.05	92.62	90.78	1018.11	3370.12	10586.80	61.54	29.61	819.41
magnetite	YM82-26	0.03	92.13	29.21	1784.59	4019.49	4820.08	43.69	35.80	214.41
magnetite	YM82-26	0.00	92.34	2.54	127.93	791.36	1070.90	36.50	<D.L	<D.L
magnetite	YM82-26	0.05	92.15	54.31	461.74	790.66	4311.13	41.84	12.42	344.93
magnetite	YM82-26	0.00	92.52	107.13	1808.54	3158.21	15213.55	48.49	25.54	2898.12
magnetite	YM82-26	0.02	92.04	7.12	318.98	1505.54	1159.99	705.89	<D.L	2602.64
magnetite	YM82-26	0.00	92.07	6.22	140.81	1450.86	1040.58	61.11	<D.L	150.11
magnetite	YM82-26	0.00	91.85	43.75	891.65	736.93	4400.15	52.54	<D.L	1659.02
magnetite	YM82-26	0.01	92.18	71.28	2342.17	3472.22	8354.52	57.10	12.48	1638.55
magnetite	YM82-26	0.00	92.31	18.83	771.57	1171.92	3728.28	32.04	<D.L	673.84
magnetite	YM82-26	0.05	92.04	4.18	248.11	874.16	1481.90	43.85	<D.L	149.41
magnetite	YM82-26	0.01	92.22	45.92	1966.20	996.92	9661.02	46.77	8.75	1813.61
magnetite	YM82-26	0.02	91.84	25.78	886.96	2484.36	5377.09	41.84	10.51	729.60
magnetite	YM82-26	0.00	92.00	10.53	430.98	4916.96	2121.05	41.66	<D.L	367.58
magnetite	YM82-26	0.00	92.19	21.90	590.28	4362.92	2134.52	35.14	<D.L	468.94
magnetite	YM82-26	0.03	98.12	3088.54	58494.97	8664.21	467439.38	389.63	118.60	146953.55
magnetite	YM82-26	0.03	92.24	43.94	1277.32	812.63	7281.54	53.80	8.44	931.11
magnetite	YM82-26	0.05	91.82	14.24	244.41	980.42	1446.30	65.75	10.93	291.29
magnetite	YM82-26	0.00	91.77	4.62	102.83	690.94	803.81	51.02	<D.L	<D.L
magnetite	YM82-26	0.04	91.90	5.80	128.95	1304.12	775.30	45.10	<D.L	<D.L
magnetite	YM82-26	0.03	91.84	92.01	1718.79	851.83	9441.69	48.01	<D.L	2444.99
magnetite	YM82-26	0.00	91.89	7.33	275.42	633.58	1941.49	43.14	<D.L	335.59
magnetite	YM82-26	0.00	91.10	0.88	89.38	733.87	856.30	41.29	<D.L	<D.L
magnetite	YM82-26	0.03	91.81	0.76	91.93	1307.16	876.66	45.75	<D.L	<D.L
magnetite	YM82-26	0.02	92.63	9.69	493.35	931.33	2634.47	34.51	<D.L	531.40
magnetite	YM82-26	0.00	91.75	58.67	585.98	1316.10	2791.26	54.59	79.97	493.23
magnetite	YM82-26	0.00	92.25	5.32	879.22	2408.11	2240.55	40.48	20.55	190.43

Continued on next page

Min phase	Sample	Ti48	V51	Cr52	Mn55	Fe56	Fe57	Ni58	Ni60	Ni62
magnetite	YM82-26	765.37	61.73	161.45	1449.74	722899.25	647051.25	5934.66	94.97	95.42
magnetite	YM82-26	1125.78	59.89	189.25	1330.13	722899.25	638109.00	5966.11	72.75	70.96
magnetite	YM82-26	1101.62	63.02	170.31	1166.94	722899.25	652232.06	5974.58	75.10	85.40
magnetite	YM82-26	1125.14	62.79	179.32	1174.47	722899.25	643887.44	5947.32	75.68	66.99
magnetite	YM82-26	416.76	63.93	244.14	2712.19	722899.13	658663.75	6014.75	98.56	100.50
magnetite	YM82-26	951.00	63.03	245.16	2070.91	722899.13	646782.81	6057.16	91.78	85.27
magnetite	YM82-26	881.56	61.89	243.69	1196.40	722899.19	654861.94	5985.12	92.33	83.90
magnetite	YM82-26	1114.55	63.05	120.69	1351.23	722899.13	644898.50	5962.56	86.40	88.19
magnetite	YM82-26	1125.03	64.95	145.06	1680.72	722899.19	654456.63	5895.86	87.89	76.04
magnetite	YM82-26	1290.61	59.66	104.70	1449.56	722899.13	658753.56	6007.32	88.75	87.84
magnetite	YM82-26	924.85	58.97	100.53	1133.40	722899.13	652683.44	6035.07	84.75	87.18
magnetite	YM82-26	1059.22	61.57	70.94	1489.12	722899.19	680302.69	6140.49	89.21	93.95
magnetite	YM82-26	1076.98	62.05	71.94	1377.60	722899.19	677696.81	6058.92	93.14	92.49
magnetite	YM82-26	1307.67	63.73	81.96	1486.30	722899.13	655903.50	6051.69	96.45	86.60
magnetite	YM82-26	1082.76	61.42	102.40	1621.83	722899.13	648059.56	5879.98	85.39	89.25
magnetite	YM82-26	383.40	3.55	10.09	10338.26	148562.72	151059.11	1325.96	52.66	47.44
magnetite	YM82-26	1001.98	60.99	111.17	1494.10	722899.19	662759.94	5985.22	80.76	85.60
magnetite	YM82-26	1137.39	60.12	159.71	1196.20	722899.13	668132.81	5985.23	82.27	77.24
magnetite	YM82-26	908.96	63.88	174.94	1080.06	722899.13	662019.56	6123.49	85.58	83.18
magnetite	YM82-26	1106.53	62.57	173.60	1232.59	722899.13	662927.94	6103.36	92.17	87.93
magnetite	YM82-26	969.52	59.63	164.14	1480.11	722899.13	652803.94	6020.20	89.75	74.24
magnetite	YM82-26	1396.86	60.46	175.19	1375.62	722899.13	673995.31	6087.52	84.05	84.70
magnetite	YM82-26	1204.43	111.67	396.28	991.27	722899.00	682740.56	6112.42	81.30	91.30
magnetite	YM82-26	1084.01	119.26	402.02	986.56	722899.06	689821.00	6067.12	88.73	92.99
magnetite	YM82-26	1402.46	124.84	368.43	1043.07	722899.19	676847.00	6044.92	88.70	78.50
magnetite	YM82-26	1333.96	122.10	294.06	1038.56	722899.13	659844.88	5899.41	85.12	80.36
magnetite	YM82-26	1452.58	103.59	354.49	993.62	722899.13	692645.56	6138.77	80.80	75.86

Continued on next page

Min phase	Sample	Co59	Cu63	Zn64	Ga69	Ge74	Sr88	Y89	Zr90	Nb93
magnetite	YM82-26	22.48	1.58	1020.92	9.43	15.51	0.33	<D.L	<D.L	0.49
magnetite	YM82-26	20.20	65.63	57.23	9.65	14.41	1.15	0.03	0.18	0.72
magnetite	YM82-26	18.48	0.60	55.07	9.12	15.02	0.05	<D.L	0.10	1.05
magnetite	YM82-26	16.92	0.44	48.24	9.04	13.16	0.15	<D.L	<D.L	0.86
magnetite	YM82-26	20.76	5.40	44.31	9.42	15.90	0.81	2.70	<D.L	0.31
magnetite	YM82-26	20.25	<D.L	258.29	9.25	13.09	9.78	0.46	<D.L	0.66
magnetite	YM82-26	19.78	<D.L	90.44	9.58	14.40	<D.L	<D.L	<D.L	0.53
magnetite	YM82-26	18.40	<D.L	46.52	8.62	15.10	0.77	0.05	0.21	1.02
magnetite	YM82-26	19.60	31.87	54.83	9.46	14.28	0.93	0.07	0.17	0.89
magnetite	YM82-26	19.69	<D.L	53.93	8.25	13.60	0.23	<D.L	<D.L	1.24
magnetite	YM82-26	19.90	0.28	36.30	8.23	14.37	<D.L	0.04	0.10	0.73
magnetite	YM82-26	22.34	<D.L	42.86	8.66	15.76	0.45	0.02	0.21	1.20
magnetite	YM82-26	21.52	2.11	1214.83	9.44	15.51	0.41	0.02	0.17	1.15
magnetite	YM82-26	23.03	0.56	2866.78	8.89	15.37	0.24	<D.L	0.17	1.27
magnetite	YM82-26	20.44	<D.L	2303.00	9.38	14.93	0.20	<D.L	<D.L	1.02
magnetite	YM82-26	20.87	99.43	87.94	1.06	25.59	75.25	3.20	22.50	<D.L
magnetite	YM82-26	19.99	0.61	53.39	8.67	14.87	0.20	<D.L	<D.L	0.84
magnetite	YM82-26	18.92	<D.L	36.43	8.36	14.47	0.19	<D.L	0.16	1.29
magnetite	YM82-26	19.11	<D.L	30.38	8.35	15.76	0.04	0.03	0.11	0.74
magnetite	YM82-26	18.63	<D.L	73.60	9.04	17.08	0.10	<D.L	0.12	1.12
magnetite	YM82-26	20.19	2.15	26.15	8.69	13.64	1.04	<D.L	0.14	1.03
magnetite	YM82-26	18.14	<D.L	32.59	8.16	14.17	0.11	0.02	<D.L	1.00
magnetite	YM82-26	18.32	<D.L	40.87	8.01	12.40	<D.L	<D.L	<D.L	0.41
magnetite	YM82-26	18.24	<D.L	479.58	8.77	14.12	0.01	0.02	<D.L	0.51
magnetite	YM82-26	17.11	<D.L	34.14	7.95	13.27	0.16	<D.L	0.18	0.69
magnetite	YM82-26	17.80	1.35	31.24	7.54	13.21	1.10	<D.L	0.15	0.53
magnetite	YM82-26	15.67	2.36	35.78	7.66	14.28	0.72	<D.L	<D.L	0.66

Continued on next page

Min phase	Sample	Mo98	Sn120	Ba138	Min phase	Sample	TiO2	MgO	SiO2	FeO
magnetite	YM82-26	2.78	0.88	0.28	Quartz	YM82-26	0.00	0.01	99.06	0.10
magnetite	YM82-26	2.07	0.48	3.49	Quartz	YM82-26	0.00	0.00	98.60	0.07
magnetite	YM82-26	2.98	0.50	0.06	Quartz	YM82-26	0.00	0.02	98.96	0.10
magnetite	YM82-26	2.91	0.37	0.14	Clinopx	YM82-26	0.01	9.85	50.46	16.08
magnetite	YM82-26	2.33	<D.L	0.71	Clinopx	YM82-72	0.12	10.90	51.48	11.70
magnetite	YM82-26	2.09	0.37	0.15	Clinopx	YM82-72	0.10	10.99	52.36	12.38
magnetite	YM82-26	2.54	0.53	<D.L	Clinopx	YM82-72	0.07	11.57	49.10	11.93
magnetite	YM82-26	2.66	0.33	0.05	Clinopx	YM82-72	0.10	11.12	52.15	12.31
magnetite	YM82-26	1.93	0.40	1.61	Clinopx	YM82-72	0.07	11.23	52.19	11.30
magnetite	YM82-26	2.51	<D.L	0.39	Clinopx	YM82-72	0.12	11.05	52.11	12.44
magnetite	YM82-26	2.03	<D.L	0.18	Clinopx	YM82-72	0.09	11.16	51.89	12.33
magnetite	YM82-26	2.05	0.50	0.31	Clinopx	YM82-72	0.09	9.39	48.41	13.14
magnetite	YM82-26	3.31	0.75	0.42	Clinopx	YM82-72	0.08	11.35	52.23	12.43
magnetite	YM82-26	2.81	1.02	0.25	Clinopx	YM82-72	0.07	11.80	52.20	13.15
magnetite	YM82-26	2.68	0.82	0.53	Clinopx	YM82-72	0.09	11.09	51.57	12.37
magnetite	YM82-26	2.25	<D.L	19.09	Clinopx	YM82-72	0.09	11.10	51.65	12.24
magnetite	YM82-26	3.13	0.63	0.49	Clinopx	YM82-72	0.16	11.19	51.58	12.42
magnetite	YM82-26	2.89	0.68	0.71	Clinopx	YM82-72	0.16	11.32	52.12	12.41
magnetite	YM82-26	3.03	0.42	0.24	Clinopx	YM82-72	0.04	8.53	50.22	14.54
magnetite	YM82-26	3.19	0.51	0.34	Clinopx	YM82-72	0.11	9.70	50.67	13.14
magnetite	YM82-26	2.50	0.64	0.55	Clinopx	YM82-72	0.15	9.84	50.52	13.28
magnetite	YM82-26	2.84	0.59	0.13	Clinopx	YM82-72	0.14	9.99	50.61	13.29
magnetite	YM82-26	2.39	0.49	<D.L	Clinopx	YM82-72	0.02	11.14	52.48	18.48
magnetite	YM82-26	2.93	0.59	<D.L	Clinopx	YM82-72	0.04	14.09	54.77	13.66
magnetite	YM82-26	2.63	0.38	0.09	Clinopx	YM82-26	0.04	10.13	52.32	20.51
magnetite	YM82-26	2.95	<D.L	6.06	Clinopx	YM82-26	0.00	10.83	52.48	19.85
magnetite	YM82-26	3.16	<D.L	3.89	Clinopx	YM82-26	0.02	11.05	53.14	19.48

Continued on next page

Min phase	Sample	K2O	Na2O	Al2O3	MnO	CaO	P2O5	Total	Na23	Mg24
Quartz	YM82-26	0.00	0.00	0.04	0.03	0.03	0.04	99.32	8.60	88.46
Quartz	YM82-26	0.00	0.00	0.03	0.00	0.01	0.00	98.71	25.01	454.21
Quartz	YM82-26	0.00	0.00	0.02	0.01	0.04	0.00	99.16	30.28	491.87
Clinopx	YM82-26	0.01	0.47	1.47	1.37	20.24	0.01	99.96	3458.28	57608.60
Clinopx	YM82-72	0.00	0.73	2.19	1.14	21.38	0.04	99.68	3528.29	61481.00
Clinopx	YM82-72	0.01	0.50	1.60	1.20	20.98	0.04	100.14	3658.74	62123.45
Clinopx	YM82-72	0.01	0.37	2.02	1.06	20.03	0.00	96.16	2418.46	56701.82
Clinopx	YM82-72	0.01	0.47	1.62	1.02	21.44	0.05	100.30	3560.86	63164.23
Clinopx	YM82-72	0.02	0.41	1.18	1.23	21.91	0.00	99.52	2667.40	63874.26
Clinopx	YM82-72	0.01	0.44	1.33	0.85	21.52	0.04	99.90	2349.08	63537.68
Clinopx	YM82-72	0.01	0.39	1.26	0.76	21.61	0.03	99.52	2559.38	61883.14
Clinopx	YM82-72	0.17	0.37	3.28	1.07	18.87	0.05	94.83	2653.83	61754.96
Clinopx	YM82-72	0.00	0.44	1.25	0.86	21.72	0.00	100.36	2972.18	62976.13
Clinopx	YM82-72	0.05	0.33	1.67	0.84	17.92	0.00	98.03	3017.88	61958.41
Clinopx	YM82-72	0.03	0.46	1.33	0.85	21.30	0.03	99.13	3087.17	61356.33
Clinopx	YM82-72	0.00	0.57	1.43	1.19	21.03	0.04	99.33	1725.06	64196.67
Clinopx	YM82-72	0.00	0.51	1.67	1.06	20.92	0.01	99.49	2881.32	63599.53
Clinopx	YM82-72	0.01	0.51	1.64	0.90	21.31	0.00	100.37	2653.15	63803.39
Clinopx	YM82-72	0.00	0.51	2.14	1.59	21.58	0.00	99.15	860.76	63782.05
Clinopx	YM82-72	0.00	0.53	2.47	1.44	21.06	0.02	99.13	3331.29	46614.11
Clinopx	YM82-72	0.00	0.57	2.66	1.36	21.06	0.03	99.47	3290.32	45892.27
Clinopx	YM82-72	0.00	0.55	2.07	1.41	21.20	0.01	99.26	735.50	48532.35
Clinopx	YM82-72	0.05	0.19	1.73	1.30	11.97	0.02	97.39	797.18	70426.37
Clinopx	YM82-72	0.04	0.15	1.53	1.03	12.13	0.00	97.41	796.74	59509.77
Clinopx	YM82-26	0.02	0.12	1.00	0.99	11.81	0.02	96.96	1069.86	57473.17
Clinopx	YM82-26	0.02	0.18	1.37	0.98	11.55	0.00	97.26	1300.85	57223.87
Clinopx	YM82-26	0.04	0.17	1.14	1.06	12.02	0.00	98.12	1323.33	61396.64

Continued on next page

Min phase	Sample	Al27	Si28	P31	K39	Ca44	Ti48	V51	Cr52	Mn55
Quartz	YM82-26	137.07	467439.41	54.69	<D.L	737.05	36.47	6.41	30.88	143.99
Quartz	YM82-26	125.45	467439.44	57.48	6.37	1141.24	22.91	2.73	11.36	158.26
Quartz	YM82-26	173.66	467439.41	61.55	<D.L	1216.58	37.24	3.11	7.44	163.90
Clinopx	YM82-26	8517.40	236056.89	179.58	65.28	156753.55	410.92	4.30	13.08	10784.46
Clinopx	YM82-72	9057.82	240731.31	88.89	12.61	158288.53	808.97	63.12	35.19	8056.73
Clinopx	YM82-72	9380.65	244938.27	86.50	22.33	157677.14	798.40	67.76	34.90	8245.48
Clinopx	YM82-72	6234.32	229045.33	77.99	94.79	139203.89	874.36	71.07	31.06	7715.75
Clinopx	YM82-72	11696.61	243535.95	87.72	201.69	158270.67	799.39	71.39	39.76	8862.78
Clinopx	YM82-72	9173.67	244003.39	86.91	201.69	154524.97	838.52	71.80	33.69	9297.81
Clinopx	YM82-72	6055.53	243535.92	82.51	87.83	162332.48	740.16	120.31	59.59	7835.29
Clinopx	YM82-72	6632.10	242601.05	80.21	118.96	154534.86	683.91	137.43	58.00	6401.84
Clinopx	YM82-72	5820.34	226240.67	71.23	16.87	148345.48	591.12	136.68	81.09	5407.20
Clinopx	YM82-72	7071.11	244003.38	82.94	33.77	156882.14	681.00	133.09	35.44	7063.60
Clinopx	YM82-72	6642.76	244003.38	81.27	24.00	152914.23	655.24	124.04	31.39	7051.14
Clinopx	YM82-72	7357.18	241198.73	83.25	<D.L	153664.22	691.88	130.00	26.71	6735.17
Clinopx	YM82-72	6978.27	241198.75	78.03	363.65	152272.44	747.70	102.79	36.23	8326.16
Clinopx	YM82-72	6512.72	241198.75	81.38	<D.L	157425.00	661.37	127.71	60.88	6025.58
Clinopx	YM82-72	9691.32	243535.94	87.51	360.34	148667.80	658.58	112.72	27.41	7176.48
Clinopx	YM82-72	8436.27	234654.59	82.78	393.26	79910.27	308.74	61.19	203.80	6910.63
Clinopx	YM82-72	10106.73	236991.81	77.28	10.64	159708.86	577.59	22.10	20.62	10743.79
Clinopx	YM82-72	9672.48	234654.61	70.01	<D.L	154096.41	557.62	21.72	26.59	10637.56
Clinopx	YM82-72	6374.99	236524.34	70.54	331.89	74394.43	299.11	23.72	26.78	7425.63
Clinopx	YM82-72	7327.60	245405.72	80.97	372.51	134099.11	660.21	65.75	236.67	8153.59
Clinopx	YM82-72	9427.61	256156.83	71.78	152.21	94863.31	352.49	86.17	39.94	6306.06
Clinopx	YM82-26	6946.65	244470.81	70.71	224.32	90894.65	274.60	4.19	9.71	8078.80
Clinopx	YM82-26	17594.74	245405.67	103.85	328.05	93425.76	383.34	6.58	21.40	19098.96
Clinopx	YM82-26	9241.67	248210.30	91.80	292.29	91376.78	250.70	2.80	<D.L	8006.57

Continued on next page

Min phase	Sample	Fe56	Fe57	Ni58	Ni60	Ni62	Co59	Cu63	Zn64	Ga69
Quartz	YM82-26	60801.70	73394.49	613.06	11.25	15.45	2.34	<D.L	7.31	1.08
Quartz	YM82-26	31567.73	31859.19	275.11	5.94	10.64	1.46	0.39	6.55	0.70
Quartz	YM82-26	28051.78	26937.00	226.71	5.75	5.67	1.19	1.89	5.05	0.44
Clinopx	YM82-26	166751.28	158211.22	1418.15	62.91	53.51	18.06	95.36	102.70	0.90
Clinopx	YM82-72	87946.66	90969.42	848.75	111.12	112.11	41.62	1.13	2295.87	10.29
Clinopx	YM82-72	91223.96	94820.99	901.31	140.92	144.94	40.32	2.03	2330.77	10.83
Clinopx	YM82-72	73747.41	77015.94	687.01	69.37	70.65	28.16	0.36	1008.48	6.39
Clinopx	YM82-72	91391.77	93836.02	929.44	165.24	166.12	39.30	3.67	1829.97	10.08
Clinopx	YM82-72	87692.28	91154.98	843.16	88.80	88.51	33.66	0.96	1091.49	8.01
Clinopx	YM82-72	86666.80	89108.41	839.03	100.90	94.10	31.33	2.72	1011.37	6.08
Clinopx	YM82-72	88972.36	91079.48	854.91	105.68	98.73	30.97	2.90	1219.44	7.91
Clinopx	YM82-72	78608.17	79978.25	721.63	56.70	55.09	27.27	1.35	945.98	6.91
Clinopx	YM82-72	90676.54	91387.62	842.99	71.67	67.61	29.06	0.51	1096.75	8.79
Clinopx	YM82-72	88769.10	90028.27	822.51	71.14	76.00	29.26	<D.L	1134.49	8.14
Clinopx	YM82-72	91766.73	92468.41	855.49	73.35	76.60	29.98	<D.L	1399.63	8.59
Clinopx	YM82-72	87346.67	87877.80	845.52	109.00	105.65	33.97	3.15	1214.82	6.80
Clinopx	YM82-72	88067.13	87957.63	808.90	69.40	65.44	29.46	1.58	1198.65	8.10
Clinopx	YM82-72	90214.49	90844.68	849.97	88.48	89.13	32.74	3.00	1012.46	7.82
Clinopx	YM82-72	88334.15	89505.61	855.76	90.00	84.49	33.95	0.40	748.76	5.01
Clinopx	YM82-72	105481.34	105552.12	1037.66	157.59	139.04	40.35	<D.L	1705.78	6.62
Clinopx	YM82-72	105982.38	106308.63	1055.97	153.65	161.27	41.11	0.27	1734.74	6.71
Clinopx	YM82-72	113401.34	112433.11	1128.73	182.93	165.56	35.18	1.97	776.29	3.41
Clinopx	YM82-72	93434.33	94252.90	901.81	113.10	110.74	32.92	246.85	1174.90	3.15
Clinopx	YM82-72	83835.11	85063.55	822.47	119.72	113.54	32.18	2.86	873.95	9.14
Clinopx	YM82-26	182768.11	178039.25	1594.06	51.45	50.11	32.58	7.60	149.61	1.68
Clinopx	YM82-26	201000.09	195637.52	1744.94	63.39	72.10	26.64	30.13	155.49	2.26
Clinopx	YM82-26	159594.20	158172.38	1376.70	51.76	54.16	31.69	1.55	181.71	0.88

Continued on next page

Min phase	Sample	Ge74	Sr88	Y89	Zr90	Nb93	Mo98	Sn120	Ba138
Quartz	YM82-26	4.20	0.14	<D.L	<D.L	<D.L	0.63	<D.L	0.63
Quartz	YM82-26	4.22	0.61	0.01	0.09	<D.L	<D.L	0.33	2.09
Quartz	YM82-26	3.27	0.39	<D.L	<D.L	<D.L	<D.L	<D.L	1.62
Clinopx	YM82-26	22.57	73.78	5.80	25.94	<D.L	1.43	0.41	4.81
Clinopx	YM82-72	6.65	3.99	23.50	33.63	1.11	<D.L	1.44	0.45
Clinopx	YM82-72	6.27	4.99	23.51	32.93	1.03	<D.L	1.29	1.20
Clinopx	YM82-72	6.04	3.66	15.83	19.30	0.61	<D.L	1.01	4.51
Clinopx	YM82-72	7.21	5.68	21.97	33.11	1.51	<D.L	1.35	5.80
Clinopx	YM82-72	6.76	6.00	19.13	33.19	1.98	0.09	1.21	8.29
Clinopx	YM82-72	6.69	5.22	19.92	8.01	0.46	<D.L	1.01	6.48
Clinopx	YM82-72	6.69	5.58	27.61	8.43	0.18	<D.L	1.50	9.94
Clinopx	YM82-72	5.55	4.96	26.27	5.60	0.08	<D.L	1.15	2.11
Clinopx	YM82-72	6.24	5.09	30.17	12.71	0.16	<D.L	1.58	0.91
Clinopx	YM82-72	7.05	4.65	27.08	12.70	0.10	0.11	1.28	1.10
Clinopx	YM82-72	7.27	4.71	27.19	16.19	0.23	<D.L	1.52	0.35
Clinopx	YM82-72	7.38	3.95	14.70	24.31	0.42	<D.L	1.31	16.19
Clinopx	YM82-72	6.17	4.97	28.15	9.40	0.18	0.04	1.28	0.29
Clinopx	YM82-72	7.00	4.34	33.82	16.26	0.55	<D.L	1.87	2.15
Clinopx	YM82-72	7.22	3.95	5.84	27.74	0.21	<D.L	0.65	3.03
Clinopx	YM82-72	6.22	10.04	18.29	16.54	0.82	0.05	0.90	0.59
Clinopx	YM82-72	6.15	10.44	17.91	14.97	0.84	<D.L	0.98	<D.L
Clinopx	YM82-72	6.78	2.63	3.25	6.37	0.33	<D.L	0.61	2.47
Clinopx	YM82-72	7.66	7.52	4.83	2.15	0.73	<D.L	0.55	3.57
Clinopx	YM82-72	6.55	12.56	30.72	2.77	0.36	<D.L	1.00	3.54
Clinopx	YM82-26	21.46	20.16	2.33	11.45	0.34	0.21	1.18	12.58
Clinopx	YM82-26	26.08	21.46	5.35	21.59	0.26	0.78	1.17	15.37
Clinopx	YM82-26	24.79	19.25	2.06	21.82	<D.L	0.13	1.44	11.64

Continued on next page

Min phase	Sample	TiO2	MgO	SiO2	FeO	K2O	Na2O	Al2O3	MnO	CaO
Clinopx	YM82-26	0.04	10.27	52.45	20.06	0.02	0.19	1.81	1.03	11.99
Clinopx	YM82-26	0.04	11.54	53.83	18.87	0.02	0.13	0.93	1.03	11.77
Clinopx	YM82-26	0.03	7.83	51.75	23.71	0.09	0.24	1.90	1.16	11.47
Clinopx	YM82-26	0.01	10.40	53.38	20.65	0.07	0.23	1.95	1.39	10.49
Clinopx	YM82-26	0.03	11.78	52.17	27.15	0.06	0.06	0.52	3.63	0.88
Clinopx	YM82-26	0.02	10.62	53.56	23.25	0.04	0.15	1.18	2.58	4.82
Clinopx	YM82-26	0.00	10.63	52.80	20.04	0.03	0.16	1.53	1.02	11.93
Clinopx	YM82-26	0.02	10.75	52.88	20.08	0.05	0.22	1.77	0.91	11.75
Clinopx	P-3-2-2	0.02	18.66	56.12	8.22	0.09	0.19	1.19	0.42	12.55
Clinopx	YM82-26	0.11	7.34	41.75	22.09	1.64	1.47	11.58	0.68	11.02
Clinopx	YM82-26	0.12	7.53	41.71	22.38	1.72	1.42	11.46	0.66	10.91
Clinopx	YM82-26	0.11	7.61	41.54	22.13	1.51	1.51	10.97	0.67	10.76
Clinopx	YM82-26	0.17	7.76	42.10	21.95	1.57	1.47	11.35	0.59	10.85
Clinopx	YM82-26	0.13	7.44	41.77	22.50	1.73	1.40	11.30	0.65	10.81
Clinopx	YM82-26	0.12	7.41	41.70	22.57	1.73	1.45	11.40	0.67	10.92
Clinopx	YM82-26	0.19	7.34	41.64	22.30	1.72	1.54	11.35	0.70	10.74
Clinopx	YM82-26	0.05	9.42	59.87	17.45	0.03	0.17	1.61	0.86	9.84
Clinopx	YM82-26	0.00	9.26	57.63	25.54	0.03	0.06	0.58	3.50	2.91
Clinopx	YM82-26	0.03	8.96	57.22	18.72	0.06	0.23	2.05	1.00	10.43

Continued on next page

Min phase	Sample	P2O5	Total	Na23	Mg24	Al27	Si28	P31	K39	Ca44
Clinopx	YM82-26	0.05	97.89	7086.79	48074.71	84906.78	244938.23	534.80	4541.33	66115.27
Clinopx	YM82-26	0.01	98.16	1251.15	62247.07	8085.16	251482.38	94.29	258.54	87750.95
Clinopx	YM82-26	0.02	98.20	1297.41	57853.84	9447.77	241666.16	69.50	314.58	83547.31
Clinopx	YM82-26	0.00	98.56	1208.37	52707.87	8248.51	249612.63	87.45	307.58	82277.34
Clinopx	YM82-26	0.01	96.28	529.11	63970.13	3522.82	244003.34	80.86	168.26	24550.86
Clinopx	YM82-26	0.07	96.29	1197.16	56960.27	8281.91	250547.50	77.72	317.97	88799.98
Clinopx	YM82-26	0.02	98.17	1553.22	56504.53	9792.98	246807.98	73.15	394.61	85167.19
Clinopx	YM82-26	0.03	98.46	1395.90	54397.09	7920.59	247275.39	73.77	336.78	76836.66
Clinopx	P-3-2-2	0.00	97.48	10478.76	42264.32	64207.20	194922.23	77.77	11840.62	89779.85
Clinopx	YM82-26	0.02	97.71	11025.05	42711.21	64672.47	194922.23	78.45	11837.87	89750.87
Clinopx	YM82-26	0.05	97.95	10683.16	40817.10	61108.77	193052.47	104.42	12008.91	82727.15
Clinopx	YM82-26	0.02	96.81	510.29	59264.13	3423.00	193987.34	59.47	98.98	19993.43
Clinopx	YM82-26	0.00	97.81	494.12	60923.12	3610.32	196791.97	60.55	150.11	11919.53
Clinopx	YM82-26	0.00	97.72	9268.59	38886.02	55467.01	194454.75	106.05	12937.54	77890.19
Clinopx	YM82-26	0.02	97.97	10345.32	39492.69	59427.15	195389.63	81.27	13978.58	83393.34
Clinopx	YM82-26	0.01	97.53	10585.69	40405.75	60046.55	194454.78	84.79	13873.78	83167.29
Clinopx	YM82-26	0.00	99.29	1462.95	69396.73	9831.18	279996.22	74.94	260.83	99801.81
Clinopx	YM82-26	0.06	99.57	1509.72	55213.54	9213.10	269245.06	109.81	474.08	52264.20
Clinopx	YM82-26	0.04	98.73	2754.47	63351.66	11951.03	267375.31	230.25	393.60	135582.81

Continued on next page

Min phase	Sample	Total	Na23	Mg24	Al27	Si28	P31	K39	Ca44	Ti48
Clinopx	YM82-26	97.89	7086.79	48074.71	84906.78	244938.23	534.80	4541.33	66115.27	2986.75
Clinopx	YM82-26	98.16	1251.15	62247.07	8085.16	251482.38	94.29	258.54	87750.95	236.68
Clinopx	YM82-26	98.20	1297.41	57853.84	9447.77	241666.16	69.50	314.58	83547.31	228.40
Clinopx	YM82-26	98.56	1208.37	52707.87	8248.51	249612.63	87.45	307.58	82277.34	240.83
Clinopx	YM82-26	96.28	529.11	63970.13	3522.82	244003.34	80.86	168.26	24550.86	89.47
Clinopx	YM82-26	96.29	1197.16	56960.27	8281.91	250547.50	77.72	317.97	88799.98	247.15
Clinopx	YM82-26	98.17	1553.22	56504.53	9792.98	246807.98	73.15	394.61	85167.19	265.19
Clinopx	YM82-26	98.46	1395.90	54397.09	7920.59	247275.39	73.77	336.78	76836.66	215.01
Clinopx	P-3-2-2	97.48	10478.76	42264.32	64207.20	194922.23	77.77	11840.62	89779.85	648.51
Clinopx	YM82-26	97.71	11025.05	42711.21	64672.47	194922.23	78.45	11837.87	89750.87	659.11
Clinopx	YM82-26	97.95	10683.16	40817.10	61108.77	193052.47	104.42	12008.91	82727.15	1072.30
Clinopx	YM82-26	96.81	510.29	59264.13	3423.00	193987.34	59.47	98.98	19993.43	61.78
Clinopx	YM82-26	97.81	494.12	60923.12	3610.32	196791.97	60.55	150.11	11919.53	52.96
Clinopx	YM82-26	97.72	9268.59	38886.02	55467.01	194454.75	106.05	12937.54	77890.19	603.25
Clinopx	YM82-26	97.97	10345.32	39492.69	59427.15	195389.63	81.27	13978.58	83393.34	631.61
Clinopx	YM82-26	97.53	10585.69	40405.75	60046.55	194454.78	84.79	13873.78	83167.29	679.86
Clinopx	YM82-26	99.29	1462.95	69396.73	9831.18	279996.22	74.94	260.83	99801.81	292.40
Clinopx	YM82-26	99.57	1509.72	55213.54	9213.10	269245.06	109.81	474.08	52264.20	209.68
Clinopx	YM82-26	98.73	2754.47	63351.66	11951.03	267375.31	230.25	393.60	135582.81	391.54

Continued on next page

Min phase	Sample	V51	Cr52	Mn55	Fe56	Fe57	Ni58	Ni60	Ni62	Co59
Clinopx	YM82-26	105.74	212.22	11709.85	1184935.75	1089297.75	10164.83	386.97	393.46	78.87
Clinopx	YM82-26	2.54	7.85	7402.80	153470.77	153381.41	1323.39	47.01	44.04	30.12
Clinopx	YM82-26	3.01	12.02	7274.58	153749.61	151935.67	1335.64	49.84	47.07	25.51
Clinopx	YM82-26	3.33	9.75	7005.72	139036.33	140985.05	1244.96	50.87	49.84	27.08
Clinopx	YM82-26	1.47	6.76	22816.81	201669.17	200659.20	1725.66	52.58	36.68	37.39
Clinopx	YM82-26	2.84	9.03	7314.98	151653.75	152481.03	1348.16	45.19	45.11	28.32
Clinopx	YM82-26	3.16	10.41	8696.63	159640.83	156414.13	1390.26	63.10	61.44	35.14
Clinopx	YM82-26	5.05	19.11	6310.71	136167.48	133307.30	1159.50	43.30	37.63	24.63
Clinopx	P-3-2-2	9.87	27.28	6020.25	205311.31	191108.14	1811.68	89.39	92.86	29.30
Clinopx	YM82-26	8.66	19.29	5561.29	193548.34	186356.42	1685.87	93.42	91.01	29.30
Clinopx	YM82-26	36.64	88.21	5892.57	538941.56	504532.63	4582.20	138.87	134.68	37.63
Clinopx	YM82-26	0.77	12.07	17179.23	158254.03	156921.94	1369.95	41.37	44.50	23.33
Clinopx	YM82-26	1.80	6.70	19121.58	178919.53	176730.08	1559.49	43.81	46.75	23.45
Clinopx	YM82-26	14.31	42.86	4873.64	162014.94	159046.80	1386.59	81.75	81.93	24.72
Clinopx	YM82-26	15.09	45.75	5307.02	169039.52	170392.02	1531.97	89.77	90.14	26.88
Clinopx	YM82-26	17.44	45.43	5274.10	177508.17	178259.45	1582.91	81.32	87.81	26.97
Clinopx	YM82-26	4.41	14.48	10007.62	203054.58	195845.34	1684.94	67.81	63.43	38.34
Clinopx	YM82-26	2.28	<D.L	16754.94	182695.86	178860.64	1615.17	104.64	91.42	39.78
Clinopx	YM82-26	4.79	14.87	10464.04	178894.03	175727.77	1543.99	61.91	56.83	25.78

Continued on next page

Min phase	Sample	Cu63	Zn64	Ga69	Ge74	Sr88	Y89	Zr90	Nb93	Mo98
Clinopx	YM82-26	266.53	369.04	25.89	37.50	36.80	1.27	6.06	3.95	4.85
Clinopx	YM82-26	2.63	181.89	1.44	25.15	19.31	1.75	22.89	0.12	<D.L
Clinopx	YM82-26	10.75	159.35	1.10	23.12	18.19	3.76	34.06	0.11	0.12
Clinopx	YM82-26	5.49	138.50	0.98	20.95	21.20	1.17	17.54	0.21	0.11
Clinopx	YM82-26	5.61	257.27	<0.60	24.08	13.90	0.11	0.73	0.18	<D.L
Clinopx	YM82-26	16.54	160.98	1.21	23.22	18.69	1.05	19.85	0.26	<D.L
Clinopx	YM82-26	1.54	180.62	1.44	22.46	18.59	1.64	21.03	0.35	<D.L
Clinopx	YM82-26	4.42	150.22	1.36	17.93	20.40	3.79	28.01	0.09	<D.L
Clinopx	P-3-2-2	3.21	104.09	11.16	18.33	220.77	14.41	44.29	9.73	0.25
Clinopx	YM82-26	10.72	97.79	10.88	18.41	212.00	11.98	43.40	10.32	<D.L
Clinopx	YM82-26	39.01	154.26	14.12	25.71	207.89	14.01	41.51	8.92	1.58
Clinopx	YM82-26	4.35	156.98	0.71	20.23	11.03	0.48	0.84	<D.L	<D.L
Clinopx	YM82-26	6.03	151.65	0.63	19.54	8.96	0.30	0.77	<D.L	<D.L
Clinopx	YM82-26	6.09	98.92	11.71	15.08	206.95	22.70	43.48	7.65	<D.L
Clinopx	YM82-26	1.26	98.68	11.49	16.61	237.74	24.44	47.95	7.35	<D.L
Clinopx	YM82-26	0.55	96.39	12.95	16.11	224.49	22.27	44.91	6.89	<D.L
Clinopx	YM82-26	3.67	214.09	1.78	26.14	20.46	3.17	26.01	0.24	<D.L
Clinopx	YM82-26	20.03	265.53	1.89	26.54	15.08	0.53	1.91	0.66	0.24
Clinopx	YM82-26	73.91	116.75	1.37	23.16	57.06	2.38	23.73	0.26	1.19

Continued on next page

Min phase	Sample	Sn120	Ba138
Clinopx	YM82-26	6.20	240.10
Clinopx	YM82-26	0.68	8.85
Clinopx	YM82-26	0.82	9.88
Clinopx	YM82-26	1.14	16.90
Clinopx	YM82-26	0.56	21.71
Clinopx	YM82-26	0.54	10.55
Clinopx	YM82-26	1.26	19.16
Clinopx	YM82-26	0.85	12.10
Clinopx	P-3-2-2	1.39	866.85
Clinopx	YM82-26	1.45	834.24
Clinopx	YM82-26	1.75	720.69
Clinopx	YM82-26	0.39	9.82
Clinopx	YM82-26	0.39	13.86
Clinopx	YM82-26	1.06	802.45
Clinopx	YM82-26	0.77	804.07
Clinopx	YM82-26	1.00	925.67
Clinopx	YM82-26	0.88	12.66
Clinopx	YM82-26	1.48	23.35
Clinopx	YM82-26	1.40	23.08

Appendix F. Growth rate, cell viability data, and UV attenuation data for *Synechococcus* sp. PCC 7002 UV irradiation experiments

‘- - ‘ indicates that the culture has died

Table F1. Optical density measurements at 750 nm for UV doses ranging from 100 to 1000 J/m^2.

Day/OD750	0 J/m2	100 J/m2	300 J/m2	600 J/m2	1000 J/m2
0	0.068	0.04725	0.045	0.056	0.069
1	0.21	0.14595	0.143	0.119	0.13
2	0.466	0.28665	0.286	0.16	0.084
3	0.644	0.41055	0.371	0.213	0.106
4	0.771	0.556	0.497	0.263	0.103
5	0.822	0.641	0.534	0.283	0.121
6	0.882	0.675	0.601	0.32	0.134
7	0.901	0.721	0.658	0.364	0.165

Table F2. Chlorophyll a measurements for *Synechococcus* sp. PCC 7002 cultures irradiated at 1000 J/m^2

1000 J/m2	OD652	duplicate	OD665	duplicate	OD652 avg	OD665 avg	Chl a (ug/mL)
Day 0 pre-irradiation							
Fe 0.15/Si 0.2	0.23	0.195	0.32	0.399	0.2125	0.3595	4.04
Fe 0.35/Si 0.2	0.255	0.302	0.49	0.544	0.2785	0.517	6.04
Fe 0.55/Si 0.2	0.196	0.216	0.389	0.396	0.206	0.3925	4.63
Fe 0.15/Si 0.6	0.185	0.23	0.391	0.404	0.2075	0.3975	4.70
Fe 0.35/Si 0.6	0.249	0.233	0.48	0.488	0.241	0.484	5.83
Fe 0.55/Si 0.6	0.158	0.169	0.327	0.304	0.1635	0.3155	3.74
Fe 0.15/Si 2.0	0.161	0.166	0.334	0.347	0.1635	0.3405	4.15
Fe 0.35/Si 2.0	0.115	0.111	0.245	0.242	0.113	0.2435	3.00
Fe 0.55/Si 2.0	0.148	0.152	0.343	0.371	0.15	0.357	4.53
Fe 0/Si 0.2	0.145	0.188	0.338	0.432	0.1665	0.385	4.85
Fe 0/Si 0.6	0.197	0.189	0.36	0.405	0.193	0.3825	4.58
Fe 0/Si 2.0	0.128	0.146	0.26	0.258	0.137	0.259	3.05
Fe 0/Si 0 UV	0.175	0.132	0.326	0.272	0.1535	0.299	3.56
Fe 0/Si 0 no UV	0.134	0.1	0.257	0.254	0.117	0.2555	3.16
Day 0 post-irradiation							
Fe 0.15/Si 0.2	0.031	0.029	0.089	0.095	0.03	0.092	1.24
Fe 0.35/Si 0.2	0.047	0.039	0.112	0.112	0.043	0.112	1.46
Fe 0.55/Si 0.2	0.037	0.023	0.07	0.067	0.03	0.0685	0.86
Fe 0.15/Si 0.6	0.029	0.029	0.09	0.094	0.029	0.092	1.25
Fe 0.35/Si 0.6	0.031	0.021	0.095	0.083	0.026	0.089	1.23
Fe 0.55/Si 0.6	0.021	0.029	0.066	0.078	0.025	0.072	0.96
Fe 0.15/Si 2.0	0.039	0.032	0.096	0.092	0.0355	0.094	1.23
Fe 0.35/Si 2.0	0.018	0.021	0.07	0.071	0.0195	0.0705	0.98
Fe 0.55/Si 2.0	0.015	0.033	0.072	0.089	0.024	0.0805	1.11
Fe 0/Si 0.2	0.031	0.036	0.086	0.101	0.0335	0.0935	1.24
Fe 0/Si 0.6	0.023	0.026	0.081	0.083	0.0245	0.082	1.13
Fe 0/Si 2.0	0.053	0.052	0.071	0.085	0.0525	0.078	0.82
Fe 0/Si 0 UV	0.028	0.021	0.084	0.075	0.0245	0.0795	1.09
Fe 0/Si 0 no UV	0.134	0.13	0.253	0.258	0.132	0.2555	3.03
Day 1							
Fe 0.15/Si 0.2	0.034	0.033	0.056	0.07	0.0335	0.063	0.74
Fe 0.35/Si 0.2	0.062	0.052	0.096	0.102	0.057	0.099	1.13
Fe 0.55/Si 0.2	0.021	0.014	0.033	0.02	0.0175	0.0265	0.28
Fe 0.15/Si 0.6	0.04	0.039	0.075	0.083	0.0395	0.079	0.95
Fe 0.35/Si 0.6	0.044	0.053	0.084	0.082	0.0485	0.083	0.94
Fe 0.55/Si 0.6	0.033	0.035	0.052	0.058	0.034	0.055	0.61
Fe 0.15/Si 2.0	0.056	0.055	0.108	0.077	0.0555	0.0925	1.03
Fe 0.35/Si 2.0	0.04	0.039	0.066	0.055	0.0395	0.0605	0.65
Fe 0.55/Si 2.0	0.056	0.042	0.088	0.093	0.049	0.0905	1.06
Fe 0/Si 0.2	0.061	0.053	0.093	0.084	0.057	0.0885	0.95
Fe 0/Si 0.6	0.05	0.041	0.059	0.061	0.0455	0.06	0.59
Fe 0/Si 2.0	0.038	0.038	0.061	0.057	0.038	0.059	0.64
Fe 0/Si 0 UV	0.047	0.045	0.066	0.067	0.046	0.0665	0.69
Fe 0/Si 0 no UV	0.16	0.172	0.366	0.373	0.166	0.3695	4.60

Continued on next page

	OD652	duplicate	OD665	duplicate	OD652 avg	OD665 avg	Chl a (ug/mL)
			Day 2				
Fe 0.15/Si 0.2	0.044	0.039	0.05	0.048	0.0415	0.049	0.44
Fe 0.35/Si 0.2	0.074	0.065	0.127	0.116	0.0695	0.1215	1.39
Fe 0.55/Si 0.2	0.016	0.02	0.02	0.018	0.018	0.019	0.16
Fe 0.15/Si 0.6	0.036	0.044	0.064	0.069	0.04	0.0665	0.74
Fe 0.35/Si 0.6	0.046	0.051	0.079	0.089	0.0485	0.084	0.95
Fe 0.55/Si 0.6	0.033	0.038	0.048	0.053	0.0355	0.0505	0.52
Fe 0.15/Si 2.0	0.022	0.035	0.027	0.052	0.0285	0.0395	0.40
Fe 0.35/Si 2.0	0.021	0.032	0.043	0.056	0.0265	0.0495	0.58
Fe 0.55/Si 2.0	0.032	0.037	0.066	0.075	0.0345	0.0705	0.85
Fe 0/Si 0.2	0.041	0.044	0.082	0.084	0.0425	0.083	0.99
Fe 0/Si 0.6	0.033	0.034	0.057	0.062	0.0335	0.0595	0.68
Fe 0/Si 2.0	0.026	0.025	0.054	0.048	0.0255	0.051	0.61
Fe 0/Si 0 UV	0.031	0.036	0.057	0.065	0.0335	0.061	0.71
Fe 0/Si 0 no UV	0.229	0.251	0.441	0.401	0.24	0.421	4.81
			Day 3				
Fe 0.15/Si 0.2	0.043	0.039	0.042	0.047	0.041	0.0445	0.37
Fe 0.35/Si 0.2	0.048	0.038	0.065	0.052	0.043	0.0585	0.59
Fe 0.55/Si 0.2	0.022	0.022	0.015	0.017	0.022	0.016	0.07
Fe 0.15/Si 0.6	0.027	0.021	0.042	0.033	0.024	0.0375	0.41
Fe 0.35/Si 0.6	0.035	0.036	0.064	0.065	0.0355	0.0645	0.75
Fe 0.55/Si 0.6	0.027	0.025	0.043	0.044	0.026	0.0435	0.49
Fe 0.15/Si 2.0	0.022	0.02	0.023	0.024	0.021	0.0235	0.20
Fe 0.35/Si 2.0	0.025	0.029	0.04	0.043	0.027	0.0415	0.45
Fe 0.55/Si 2.0	0.032	0.038	0.061	0.064	0.035	0.0625	0.72
Fe 0/Si 0.2	0.029	0.038	0.066	0.055	0.0335	0.0605	0.70
Fe 0/Si 0.6	0.029	0.024	0.052	0.064	0.0265	0.058	0.72
Fe 0/Si 2.0	0.021	0.017	0.045	0.038	0.019	0.0415	0.51
Fe 0/Si 0 UV	0.024	0.021	0.034	0.029	0.0225	0.0315	0.32
Fe 0/Si 0 no UV	0.237	0.252	0.467	0.4	0.2445	0.4335	4.97
			Day 4				
Fe 0.15/Si 0.2	0.02	0.016	0.022		0.018	0.022	0.20
Fe 0.35/Si 0.2	0.035	0.027	0.056	0.051	0.031	0.0535	0.61
Fe 0.55/Si 0.2	0.012	0.015	0.013	0.012	0.0135	0.0125	0.09
Fe 0.15/Si 0.6	0.028	0.023	0.038	0.036	0.0255	0.037	0.38
Fe 0.35/Si 0.6	0.034	0.03	0.053	0.047	0.032	0.05	0.54
Fe 0.55/Si 0.6	0.02	0.021	0.029	0.034	0.0205	0.0315	0.34
Fe 0.15/Si 2.0	0.013	0.012	0.016	0.016	0.0125	0.016	0.15
Fe 0.35/Si 2.0	0.03	0.033	0.06	0.048	0.0315	0.054	0.61
Fe 0.55/Si 2.0	0.05	0.054	0.091	0.099	0.052	0.095	1.10
Fe 0/Si 0.2	0.038	0.028	0.065	0.046	0.033	0.0555	0.62
Fe 0/Si 0.6	0.022	0.018	0.035	0.034	0.02	0.0345	0.39
Fe 0/Si 2.0	0.012	0.013	0.016	0.014	0.0125	0.015	0.14
Fe 0/Si 0 UV	0.018	0.025	0.038	0.026	0.0215	0.032	0.34
Fe 0/Si 0 no UV	0.306	0.31	0.402	0.45	0.308	0.426	4.31

Continued on next page

	OD652	duplicate	OD665	duplicate	OD652 avg	OD665 avg	Chl a (ug/mL)
			Day 5				
Fe 0.15/Si 0.2	0.015	0.011	0.029	0.023	0.013	0.026	0.31
Fe 0.35/Si 0.2	0.024	0.022	0.031	0.032	0.023	0.0315	0.32
Fe 0.55/Si 0.2	0.012	0.014	0.016	0.016	0.013	0.016	0.15
Fe 0.15/Si 0.6	0.018	0.022	0.017	0.02	0.02	0.0185	0.13
Fe 0.35/Si 0.6	0.029	0.027	0.032	0.031	0.028	0.0315	0.27
Fe 0.55/Si 0.6	0.027	0.0203	0.028	0.023	0.02365	0.0255	0.21
Fe 0.15/Si 2.0	0.014	0.016	0.014	0.013	0.015	0.0135	0.09
Fe 0.35/Si 2.0	0.043	0.043	0.054	0.04	0.043	0.047	0.40
Fe 0.55/Si 2.0	0.126	0.136	0.251	0.272	0.131	0.2615	3.14
Fe 0/Si 0.2	0.041	0.037	0.067	0.055	0.039	0.061	0.66
Fe 0/Si 0.6	0.031	0.027	0.042	0.028	0.029	0.035	0.32
Fe 0/Si 2.0	0.024	0.021	0.023	0.02	0.0225	0.0215	0.16
Fe 0/Si 0 UV	0.028	0.033	0.033		0.0305	0.033	0.28
Fe 0/Si 0 no UV	0.423	0.4	0.665	0.603	0.4115	0.634	6.81
			Day 6				
Fe 0.15/Si 0.2	0.053	0.036	0.053	0.028	0.0445	0.0405	0.28
Fe 0.35/Si 0.2	0.046	0.048	0.076	0.085	0.047	0.0805	0.91
Fe 0.55/Si 0.2	0.017	0.011	0.011	0.008	0.014	0.0095	0.04
Fe 0.15/Si 0.6	0.053	0.023	0.033	0.021	0.038	0.027	0.12
Fe 0.35/Si 0.6	0.041	0.041	0.062	0.061	0.041	0.0615	0.65
Fe 0.55/Si 0.6	0.051	0.048	0.092	0.081	0.0495	0.0865	0.99
Fe 0.15/Si 2.0	0.033	0.064	0.047	0.048	0.0485	0.0475	0.36
Fe 0.35/Si 2.0	0.107	0.106	0.22	0.213	0.1065	0.2165	2.62
Fe 0.55/Si 2.0	0.192	0.217	0.418	0.457	0.2045	0.4375	5.38
Fe 0/Si 0.2	0.043	0.035	0.059	0.044	0.039	0.0515	0.51
Fe 0/Si 0.6	0.025	0.026	0.032	0.016	0.0255	0.024	0.17
Fe 0/Si 2.0	0.022	0.024	0.02	0.025	0.023	0.0225	0.17
Fe 0/Si 0 UV	0.03	0.023	0.04	0.026	0.0265	0.033	0.31
Fe 0/Si 0 no UV	0.425	0.484	0.916	0.901	0.4545	0.9085	10.92
			Day 7				
Fe 0.15/Si 0.2	0.058	0.039	0.105	0.065	0.0485	0.085	0.97
Fe 0.35/Si 0.2	0.046	0.048	0.076	0.085	0.047	0.0805	0.91
Fe 0.55/Si 0.2	0.016	0.015	0.011	0.009	0.0155	0.01	0.03
Fe 0.15/Si 0.6	0.025	0.023	0.027	0.026	0.024	0.0265	0.23
Fe 0.35/Si 0.6	0.03	0.022	0.04	0.028	0.026	0.034	0.33
Fe 0.55/Si 0.6	0.088	0.095	0.158	0.184	0.0915	0.171	2.00
Fe 0.15/Si 2.0	0.051	0.055	0.09	0.094	0.053	0.092	1.05
Fe 0.35/Si 2.0	0.178	0.173	0.361	0.358	0.1755	0.3595	4.36
Fe 0.55/Si 2.0	0.209	0.205	0.418	0.427	0.207	0.4225	5.11
Fe 0/Si 0.2	0.045	0.029	0.081	0.039	0.037	0.06	0.66
Fe 0/Si 0.6	0.03	0.029	0.039	0.039	0.0295	0.039	0.38
Fe 0/Si 2.0	0.037	0.026	0.056	0.035	0.0315	0.0455	0.47
Fe 0/Si 0 UV	0.026	0.021	0.029	0.019	0.0235	0.024	0.19
Fe 0/Si 0 no UV	0.482	0.527	0.932	0.813	0.5045	0.8725	9.90

Continued on next page

	OD652	duplicate	OD665	duplicate	OD652 avg	OD665 avg	Chl a (ug/mL)
			Day 8				
Fe 0.15/Si 0.2	0.132	0.119	0.218	0.219	0.1255	0.2185	2.49
Fe 0.35/Si 0.2	0.077	0.078	0.145	0.146	0.0775	0.1455	1.71
Fe 0.55/Si 0.2	0.023	0.018	0.032	0.026	0.0205	0.029	0.30
Fe 0.15/Si 0.6	0.029	0.02	0.044	0.027	0.0245	0.0355	0.37
Fe 0.35/Si 0.6	0.038	0.032	0.06	0.046	0.035	0.053	0.56
Fe 0.55/Si 0.6	0.171	0.158	0.311	0.312	0.1645	0.3115	3.67
Fe 0.15/Si 2.0	0.119	0.113	0.245	0.247	0.116	0.246	3.02
Fe 0.35/Si 2.0	0.168	0.187	0.344	0.384	0.1775	0.364	4.41
Fe 0.55/Si 2.0	0.185	0.183	0.377	0.372	0.184	0.3745	4.53
Fe 0/Si 0.2	0.05	0.03	0.091	0.054	0.04	0.0725	0.84
Fe 0/Si 0.6	0.028	0.038	0.046	0.059	0.033	0.0525	0.57
Fe 0/Si 2.0	0.05	0.045	0.083	0.072	0.0475	0.0775	0.86
Fe 0/Si 0 UV	0.031	0.044	0.072	0.047	0.0375	0.0595	0.65
Fe 0/Si 0 no UV	0.555	0.586	1.044	0.845	0.5705	0.9445	10.51

Table F3. Chlorophyll a measurements for *Synechococcus* sp. PCC 7002 cultures irradiated at 500 J/m^2

500 J/m2	OD652	duplicate	OD665	duplicate	OD652 avg	OD665 avg	Chl a (ug/mL)
Day 0 post-irradiation							
Fe 0.15/Si 0.2	0.017	0.019	0.044	0.025	0.018	0.0345	0.41
Fe 0.35/Si 0.2	0.022	0.019	0.034	0.034	0.0205	0.034	0.38
Fe 0.55/Si 0.2	0.033	0.077	0.069	0.066	0.055	0.0675	0.63
Fe 0.15/Si 0.6	0.027	0.039	0.04	0.049	0.033	0.0445	0.44
Fe 0.35/Si 0.6	0.028	0.0473	0.043	0.053	0.03765	0.048	0.46
Fe 0.55/Si 0.6	0.048	0.056	0.048	0.047	0.052	0.0475	0.33
Fe 0.15/Si 2.0	0.014	0.017	0.03	0.048	0.0155	0.039	0.50
Fe 0.35/Si 2.0	0.034	0.037	0.07	0.062	0.0355	0.066	0.77
Fe 0.55/Si 2.0	0.025	0.028	0.056	0.037	0.0265	0.0465	0.53
Fe 0/Si 0.2	0.039	0.041	0.043	0.04	0.04	0.0415	0.33
Fe 0/Si 0.6	0.038	0.025	0.034	0.031	0.0315	0.0325	0.26
Fe 0/Si 2.0	0.034	0.028	0.023	0.021	0.031	0.022	0.09
Fe 0/Si 0 UV	0.167	0.101	0.0585	0.134	1.68327	0.077	0.70
Fe 0/Si 0 no UV	0.048	0.049	0.049	0.051	0.0485	0.05	0.40
Day 1							
Fe 0.15/Si 0.2	0.059	0.084	0.058	0.085	0.0715	0.0715	0.55
Fe 0.35/Si 0.2	0.044	0.049	0.056	0.064	0.0465	0.06	0.58
Fe 0.55/Si 0.2	0.015	0.008	0.028	0.028	0.0115	0.028	0.36
Fe 0.15/Si 0.6	0.034	0.035	0.026	0.037	0.0345	0.0315	0.22
Fe 0.35/Si 0.6	0.042	0.038	0.053	0.041	0.04	0.047	0.42
Fe 0.55/Si 0.6	0.05	0.042	0.051	0.049	0.046	0.05	0.42
Fe 0.15/Si 2.0	0.026	0.029	0.024	0.022	0.0275	0.023	0.14
Fe 0.35/Si 2.0	--	--	--	--	--	--	--
Fe 0.55/Si 2.0	0.033	0.034	0.028	0.026	0.0335	0.027	0.15
Fe 0/Si 0.2	0.012	0.016	0.033	0.035	0.014	0.034	0.43
Fe 0/Si 0.6	0.011	0.017	0.034	0.037	0.014	0.0355	0.46
Fe 0/Si 2.0	0.011	0.017	0.031	0.03	0.014	0.0305	0.38
Fe 0/Si 0 UV	0.067	0.072	0.082	0.086	0.0695	0.084	0.77
Fe 0/Si 0 no UV	0.095	0.077	0.102	0.112	0.086	0.107	1.01
Day 4							
Fe 0.15/Si 0.2	0.147	0.19	0.305	0.345	0.1685	0.325	3.86
Fe 0.35/Si 0.2	0.181	0.217	0.379	0.426	0.199	0.4025	4.86
Fe 0.55/Si 0.2	0.006		0.017		0.006	0.017	0.23
Fe 0.15/Si 0.6	0.012	0.017	0.039	0.051	0.0145	0.045	0.61
Fe 0.35/Si 0.6	0.036	0.032	0.076	0.076	0.034	0.076	0.95
Fe 0.55/Si 0.6	0.117	0.158	0.261	0.34	0.1375	0.3005	3.72
Fe 0.15/Si 2.0	0.085	0.085	0.164	0.171	0.085	0.1675	2.00
Fe 0.35/Si 2.0	0.109	0.131	0.062	0.107	0.12	0.0845	0.35
Fe 0.55/Si 2.0	0.035		0.215		0.035	0.215	3.20
Fe 0/Si 0.2	0.015		0.038	0.048	0.015	0.043	0.57
Fe 0/Si 0.6	0.004		0.008		0.004	0.008	0.10
Fe 0/Si 2.0		0.014		0.175	0.014	0.175	2.73
Fe 0/Si 0 UV	0.014	0.022	0.063	0.065	0.018	0.064	0.89
Fe 0/Si 0 no UV	0.241	0.291	0.573	0.665	0.266	0.619	7.81

Continued on next page

	OD652	duplicate	OD665	duplicate	OD652 avg	OD665 avg	Chl a (ug/mL)
			Day 8				
Fe 0.15/Si 0.2	0.238	0.453	0.505	0.943	0.3455	0.724	8.84
Fe 0.35/Si 0.2	0.336	0.73	0.738	1.42	0.533	1.079	13.03
Fe 0.55/Si 0.2							
Fe 0.15/Si 0.6	0.222	0.39	0.505	0.846	0.306	0.6755	8.39
Fe 0.35/Si 0.6	0.184	0.343	0.425	0.733	0.2635	0.579	7.18
Fe 0.55/Si 0.6	0.317	0.568	0.703	1.159	0.4425	0.931	11.39
Fe 0.15/Si 2.0	0.131	0.252	0.321	0.544	0.1915	0.4325	5.41
Fe 0.35/Si 2.0	0.258	0.654	0.569	1.016	0.456	0.7925	9.02
Fe 0.55/Si 2.0	0.3	0.512	0.648	1.066	0.406	0.857	10.49
Fe 0/Si 0.2	0.047	0.071	0.139	0.172	0.059	0.1555	2.03
Fe 0/Si 0.6	0.062	0.132	0.156	0.288	0.097	0.222	2.79
Fe 0/Si 2.0	0.022	0.041	0.062	0.096	0.0315	0.079	1.02
Fe 0/Si 0 UV	0.051	0.053	0.123	0.117	0.052	0.12	1.51
Fe 0/Si 0 no UV	0.388	0.687	0.742	1.308	0.5375	1.025	12.11
			Day 12				
Fe 0.15/Si 0.2	0.796	0.62	1.39	1.34	0.708	1.365	8.09
Fe 0.35/Si 0.2	0.4	0.75	1.77	1.2	0.575	1.485	9.64
Fe 0.55/Si 0.2	--	--	--	--	--	--	--
Fe 0.15/Si 0.6	1.1	1.19	1.94	2.14	1.145	2.04	11.73
Fe 0.35/Si 0.6	1.23	1.44	1.97	2.52	1.335	2.245	12.59
Fe 0.55/Si 0.6	1.43	1.68	2.22	2.95	1.555	2.585	14.41
Fe 0.15/Si 2.0	1.18	0.92	1.54	2.02	1.05	1.78	10.01
Fe 0.35/Si 2.0	1.41	1.36	2.63	2.87	1.385	2.75	16.48
Fe 0.55/Si 2.0	1.43	1.34	3.01	2.77	1.385	2.89	17.63
Fe 0/Si 0.2	0.6	0.57	0.97	1.21	0.585	1.09	6.38
Fe 0/Si 0.6	0.29	0.29	0.65	0.58	0.29	0.615	3.77
Fe 0/Si 2.0							
Fe 0/Si 0 UV	0.069	0.059	0.158	0.131	0.064	0.1445	1.81
Fe 0/Si 0 no UV	1.1	1.48	3.2	3.78	1.29	3.49	22.92
			Day 16				
Fe 0.15/Si 0.2	2.14	2.22	3.26	2.52	2.18	2.89	14.23
Fe 0.35/Si 0.2	2.46	2.2	3.44	2.92	2.33	3.18	15.95
Fe 0.55/Si 0.2	--	--	--	--	--	--	--
Fe 0.15/Si 0.6	1.96	2.24	3.76	3.16	2.1	3.46	19.21
Fe 0.35/Si 0.6	2.1	2.3	3.86	3.48	2.2	3.67	20.50
Fe 0.55/Si 0.6	2.24	2.48	4.16	4.44	2.36	4.3	24.95
Fe 0.15/Si 2.0	1.96	1.87	3.78	3.56	1.915	3.67	21.72
Fe 0.35/Si 2.0	2.04	2.8	3.74	5.42	2.42	4.58	26.97
Fe 0.55/Si 2.0	2.62	2.78	4.82	5.22	2.7	5.02	29.36
Fe 0/Si 0.2	1.86	1.16	1.84	1.52	1.51	1.68	7.24
Fe 0/Si 0.6	1.6	1.76	0.96	2.4	1.68	1.68	6.51
Fe 0/Si 2.0	0.86	0.78	1	0.96	0.82	0.98	4.48
Fe 0/Si 0 UV	0.077	0.071	0.155	0.161	0.074	0.158	1.94
Fe 0/Si 0 no UV	1.76	2.08	5.48	5.9	1.92	5.69	38.15

Continued on next page

	OD652	duplicate	OD665	duplicate	OD652 avg	OD665 avg	Chl a (ug/mL)
			Day 19				
Fe 0.15/Si 0.2	2.4	2.22	3.68	3.45	2.31	3.565	19.17
Fe 0.35/Si 0.2	2.12	2.42	3.87	3.2	2.27	3.535	19.10
Fe 0.55/Si 0.2							
Fe 0.15/Si 0.6	1.9	1.86	3.9	3.56	1.88	3.73	22.35
Fe 0.35/Si 0.6	2.22	2.14	3.95	4.1	2.18	4.025	23.48
Fe 0.55/Si 0.6	2.46	2.32	5.14	5.42	2.39	5.28	32.80
Fe 0.15/Si 2.0	2.32	2.26	4.53	4.67	2.29	4.6	27.69
Fe 0.35/Si 2.0	1.34	1.28	3.9	4.58	1.31	4.24	28.94
Fe 0.55/Si 2.0	1.84	1.78	5.2	5.7	1.81	5.45	36.66
Fe 0/Si 0.2	1.18	1.62	2.24	2.16	1.4	2.2	11.94
Fe 0/Si 0.6	1.26	1.4	2.14	1.28	1.33	1.71	8.25
Fe 0/Si 2.0	1.56	1.4	1.82	1	1.48	1.41	5.16
Fe 0/Si 0 UV	0.039	0.443	0.093	0.408	0.241	0.2505	2.02
Fe 0/Si 0 no UV	1.62	1.18	6.14	6.44	1.4	6.29	45.25

Table F4. Cell viability measurements as colony forming unit (CFU) counts.

Conc. In mM	CFU	cells/mL surv	% survival
Fe 0.15/Si 0.2	6	60	0.29
Fe 0.35/Si 0.2	7.5	75	0.36
Fe 0.55/Si 0.2	0	0	0.00
Fe 0.15/Si 0.6	10.5	105	0.50
Fe 0.35/Si 0.6	16.5	165	0.79
Fe 0.55/Si 0.6	19.5	195	0.94
Fe 0.15/Si 2.0	24	240	1.15
Fe 0.35/Si 2.0	30	300	1.44
Fe 0.55/Si 2.0	57.5	575	2.76
Fe 0/Si 0.2	2.5	25	0.12
Fe 0/Si 0.6	6.5	65	0.31
Fe 0/Si 2.0	8	80	0.38
Fe 0/Si 0 no UV.	208	20800	100.00
Fe 0/Si 0 UV.	2.75	27.5	0.13

Table F5. Transmission at 254 nm through Fe and Si supplemented A+ growth media

0 Si	% Trans.					% abs
[Fe+3] mM	1	2	3	avg trans	% abs	no bkrnd
0.0144	72.8	73.5	72.7	73.00	27.00	0.00
0.025	57.1	55.9	56.8	56.60	43.40	16.40
0.05	39.25	38.35	37.9	38.50	61.50	34.50
0.075	27.85	27.4	29.4	28.22	71.78	44.78
0.15	17.88	17.32	17.26	17.49	82.51	55.51
0.3	5.51	6.48	5.11	5.70	94.30	67.30
0.4	1.58	1.49	1.69	1.59	98.41	71.41
0.55	0.5	0.61	0.67	0.59	99.41	72.41
0.6 Si	% Trans.					
[Fe+3] mM	1	2	3	avg trans	% abs	
0.0144	57.1	55.4	54.3	55.60	44.40	17.40
0.025	49.6	45.6	46.8	47.33	52.67	25.67
0.05	31.7	33.25	31.8	32.25	67.75	40.75
0.075	21.6	19.5	21.6	20.90	79.10	52.10
0.15	10.76	8.98	10.28	10.01	89.99	62.99
0.3	5.41	4.67	5.22	5.10	94.90	67.90
0.4	1.57	1.67	1.77	1.67	98.33	71.33
0.55	0.48	0.57	0.49	0.51	99.49	72.49
2.0 Si	% Trans.					% abs
[Fe+3] mM	1	2	3	avg trans	% abs	no bkrnd
0.0144	51.7	51.7	51.3	51.57	48.43	21.43
0.025	35	32	35	34.00	66.00	39.00
0.05	20.98	21.8	21.9	21.56	78.44	51.44
0.075	14.14	12.64	12.6	13.13	86.87	59.87
0.15	4.12	3.83	3.61	3.85	96.15	69.15
0.3	1.52	2.03	1.92	1.82	98.18	71.18
0.4	0.4	0.51	0.32	0.41	99.59	72.59
0.55	0.1	0.1	0.07	0.09	99.91	72.91

Appendix G. Growth rate and intracellular ROS data for *Synechococcus* sp. PCC 7002 high iron/silica experiments

‘- - ‘ indicates that the culture has died

Table G1. Chlorophyll a measurements for *Synechococcus* sp. PCC 7002 cultures grown in Fe(III) and Si supplemented A+ growth media containing EDTA

Conc. In mM	OD652	duplicate	OD665	duplicate	OD652 avg	OD665 avg	chl a (ug/mL)
Day 0							
Fe 0.03/Si 0.6	0.015	0.022	0.021	0.042	0.0185	0.032	0.36
Fe 0.15/Si 0.6	0.035	0.029	0.061	0.058	0.032	0.060	0.71
Fe0.35/Si 0.6	0.028	0.025	0.046	0.045	0.0265	0.046	0.52
Fe 0.55/Si 0.6	0.02	0.024	0.039	0.059	0.022	0.049	0.62
Fe 0.75/Si 0.6	0.028	0.02	0.04	0.043	0.024	0.042	0.48
Fe 0.03/Si 0	0.024	0.024	0.047	0.046	0.024	0.047	0.56
Fe 0.15/Si 0	0.032	0.033	0.06	0.053	0.0325	0.057	0.65
Fe0.35/Si 0	0.027	0.025	0.042	0.049	0.026	0.046	0.53
Fe 0.55/Si 0	0.02	0.025	0.033	0.035	0.0225	0.034	0.37
Fe 0.75/Si 0	0.018	0.016	0.031	0.028	0.017	0.030	0.34
Fe 0/Si 0.2	0.026	0.021	0.046	0.047	0.0235	0.047	0.56
Fe 0/Si 0.6	0.027	0.023	0.045	0.047	0.025	0.046	0.54
Fe 0/Si 2.0	0.022	0.023	0.045	0.04	0.0225	0.043	0.51
Fe 0/Si 0	0.021	0.031	0.045	0.043	0.026	0.044	0.50
Day 1							
Fe 0.03/Si 0.6	0.05	0.046	0.075	0.089	0.048	0.082	0.94
Fe 0.15/Si 0.6	0.03	0.05	0.08	0.072	0.04	0.076	0.91
Fe0.35/Si 0.6	0.05	0.025	0.069	0.073	0.0375	0.071	0.85
Fe 0.55/Si 0.6	0.025	0.022	0.061	0.072	0.0235	0.067	0.89
Fe 0.75/Si 0.6	0.036	0.034	0.052	0.061	0.035	0.057	0.63
Fe 0.03/Si 0	0.042	0.041	0.069	0.071	0.0415	0.070	0.80
Fe 0.15/Si 0	0.03	0.015	0.02	0.035	0.0225	0.028	0.26
Fe0.35/Si 0	0.005	0.009	0.01	0.011	0.007	0.011	0.11
Fe 0.55/Si 0	--	--	--	--	--	--	--
Fe 0.75/Si 0	--	--	--	--	--	--	--
Fe 0/Si 0.2	0.041	0.044	0.099	0.095	0.0425	0.097	1.23
Fe 0/Si 0.6	0.037	0.042	0.091	0.089	0.0395	0.090	1.14
Fe 0/Si 2.0	0.039	0.045	0.089	0.096	0.042	0.093	1.16
Fe 0/Si 0	0.042	0.049	0.095	0.092	0.0455	0.094	1.15
Day 2							
Fe 0.03/Si 0.6	0.075	0.069	0.115	0.119	0.072	0.117	1.31
Fe 0.15/Si 0.6	0.071	0.072	0.11	0.105	0.0715	0.108	1.16
Fe0.35/Si 0.6	0.081	0.074	0.112	0.11	0.0775	0.111	1.17
Fe 0.55/Si 0.6	0.085	0.081	0.109	0.1	0.083	0.105	1.02
Fe 0.75/Si 0.6	0.082	0.085	0.1	0.105	0.0835	0.103	0.98
Fe 0.03/Si 0	0.085	0.081	0.102	0.11	0.083	0.106	1.04
Fe 0.15/Si 0	--	--	--	--	--	--	--
Fe0.35/Si 0	--	--	--	--	--	--	--
Fe 0.55/Si 0	--	--	--	--	--	--	--
Fe 0.75/Si 0	--	--	--	--	--	--	--
Fe 0/Si 0.2	0.065	0.052	0.135	0.132	0.0585	0.134	1.69
Fe 0/Si 0.6	0.061	0.059	0.139	0.134	0.06	0.137	1.73
Fe 0/Si 2.0	0.064	0.065	0.142	0.145	0.0645	0.144	1.81
Fe 0/Si 0	0.069	0.075	0.152	0.143	0.072	0.148	1.81

Continued on next page

Conc. In mM	OD652	duplicate	OD665	duplicate	OD652 avg	OD665 avg	chl a (ug/mL)
				Day 3			
Fe 0.03/Si 0.6	0.109	0.109	0.169	0.156	0.109	0.163	1.75
Fe 0.15/Si 0.6	0.105	0.101	0.142	0.152	0.103	0.147	1.55
Fe0.35/Si 0.6	0.1	0.099	0.135	0.141	0.0995	0.138	1.43
Fe 0.55/Si 0.6	0.1	0.102	0.139	0.138	0.101	0.139	1.42
Fe 0.75/Si 0.6	0.109	0.105	0.13	0.135	0.107	0.133	1.28
Fe 0.03/Si 0	0.11	0.111	0.156	0.149	0.1105	0.153	1.57
Fe 0.15/Si 0	--	--	--	--	--	--	--
Fe0.35/Si 0	--	--	--	--	--	--	--
Fe 0.55/Si 0	--	--	--	--	--	--	--
Fe 0.75/Si 0	--	--	--	--	--	--	--
Fe 0/Si 0.2	0.129	0.12	0.192	0.192	0.1245	0.192	2.10
Fe 0/Si 0.6	0.122	0.121	0.185	0.192	0.1215	0.189	2.07
Fe 0/Si 2.0	0.119	0.109	0.179	0.185	0.114	0.182	2.03
Fe 0/Si 0	0.125	0.132	0.201	0.215	0.1285	0.208	2.33
				Day 4			
Fe 0.03/Si 0.6	0.156	0.152	0.221	0.219	0.154	0.220	2.31
Fe 0.15/Si 0.6	0.132	0.129	0.198	0.185	0.1305	0.192	2.04
Fe0.35/Si 0.6	0.142	0.125	0.182	0.179	0.1335	0.181	1.84
Fe 0.55/Si 0.6	0.141	0.14	0.179	0.181	0.1405	0.180	1.77
Fe 0.75/Si 0.6	0.145	0.138	0.185	0.189	0.1415	0.187	1.88
Fe 0.03/Si 0	0.129	0.125	0.181	0.188	0.127	0.185	1.96
Fe 0.15/Si 0	--	--	--	--	--	--	--
Fe0.35/Si 0	--	--	--	--	--	--	--
Fe 0.55/Si 0	--	--	--	--	--	--	--
Fe 0.75/Si 0	--	--	--	--	--	--	--
Fe 0/Si 0.2	0.182	0.198	0.241	0.241	0.19	0.241	2.36
Fe 0/Si 0.6	0.17	0.165	0.259	0.241	0.1675	0.250	2.69
Fe 0/Si 2.0	0.175	0.17	0.256	0.251	0.1725	0.254	2.71
Fe 0/Si 0	0.182	0.179	0.28	0.279	0.1805	0.280	3.07
				Day 4			
Fe 0.03/Si 0.6	0.214	0.207	0.326	0.321	0.2105	0.324	3.54
Fe 0.15/Si 0.6	0.2	0.205	0.279	0.286	0.2025	0.283	2.93
Fe0.35/Si 0.6	0.204	0.204	0.25	0.261	0.204	0.256	2.48
Fe 0.55/Si 0.6	0.208	0.215	0.242	0.238	0.2115	0.240	2.17
Fe 0.75/Si 0.6	0.198	0.211	0.249	0.225	0.2045	0.237	2.18
Fe 0.03/Si 0	0.201	0.208	0.269	0.267	0.2045	0.268	2.68
Fe 0.15/Si 0	--	--	--	--	--	--	--
Fe0.35/Si 0	--	--	--	--	--	--	--
Fe 0.55/Si 0	--	--	--	--	--	--	--
Fe 0.75/Si 0	--	--	--	--	--	--	--
Fe 0/Si 0.2	0.341	0.328	0.45	0.449	0.3345	0.450	4.57
Fe 0/Si 0.6	0.325	0.332	0.462	0.411	0.3285	0.437	4.40
Fe 0/Si 2.0	0.311	0.321	0.42	0.449	0.316	0.435	4.47
Fe 0/Si 0	0.324	0.331	0.451	0.449	0.3275	0.450	4.63

Continued on next page

Conc. In mM	OD652	duplicate	OD665	duplicate	OD652 avg	OD665 avg	chl a (ug/mL)
				Day 6			
Fe 0.03/Si 0.6	0.262	0.285	0.45	0.449	0.2735	0.450	5.07
Fe 0.15/Si 0.6	0.231	0.242	0.364	0.371	0.2365	0.368	4.04
Fe0.35/Si 0.6	0.22	0.215	0.31	0.305	0.2175	0.308	3.22
Fe 0.55/Si 0.6	0.217	0.225	0.298	0.31	0.221	0.304	3.13
Fe 0.75/Si 0.6	0.235	0.241	0.331	0.319	0.238	0.325	3.33
Fe 0.03/Si 0	0.24	0.249	0.359	0.355	0.2445	0.357	3.80
Fe 0.15/Si 0	--	--	--	--	--	--	--
Fe0.35/Si 0	--	--	--	--	--	--	--
Fe 0.55/Si 0	--	--	--	--	--	--	--
Fe 0.75/Si 0	--	--	--	--	--	--	--
Fe 0/Si 0.2	0.461	0.459	0.59	0.6	0.46	0.595	5.90
Fe 0/Si 0.6	0.45	0.461	0.572	0.569	0.4555	0.571	5.54
Fe 0/Si 2.0	0.44	0.438	0.59	0.572	0.439	0.581	5.85
Fe 0/Si 0	0.452	0.461	0.598	0.605	0.4565	0.602	6.04
				Day 7			
Fe 0.03/Si 0.6	0.3	0.297	0.519	0.501	0.2985	0.510	5.85
Fe 0.15/Si 0.6	0.279	0.291	0.441	0.44	0.285	0.441	4.83
Fe0.35/Si 0.6	0.279	0.281	0.369	0.362	0.28	0.366	3.65
Fe 0.55/Si 0.6	0.3	0.299	0.405	0.4	0.2995	0.403	4.09
Fe 0.75/Si 0.6	0.298	0.301	0.397	0.401	0.2995	0.399	4.03
Fe 0.03/Si 0	0.305	0.31	0.433	0.432	0.3075	0.433	4.51
Fe 0.15/Si 0	--	--	--	--	--	--	--
Fe0.35/Si 0	--	--	--	--	--	--	--
Fe 0.55/Si 0	--	--	--	--	--	--	--
Fe 0.75/Si 0	--	--	--	--	--	--	--
Fe 0/Si 0.2	0.48	0.502	0.615	0.629	0.491	0.622	6.09
Fe 0/Si 0.6	0.49	0.498	0.619	0.615	0.494	0.617	5.98
Fe 0/Si 2.0	0.489	0.49	0.621	0.639	0.4895	0.630	6.23
Fe 0/Si 0	0.492	0.501	0.641	0.64	0.4965	0.641	6.34

Table G2. Chlorophyll a measurements for *Synechococcus* sp. PCC 7002 cultures grown in Fe(III) and Si supplemented A+ growth media containing citrate

Conc. In mM	OD652	duplicate	OD665	duplicate	OD652 avg	OD665 avg	chl a (ug/mL)
				day 0			
Fe 0.03/Si 0.6	0	0	0.03	0.04	0	0.035	0.57
Fe 0.15/Si 0.6	0	0.003	0.03	0.035	0.0015	0.0325	0.52
Fe0.35/Si 0.6	0.001	0.004	0.039	0.039	0.0025	0.039	0.61
Fe 0.55/Si 0.6	0.003	0.001	0.04	0.04	0.002	0.04	0.63
Fe 0.75/Si 0.6	0.015	0.01	0.039	0.042	0.0125	0.0405	0.55
Fe 0.03/Si 0	0.001	0.006	0.026	0.045	0.0035	0.0355	0.55
Fe 0.15/Si 0	0	0.001	0.031	0.041	0.0005	0.036	0.58
Fe0.35/Si 0	0.002	0.001	0.029	0.028	0.0015	0.0285	0.45
Fe 0.55/Si 0	0.002	0.004	0.024	0.043	0.003	0.0335	0.52
Fe 0.75/Si 0	0.001	0.004	0.026	0.036	0.0025	0.031	0.48
Fe 0/Si 0	0.002	0.004	0.036	0.042	0.003	0.039	0.61
				day 1			
Fe 0.03/Si 0.6	0.038	0.037	0.052	0.057	0.0375	0.0545	0.57
Fe 0.15/Si 0.6	0.006	0.005	0.008	0.006	0.0055	0.007	0.07
Fe0.35/Si 0.6	0.004	0.003	0.009	0.008	0.0035	0.0085	0.11
Fe 0.55/Si 0.6	0.004	0.003	0.007	0.007	0.0035	0.007	0.08
Fe 0.75/Si 0.6	0.004	0.005	0.004	0.005	0.0045	0.0045	0.03
Fe 0.03/Si 0	0.022	0.023	0.058	0.057	0.0225	0.0575	0.74
Fe 0.15/Si 0	0.023	0.027	0.049	0.044	0.025	0.0465	0.54
Fe0.35/Si 0	0.02	0.02	0.043	0.037	0.02	0.04	0.48
Fe 0.55/Si 0	0.02	0.019	0.035	0.039	0.0195	0.037	0.44
Fe 0.75/Si 0	0.001	0.001	0.02	0.019	0.001	0.0195	0.31
Fe 0/Si 0	0.045	0.049	0.082	0.117	0.047	0.0995	1.22
				day 2			
Fe 0.03/Si 0.6	0.058	0.061	0.089	0.085	0.0595	0.087	0.91
Fe 0.15/Si 0.6	--	--	0.005	0.006	--	0.0055	0.09
Fe0.35/Si 0.6	--	--	0.004	--	--	0.002	0.03
Fe 0.55/Si 0.6	--	--	--	--	--	--	0.00
Fe 0.75/Si 0.6	--	--	--	--	--	--	0.00
Fe 0.03/Si 0	0.059	0.062	0.098	0.103	0.0605	0.1005	1.12
Fe 0.15/Si 0	0.052	0.055	0.081	0.082	0.0535	0.0815	0.87
Fe0.35/Si 0	0.055	0.049	0.075	0.081	0.052	0.078	0.83
Fe 0.55/Si 0	0.045	0.04	0.072	0.073	0.0425	0.0725	0.82
Fe 0.75/Si 0	0.006	0.005	0.009	0.003	0.0055	0.006	0.05
Fe 0/Si 0	0.081	0.088	0.156	0.133	0.0845	0.1445	1.63

Continued on next page

Conc. In mM	OD652	duplicate	OD665	duplicate	OD652 avg	OD665 avg	chl a (ug/mL)
				day 3			
Fe 0.03/Si 0.6	0.069	0.072	0.101	0.102	0.0705	0.1015	1.05
Fe 0.15/Si 0.6	--	--	--	--	--	--	--
Fe0.35/Si 0.6	--	--	--	--	--	--	--
Fe 0.55/Si 0.6	--	--	--	--	--	--	--
Fe 0.75/Si 0.6	--	--	--	--	--	--	--
Fe 0.03/Si 0	0.116	0.148	0.185	0.196	0.132	0.1905	1.98
Fe 0.15/Si 0	0.165	0.172	0.201	0.209	0.1685	0.205	1.90
Fe0.35/Si 0	0.156	0.154	0.182	0.193	0.155	0.1875	1.73
Fe 0.55/Si 0	0.105	0.102	0.145	0.149	0.1035	0.147	1.51
Fe 0.75/Si 0	--	--	--	--	--	--	--
Fe 0/Si 0	0.243	0.239	0.33	0.325	0.241	0.3275	3.28
				day 4			
Fe 0.03/Si 0.6	0.099	0.089	0.125	0.129	0.094	0.127	1.27
Fe 0.15/Si 0.6	--	--	--	--	--	--	--
Fe0.35/Si 0.6	--	--	--	--	--	--	--
Fe 0.55/Si 0.6	--	--	--	--	--	--	--
Fe 0.75/Si 0.6	--	--	--	--	--	--	--
Fe 0.03/Si 0	0.146	0.15	0.275	0.281	0.148	0.278	3.27
Fe 0.15/Si 0	0.182	0.179	0.232	0.239	0.1805	0.2355	2.30
Fe0.35/Si 0	0.183	0.189	0.215	0.221	0.186	0.218	1.97
Fe 0.55/Si 0	0.131	0.139	0.182	0.175	0.135	0.1785	1.76
Fe 0.75/Si 0	--	--	--	--	--	--	--
Fe 0/Si 0	0.286	0.281	0.412	0.413	0.2835	0.4125	4.30
				day 5			
Fe 0.03/Si 0.6	0.126	0.132	0.179	0.174	0.129	0.1765	1.78
Fe 0.15/Si 0.6							
Fe0.35/Si 0.6							
Fe 0.55/Si 0.6							
Fe 0.75/Si 0.6							
Fe 0.03/Si 0	0.176	0.182	0.335	0.329	0.179	0.332	3.88
Fe 0.15/Si 0	0.201	0.211	0.285	0.281	0.206	0.283	2.85
Fe0.35/Si 0	0.2	0.209	0.245	0.257	0.2045	0.251	2.35
Fe 0.55/Si 0	0.165	0.172	0.201	0.205	0.1685	0.203	1.87
Fe 0.75/Si 0	--	--	--	--	--	--	--
Fe 0/Si 0	0.315	0.311	0.487	0.492	0.313	0.4895	5.31

Continued on next page

Conc. In mM	OD652	duplicate	OD665	duplicate	OD652 avg	OD665 avg	chl a (ug/mL)
				day 6			
Fe 0.03/Si 0.6	0.149	0.156	0.272	0.289	0.1525	0.2805	3.27
Fe 0.15/Si 0.6	--	--	--	--	--	--	--
Fe0.35/Si 0.6	--	--	--	--	--	--	--
Fe 0.55/Si 0.6	--	--	--	--	--	--	--
Fe 0.75/Si 0.6	--	--	--	--	--	--	--
Fe 0.03/Si 0	0.211	0.213	0.382	0.379	0.212	0.3805	4.39
Fe 0.15/Si 0	0.225	0.231	0.321	0.329	0.228	0.325	3.35
Fe0.35/Si 0	0.235	0.241	0.289	0.285	0.238	0.287	2.65
Fe 0.55/Si 0	0.189	0.195	0.249	0.251	0.192	0.25	2.44
Fe 0.75/Si 0	--	--	--	--	--	--	--
Fe 0/Si 0	0.398	0.412	0.582	0.573	0.405	0.5775	5.96
				day 7			
Fe 0.03/Si 0.6	0.183	0.181	0.259	0.253	0.182	0.256	2.62
Fe 0.15/Si 0.6	--	--	--	--	--	--	--
Fe0.35/Si 0.6	--	--	--	--	--	--	--
Fe 0.55/Si 0.6	--	--	--	--	--	--	--
Fe 0.75/Si 0.6	--	--	--	--	--	--	--
Fe 0.03/Si 0	0.256	0.261	0.462	0.471	0.2585	0.4665	5.40
Fe 0.15/Si 0	0.265	0.276	0.389	0.403	0.2705	0.396	4.15
Fe0.35/Si 0	0.292	0.296	0.358	0.356	0.294	0.357	3.31
Fe 0.55/Si 0	0.252	0.259	0.31	0.309	0.2555	0.3095	2.86
Fe 0.75/Si 0							
Fe 0/Si 0	0.245	0.249	0.567	0.568	0.247	0.5675	7.14
				day 8			
Fe 0.03/Si 0.6	0.242	0.249	0.335	0.341	0.2455	0.338	3.41
Fe 0.15/Si 0.6	--	--	--	--	--	--	--
Fe0.35/Si 0.6	--	--	--	--	--	--	--
Fe 0.55/Si 0.6	--	--	--	--	--	--	--
Fe 0.75/Si 0.6	--	--	--	--	--	--	--
Fe 0.03/Si 0	0.319	0.331	0.512	0.509	0.325	0.5105	5.55
Fe 0.15/Si 0	0.312	0.307	0.436	0.432	0.3095	0.434	4.43
Fe0.35/Si 0	0.315	0.309	0.389	0.401	0.312	0.395	3.78
Fe 0.55/Si 0	0.278	0.288	0.361	0.372	0.283	0.3665	3.56
Fe 0.75/Si 0	--	--	--	--	--	--	--
Fe 0/Si 0	0.299	0.305	0.623	0.629	0.302	0.626	7.62

Table G3. Chlorophyll a measurements for *Synechococcus* sp. PCC 7002 cultures grown in anoxic conditions, in Fe(II) and Si supplemented A+ growth media.

Conc. In mM	OD652	duplicate	OD665	duplicate	OD652 avg	OD665 avg	chl a (ug/mL)
				Day 0			
Fe 0.03/Si 0	0.023	0.029	0.065	0.061	0.026	0.063	0.80
Fe 0.55/Si 0	0.046	0.042	0.094	0.084	0.044	0.089	1.07
Fe 1/Si 0	0.036	0.034	0.082	0.086	0.035	0.084	1.07
Fe 0.03/Si 0.6	0.045	0.042	0.086	0.071	0.0435	0.0785	0.91
Fe 0.55/Si 0.6	0.039	0.047	0.087	0.092	0.043	0.0895	1.09
Fe 1/0Si 0.6	0.047	0.047	0.103	0.121	0.047	0.112	1.42
Fe 0/Si 0	0.034	0.038	0.085	0.091	0.036	0.088	1.13
				Day 1			
Fe 0.03/Si 0	0.096	0.103	0.193	0.208	0.0995	0.2005	2.42
Fe 0.55/Si 0	0.131	0.144	0.25	0.277	0.1375	0.2635	3.12
Fe 1/Si 0	0.054	0.059	0.118	0.128	0.0565	0.123	1.52
Fe 0.03/Si 0.6	0.116	0.121	0.236	0.257	0.1185	0.2465	3.00
Fe 0.55/Si 0.6	0.122	0.131	0.323	0.285	0.1265	0.304	3.87
Fe 1/0Si 0.6	0.07	0.074	0.144	0.149	0.072	0.1465	1.77
Fe 0/Si 0	0.101	0.109	0.215	0.228	0.105	0.2215	2.71
				Day 2			
Fe 0.03/Si 0	0.237	0.241	0.506	0.502	0.239	0.504	6.17
Fe 0.55/Si 0	0.324	0.385	0.575	0.699	0.3545	0.637	7.35
Fe 1/Si 0	0.161	0.09	0.131	0.112	0.1255	0.1215	0.91
Fe 0.03/Si 0.6	0.184	0.215	0.3	0.364	0.1995	0.332	3.70
Fe 0.55/Si 0.6	0.337	0.372	0.602	0.706	0.3545	0.654	7.63
Fe 1/0Si 0.6	0.176	0.144	0.243	0.208	0.16	0.2255	2.31
Fe 0/Si 0	0.239	0.275	0.495	0.535	0.257	0.515	6.19
				Day 3			(ug/mL)
Fe 0.03/Si 0	0.337	0.476	0.58	0.878	0.4065	0.729	8.40
Fe 0.55/Si 0	0.573	0.611	1.073	1.156	0.592	1.1145	13.10
Fe 1/Si 0	0.214	0.223	0.317	0.323	0.2185	0.32	3.35
Fe 0.03/Si 0.6	0.395	0.434	0.699	0.783	0.4145	0.741	8.53
Fe 0.55/Si 0.6	0.5	0.631	0.927	1.195	0.5655	1.061	12.45
Fe 1/0Si 0.6	0.305	0.311	0.492	0.52	0.308	0.506	5.61
Fe 0/Si 0	0.417	0.51	0.739	0.944	0.4635	0.8415	9.75

Continued on next page

Conc. In mM	OD652	duplicate	OD665	duplicate	OD652 avg	OD665 avg	chl a
				Day 4			
Fe 0.03/Si 0	0.635	0.94	0.74	1.445	0.7875	1.0925	11.07
Fe 0.55/Si 0	0.77	1.335	1.105	2.18	1.0525	1.6425	17.77
Fe 1/Si 0	0.6	0.69	0.69	0.83	0.645	0.76	6.87
Fe 0.03/Si 0.6	0.75	1.095	0.98	1.77	0.9225	1.375	14.52
Fe 0.55/Si 0.6	0.815	1.005	1.2	1.57	0.91	1.385	14.79
Fe 1/0Si 0.6	0.66	0.76	0.855	1.055	0.71	0.955	9.49
Fe 0/Si 0	0.83	1.3	1.175	2.12	1.065	1.6475	17.74
				Day 5			
Fe 0.03/Si 0	0.83	0.885	1.44	1.415	0.8575	1.4275	15.93
Fe 0.55/Si 0	1	1.295	1.66	2.27	1.1475	1.965	22.21
Fe 1/Si 0	0.745	0.805	1.16	1.195	0.775	1.1775	12.56
Fe 0.03/Si 0.6	1.01	1.155	1.605	1.925	1.0825	1.765	19.51
Fe 0.55/Si 0.6	1.215	1.065	2.065	1.68	1.14	1.8725	20.77
Fe 1/0Si 0.6	0.71	0.8	0.995	1.355	0.755	1.175	12.69
Fe 0/Si 0	1.27	1.99	2.145	3.73	1.63	2.9375	33.93

Table G4. Intracellular reactive oxygen species (ROS) data for *Synechococcus* sp. PCC 7002 grown in oxygenic and anoxic conditions in the presence/absence of a metal chelator

	n-fold increase in ROS	
	un-acclimated	acclimated
oxygenic-EDTA		
Fe 0.03/Si 0	3	4
Fe 0.15/Si 0	9	DEAD
Fe 0.35/Si 0	13	DEAD
Fe 0.55/Si 0	19	DEAD
Fe 0.75/Si 0	32	DEAD
Fe 0.03/Si 0.6	4	4
Fe 0.15/Si 0.6	10	6
Fe 0.35/Si 0.6	21	14
Fe 0.55/Si 0.6	32	27
Fe 0.75/Si 0.6	39	DEAD
oxygenic-citrate		
Fe 0.03/Si 0	18	4
Fe 0.15/Si 0	21	8
Fe 0.35/Si 0	27	DEAD
Fe 0.55/Si 0	36	DEAD
Fe 0.75/Si 0	110	DEAD
Fe 0.03/Si 0.6	9	3
Fe 0.15/Si 0.6	18	4
Fe 0.35/Si 0.6	21	12
Fe 0.55/Si 0.6	22	33
Fe 0.75/Si 0.6	46	DEAD
anoxic		
Fe 0.03/Si 0	5	1
Fe 0.5/Si 0	12	3
Fe 1/Si 0	14	4
Fe 0.03/Si 0.6	5	1
Fe 0.5/Si 0.6	7	2
Fe 1/Si 0.6	11	3